UNIVERSITY OF OKLAHOMA

GRADUATE COLLEGE

SEISMIC EXPRESSION OF IGNEOUS BODIES IN SEDIMENTARY BASINS AND THEIR IMPACT ON HYDROCARBON EXPLORATION: EXAMPLES FROM A COMPRESSIVE TECTONIC SETTING, TARANAKI BASIN, NEW ZEALAND

A DISSERTATION

SUBMITTED TO THE GRADUATE FACULTY

in partial fulfillment of the requirements for the

Degree of

DOCTOR OF PHILOSOPHY

By

LENNON INFANTE-PAEZ
Norman, Oklahoma
2018

SEISMIC EXPRESSION OF IGNEOUS BODIES IN SEDIMENTARY BASINS AND THEIR IMPACT ON HYDROCARBON EXPLORATION: EXAMPLES FROM A COMPRESSIVE TECTONIC SETTING, TARANAKI BASIN, NEW ZEALAND

A DISSERTATION APPROVED FOR THE
CONOCOPHILLIPS SCHOOL OF GEOLOGY AND GEOPHYSICS

BY

Dr. Kurt J. Marfurt, Chair

Dr. Roger Slatt

Dr. John Pigott

Dr. Bradley Wallet

Dr. Deepak Devegowda

To God almighty and my family, specially my grandpa Dr. Oscar Infante.

Acknowledgements

would like to thank almighty God, for giving me wisdom whenever I asked him and for an amazing life filled with health, joy, and happiness. I think it is implicit that such an outstanding achievement (I'm a doctor now !!) is not only because my own merits. There is a large list of people that have helped me achieve Todays (May 11th, 2018) goal.

First, I want to thank my mom Janeth Paez and my dad Julian Infante for the love, care and all the life lessons, especially for teaching me that you can always achieve your goals if you work hard enough and trust in God. To my older brother Julian (Zorro), I would like to thank him for all the adventures we had when we were kids and for making my childhood incredibly fun, which have ultimately made me think the way I do. To the lovely, smart, beautiful and kind-hearted, Miss Andreina Liborius, I would like to thank her for all the love, patience and support this last few years, for being there unconditionally every time I needed her and for caring so much about me.

would like to express my sincere gratitude to my committee chair: Dr. K. J. Marfurt and my committee members Dr. Roger Slatt, Dr. John Pigott, Dr. Bradley Wallet and Dr. Deepak Davegowda. To my advisor and friend Dr. Kurt Marfurt, I thank him for taking me under his wing even though I told him I did not want to program. Also, I thank him for showing me that you can be brilliant, passionate, happy, wise, and still be humble and kind to others. I 'm infinitely grateful to Dr. Roger Slatt because he took me as his student when I was a recent graduate from Venezuela. I will be forever in his debt, because he changed my life (I promise I will pay forward whenever I become a professor). To Dr. John Pigott, a man who is incredibly knowledgeable about several aspects in geosciences, I thank him for all the constructive criticisms, teaching moments and for showing me that you can be a specialist who can also be a generalist. Also, I thank him for teaching me how to hold the laser pointer the proper way while presenting (This is very, very important). To Dr. Davegowda, I thank him for being very supportive regarding my technical work and for always being so professional and available for me. To Dr. Wallet. I thank him for showing me that you can always achieve your goals no matter how long they may take, and for always being respectful and available for me (while being in a different country).

Lastly, but not less important, many thanks to all the staff in the geology and geophysics department and professors and friends at the University of Oklahoma who were kind and helped me in this past 3 years (I'm deeply sorry if I forgot to mention your name, it's because I really want to sleep!!). Rebecca Fay, Ginny Gandy-Guedes, Ginger Leivas, Leah Mohser, Ashley Tullius, Donna Mulling, Teresa Hackney, Nacy Leonard, Robert Turner, Dalton Brasington, Dr. Lyn Soreghan, Dr. Barry Weaver, Dr. Zeev Reches, Charles Gilbert, Michael Behm, Nori Nakata, Dr. Jie Qi, Dr. Matt Pranter, Dr. Shankar Mitra, Dr. Michael Engel, Dr. Brett Carpenter, David Lubo, Gabriel Machado, Elizabeth Da Silva, Emilio Torres, Carl Symcox, Alex Besov, Suarabh Sinha, Javier Tellez, Tang Ha, Antonio Cervantes, Rafael Pires-De Lima, Folarin Kolawole, Abdulmohsen Alali, Jing Zhang, Cecilia Lopez-Gamundi, Lily Pfeifer, Abidin Caf, Tengfei Wu, Bin Lyu, Suriamin, Murphey Casesl, Swetal Patel, Kayla Miller, Laura Sanchez, Carlos Molinares, David Prado, Henry Galvis, Daniela Becerra, David Duarte, Benmadi Millad, Yan Qin, Muiz Matemilola, Oluwatobiloba Francis, Kelsy Lewis, Benjamin Slechtaa and many others. Additionally, I would like to thank Dr. Henry

Posamentier, Dr. Justin Mcdonal, Dr. Christopher Jackson, Dr. Steve Shuctter, Dr. Bergman, Dr. Satinder Chopra, Don Herron and Luis Vernengo for all the excellent technical advice and support on my dissertation.

Especial thanks go to “Team Lennon” (Andreina Liborius, David Lubo, Carl Symcox, Folarin Kolawole, Gabriel Machado, Emilio Torres, Javier Tellez, Rafael Pires-De Lima and Saurahb Sinha) without their direct help, I would not have been able to meet the deadlines.

Table of Contents

List of Figures

ABSTRACT

The impact of Neogene volcanism on hydrocarbon exploration in the Taranaki Basin, New Zealand remains under-explored. To better understand these effects, I performed detailed seismic interpretation coupled with examination of data from exploratory wells drilled into andesitic volcanoes. I discovered that igneous bodies can mimic the seismic expression of common sedimentary exploration targets such as bright spots, carbonate mounds and sinuous sand-prone channels. I find that by understanding the context of volcanic systems, one can avoid misinterpreting them as something else. Important clues that help distinguishing volcanoes from carbonate mounds in seismic data are not in the actual mound-like reflectors, but rather in features around and below these ambiguous facies. These clues are the disruption of reflectors immediately below volcanoes and igneous sills forming forced folds nearby and below the volcanic edifices. Secondly, in good quality seismic surveys, volcanic rocks of intermediate magma composition (andesitic) present distinctive patterns in seismic data. Such patterns are easy for machine learning to identify using a combination of seismic attributes that highlight the continuity, amplitude and frequency of the reflectors at the same voxels. Clustering of these seismic attributes using Self-Organizing Maps (SOM) allowed for the identification of different architectural elements such as lava flows, subaqueous landslides and pyroclastic flows associated with the andesitic Kora volcano. Finally, by 3D mapping of the Eocene, Miocene and Pleistocene strata in the Kora 3D seismic survey, I reveal that the andesitic volcanoes are capable of large structural trapping (Mega forced folds) in both the strata predating and postdating the volcanism. These traps are four way-

dip closures with the potential to store more than 1.0 billion of barrels of oil if filled to spill point.

CHAPTER 1

INTRODUCTION

Though igneous rocks are common in many sedimentary basins, their expression in 3D seismic data is underreported in the published literature. While excellent descriptions of igneous intrusions and extrusions can be found in the global geophysics literature, most case studies have been limited to 2D marine seismic data. (e.g., Planke et al., 2000; Jackson et al., 2013; Magee et al., 2013) . Although the oil and gas industry has acquired numerous high-quality 3D seismic surveys in the last 30 years, many over volcanogenic terrains, only a few dozen peer-reviewed papers have been written addressing the seismic expression of igneous bodies. Schutter (2003) attributed this lack of documentation to the belief by the oil industry that these rocks cannot be "good reservoirs" and that their presence may be hostile to the preservation of hydrocarbons. Nevertheless, significant quantities of hydrocarbons have been produced over the last two decades from igneous rocks in Argentina, India, Thailand, New Zealand, Namibia, Japan, Alaska, Venezuela, Cuba, Congo, Brazil, Algeria, Russia, Georgia, Italy and even the U.S.A (Zou, 2013). The largest field producing from an igneous reservoir is found in Jatibarang, Indonesia, in northwestern Java, which has produced more than 1.2 billion barrels of oil from fractured andesitic volcanics between 1969 to 1994 (Schutter, 2003).

In most cases, igneous rocks have limited impact on the exploration objective, unless someone is unfortune to drill a bright spot having the wrong polarity (Mark et al., 2017; Arawa-1 well series report), a volcanic plug in a carbonate terrain (Klarner and Klarner, 2012; Reynolds et al., 2016; Holdford et al., 2017) or a mafic lava flow with similar morphology as a meandering channel or turbidite (Vernengo per. Comm., 2017).

Klarner and Klarner (2012) find that in some cases the channel and mound features can be identified as igneous if placed in the proper stratigraphic context (below and above the target) coupled with an understanding of the basin history. Furthermore, Klarner and Klarner (2012) advise that if volcanics are present, a magnetic survey should be acquired. However, interpretation of such magnetic data can be difficult. In some cases, neighboring volcanoes can have different remnant magnetic polarization (Pena et al., 2009), while in at least one case encountered by AGIP over the western Mediterranean, a non-magnetic "carbonate buildup" was found to be a non-magnetic mafic volcano with overall mineralogy diagenetically altered to montmorillonite (Marfurt per. Comm., 2017). In addition to potentially misinterpreting igneous intrusions as bright spots, Mark et al. (2017) report that sills can be considered as geohazards that when unexpectedly encountered are detrimental to safe drilling practices and can also result in prolonged non-productive time.

Though igneous intrusions can overly "cook" a preexisting hydrocarbon accumulation (Barber et al., 1988; Kingston and Matzko, 1995), igneous intrusions can positively alter otherwise immature source rocks into the oil window (Rodriguez et al., 2009; Del Pino and Bermudez, 2009). Igneous rocks can also act as seals and traps (Holford et al., 2013). If fractured, igneous rocks can serve as migration pathways (Rateau et al., 2013) or form the reservoir (Schutter, 2003; Rodriguez and Montreal 2009; Zhang and Marfurt, 2011). Igneous rocks can create structural traps such as forced folds (Hansen and Cartwright, 2006; Holdford et al.,2012; Jackson et al., 2013; Magee et al., 2014; Gao et al., 2017) or domes by differential compaction of softer sediments around the more rigid igneous bodies (Hansen and Cartwright, 2006). Migration pathways can also be created from cooling and subsidence of volcanic edifices forming radial faults (Giba, 2013), or conversely, from growth or inflation of magma chambers, breaking through the host rock (Morley, 2018, in press). Hence, identification and mapping of igneous bodies is essential to both avoiding potential interpretation pitfalls, and in assessing their potential positive or negative impact to hydrocarbon exploration in sedimentary basins.

In general, igneous rocks exhibit a higher impedance than surrounding sedimentary rocks (due to both higher density and velocity), resulting in strong reflections. Andesitic volcanics show distinctive “salt and pepper” patterns in seismic data. These characteristics make igneous bodies amenable to semiautomated interpretation using seismic attributes as an input to machine learning algorithms. and promises to be a very effective way to accelerate the interpretation of anomalous facies (such as igneous bodies) from a more homogeneous background. Because seismic attributes are quantitative measurements of both amplitude and geometry, a key component to machine learning is determining which seismic attributes best differentiate a feature of interest from the background. For example, self-organizing maps (or SOM) simply organize the input attributes in a manner that voxels with similar characteristics (input attributes) are grouped and colored similarly. The algorithm does what it is supposed to do, it organizes the data and finds patterns. The main challenge for interpreters in applying SOM and similar algorithms to seismic data is the attribute selection.

This dissertation seeks to address the above-mentioned challenges, and is structured as follows

In Chapter 2, I investigate a few case studies from various sedimentary basins where the misinterpretation of igneous bodies in seismic data resulted in wells drilled into igneous rocks that were incorrectly interpreted to be targets of interest. I examine the seismic expression of drilled andesitic volcanoes and related igneous intrusions in the Taranaki Basin, and then use well control and principles of 3D seismic interpretation to propose a contextual interpretation workflow to avoid misinterpreting such igneous bodies.

In Chapter 3, I examine the seismic patterns associated with igneous bodies and identify seismic attributes that provide quantitative measures for subsequent machine learning. Key to this effort is identifying attributes that separate seismic patterns that represent volcanics from the surrounding sedimentary strata. I validate this analysis by using attributes from the Kora 3D survey to highlight geomorphologic features using self-organizing maps.

Chapter 4 uses the Kora 3D survey to illustrate the geologic cause and seismic expression of Mega forced folds. By 3D mapping of the folded strata below and above the Kora volcano, I find that there is causal relationship between the two. Using this case study, I propose that similar structural traps occur in other sedimentary basins affected by subduction-related volcanism.

I summarize my findings in Chapter 5 with the major conclusion being that igneous bodies, contrary to the common belief can positively as well as negatively impact hydrocarbon exploration. In both cases, the interpreter needs to know that they are present in the basin.

REFERENCES

Barber, P. M., T. Rasmussen, S. S. Rey, and R. Myklebust, 1988, The Exmouth Plateau deep water frontier: A case history, in P. G. Purcell and R. R. Purcell, eds., The North West Shelf, Australia, Proceedings of the Petroleum Exploration Society of Australia Symposium, 63–76.

Crown Minerals, Arawa-1 well completion report. 2016. Web. 12 Dec. 2016. Petroleum Report Series PR 1824.

Delpino, D. H., and A. M. Bermudez, 2009, Petroleum sys- tems including unconventional reservoirs in intrusive igneous rocks (sills and laccoliths): The Leading Edge, **28**, 804–811, doi: 10.1190/1.3167782.

Gao, Z., W. Tian, L. Wang, Y. Shi, and M. Pan, 2017, Emplacement of intrusions of the Tarim Flood Basalt Province and their impacts on oil and gas reservoirs: A 3D seismic reflection study in Yingmaili fields, Tarim Basin, northwest China: Interpretation, **5**, no. 3, SK51-SK63, doi:10.1190/INT-2016-0165.1.

Giba, M., J. J. Walsh, A. Nicol, V. Mouslopoulou, and H. Seebeck, 2013, Investigation of the spatio-temporal relationship between normal faulting and arc volcanism on million-year time scales: Journal of the Geological Society, **170**, no. 6, 951–962, doi:10.1144/jgs2012-121.

Hansen, D. M., and J. Cartwright, 2006, Saucer-shaped sill with lobate morphology revealed by 3D seismic data: implications for resolving a shallow-level sill emplacement mechanism: Journal of the Geological Society, **163**, no. 3, 509–523, doi:10.1144/0016-764905-073.

Holford, S. P., N. Schofield, and P. Reynolds, 2017, Subsurface fluid flow focused by buried volcanoes in sedimentary basins: Evidence from 3D seismic data, Bass Basin, offshore southeastern Australia: Interpretation, **5**, no. 3, SK39-SK50, doi:10.1190/INT-2016-0205.1.

Holford, S. P., N. Schofield, C. A. L. Jackson, C. Magee, P. F. Green, and I. R. Duddy, 2013, Impacts of igneous in- trusions on source and reservoir potential in prospective sedimentary basins along the Western Australian continental margin: West Australian Basins Symposium, Proceedings of the Petroleum Exploration Society of Australia Symposium, 1–12.

Holford, S., N. Schofield, J. MacDonald, I. Duddy, and P. Green, 2012, Seismic analysis of igneous systems in sedimentary basins and their impacts on hydrocarbon prospectivity: examples from the southern Australian margin: The APPEA Journal, **52**, no. 1, 229-252, doi:10.1071/AJ11017.

Jackson, C. A. L., N. Schofield, and B. Golenkov, 2013, Geometry and controls on the development of igneous sill-related forced folds: A 2-D seismic reflection case study from offshore southern Australia: Bulletin of the Geological Society of America, **125**, no. 11–12, 1874–1890, doi:10.1130/B30833.1.

Kartanegara, A.L., Baik, R.N. and Ibrahim, M.A., 1996, Volcanics oil bearing in Indonesia. American Association of Petroleum Geologists, **A**73.

Kingston, J., and J. R. Matzko, 1995, Undiscovered petro- leum of the Brazilian interior sag basins: Interna- tional Geology Review, **37**, 959–980, doi: 10.1080/ 00206819509465435.

Klarner S., O. Klarner,2012, Identification of Paleo-Volcanic Rocks on Seismic Data: Updates in Volcanology – A Comprehensive Approach to Volcanological Problems, InTech.

Magee, C., C. A. L. Jackson, and N. Schofield, 2014, Diachronous sub-volcanic intrusion along deep-water margins: Insights from the Irish Rockall Basin: Basin Research, **26**, no. 1, 85–105, doi:10.1111/bre.12044.

Magee, C., E. Hunt-Stewart, and C. A. L. Jackson, 2013, Volcano growth mechanisms and the role of sub-volcanic intrusions: Insights from 2D seismic reflection data: Earth and Planetary Science Letters, **373**, 41–53, doi:10.1016/j.epsl.2013.04.041.

Mark, N. J., N. Schofield, S. Pugliese, D. Watson, S. Holford, D. Muirhead, R. Brown, and D. Healy, 2017, Igneous intrusions in the Faroe Shetland basin and their implications for hydrocarbon exploration; new insights from well and seismic data: Marine and Petroleum Geology, in press, doi:10.1016/j.marpetgeo.2017.12.005.

Morley, C., 2018, 3D seismic imaging of the plumbing system of the Kora volcano, Taranaki Basin, New Zealand: The influences of syn-rift structure on shallow igneous intrusion architecture: Geosphere, in press.

Pena, V., S. Chávez-Pérez, M. Vázquez-García, and K. J. Marfurt, 2009, Impact of shallow volcanics on seismic data quality in Chicontepec Basin, Mexico: The Leading Edge, **28**, 674–679.

Planke, S., P. A. Symonds, E. Alvestad, and J. Skogseid, 2000, Seismic volcanostratigraphy of large-volume basaltic extrusive complexes on rifted margins: Journal of Geophysical Research: Solid Earth, **105**, no. B8, 19335–19351, doi:10.1029/1999JB900005.

Rateau, R., N. Schofield, and M. Smith, 2013, The potential role of igneous intrusions on hydrocarbon migration, West of Shetland: Petroleum Geoscience, **19**, 259–272, doi: 10.1144/petgeo2012-035.

Reynolds, P., N. Schofield, R. J. Brown, and S. P. Holford, 2018, The architecture of submarine monogenetic volcanoes – insights from 3D seismic data: Basin Research, **30**, 437–451, doi:10.1111/bre.12230.

Schutter, S. R., 2003, Hydrocarbon occurrence and exploration in and around igneous rocks: Geological Society of London, Special Publications, 7–33.

Zhang, K., and K. J. Marfurt, 2011, Seismic attribute illumi- nation of an igneous reservoir in China: The Leading Edge, **30**, 266–270, doi: 10.1190/1.3567256.

Zou, C. N., 2013, Volcanic reservoirs in petroleum exploration: Beijing, China, Petroleum Industry Press.

CHAPTER 2

SEISMIC EXPRESSION OF IGNEOUS INTRUSIVE AND EXTRUSIVE BODIES IN NORTH GRABEN, TARANAKI BASIN, NEW ZEALAND: IMPLICATIONS FOR AVOIDING PITFALLS IN INTERPRETATION.

ABSTRACT

In the past decades, many exploration wells have drilled into igneous rocks where the anticipated targets exhibiting similar seismic expressions were porous carbonate mounds, sheet sands or sand-prone sinuous channels. In cases where sedimentary features such as channels or fans cannot be clearly delineated, the interpretation may be driven primarily by bright spot anomalies, where a poor understanding of the wavelet polarity may lead to an erroneous interpretation. While many wells that are drilled into igneous rocks were based on interpretation of 2D seismic data, misinterpretation still occurs today using high quality 3D seismic data. To address this challenge, I analyze the seismic expression of andesitic volcanoes in the Taranaki Basin, New Zealand and use it to help understand misinterpreted igneous bodies in different parts of the world. I then propose an in-context interpretation workflow in which the seismic interpreter looks for key clues above, below and around the target of interest that may alert the interpreter to the presence of igneous facies.

INTRODUCTION

While igneous rocks are common in Australia, Argentina, Brazil, the UK-Norway continental margin, Indonesia, New Zealand, China and other oil provinces around the world, there is only limited documentation of the seismic expression of igneous bodies in 3D seismic data. Furthermore, more than 90 % of the documentation that does exist is focused on mafic intrusions (mainly sills), such as those described by Planke et al. (1999), Hansen and Cartwright (2006), Miles and Cartwright (2010), Klarner and Klarner (2012), Schofield et al. (2012), Holford et al. (2013), Jackson et al. (2013), Alves et al. (2015), Magee et al. (2016),Cortez and Santos (2016), and more recently by McLean et al. (2017), Hafeez et al. (2017), Gao et al (2017), Schmiedel et al. (2017) and Rabbel et al. (2018). Most of these studies focus on the magma mechanisms of emplacement into the sedimentary overburden, the associated deformation and the magmatic plumbing system. Moreover, the published literature is based towards the European side of the North Atlantic continental margin (UK-Norway), Australia and Brazil. Only a few studies directly address the identification of igneous rocks in seismic data Klarner and Klarner (2012) to avoid misinterpreting them as common sedimentary exploration targets.

Several publications examine igneous bodies that mimic common sedimentary exploration targets such as carbonate mounds, sinuous channels, and bright spots. For example, according to Mark et al. 2017, in press, in the Faroe-Shetland Basin, North East Atlantic, exploration companies targeting Carboniferous/Devonian, Jurassic, and Lower Cretaceous sandstones have drilled mafic igneous sills based on high amplitudes observed in seismic data (Figure 2.1). Similarly, using a legacy 2D seismic survey from 1982, in the Taranaki Basin, New Zealand, the Arawa-1 well drilled a bright spot in a structural high as a secondary target. This bright spot was andesitic volcanic tuff, probably sourced by subaqueous flows of adjacent Miocene volcanoes (Figure 2.2). In the San Jorge Basin, Argentina, exploration/development wells targeting sand prone meandering channels have drilled mafic lava flows with well-developed meander loops, filling a preexisting meander valley (Figure 2.3). In the Bass Basin, Australia, basaltic volcanoes were drilled by at least two exploration wells which were originally intended to test the hydrocarbon potential of a Miocene "reef complex" at a depth of 790 m (Holford et al., 2017; Reynolds et al., 2018) Figure (2.4).

Given these examples where clastic, carbonate and igneous bodies exhibit similar characteristics, it is clear that one should not limit an interpretation solely on the geometry or seismic expression of a preconceived or desired model. Doing so would make us a victim of confirmation bias. Krueger and Funder (2004) define *confirmation bias* as "actively looking for opinions and evidences that support one's own beliefs or hypotheses". See Bond et al., (2007) for examples of confirmation bias in seismic interpretation. My conjecture is that such confirmation bias concept was unconsciously executed in the previous examples from Argentina, Faroe Shetland and Australia (Figures 2.1-2.3) where the explorationists believed to have found in their seismic data the expression of the conceptual geological target model they had in mind. Counterintuitively, the best way for an interpreter to avoid confirmation bias is to gain a deeper understanding of features they are *not* interested in drilling, which in this paper, is a better understanding of the seismic expression and geomorphology of igneous intrusive and extrusive bodies.

My primary objective in documenting the seismic expression of igneous bodies is to alert the interpretation community of potential pitfalls when exploring for hydrocarbons in a sedimentary basin affected by volcanism. e.g., misinterpreting igneous features as hydrocarbon bright spots, carbonate mounds, or meandering channels. Perhaps the best way to avoid such a pitfall is to do an in-context interpretation. This is essentially the identification of subtler or architectural elements of igneous systems (Klarner et al., 2006; Klarner and Klarner, 2012). Specifically, the presence of deeper sills, associated forced folds, velocity pull-ups and poorly imaged vertical dykes near shallower volcanic vents serve as key indicators that the mound or channel-like features may not be a carbonate buildup or channelized turbidites.

For this reason, my goal is to document how igneous rocks appear in seismic data. Specifically, this study documents the seismic expression of andesitic (intermediate magma composition) volcanoes in the Taranaki basin, New Zealand, that have been drilled by exploration wells beginning in the 1980's. I link the presence of igneous sills, dykes, and forced folds below and around volcanoes to the same magmatic episode responsible for building the volcanic edifices. Finally, I propose an in-context interpretation workflow in which the seismic interpreter looks for key clues above, below and around the target of interest that may alert the interpreter to the presence of igneous facies.

Geological background

The study area is in the Northern Graben of the Taranaki basin, New Zealand. Although very extensive and complex, the evolution of the Taranaki Basin can be briefly summarized by three major phases of deformation. Phase one was Cretaceous to Paleocene (~84-55 Ma) extension. Phase two was Eocene to Recent (~40-0Ma) shortening, and Phase three was Late Miocene to Recent (~12-Ma) extension (Giba et al., 2010). Late Cretaceous extension was responsible for the breakup of Gondwana (King and Thrasher, 1992, 1996), while shortening in the Taranaki Basin is thought to have formed as a consequence of the subduction of the oceanic Pacific plate with the continental Australian Plate (Demets et al., 1994; Beavan et al., 2002). The last phase of deformation in the Taranaki Basin was the Miocene and younger extension. This extension was accompanied by volcanism that commenced at about 16 Ma and continues at Mt Taranaki Today (Neall et al., 1986; Hayward et al., 1987; Bergman et al., 1992; King and Thrasher, 1992) (Figure 2.5).These volcanic centers are mainly stratovolcanoes, of mostly low-medium K andesitic composition and, together with their NNE-trending alignment (Figure 2.6) parallel to the late Miocene subduction margin, suggest that the associated magmas were derived from the subducting Pacific Plate beneath the basin (Bergman et al., 1992).

Since the magmatism in New Zealand ranges from Early Miocene and Younger, the strata that predate such activity are named the pre-magmatic sequence, whereas the sediments that postdate the igneous activity are named the post-magmatic sequence.

Data set and Methods

The data set available for this study includes approximately 200 km^2 of offshore 3D pre-stack time migrated (PSTM) seismic data acquired in 2006 over the Northern Graben in the Taranaki Basin, New Zealand. Thirteen wells, four of them inside the 3D seismic survey (Kora 1-2-3-4 drilled by former Arco Petroleum NZ Inc.) with caliper, gamma ray bulk density, neutron porosity, P-sonic and resistivity logs. Well completion reports for all the wells and some offshore 2D PSTM seismic lines connecting other exploration wells nearby the Kora 3D survey were also available. The exceptional combination of factors found in the Taranaki Basin, make the study of the hydrocarbons in and around igneous rocks an exceptional laboratory for seismic interpreters whose interest is the impact of igneous rocks on hydrocarbon exploration. One key advantage is (1) the preservation of the entire volcanic arc due to its submarine (bathyal) depositional environment (Bergman et al., 1992) preventing subsequent erosion (Jackson 2012). A second advantage is that the Mohakatino Volcanic Belt (MVB) is located offshore, facilitating its illumination by high quality 3D marine seismic surveys.

The methods used in this dissertation are basic seismic interpretation techniques using commercial interpretation and seismic chronostratigraphy software. The seismic interpretation involves time slice and vertical random slices fallowed by horizon and stratal slices through the seismic data and seismic attribute volumes. Horizons were mapped using a constant phase auto tracker, well-to-seismic ties were constructed using synthetics based on the density and P-wave sonic logs to create acoustic impedance. Since the seismic data were acquired offshore, the phase of the wavelet is validated by the strong and symmetric peak observed at the water bottom boundary.

For the convenience of the reader, I will use a black-red color bar when using the Kora 3D seismic survey which has the highest quality (highest signal to noise ratio) and blue-white when displaying other surveys.

Extrusive igneous bodies in Taranaki Basin, New Zealand

Andesitic volcanoes

Some of the andesitic stratovolcanoes that form the Mohakatino Volcanic Belt (MVB) described by Bergman et al., (1992) and King and Thrasher (1996) have been penetrated in the early to late 1980s by exploration wells: Mangaa-1, Te-Kumi-1, Tua-Tua-1, and Kora-1-4 (Figures 2.7-2.10). According to the well series reports, the volcanoes were built from mid bathyal paleo seafloor (800 to 1300m).

The quality of the volcano images depends on the quality of the seismic data, with (post-2006) 3D surveys providing superior images to 2D surveys acquired in 1995. (Figure 2.10). On time migrated seismic data, they show a trapezoidal to mounded geometry with moderate to high continuous amplitude reflectors on the flanks, and a chaotic "salt and pepper" internal configuration (Figures 2.7-2.10). Wells that penetrate these volcanic cones encounter sequences of andesitic tuff to poorly sorted lapilli and breccias, with plagioclase and hornblende being major mineral components along with clay and rock fragments (Awatea-1 Te-Kumi-1, Tua-Tua-1 and Kora-1-4 well series reports).

The exact lateral extension of the volcanoes is difficult to map on the insufficiently dense 2D data grid, specifically, the 2D seismic lines may slice the volcanic cone on its flanks, rather than the summit, masking its true height and extent. Given this disclaimer, I find the volcanoes to be approximately 4-5 km in radius, rising between 500 m - 800 m above the paleo sea floor.

Whether analyzing 2D or 3D seismic surveys, the onlap of sediments onto the volcano flanks show that they were either volcanic islands or seamounts, where the age of the onlapping sediments indicate the relative age of the igneous bodies. Giba et al., (2013) used biostratigraphic dating of the sediment layers provided by offshore Taranaki Basin exploration wells to constrain the age of the Tua-Tua, Te-Kumi, Mangaa and Kora volcanoes (Figures5-8) to be between 33.7-10, 12-8, 12-5.5, and 12-5.5 Ma respectively.

The well control through several cone- to-mound-like structures seen on seismic data calibrates the unique external and internal seismic patterns of andesitic volcanoes which can be used to interpret similar nearby undrilled seismic patterns (Figure 2.11-2.14). The volcanoes exhibit a cone-to-mounded structure ranging from 500-100 ms in two-way travel time. While seamounts may retain their cone shape, subaerially exposed volcanic islands will be eroded, resulting in truncated cone to a more mounded appearance. Steep dip flanks (> 20°), internal heterogeneity, and higher velocity than the surrounding sediments give rise to imaging problems, resulting in a nearly complete disruption on the continuity of the reflectors immediately below the volcanoes. Analyzing a 3D seismic survey from Santos Basin, offshore Brazil, Cortez and Santos (2016) called a similar lack of continuity of the reflectors “shadow”. In seismic surveys from the Taranaki Basin, this disruption continues horizontally some 3000 m below the paleo seafloor at the time of eruption, which is inconsistent with vertical pipe feeder models ranging only hundreds of meters in diameter (Morley, 2018, in press). Examining the deeper reflectors below the volcanic cones, Figures 2.7-2.10 show deeper reflectors that are pulled up along with those concordant with the top of the volcano surface. For this reason, while velocity heterogeneity may lead to a poor image, most of the doming is structural (Figure 2.15), rather than a velocity pull-up artifact.

Seismic expression of the Kora volcano

Vertical slices through the 3D seismic volume showing the Kora Volcano in Figure 2.16 provide superior images when compared to older vintage data (Figures 2.7-2.9). The high amplitude at the top of the volcano is due to the high impedance contrast between the siliciclastic sediments and volcanic rocks. Within the volcano itself, it is possible to identify two different patterns: continuous high amplitude reflectors and chaotic moderate amplitude reflectors. Also, a shallow, high amplitude, low frequency flat reflector occurs above the volcano. This conspicuous feature appears to correspond to gasses emanating from the volcano. However, this feature is unlikely to represent inorganic gases -water vapor, carbon dioxide and sulphur dioxide, which are commonly found in volcanoes (USGS 2016) - because the volcano is believed to have been extinct since the Late Miocene ~12 Ma (Bergman et al., 1992).

The conic geometry of the volcano makes it necessary to study it in different orientations. Figure 2.17 shows the vertical section B-B′ in the northwest−southeast direction; the section crosses well Kora-4 illustrating, both strong amplitude, continuous and moderate amplitude chaotic reflectors within the volcanic edifice. On the flanks of the volcano, two onlapping wedges on both sides of the edifice indicate that the volcanic cone formed before these sediments were deposited. There is also evidence of a magma conduit breaking the host rocks (blue arrow) The north–south vertical section illustrates mainly chaotic seismic facies within the volcanic edifice penetrated by wells Kora-1,2 and 3, where a “transparent” amplitude zone occurs immediately below the volcanic summit similar to the pattern seen about the Te-Kumi-1, Tua-Tua-1 and Mangaa-1 wells. Note that onlapping wedges are also present (Figure 2.18). The east–west vertical section shows two distinctive seismic facies within the volcano. Wells Kora-1 and Kora- 4 drilled chaotic, moderate amplitude and continuous, high-amplitude reflectors, respectively. The onlapping wedges are also present (Figure 2.19). The presence of the onlapping wedges in different orientations suggests that these sediments were not completely blocked by the volcano, meaning that they were able to “travel” around the extrusive body.

Core pictures and descriptions available from the Kora completion well reports show that the volcanic rocks penetrated by Kora-1,2 and 3 wells represent a series of altered andesitic clasts with grain size ranging from tuff (volcanic ash) to pebbles, representing several sequences of pyroclastic flows dominated by andesine plagioclase, hornblende and pyroxene (Figure 2.20). Textural characteristics vary from sand size andesite through tuff breccia to clast-supported andesite agglomerates. Induration qualities also vary widely from unconsolidated to well consolidated (Kora-1 well series report). This series of altered andesitic clast exhibits a repeated pattern of fining-upward every 5–8 m, which serves as evidence for multistage volcanic episodes within the Kora-volcano edifice.

Integrating the core data from Kora-1,2 and 3 with the seismic data, I identify the chaotic moderate amplitude seismic facies to be pyroclastic flows. Although the completion well reports find no significant difference in mineralogic composition in volcanic rocks penetrated by Kora-1,2 and 3 to those penetrated by Kora-4, the slightly higher gamma ray in Kora-4 may be due to higher clay content which in turn implies higher alteration of plagioclase to clay rather than in *situ clay* sedimentation. At this point of the analysis, the nature of the continuous high-amplitude reflectors remains unknown. For this reason, I will use principles of seismic geomorphology to better map the architectural element represented by the continuous high-amplitude seismic pattern.

Faults associated with the Kora Volcano

Faults form an important component of the Kora volcano. A time slice through the coherence attribute at t = 2050 ms shows a semicircular, low-coherence feature that delineates the extent of the volcano (Figure 2.21). Similarly, co-rendering volumetric dip azimuth and dip magnitude, I image the volcano and the radial normal faults, showing the direction in which the reflectors are dipping. The distinct colors in the volcano indicate a dome structure (Figure 2.22). The extension of the Kora volcano is approximately 7–8 km in diameter, with a preserved summit height of approximately more than 800 m (Kora-1 well series report). These dimensions are comparable with the more modern Mount Taranaki (approximately 4-5 km in diameter and 2518 m of summit height) and Mount Ruapehu (approximately 6–7 km in diameter and 2797 m of peak height) analogs in the Taranaki Peninsula of New Zealand (Figure 2.4d). Normal faults are observed as low-coherence radial patterns similar to those created by salt diapirs (Rojo et al., 2016). Like salt diapirs, volcanism not only creates these radial-fault patterns in the pre-magmatic sequence due to growth or inflation of a magma chamber (somehow equivalent to active salt diapirs) but also in the post-magmatic sequences, where in this case the cause is due to subsidence of the volcanic body and the compaction of softer sediments against a more rigid body, the volcano (Reches and Schutter pers. Comm. 2018). Such a hypothesis can be proposed because this deformation is observed in sediments above the volcano, which postdate the volcanic activity (Figure 2.23). Radial fault patterns like those created by the Kora volcano are likewise documented by Giba et al. (2013) elsewhere in the Northern Graben of the Taranaki Basin.

To better illustrate the fault system created by the Kora volcano, Figure 2.24 shows a series of horizons from the pre-to the post-magmatic sequences. Horizon slices through dip magnitude (top) and dip azimuth co-rendered with the dip magnitude (bottom) along the pre-magmatic Paleocene, the top Eocene and the top of the Middle Miocene Kora volcano with the disconformable post-magmatic Upper Miocene Ariki Marl show a fault network. The fault network appears to be radial in both the pre- and post-magmatic sequence, although it is more pronounced in the post-volcanic sediments. Such faults associated with volcanism, potentially connect pores in an otherwise isolated pore network in the volcanics erupted by Kora and other submarine andesitic volcanoes, thus improving the reservoir quality of the volcanics.

Intrusive igneous bodies in Taranaki Basin

Igneous sills

Although not extensively documented because they are not exploration objectives, the most common features related to igneous bodies seen in seismic data are intrusive sills (Planke et al., 1999; Hansen and Cartwright, 2006; Miles and Cartwright, 2010; Holford et al., 2013; Jackson et al., 2013; Alves et al., 2015; Magee et al., 2016; Cortez and Santos, 2016; Naviset et al., 2017; McLean et al., 2017; Hafeez et al., 2017; Gao et al., 2017; Infante-Paez and Marfurt, 2017; Mark et al., 2017; Schofield et al., 2017) and more recently by Rabbel et al., 2018; Morley, 2018, in press).

A good example of episodic Miocene magmatism is the Kora volcano (Figure 2.15). Vertical sections around this edifice show multiple high amplitude, continuous (2-3 km) diameter saucer- shaped reflectors below the volcano that cross cut stratigraphy (Figures 2.25-2.26). The spatial distribution of these reflectors around the Kora volcano is illustrated using a set of co-rendered time slices through the instantaneous envelope attribute. Figure 2.27 shows the semicircular distribution of these high amplitude reflectors below and around the volcano. The spatial relationship to the Kora volcano supports the hypothesis that they are igneous bodies related to the same magmatic event that created the volcanic edifice in the Early-Mid Miocene (Bergman et al., 1992; Giba et al., 2013). These saucer-shaped high amplitude reflectors exhibit the same morphology as those documented by DuToit (1920), Planke et al. (2000) and others, from the rifted European side of the North Atlantic margin, Brazil and Australia, where rifting facilitates mafic magmatism due to decompression and partial melting of the ultramafic mantle. Furthermore, Sarkar and Marfurt (2017) describe similar andesitic saucer-shaped sills drilled and logged on the way down to deeper turbidites in the Chicontepec Basin of eastern Mexico. Regardless of their composition, the appearance of these sills below Kora is similar to those due to extension and subduction-related magmatism. Given these morphological analogues in both mafic and intermediate provinces, I interpret the saucer-shaped high amplitudes in the Kora3D survey to be sills (Figures 2.25-2.26). The host rocks into which these igneous bodies intrude may be of interest in hydrocarbon exploration. Figure 2.28 illustrates a vertical slice through a seismic amplitude section showing multiple ~2 km sills and possible laccoliths that thermally modify the Paleocene source rock, such as described by Delpino and Bermudez (2009). In this scenario, heat from the sills place immature source rocks within the oil window. Igneous intrusion will produce contact metamorphism in the host rocks nearby the intrusion. These thermally altered rocks or “hornfels” , like those studied in outcrop by Liborius and Tazzo (2012) and Sarkar et al. (2017) are often fractured, allowing hydrocarbons to migrate into the fractured igneous bodies (Rodriguez Monreal et al., 2009; Delpino and Bermudez, 2009; Senger et al. , 2017; Rabbel et al., 2018)

Though physical geology textbooks show sills being concordant to stratigraphy, seismic data exhibit such sills in their entirety (Thomson, 2007; Miles and Cartwright, 2010), where they are seen to step upward like the large scale photo of the Greenland outcrop shown in Figure 2.29. Figure 2.29 shows a sill that is concordant with stratigraphy for the most part, propagates upwards through "steps" that cross-cut stratigraphy until it finds a suitable layer where another saucer shaped sill could be developed. Upward movements of magma through sill junctions (Figures 2.30), a type of lateral magma flow (Hansen et al., 2004) seems to be the major mechanism of vertical magma transport in the upper crust (Magee et al., 2016).

Below the Kora volcano these sill-to-sill junctions can be seen to have transported magma from ~ 4.2 s TWT to ~ 2.75 s TWT (about 2 km) over a lateral distance of 10 km. In addition, they appear to connect to the flanks of the Kora Volcano forming a side vent (Figure 2.31 reddish arrows).

Forced folds

Another key feature often associated with igneous intrusions is deformation of the host rock. Jackson et al. (2013), Magee et al. (2014), Alves et al. (2015), and Schmiedel et al. (2017) report the occurrence of forced folds in seismic data. According to Schmiedel et al. (2017), most sills form folds because either the volume of the magma displaces that of the sediments or because intrusions are virtually incompressible with respect to the surrounding sedimentary rocks that do not compact, and therefore develop a structural dome. Figure 2.32a shows an example of post-emplacement deformation where a sill complex in the Upper Cretaceous sequence and corresponding forced folds directly above the igneous intrusions (green arrows). The wavelength of the fold appears to be linked to the lateral extent of the sills, while the amplitude of the fold seems to be related to the cumulative thickness. A crucial clue is that the amplitude of the fold deformation decreases stratigraphically upwards, suggesting the deformation occurred after the emplacement of the sill, probably due to differential compaction about the flanks (Schmiedel et al., 2017) and that the sill was emplaced in a zone of high pore fluid volume that may have been fluidized to accommodate the volume of the magma. In contrast, Figure 2.32b shows an example of a forced fold where terminations can be seen to lap onto the fold, suggesting syn-emplacement deformation thereby defining the time of the initial intrusion (Hansen and Cartwright, 2006). Often, sills show evidence of both syn- and post-emplacement deformation and small to no deformation respectively (Figure 2.32a grey arrow). Magee et al. (2016) find that sometimes sill emplacement shows little to no deformation, suggesting fluidization. For this reason, while deformation is an indicator of the emplacement of most igneous bodies, not all igneous intrusions generate such features.

Igneous dikes

In magmatic systems, dykes are near vertical intrusions commonly tens of meters thick and up to a few kilometers in extent (e.g. Thomson, 2007; Holdford et al., 2017; Reynolds et al., 2018) that cross-cut pre-existent strata, usually intruding into zones of weakness such as faults and other mechanically weaker layers. The imaging of these igneous bodies in seismic data is challenging since seismic data will not image near vertical features (Thomson, 2007). Nevertheless, evidence of dykes can still be observed in seismic data. (Holdford et al., 2017, Reynolds et al., 2018).

A series of near vertical, narrow, low amplitude reflectors can be seen below the flanks of the Kora volcano (Figure 2.33). These reflectors create a pattern that is very difficult to distinguish from low signal/noise zones where amplitudes may have been affected by absorption. However, they only cover a certain portion of the seismic section between 2000-4000 ms TWT in Figure 2.34. The second criteria is that they appear to be terminating on sections of the flank of the Kora Volcano where reflectors with a small conical shape appear (Figure 2.34). A coherence and dip magnitude stratal slice near the base of the flank of the volcano shows this feature to be semi-circular (Figures 2.35 a and b). Given the spatial and temporal relationship of these events, I interpret the near vertical, narrow, low amplitude pattern to be near vertical dykes that feed the small conical vents. This observation is consistent with the model proposed by Bischoff et al. (2017).

Avoiding potential seismic interpretation pitfalls

The images from the introduction section had well that penetrated the mound- to cone- shaped structures confirming them as igneous volcanoes. In the absence of well control the cone-to mound-like geometry is similar to carbonate reef exploration targets. In addition, Figure 2.36 shows examples of igneous bodies both intrusive and extrusive that mimic the seismic expression of common sedimentary exploration targets. Based on their morphology alone, many interpreters will not be able to distinguish igneous bodies from their clastic counterparts (I encourage the reader to make an educated guess before reading the figure caption).

To try to distinguish between common exploration targets from Figure 2.36 and igneous bodies that mimic their geometry/ morphology, I examine a few seismic amplitude sections of the Akira 2007 2D seismic survey acquired over the Taranaki Basin, New Zealand. The seismic data depict a series of cone-to-mound geometries with chaotic internal reflection configurations and moderate to high amplitudes on the top. Immediately below the mound-like features there is a disruption in the reflections similar to those seen in the volcanoes in Figures 2.7-2.14. The mounds exhibit base lengths of approximately 2000 meters with “steep” flanks and appear to be laterally interconnected. Based only on their geometry, these features are similar to “carbonate mounds” (Holdford et al., 2017; Reynolds et al., 2018;) or even to mud volcanoes. The only unequivocal way to determine the composition of these mounds would be by drilling a well through them and study extracted core or cuttings. An alternative way would be to use potential field methods to differentiate between generally magnetic igneous rocks and non-magnetic sedimentary rocks. However, remnant magnetization may confuse the interpretation (e.g. Pena et al., 2009) while diagenesis may result in magnetic volcanic tuff being converted to nonmagnetic montmorillonite (Marfurt personal communication with former colleagues at AGIP). An alternative and inexpensive method is to apply in-context interpretation. In this study, in-context interpretation refers to the concept implemented by Posamentier (per. Comm., 2018), in which he looks at the pattern of the features of interest as well as the surrounding elements (e.g., what’s below, what’s above and what’s around). To illustrate this concept, I cite National Geographic’s Brain Games TV show analogy illustrated in Figure (2.37). In this image, we see headshots of two former U. S.A leaders. We can easily recognize former vice president Dick Cheney on the left and former president George W. Bush on the right side. Detailed examination of this image shows that they both have the same face (analogous to the ambiguous pattern of interest in geology e.g., carbonate mounds, or volcanic mounds) with minor alterations. So, how is it that the same face gives two completely different persons? (analogous to two different interpretations) It is the context, (what's above, what's below and what's around) where the key to differentiation lies. In this case, the context is given by the glasses, the different hair style, hair and skin color that allows us to distinguish ex-vice president Cheney from ex-president Bush in Figure 2.37.

Applying the same in-context interpretation concept to Figure 2.38, I recognize other key clues that would help infer the composition of the mound-like features. Among these clues are: (1) saucer-shaped high amplitude sills around the mounds (2) forced folds that are formed due to the emplacement of the sills (Hansen and Cartwright 2006; Holford et al., 2012; Jackson et al., 2013; Magee et al., 2014; Infante-Paez and Marfurt, 2017; Schmiedel et al., 2017; Magee et al., 2017; Schofield et al., 2017) (red arrows) and (3) a sub-vertical narrow low amplitude pattern in the section below these mounds that appears to disrupt the reflectors for significant vertical distances (2250-3500 ms TWT, or more than 1km) just below the mounds. Implementing an in-context interpretation, the presence of all these elements (saucer shaped sills, forced folds in addition to the mounds) indicate an igneous composition of the mounds (Figure 2.39). In contrast, an interpretation driven by confirmation bias (Figure 2.40) where the objective is to identify carbonate build-ups to test their reservoir potential might misinterpret the mound-like features to be pinnacle reefs, as appeared to be the case documented by Holford et al., (2017) and Reynolds et al., (2018) in the Bass Basin, Australia. Figure 2.41 summarizes a proposed workflow to avoid interpretation pitfalls in the presence of igneous intrusions and extrusions. Key to this workflow is not to stop when we find what we are looking for (finding the feature of interest from our conceptual geological model), thereby confirming our bias. Rather, we perform in-context interpretation to try to match the evidence of the context to our exploration target, like the igneous evidence found in Figure 2.38b. Further examination of the literature supports the igneous interpretation where Jackson et al. (2013) and Magee et al. (2013) found similar features in the Ceduna sub-basin of Australia to be volcanoes.

CONCLUSIONS

Igneous bodies can mimic the geometry and morphology of important exploration targets such as carbonate mounds, sinuous channels and bright spots. For this reason, the interpreter cannot rely on seismic morphology and geometry alone. Whenever possible, seismic data should be complemented with other geophysical methods such as gravity and magnetic surveys to avoid drilling features like volcanic cones. An alternative and inexpensive method to avoid such pitfalls is in-context interpretation where the interpreter examines not only the pattern of the features of interest but also the patterns of the surrounding elements. In simpler terms, we need to not only identify features we want to find, but also to identify neighboring features we do not want to find.

By understanding the context of volcanic systems, one can avoid interpreting them as something else. Important clues that help to distinguish a volcano from a carbonate mound in seismic data are the disruption of reflectors immediately below the mound-like features and the igneous sills forming forced folds nearby and below the volcanic edifice. This disruption of reflectors is common in older 2D and newer 3D surveys that I have analyzed in the Taranaki Basin, New Zealand.

Igneous bodies in seismic data have much in common across compressive and extensional regimes. Saucer-shaped high amplitude discontinuous reflectors represent the real morphology of sills and are not caused by migration artifacts of seismic data.

Chapter 2 Figures

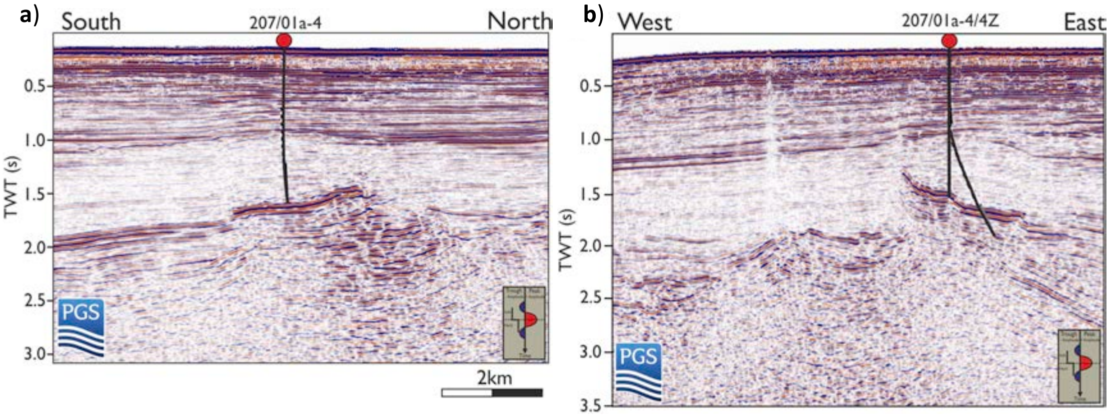

Figure 2.1. Exploration well drilling into mafic igneous sills, seismic data courtesy of PGS. Reprinted from Igneous intrusions in the Faroe Shetland basin and their implications for hydrocarbon exploration; new insights from well and seismic data, In Press N.J. Mark, N. Schofield, S. Pugliese, D. Watson, S. Holford D. Muirhead R. Brown D. Healy,1-21, Copyright (2017), with permission from Elsevier.

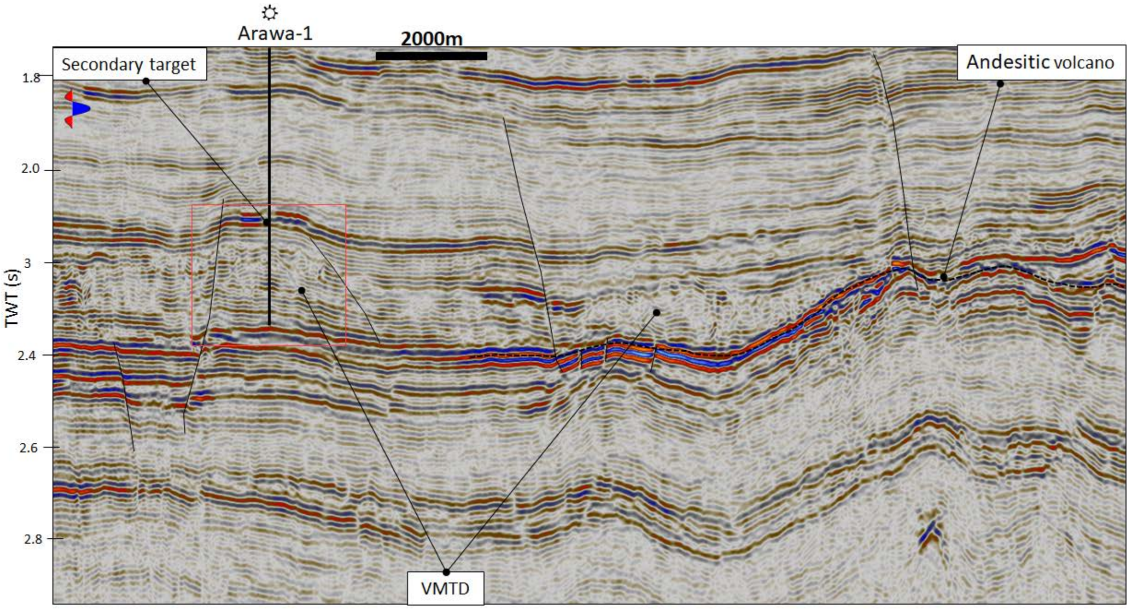

Figure 2.2. Exploration well Arawa-1 drilling into bright spot (andesitic volcanic pile). Notice the andesitic volcano on the right side. Seismic data courtesy of NZP&M. VMT= Volcanic Mass Transport Deposit.

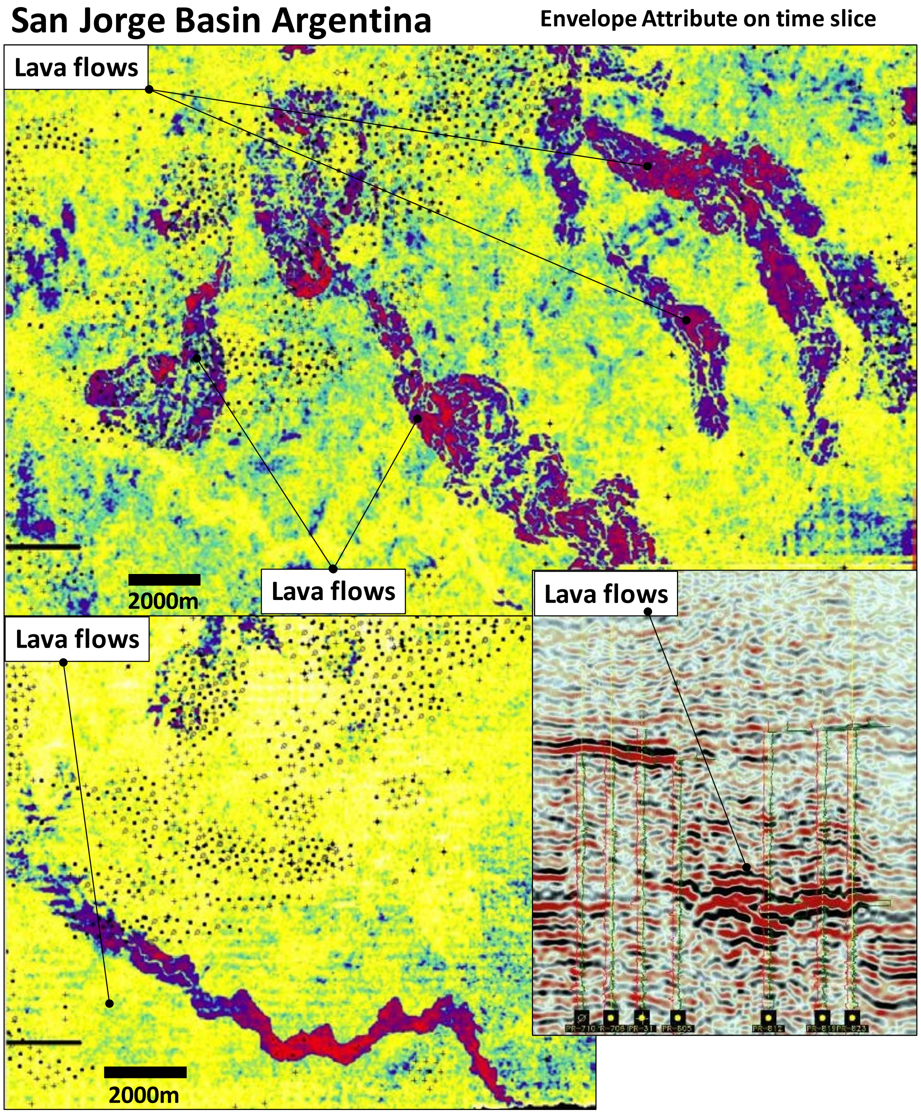

Figure 2.3. Envelope attributes in time slices and amplitude vertical section showing development wells drilled into channel-like features. The wells drilling the "channels" instead encountered lava flows that were confined to meander valleys. Courtesy of Luis Vernengo, Pan American Petroleum.

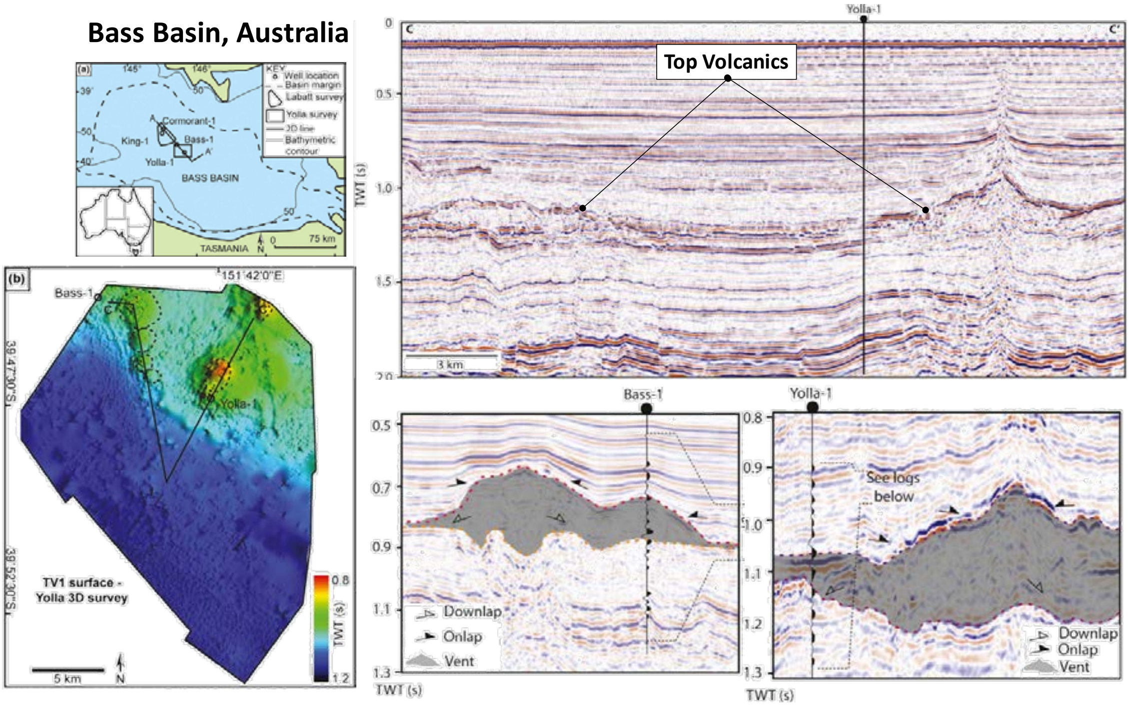

Figure 2.4. Vertical amplitude sections showing exploration wells drilling into mound-like features. The wells drilled a basaltic volcano rather than a carbonate buildup. Map on bottom left is the top of the volcanic units. Notice the dome-like shape. (After Reynolds et al., 2017).

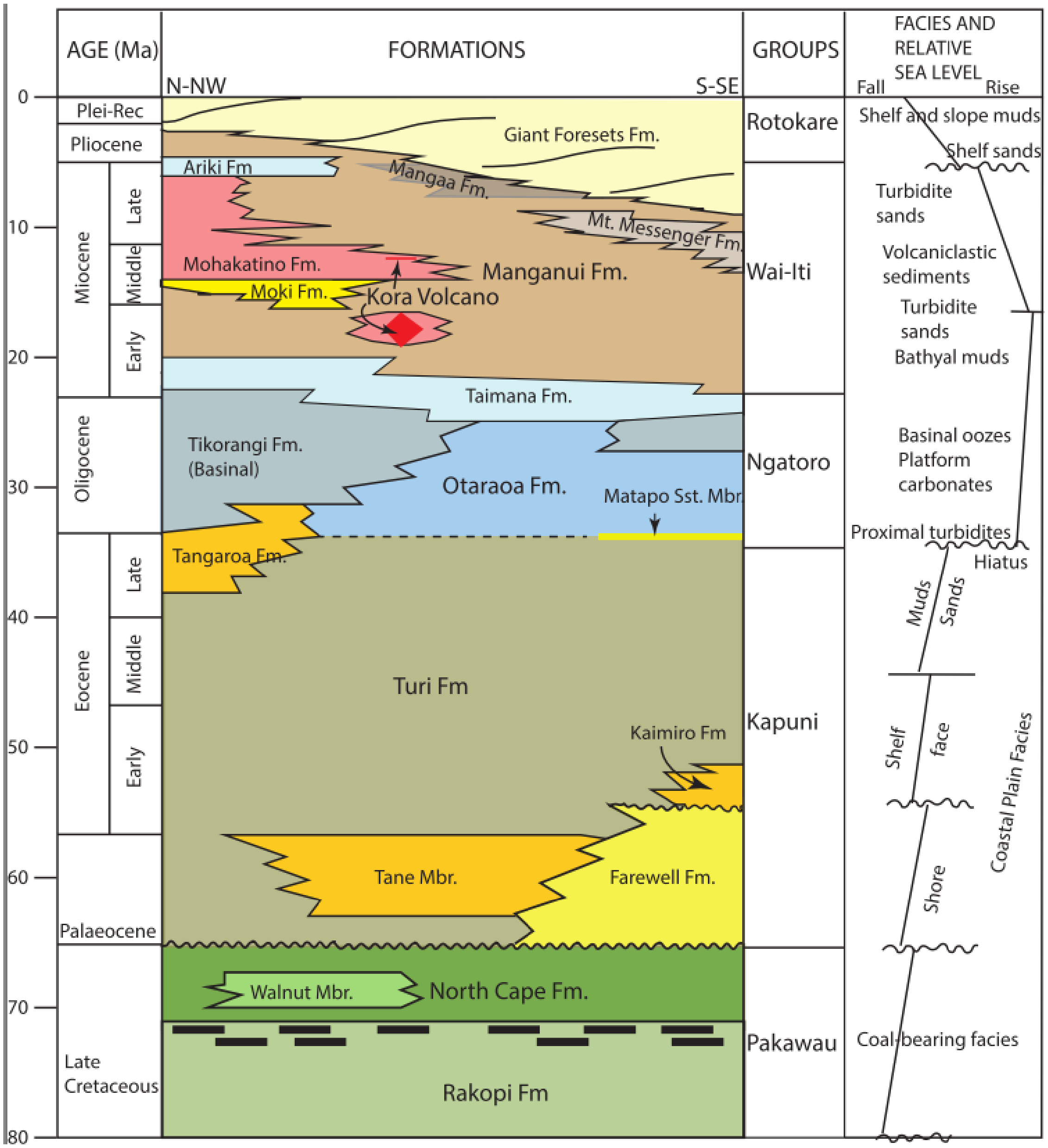

Figure 2.5. Chronostratigraphic chart and a representative section of the Geology of Taranaki Basin, New Zealand. (After Morley, 2018, in press).

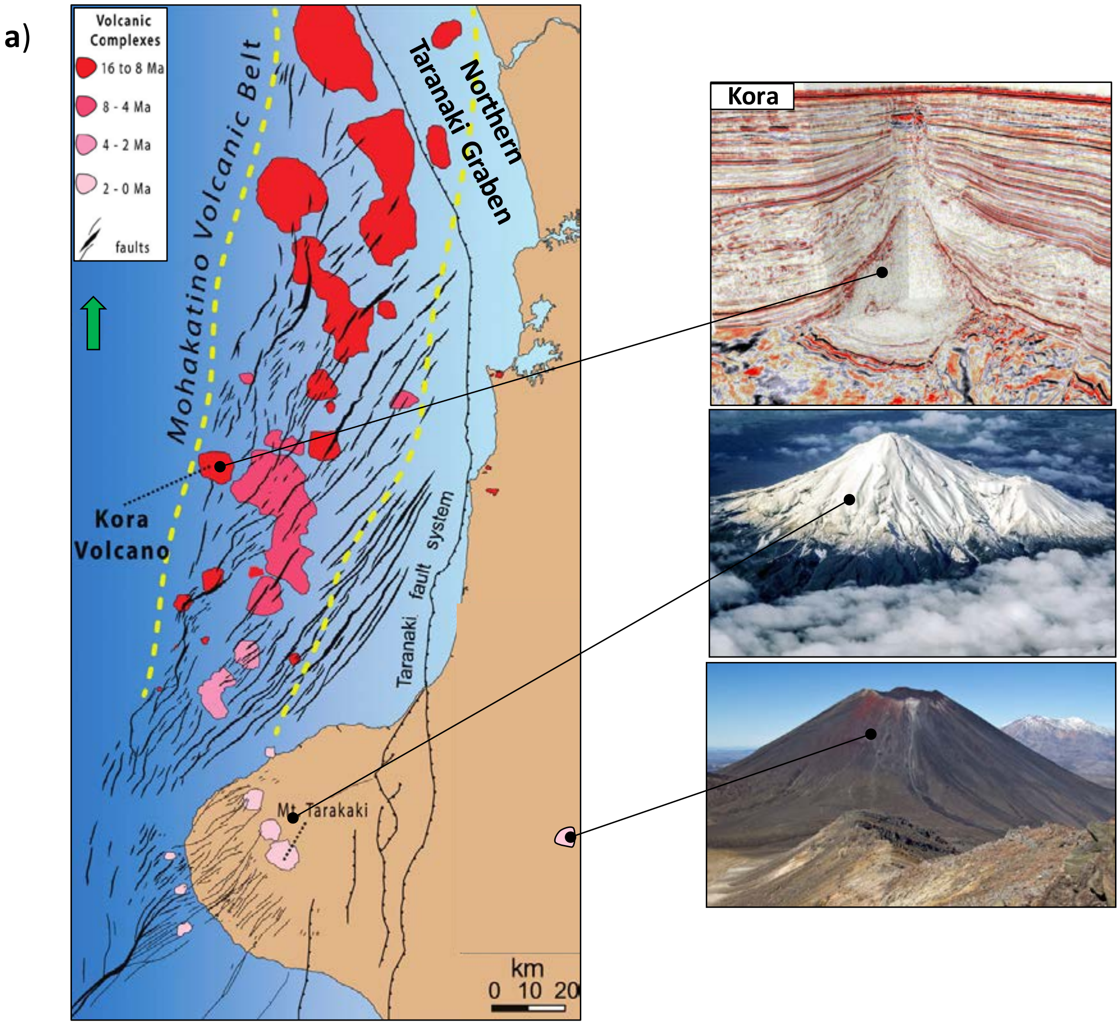

Figure 2.6. (a) location map of New Zealand showing Taranaki Basin and the size and distribution of the Mohakatino Volcanic Belt (MVB) in red. (b) Onshore younger andesitic volcanoes and 3D seismic sections showing Kora Volcano. After Giba et al. (2013) and Bischoff et al. (2017).

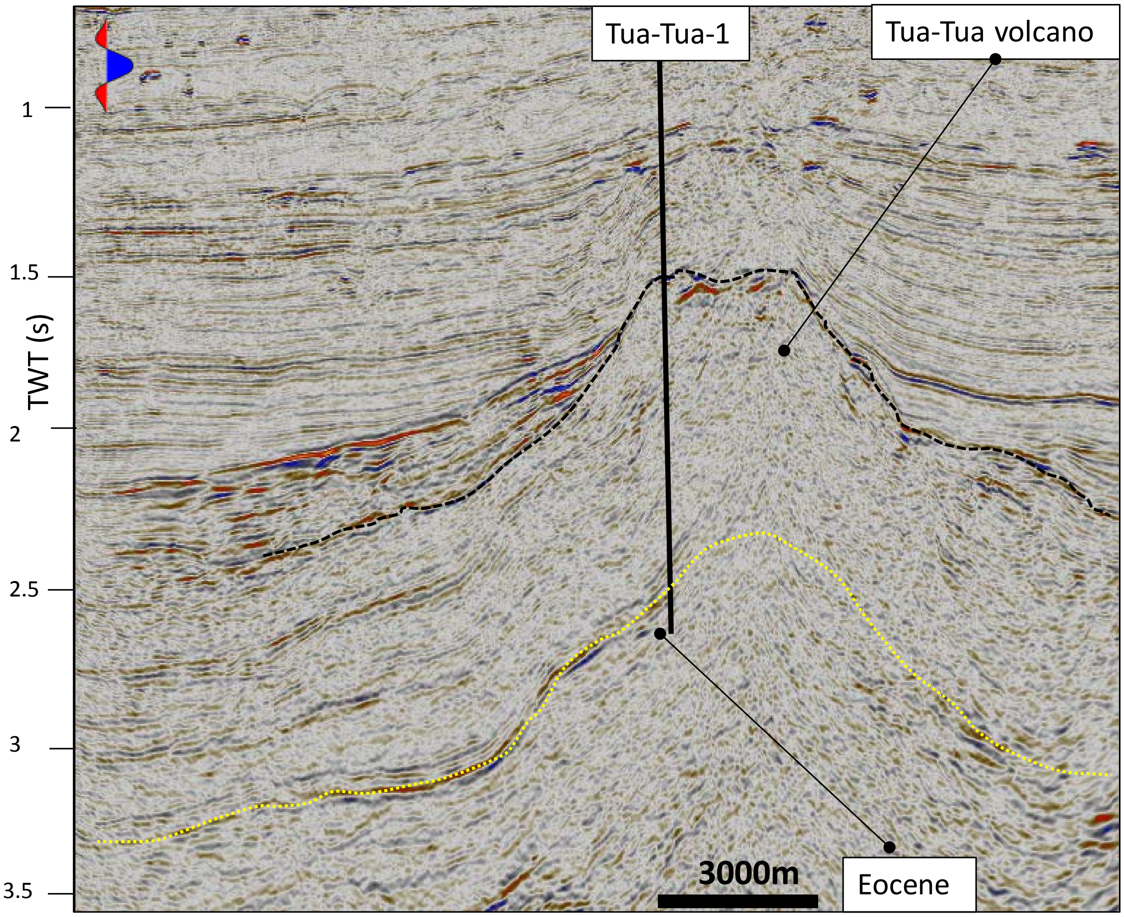

Figure 2.7. Seismic section from the 2D P95 Survey showing Well Tua-Tua-1 drilling the andesitic Tua-Tua volcano. The Tua-Tua-1 well is projected into this seismic line.

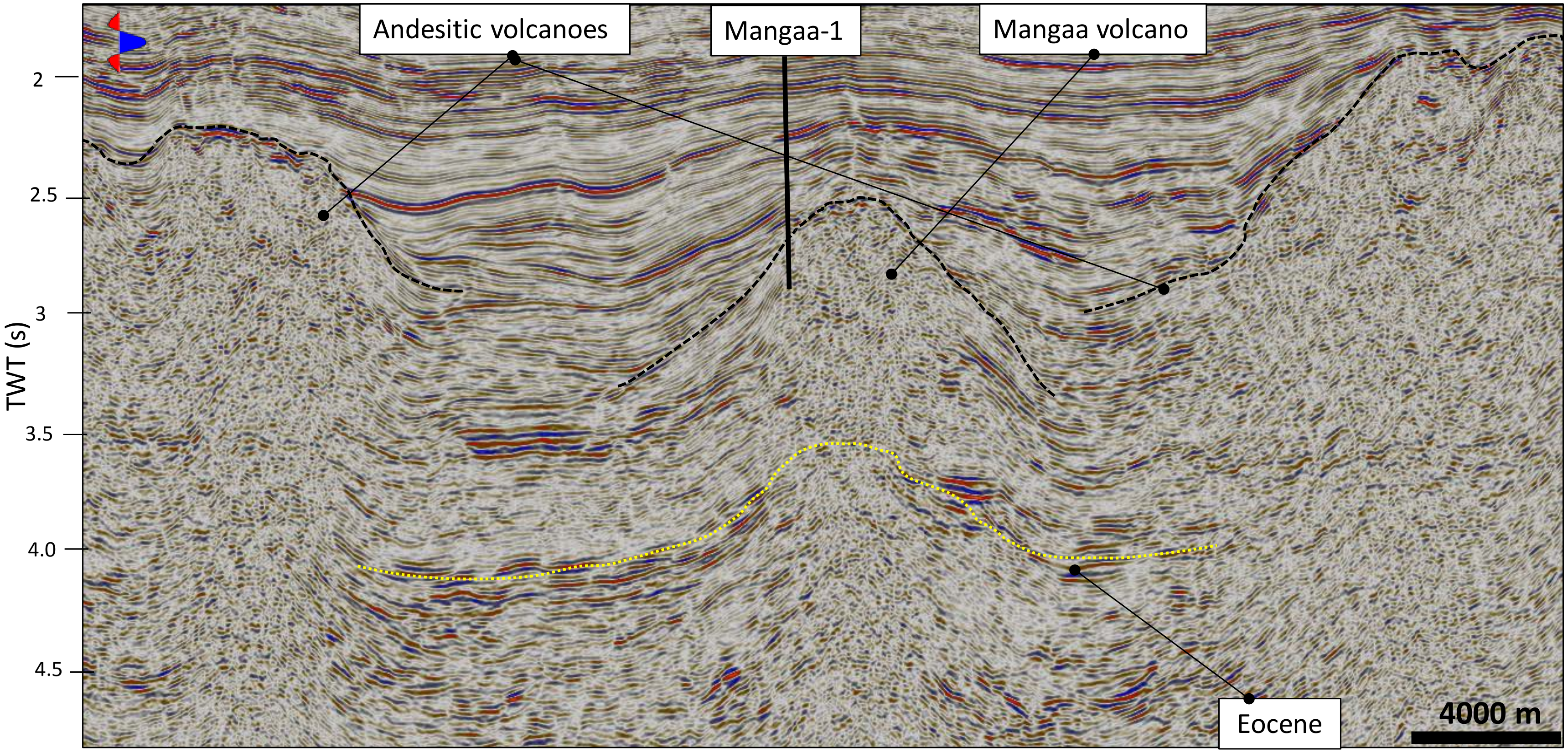

Figure 2.8. Seismic section from the P95 2D seismic survey showing well Mangaa-1 drilling the andesitic Mangaa Volcano.

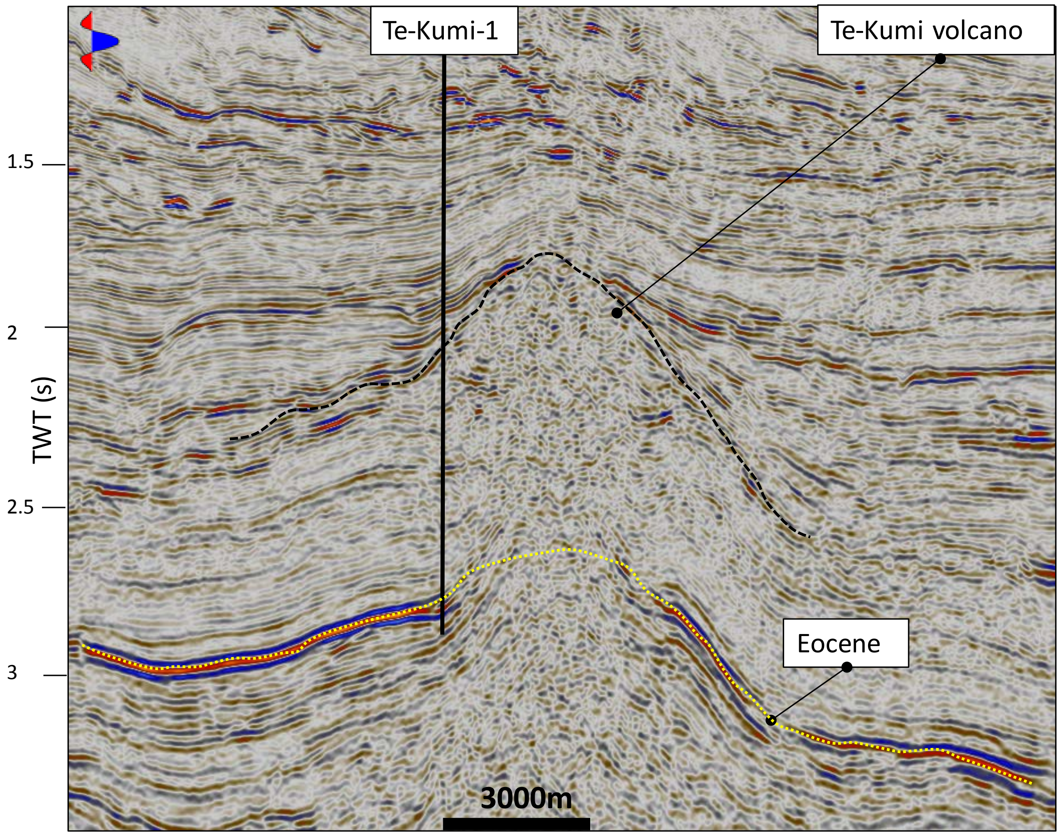

Figure 2.9. Seismic section from the 2D P95 Survey showing well Te Kumi-1 drilling the andesitic Te-Kumi Volcano.

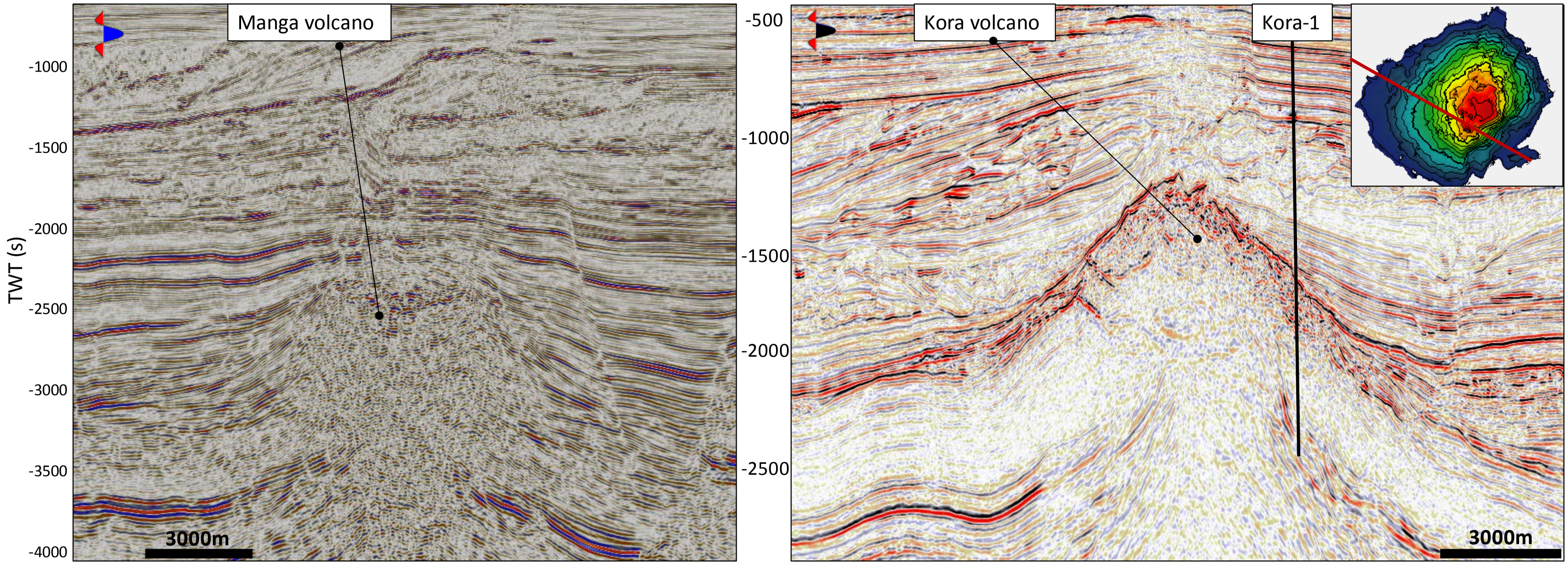

Figure 2.10 Signal/ratio comparison between: (a) legacy 2D ES-89 seismic survey and (b) modern 3D Kora 3D PSTM 2006 seismic survey. Notice the higher quality image of the Kora volcano compared to the Mangaa volcano.

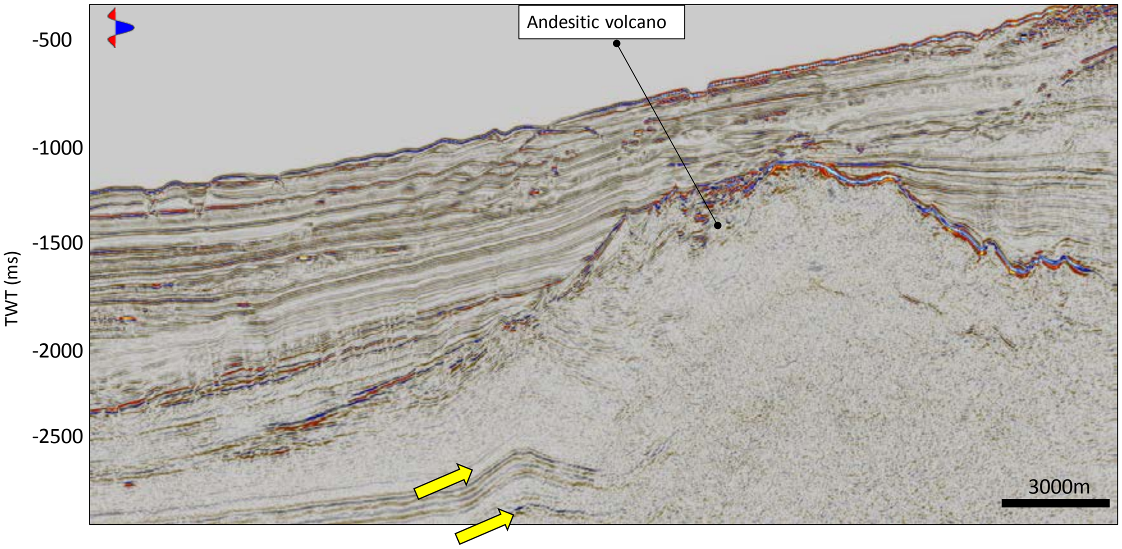

Figure 2.11. Undrilled mound-like structure interpreted to be an andesitic volcano. Yellow arrows indicate reflections below the flank of the volcano indicating the bright reflections are not the crystalline basement.

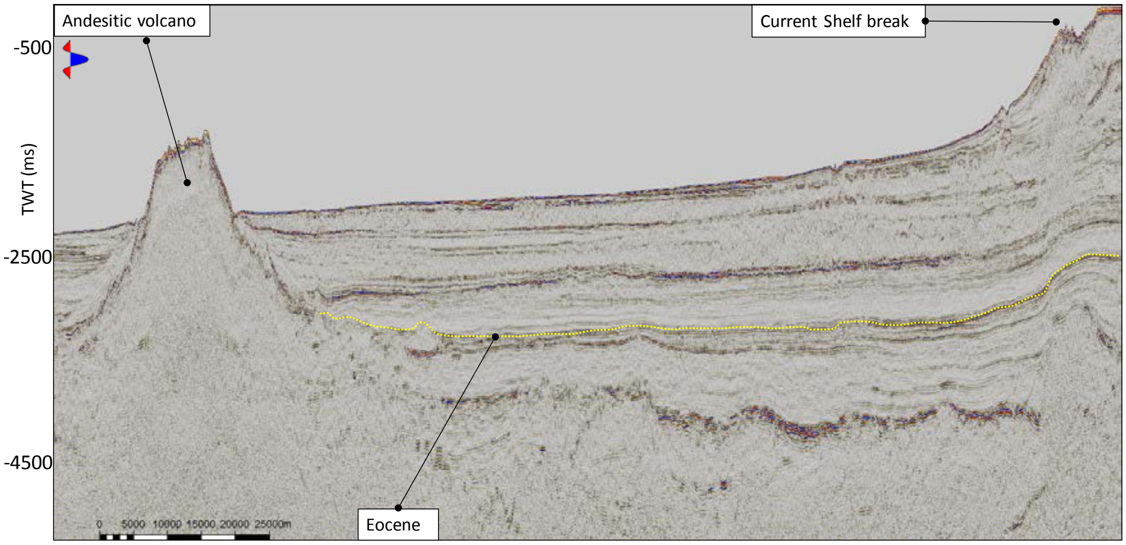

Figure 2.12. Undrilled mound-like structure interpreted to be an andesitic volcano.

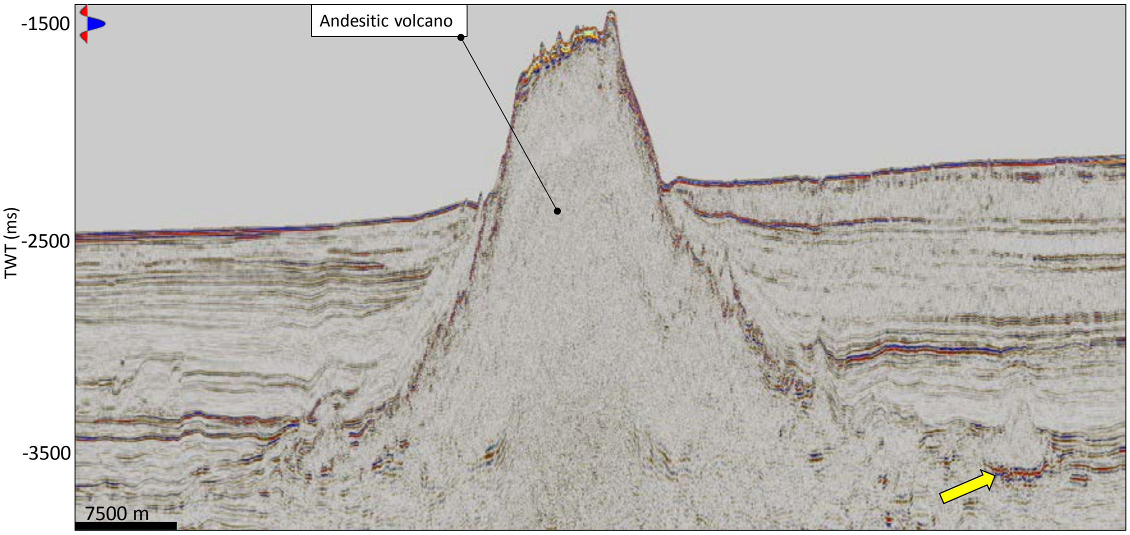

Figure 2.13. Zoomed in version of the previous undrilled mound-like structure interpreted to be an andesitic volcano. The yellow arrow indicates to reflections below the flank of the volcano indicating the mound-like structure is not crystalline basement.

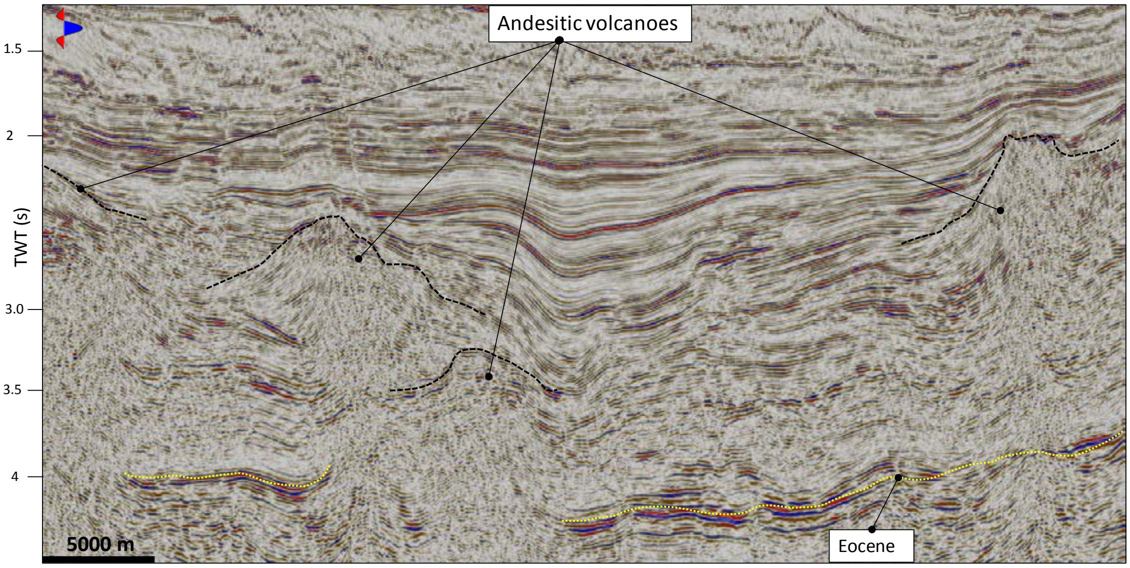

Figure 2.14. Vertical slice showing undrilled mound-like structure interpreted to be andesitic volcanoes.

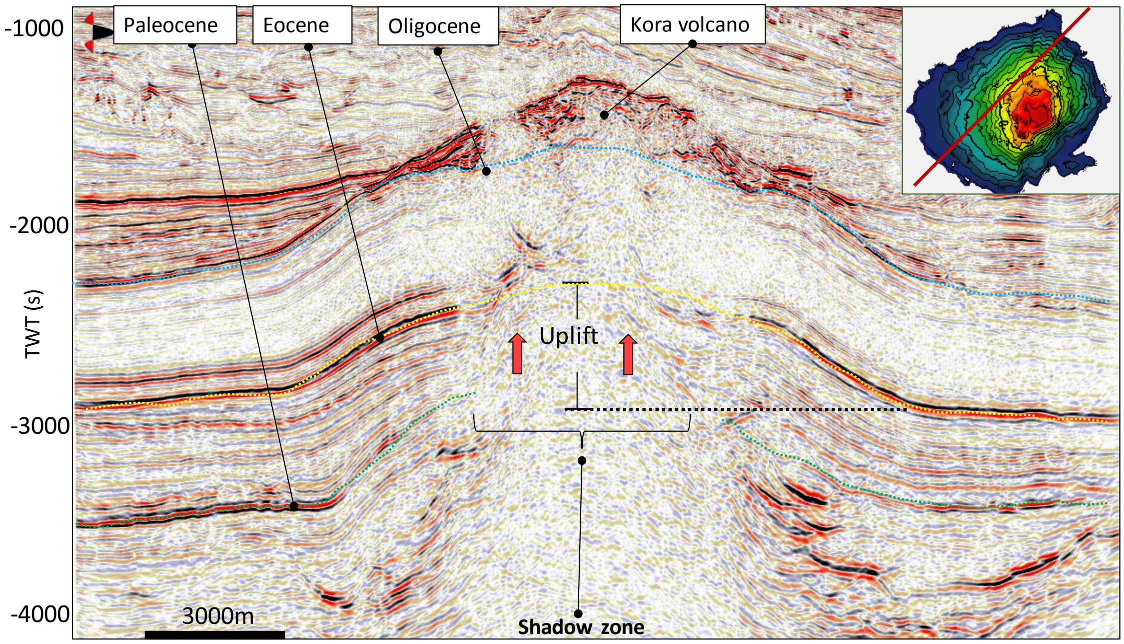

Figure 2.15. Seismic section from Kora 3D seismic survey showing the Kora volcano and the uplift of the reflectors beneath the edifice as well as the disruption of the reflectors (shadow zone).

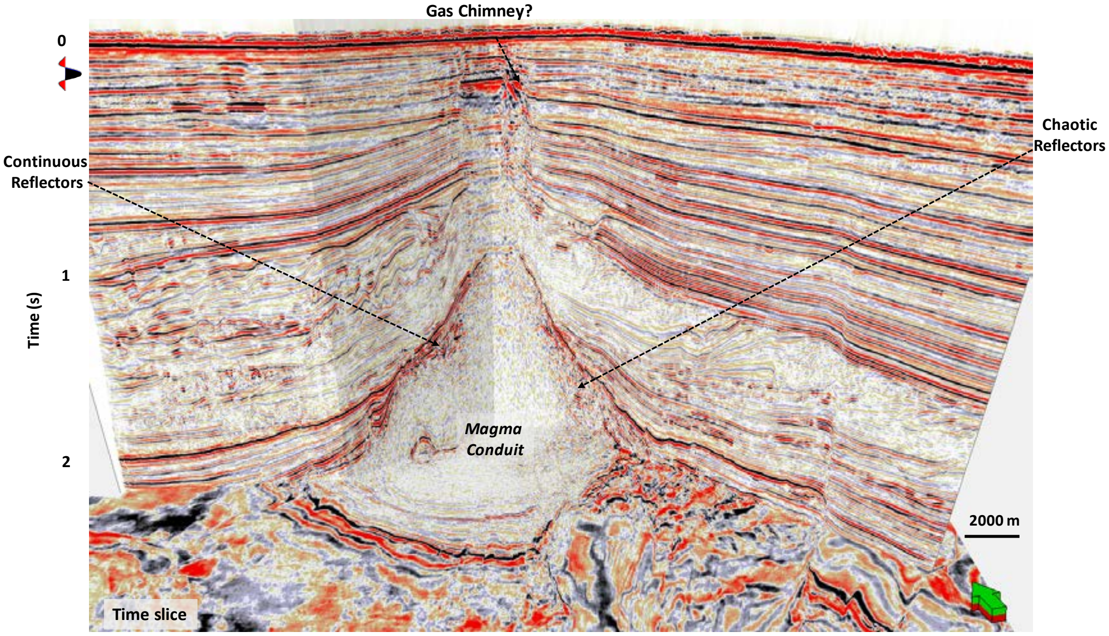

Figure 2.16. A representative 3D composite vertical slice of the amplitude data showing the Kora volcano and the good signal-to-noise ratio, allowing the identification of different seismic facies related to the volcano. After Infante-Paez and Marfurt (2017). Seismic data courtesy of NZP&M

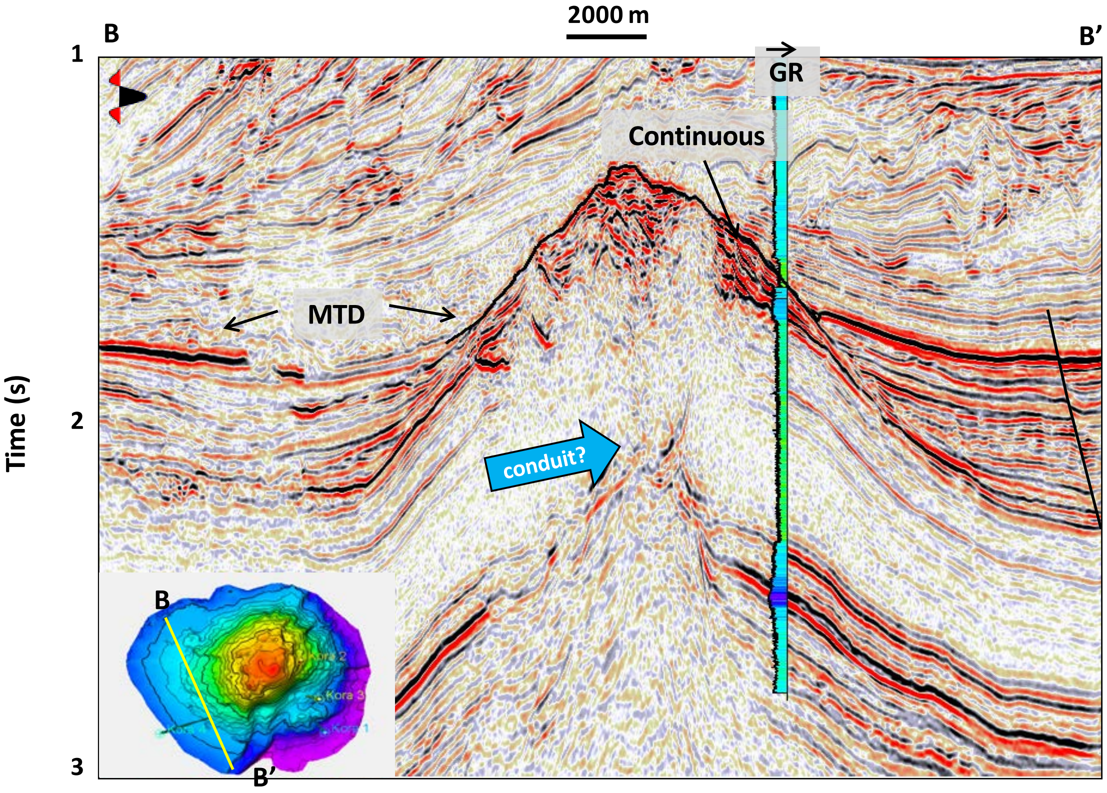

Figure 2.17. Magnified vertical magnified slice BB′ through the seismic amplitude volume showing the chaotic moderate amplitude reflectors adjacent to strong continuous reflectors penetrated by the Kora-4 well. An MTD is observed on the northwest flank of the volcano**.** After Infante-Paez and Marfurt (2017). Seismic data courtesy of NZP&M.

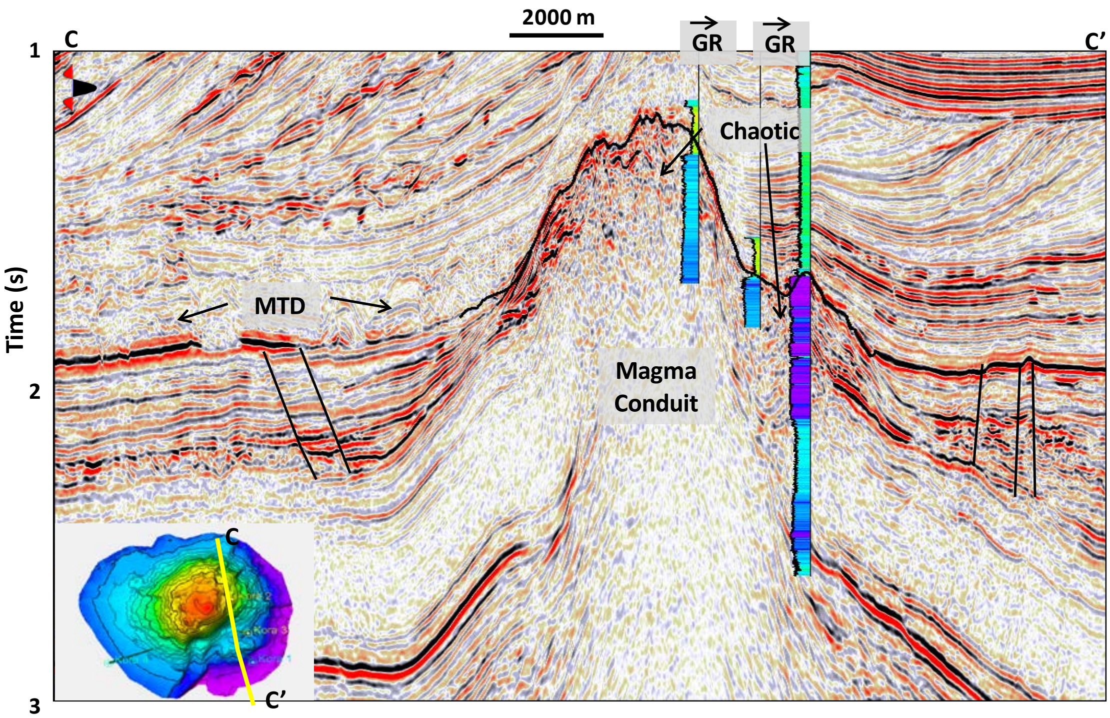

Figure 2.18. Magnified vertical slice CC′ through the seismic amplitude volume showing the chaotic moderate amplitude reflectors penetrated by wells Kora-1,2 and 3 and the strong continuous reflectors in the northwest flank. After Infante-Paez and Marfurt (2017). Seismic data courtesy of NZP&M.

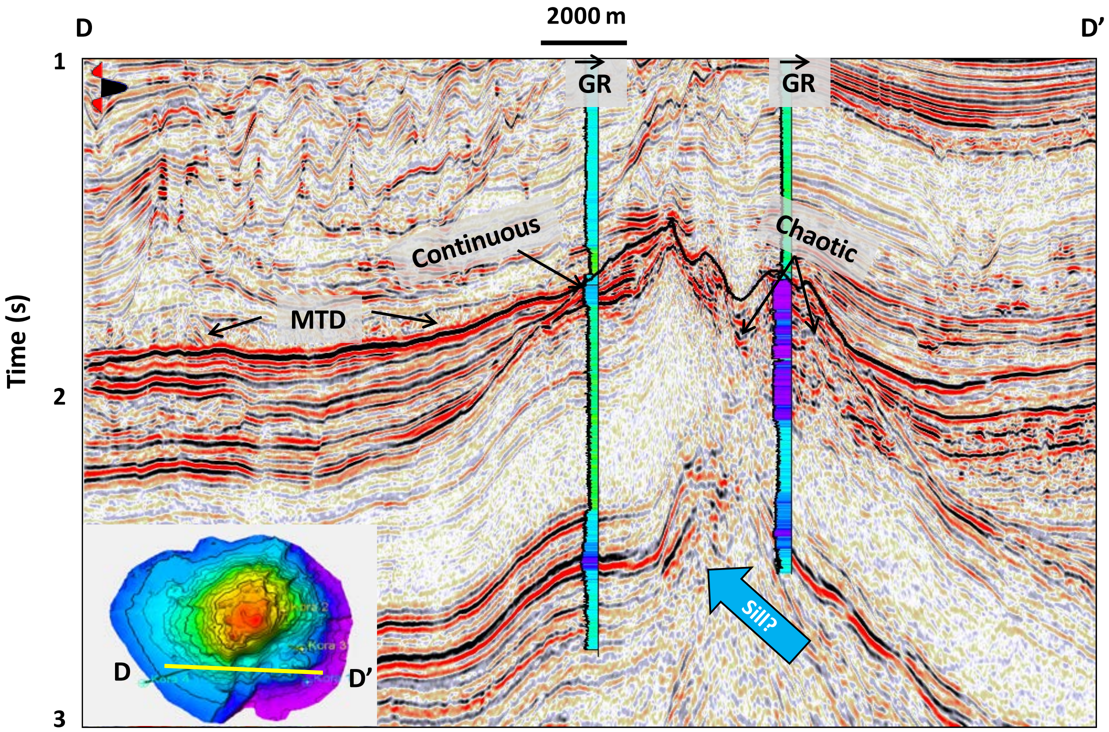

Figure 2.19. Magnified vertical slice DD′ through the seismic amplitude volume showing the chaotic moderate amplitude reflectors penetrated by the Kora-1 well, whereas the strong western continuous reflectors are penetrated only by the Kora-4 well. An MTD is observed on the western flank of the volcano. After Infante-Paez and Marfurt (2017). Seismic data courtesy of NZP&M.

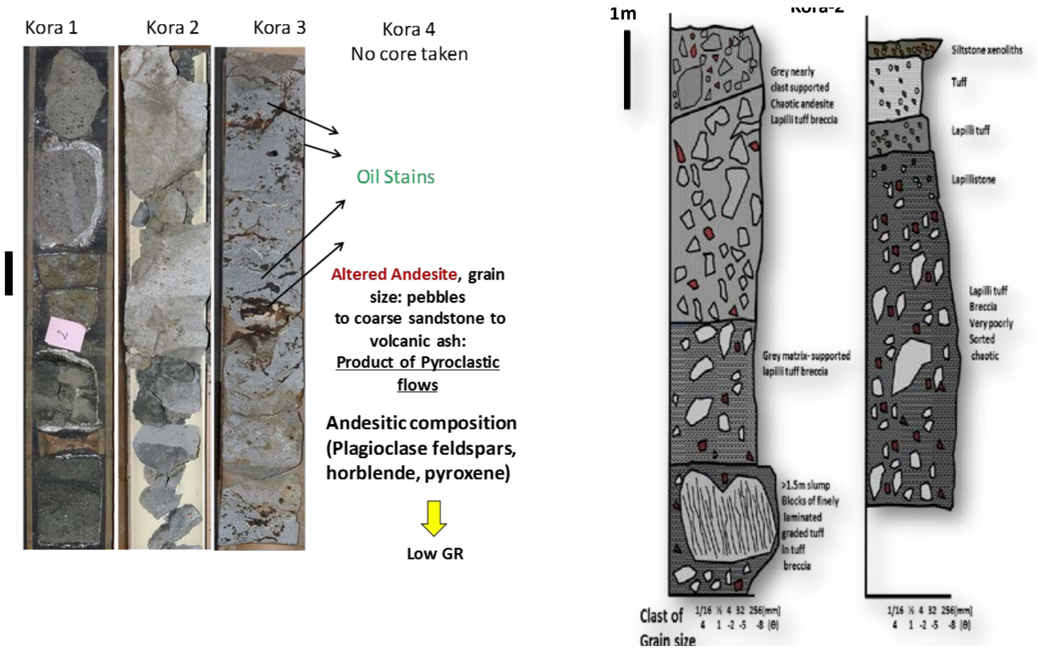

Figure 2.20. Core pictures for wells Kora 1,2 and 3 and a cartoon of the volcanic facies present in Kora-2. After Infante-Paez and Marfurt (2017).

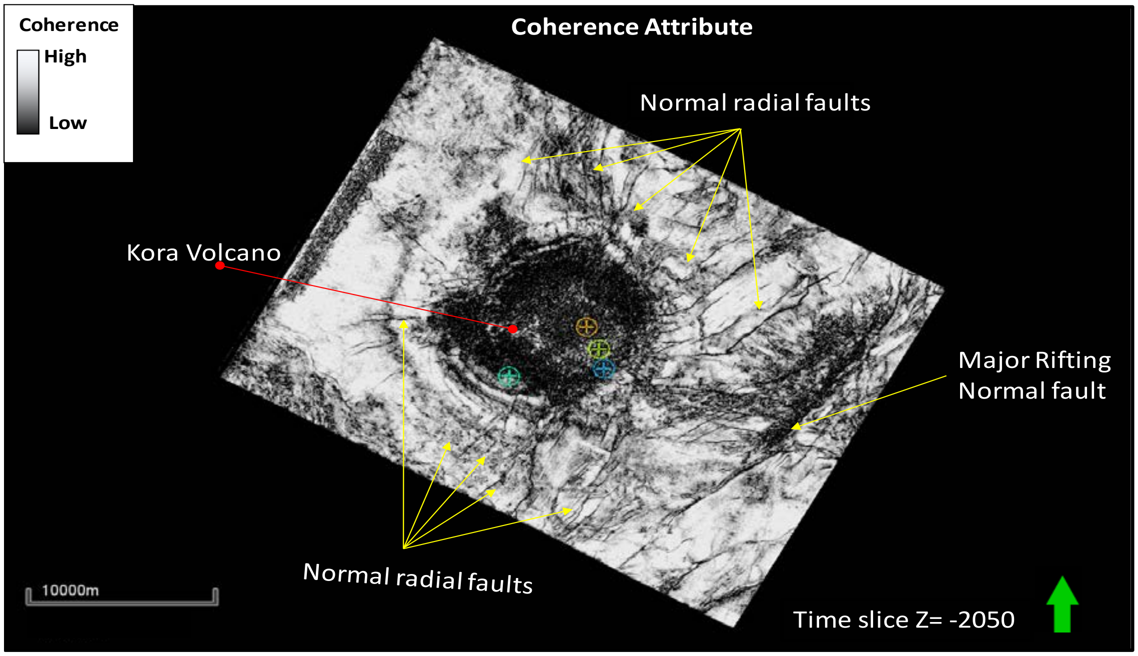

Figure 2.21. Time slice at t=2050 ms through the coherence attribute volume. The circular low-coherence feature (red arrow) delineates the extent of the volcano. Note the low-coherence radial fault pattern (yellow arrows). The four colored dots inside the volcano represent wells Kora-1–4. After Infante-Paez and Marfurt (2017). Seismic data courtesy of NZP&M.

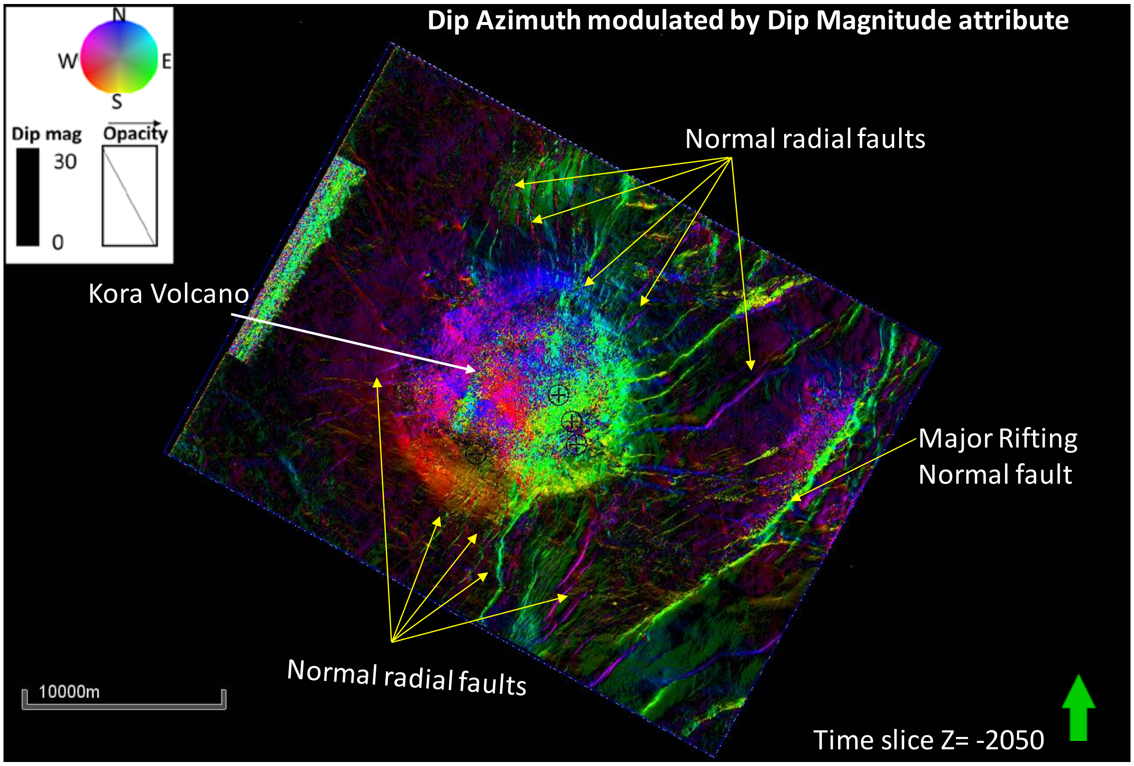

Figure 2.22. Time slice at t=2050 ms through the dip azimuth modulated by dip magnitude seismic volumes. Like the previous figure, this attribute illuminates the volcano and the radial faults, showing the direction in which both events are dipping. The different colors in the volcano indicate dips radiating from the peak of the volcano. The four black plus signs inside the volcano represent wells Kora-1–4. After Infante-Paez and Marfurt (2017). Seismic data courtesy of NZP&M.

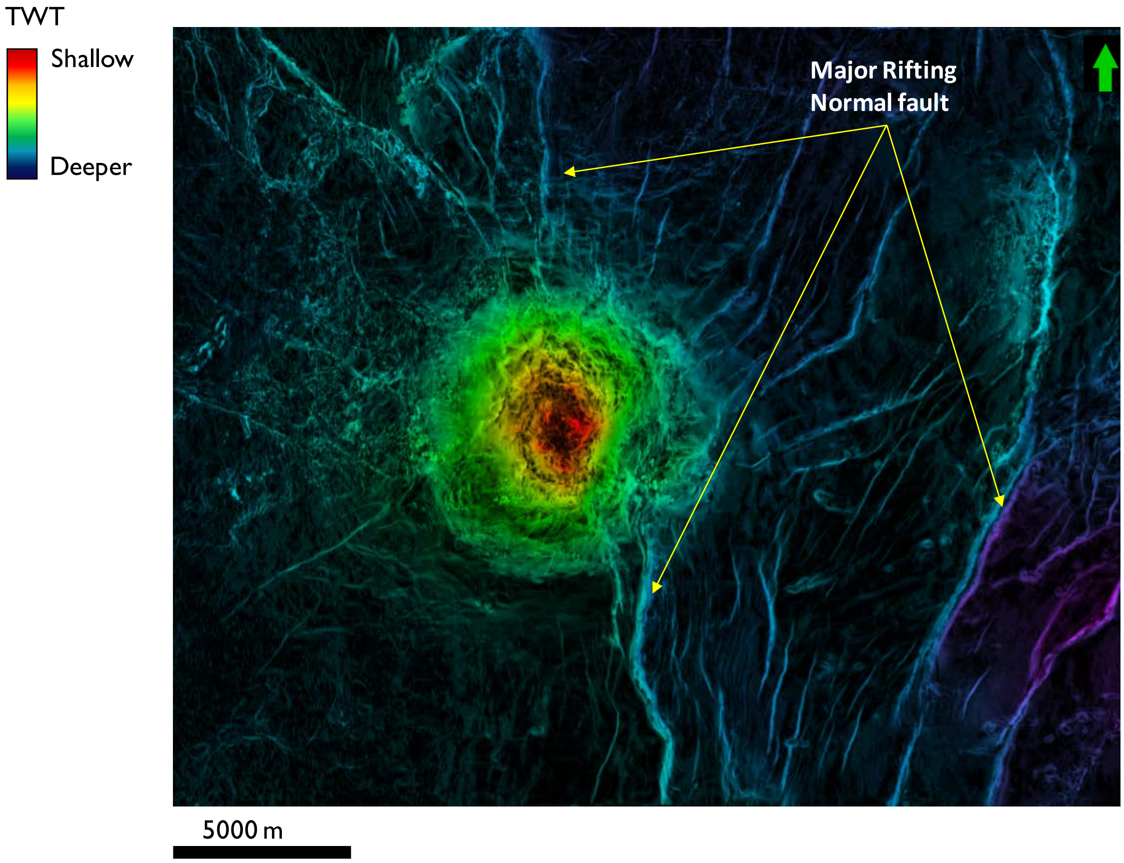

Figure 2.23. Time-structure map of the Kora volcano and top Ariki formation, showing radial fault pattern in the post-magmatic sequence. The N-S trending faults are associated with later rifting. Seismic data courtesy of NZP&M.

Figure 2.24. Dip magnitude (above) and dip magnitude modulated by dip azimuth (below) of the pre-magmatic sequence and the Miocene Volcanics, showing the evolution of the fault network. Notice the presence of the east- dipping faults (green) in the middle of the survey from the Paleocene through the Miocene. After Infante-Paez and Marfurt (2017

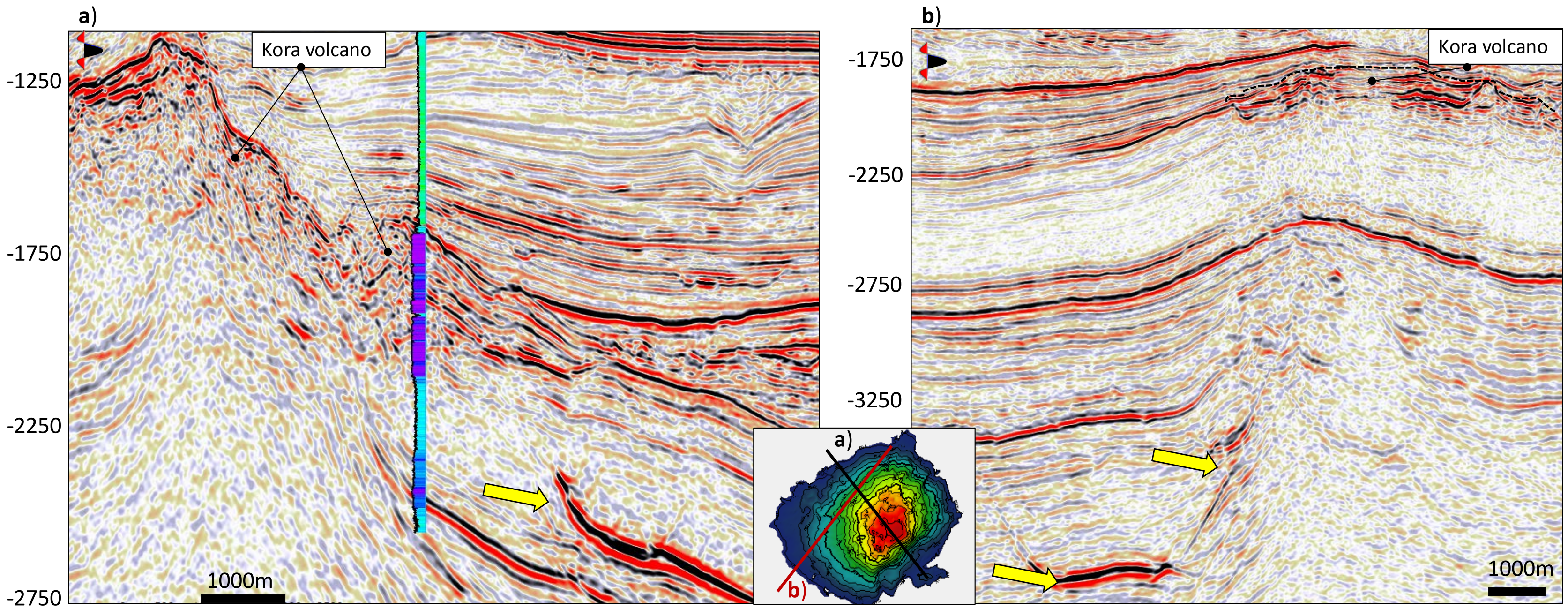

Figure 2.25. Vertical slices showing igneous sills around and below the Kora volcano.

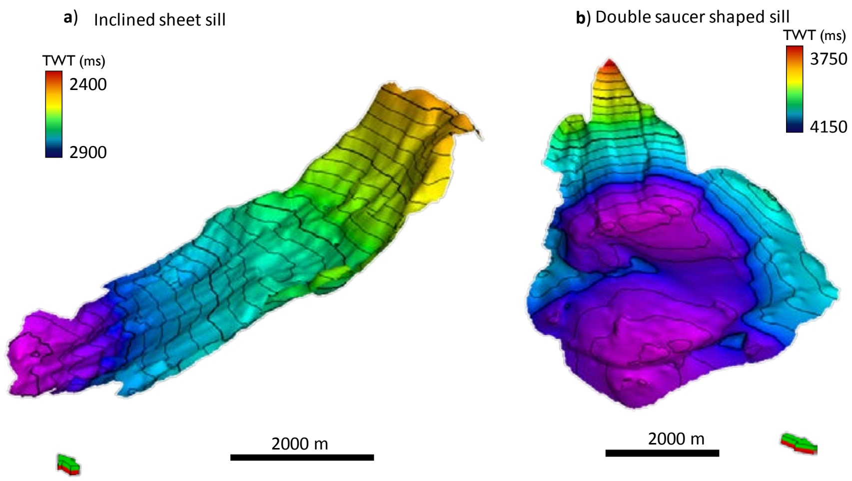

Figure 2.26. Three-dimensional view of igneous sills shown in Figure 2.25 displaying (a) an incline sheet and (b) a saucer shaped morphology.

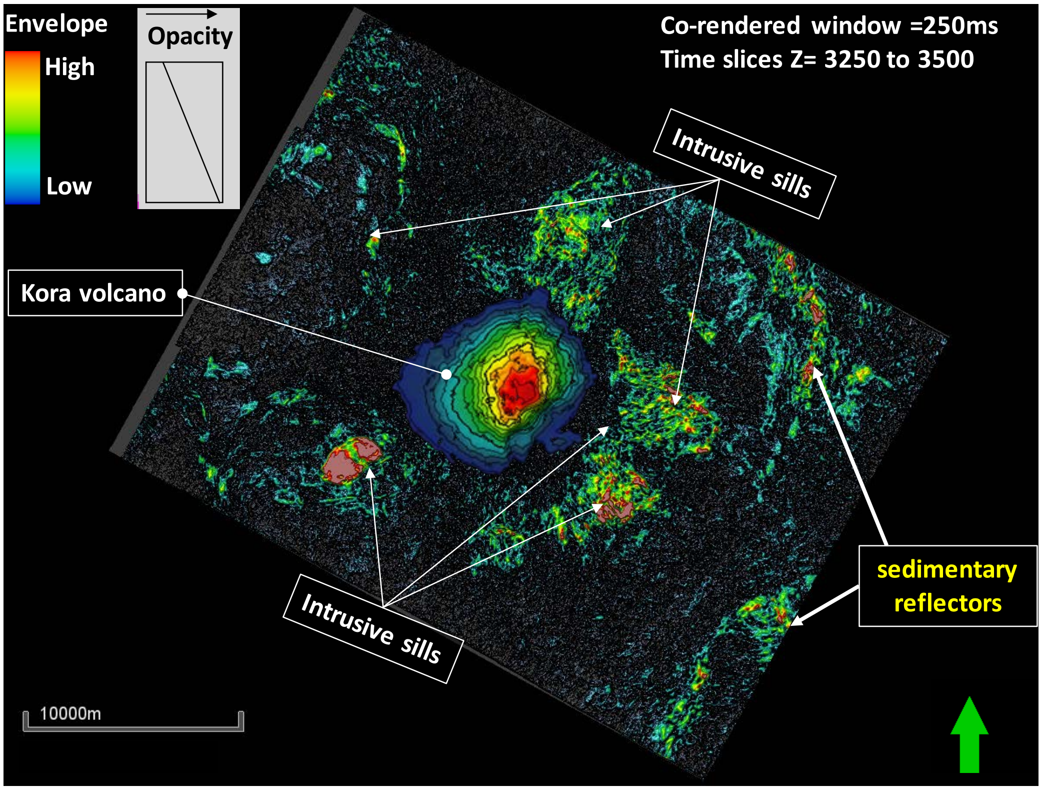

Figure 2.27. Map view of envelope attribute in a co-rendered window of 250 ms showing spatial distribution of Igneous sills around the Kora volcano. After Infante-Paez and Marfurt (2017). Seismic data courtesy of NZP&M.

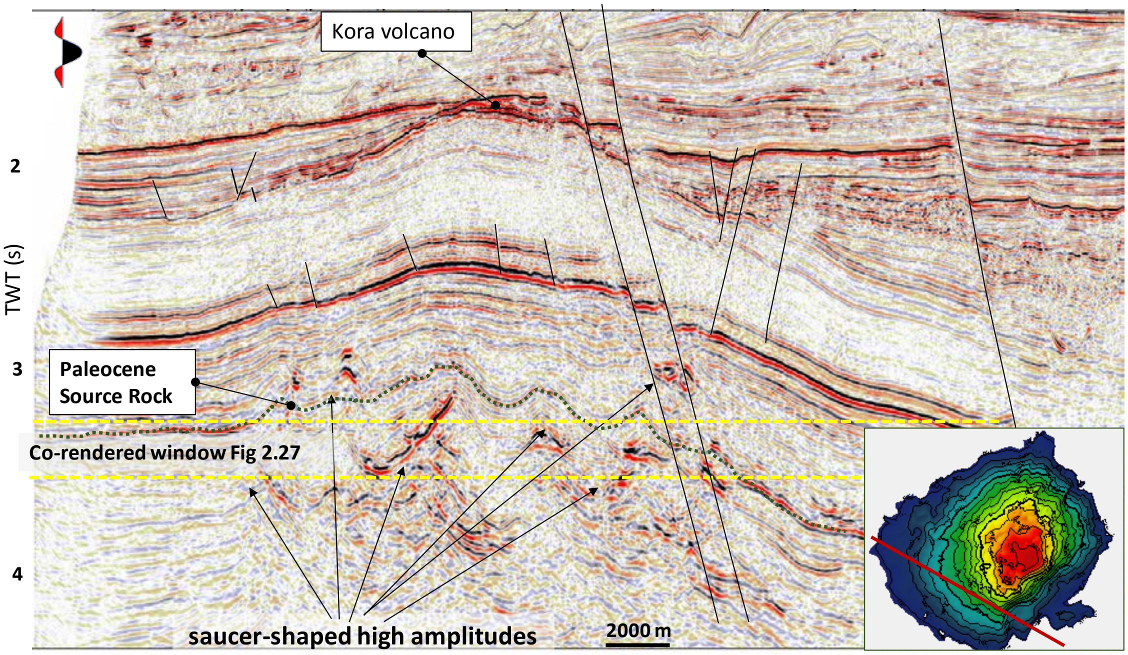

Figure 2.28. Vertical slice through the Kora 3D seismic survey showing saucer-shaped sills intruding into the Paleocene Waipawa marine source rock and possibly creating an atypical petroleum system like the one proposed by Del Pino and Bermudez (2009). After Infante-Paez and Marfurt (2017). Seismic data courtesy of NZP&M.

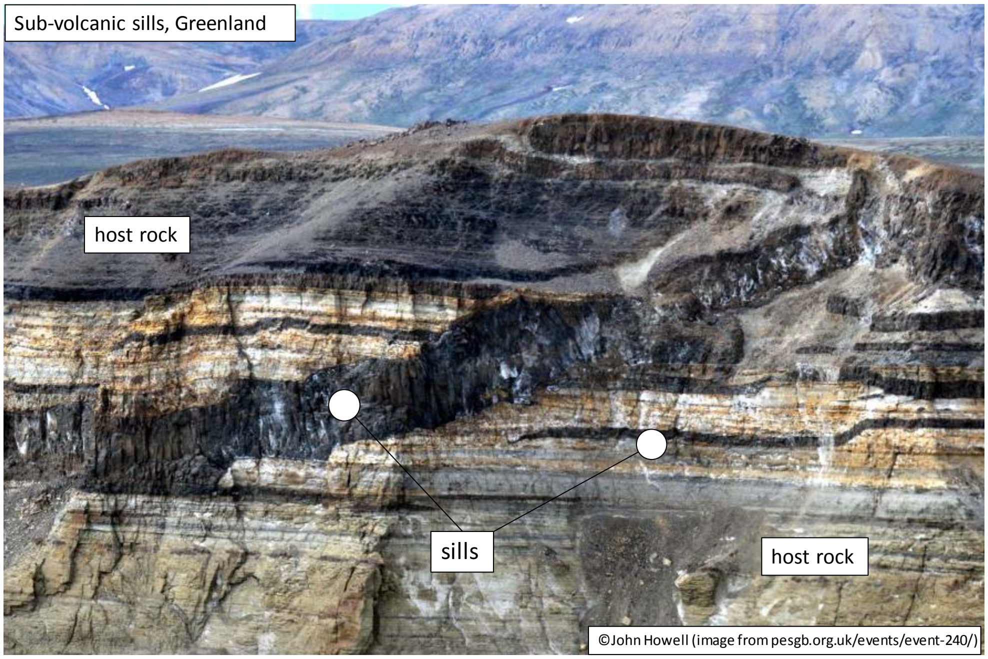

©John Howell (image from pesgb.org.uk/events/event-240/)

Figure 2.29. Igneous sills seen in outcrop in Greenland. Courtesy of John Howell. Note the sill cross cutting stratigraphy.

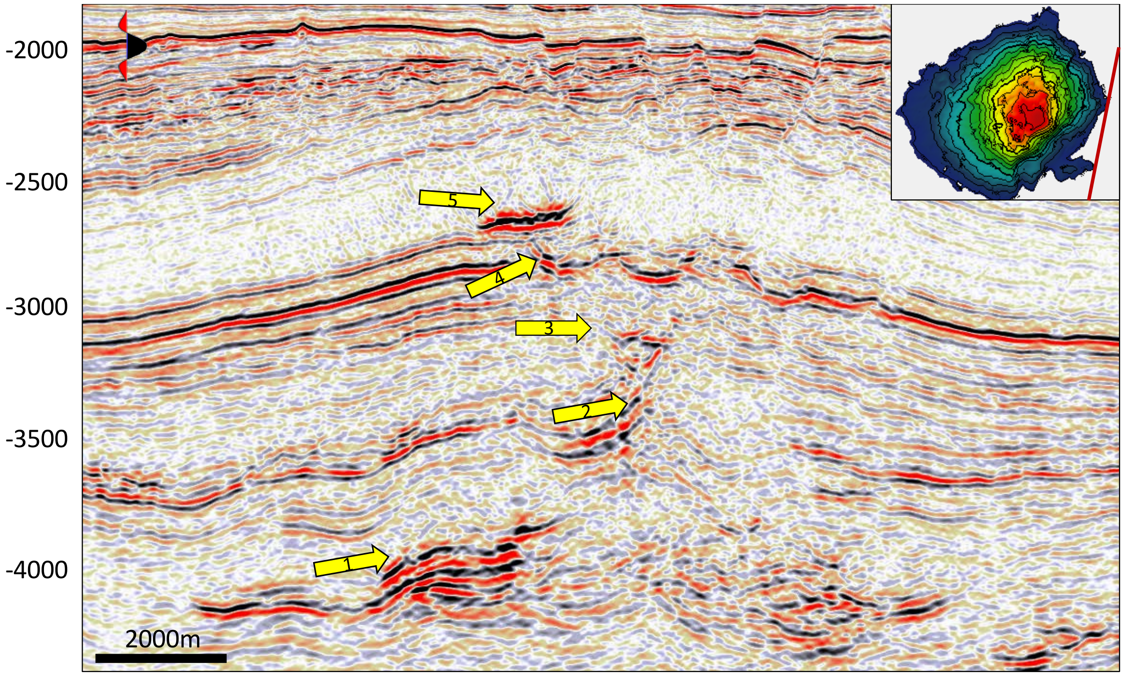

Figure 2.30. Vertical slice illustrating upward magma transport through sill junctions. Numbers in arrows indicate the stages of magma propagation through sill junctions.

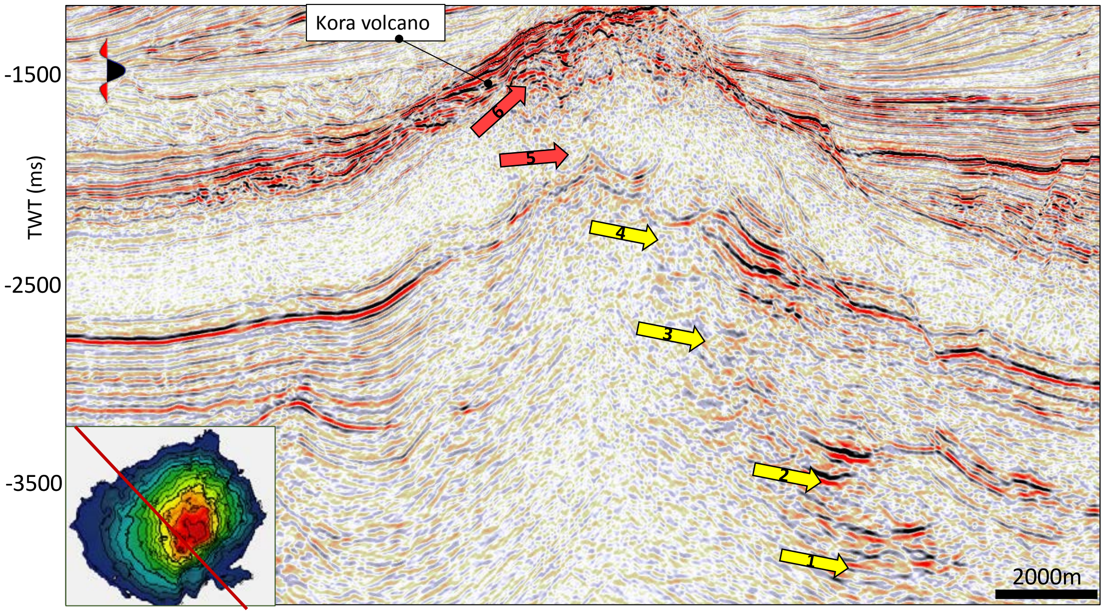

Figure 2.31. Vertical slice illustrating upwards magma transport through sill junctions. Numbers in arrows indicate the number of sill junctions. Yellow arrows indicate sills. Reddish arrows show sills reaching to the western flank of the Kora volcano.

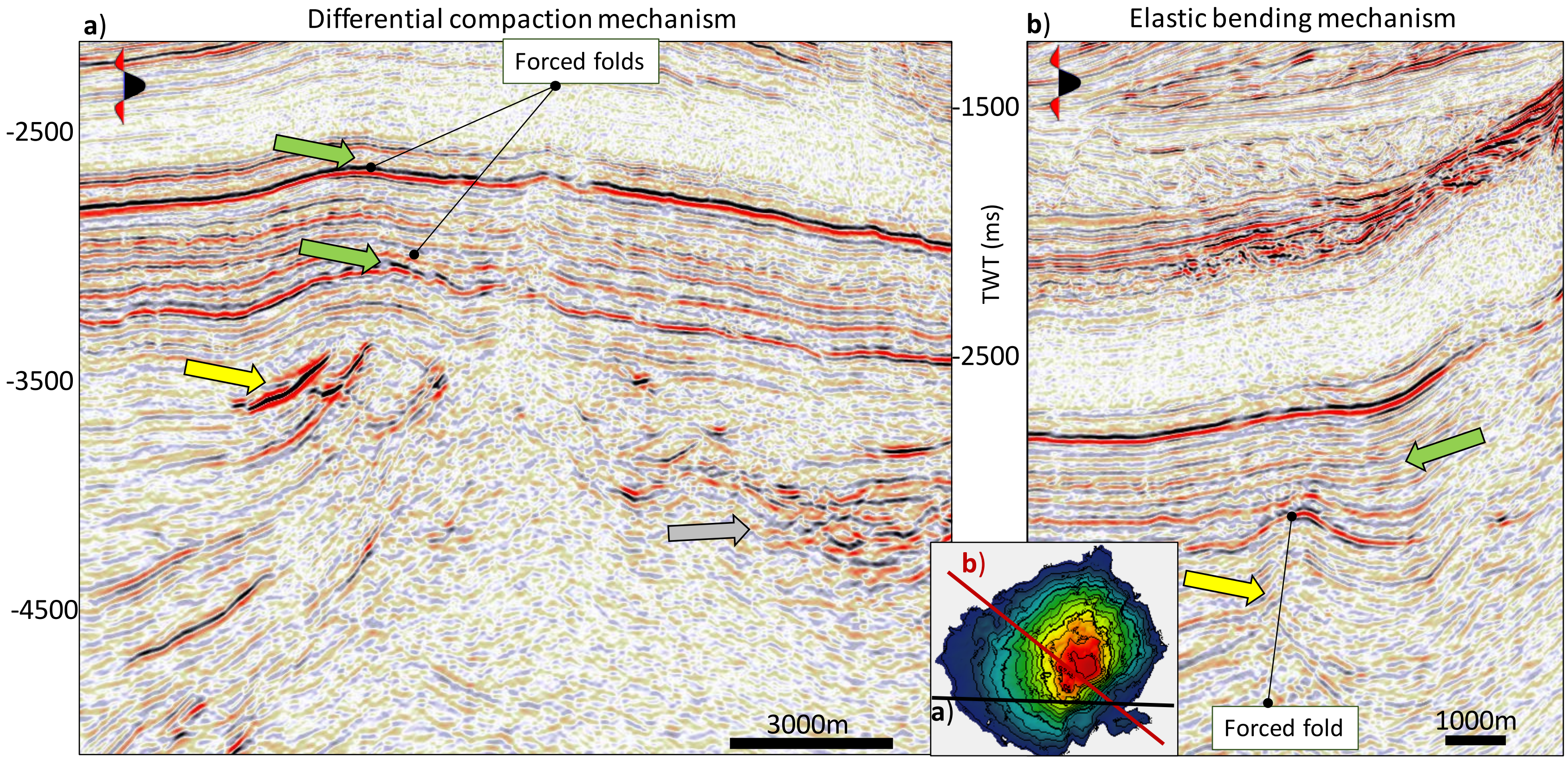

Figure 2.32. Seismic sections illustrating different mechanisms of forced folds: a) Post- emplacement b) syn-emplacement. Yellow arrows indicate sills, green arrows indicate forced folds and grey arrow points to a sill complex.

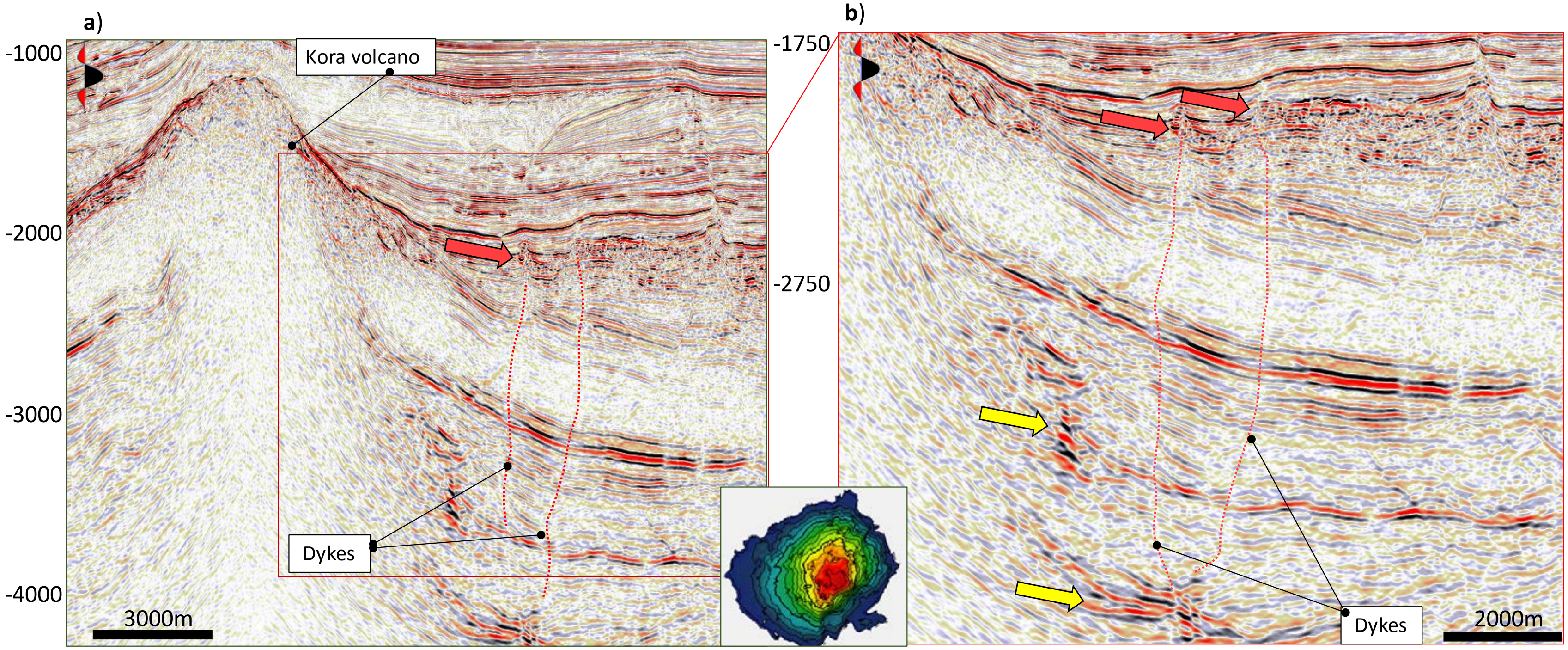

Figure 2.33. Seismic section showing (a) sub vertical low signal/noise reflections constrained to the red box zone. (b) expanded view of the area within the red box of (a). Yellow arrows indicate sills while red arrows a small volcanic mound fed by dykes (red dotted sub-vertical lines).

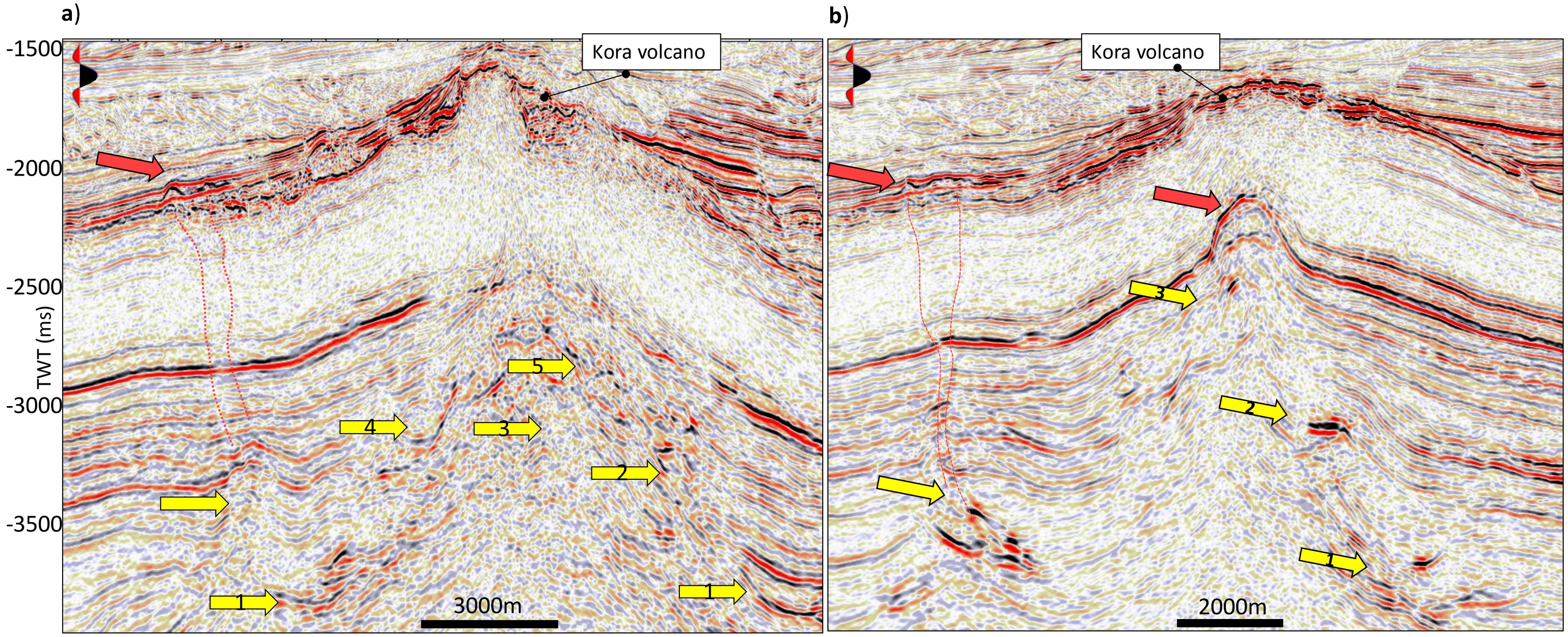

Figure 2.34. Seismic section with igneous sills below the Kora volcano and a sub vertical low signal/noise zone above the sills. Note the small-scale mound-cone structures on the flanks of Kora. (a and b) show different orientations. Yellow arrows point to the sills whereas reddish arrow point to the small cones. The Dotted reddish color represents the dykes and laccoliths. Kora 3D seismic survey courtesy of NZP&M.

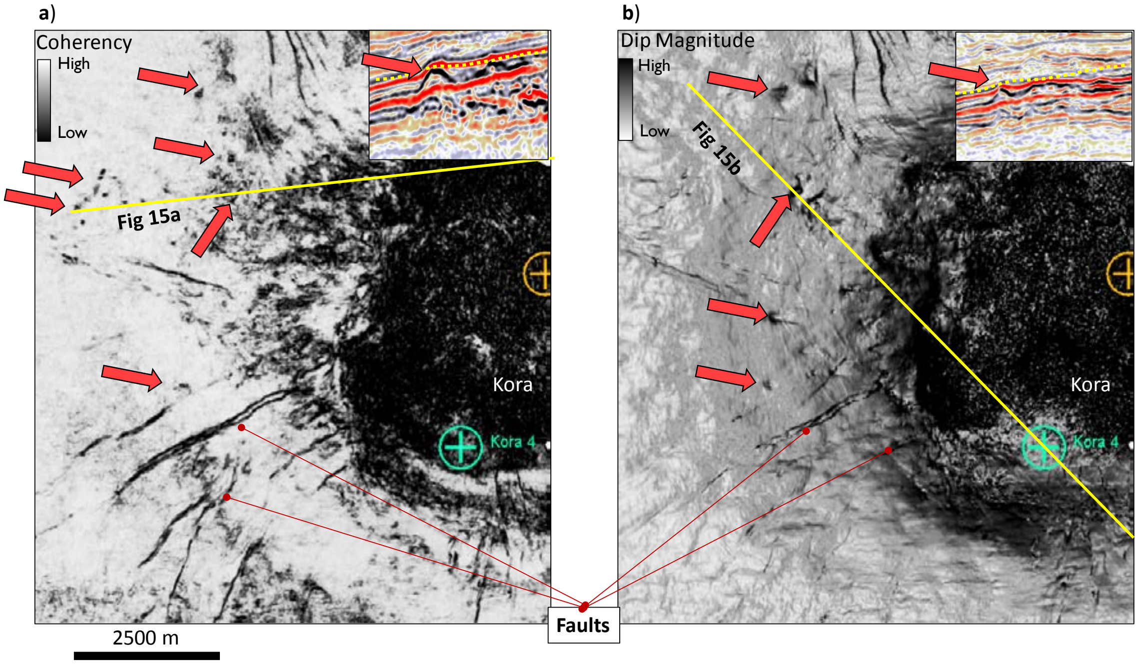

Figure 2.35. (a) Coherence and (b) Horizon slices thought dip magnitude attribute volumes close to the top of the Kora volcano. Reddish arrows point to small circular features in both attributes that represent the small cones. Yellow dotted line in the insert figure represents a reflector close to the base of Kora. Radial low coherence anomalies are normal faults. Kora 3D seismic survey courtesy of NZP&M.

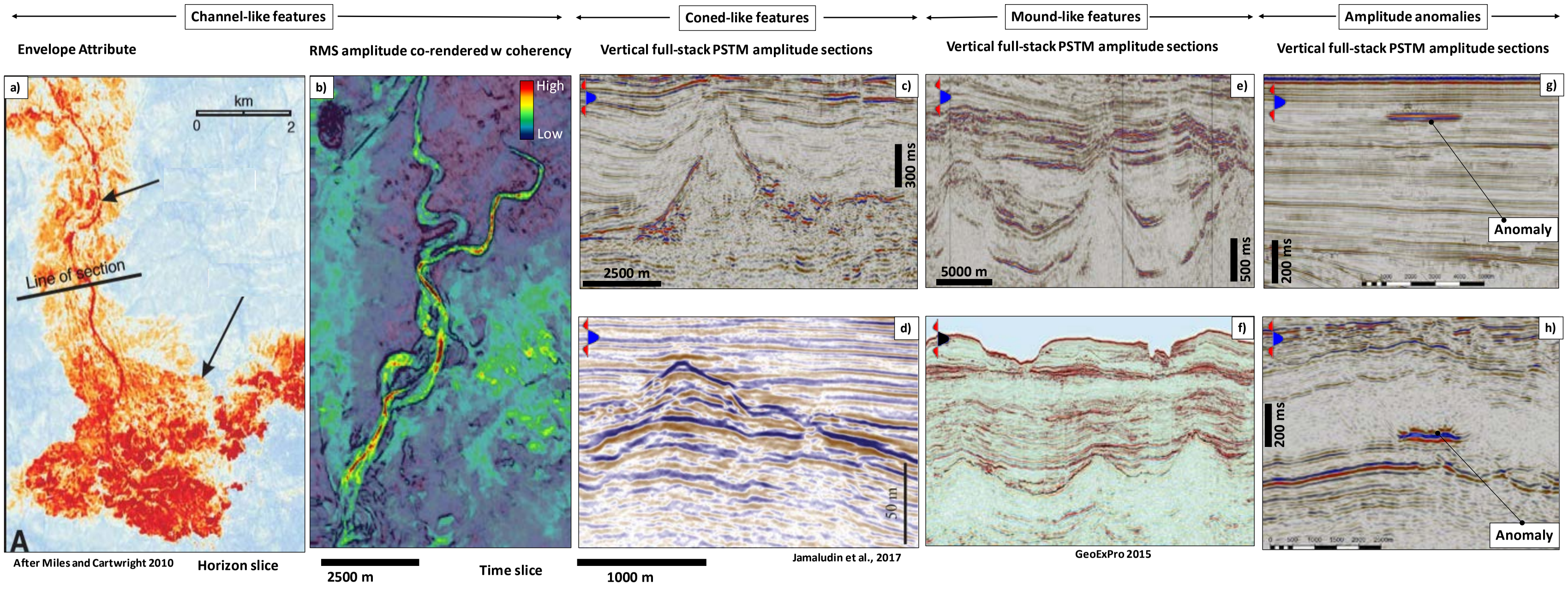

Figure 2.36. Geomorphology of igneous bodies. Vertical amplitude sections and horizon slices showing envelope attribute. In each of the four panels there are igneous bodies. Can you guess correctly which one they are? (a) Hybrid igneous flow. (b) clastic channelized turbidities from Parihaka 3D, seismic survey courtesy of NZP&M (c) Igneous volcano (andesitic? from Akira 2D, seismic survey courtesy of NZP&M (d) Carbonate build- up. (e) andesitic volcanoes from Parihaka 3D, seismic survey courtesy of NZP&M (f) Jurassic-Early Cretaceous carbonate platform, taken from https://www.geoexpro.com/articles/2015/07/offshoresenegal. (g) bright spot (gas sand?) from Parihaka 3D, seismic survey courtesy of NZP&M. h) igneous sill, from Kora 3D, seismic survey courtesy of NZP&M.

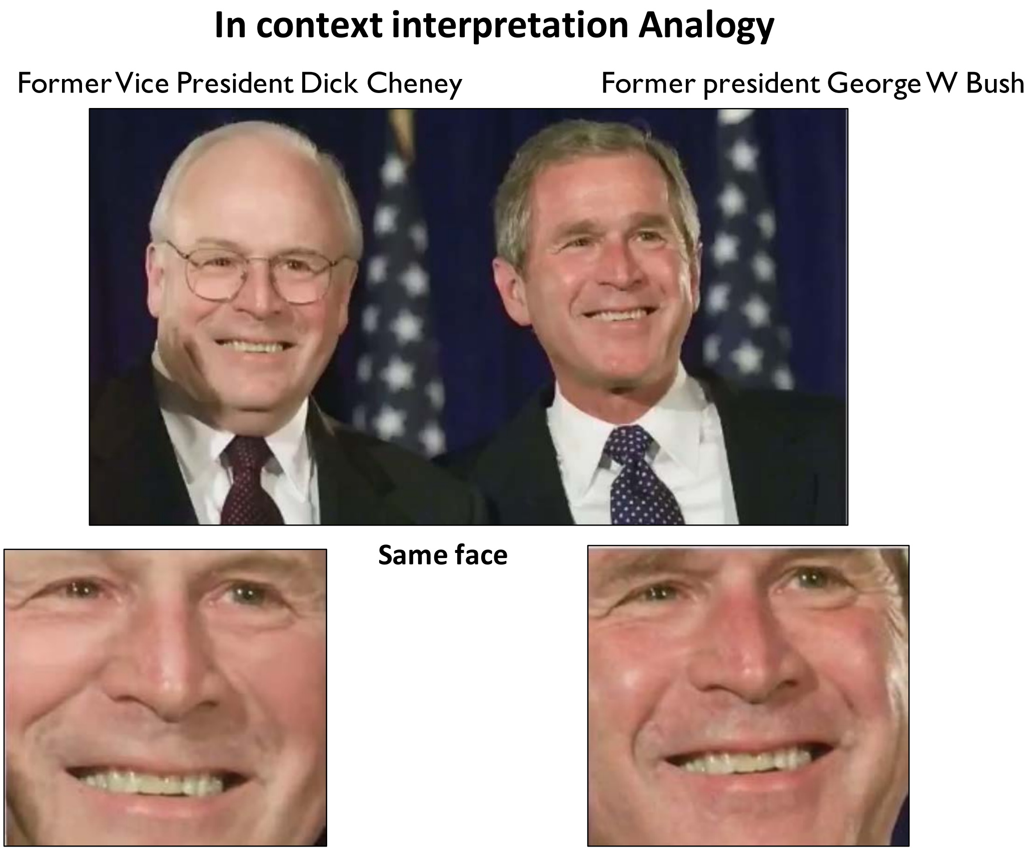

Figure 2.37. Former U.S.A leader headshot captured from Brain Games National Geographic TV show,

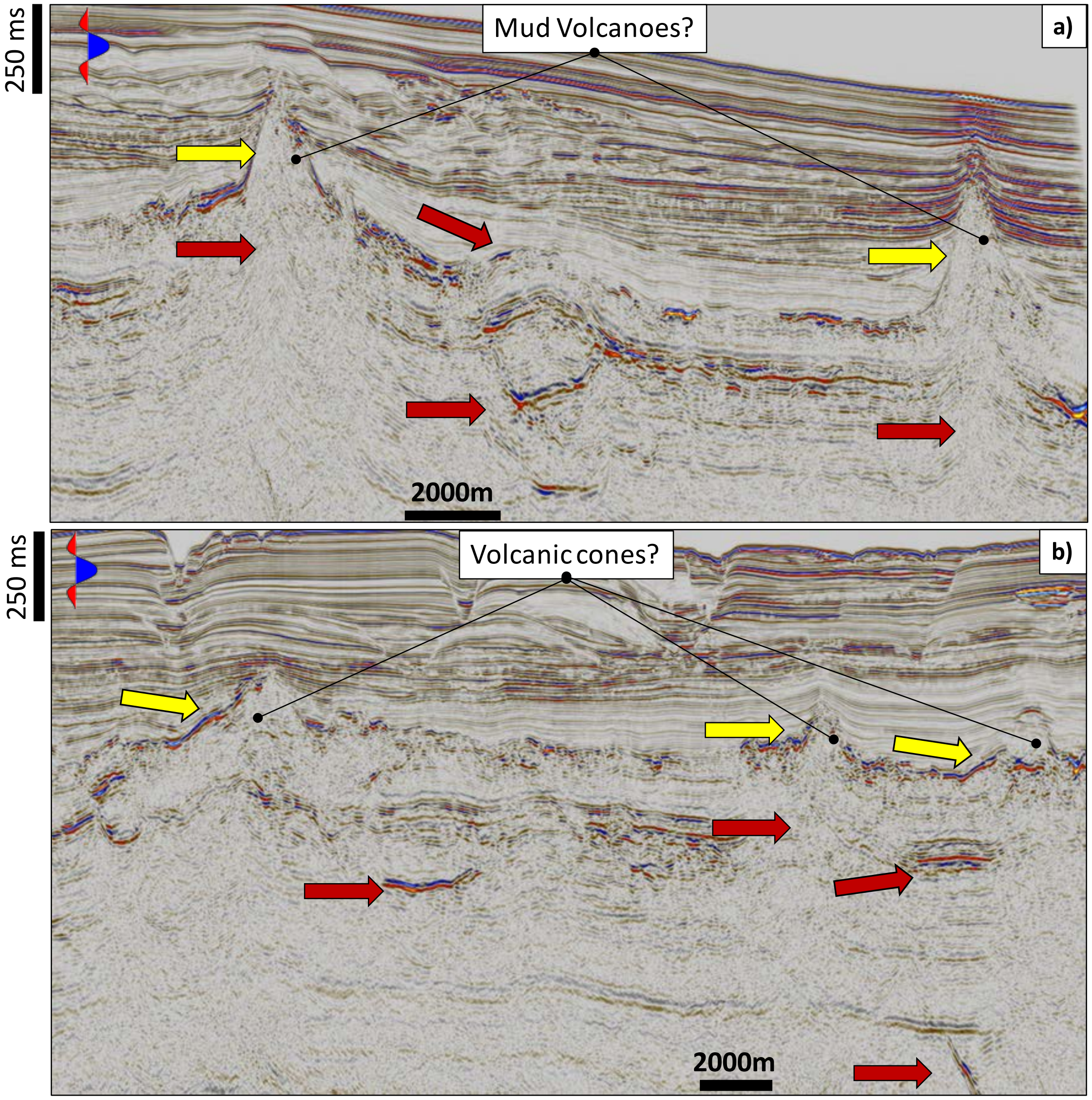

Figure 2.38. (a, and b) Seismic amplitude sections from the Akira 2D seismic survey showing mound-like structures (yellow arrows) with similar geometry to the ones in Bass, Basin Australia in Figure 24. Red arrows represent clues (sills, forced folds and dikes) for in-context interpretation. Seismic data courtesy of NZP&M.

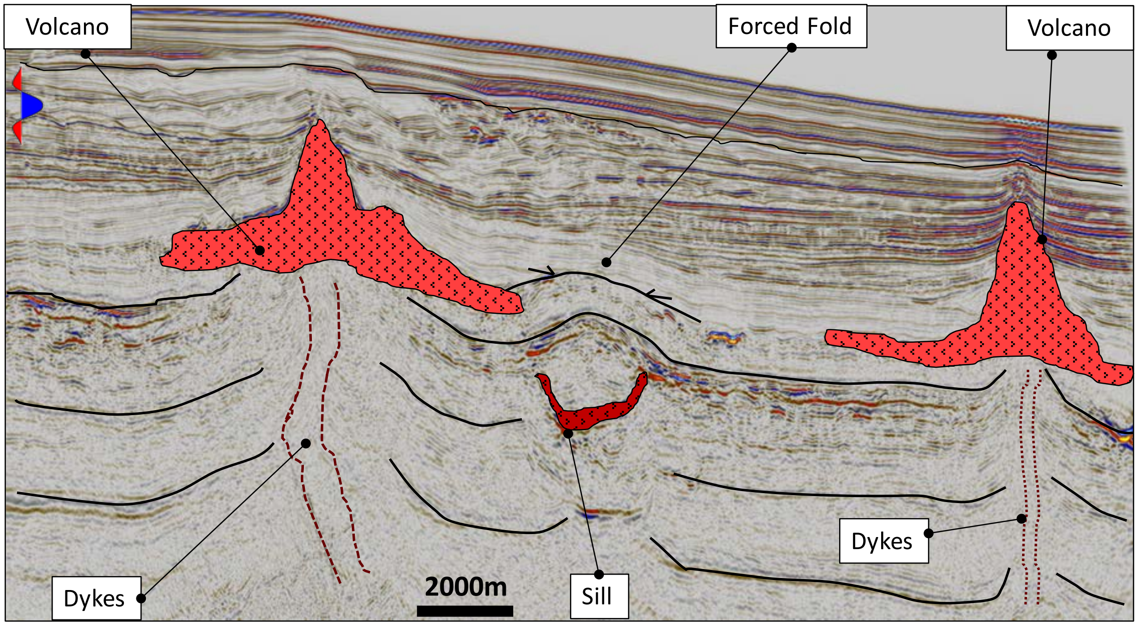

Figure 2.39. Vertical slice showing in-context interpretation suggest the mound-like features are Volcanoes. Seismic data courtesy of NZP&M.

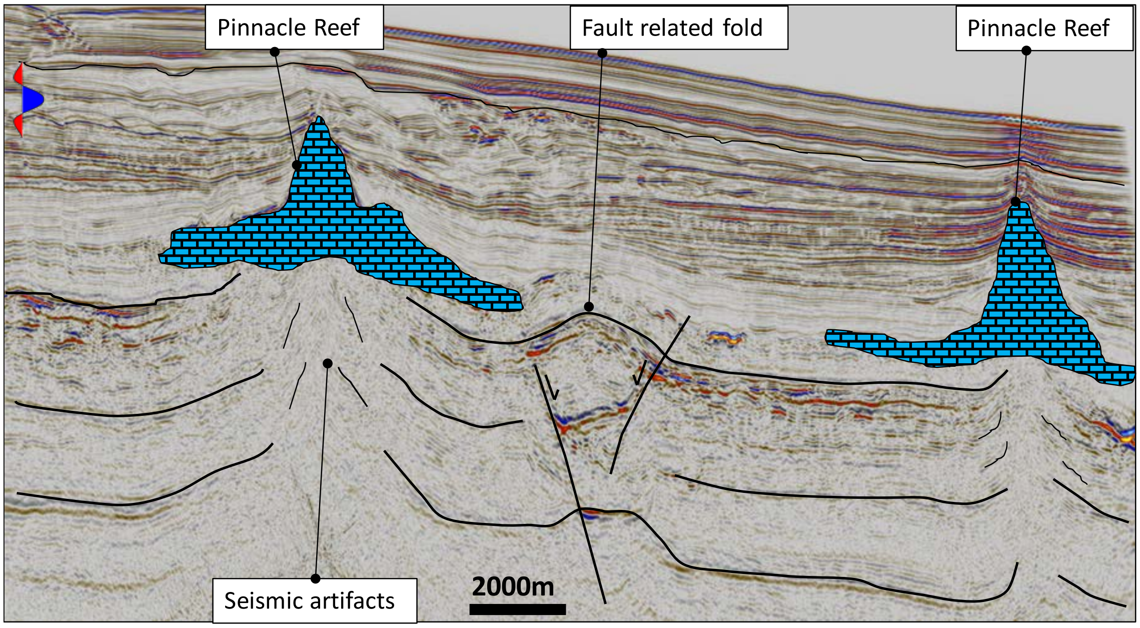

Figure 2.40. Vertical slice showing biased interpretation suggest the mound-like features are carbonate build-ups. Seismic data courtesy of NZP&M.

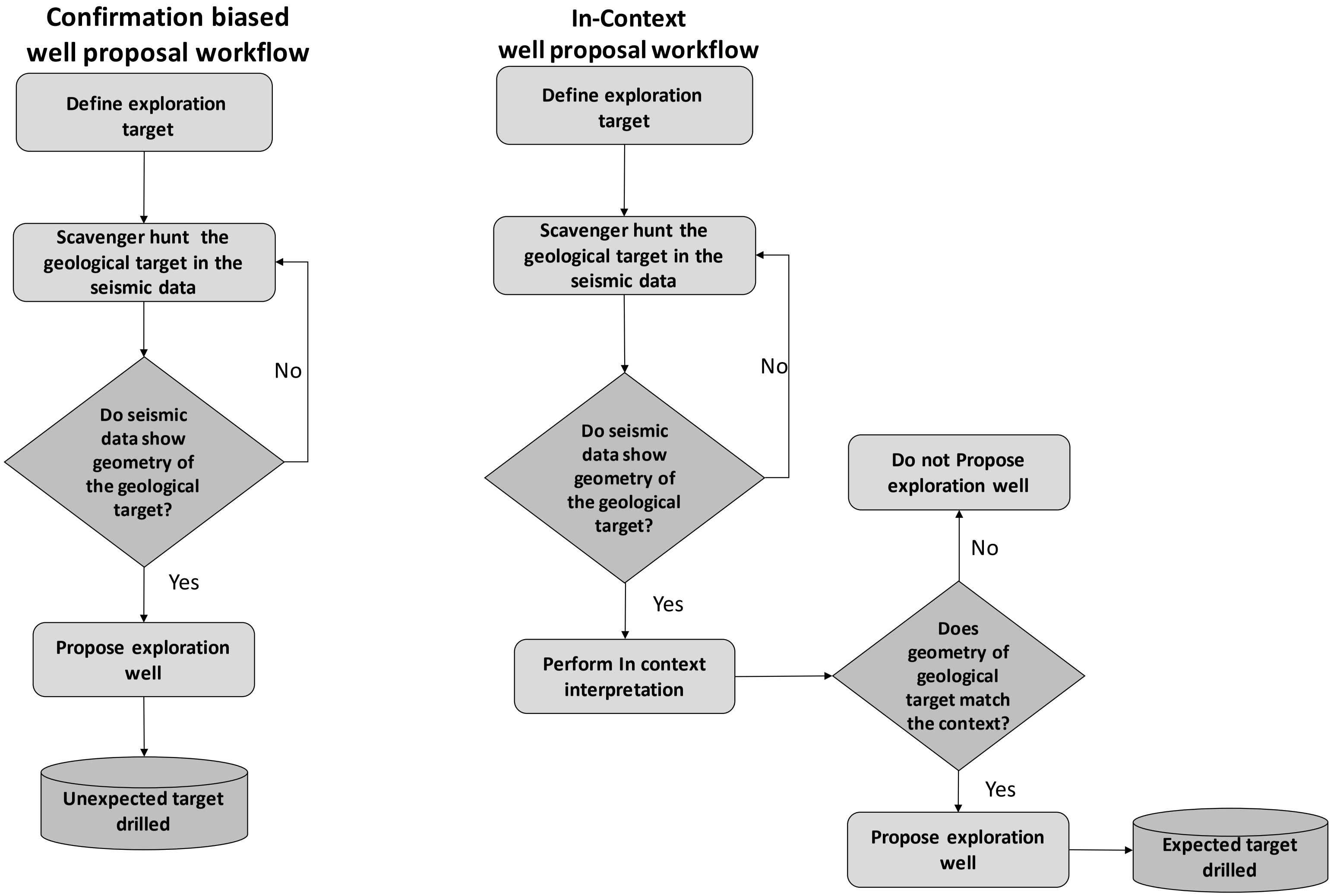

Figure 2.41. Proposed in-Context Interpretation Workflow.

REFERENCES

Alves, T., K. Omosanya, and P. Gowling, 2015, Volume rendering of enigmatic high-amplitude anomalies in southeast Brazil: A workflow to distinguish lithologic features from fluid accumulations: Interpretation, 3, A1-A14.

Bergman, S. C., J. P. Talbot, and P. R. Thompson, 1992, The Kora Miocene submarine andesite stratovolcano hydrocarbon reservoir, northern Taranaki Basin, New Zealand: 1991 New Zealand Oil Exploration Conference Proceedings: Wellington, Ministry of Commerce, p. 178–206.

Bond, C. E., A. D. Gibbs, Z. K. Shipton, and S. Jones, 2007, What do you think this is? “Conceptual uncertainty” In geoscience interpretation: GSA Today, v. 17, no. 11, p. 4–10, doi:10.1130/GSAT01711A.1.

Cortez, M. M. M., and M. A. C. Santos, 2016, Seismic interpretation, attribute analysis, and illumination study for targets below a volcanic-sedimentary succession, Santos Basin, offshore Brazil: Interpretation, v. 4, no. 1, p. 37–50, doi:10.1190/INT-2015-0097.1.

Dasgupta, R., 2013, Determination of the fractal dimension of a shore platform profile: Journal of the Geological Society of India, v. 81, no. 1, p. 122–128, doi:10.1007/s12594-013-0011-0.

Dimri, F. V. P., R. P. Srivastava, and N. Vedanti, 2011, Encyclopedia of Solid Earth Geophysics: no. 1, doi:10.1007/978-90-481-8702-7.

DuToit, A.I., 1920, The Karoo dolerites: Transactions Geological Society of South Africa 33, 1-42.

Gao, Z., W. Tian, L. Wang, Y. Shi, and M. Pan, 2017, Emplacement of intrusions of the Tarim Flood Basalt Province and their impacts on oil and gas reservoirs: A 3D seismic reflection study in Yingmaili fields, Tarim Basin, northwest China: Interpretation, v. 5, no. 3, p. SK51-SK63, doi:10.1190/INT-2016-0165.1.

Gao, Z., W. Tian, L. Wang, Y. Shi, and M. Pan, 2017, Emplacement of intrusions of the Tarim Flood Basalt Province and their impacts on oil and gas reservoirs: A 3D seismic reflection study in Yingmaili fields, Tarim Basin, northwest China: Interpretation, 5, no. 3, SK51-SK63, doi:10.1190/INT-2016-0165.1.

Giba, M., J. J. Walsh, A. Nicol, V. Mouslopoulou, and H. Seebeck, 2013, Investigation of the spatio-temporal relationship between normal faulting and arc volcanism on million-year time scales: Journal of the Geological Society, v. 170, no. 6, p. 951–962, doi:10.1144/jgs2012-121.

Hafeez, A., S. Planke, D. A. Jerram, J. M. Millett, D. Maharjan, and T. Prestvik, 2017, Upper paleocene ultramafic igneous rocks offshore mid-Norway: Re-interpretation of the vestbrona formation as a sill complex: Interpretation, v. 5, no. 3, doi:10.1190/int-2016-0143.1.

Hafeez, A., S. Planke, D. A. Jerram, J. M. Millett, D. Maharjan, and T. Prestvik, 2017, Upper paleocene ultramafic igneous rocks offshore mid-Norway: Re-interpretation of the vestbrona formation as a sill complex: Interpretation, 5, no. 3, SK103-SK120, doi:10.1190/int-2016-0143.1.

Hansen, D. M., and J. Cartwright, 2006, Saucer-shaped sill with lobate morphology revealed by 3D seismic data: implications for resolving a shallow-level sill emplacement mechanism: Journal of the Geological Society, 163, no. 3, 509–523, doi:10.1144/0016-764905-073.

Hansen, D. M., and J. Cartwright, 2006, Saucer-shaped sill with lobate morphology revealed by 3D seismic data: implications for resolving a shallow-level sill emplacement mechanism: Journal of the Geological Society, 163, no. 3, 509–523, doi:10.1144/0016-764905-073.

Hansen, D. Mø., J. A. Cartwright, and D. Thomas, 2004, 3D Seismic Analysis of the Geometry of Igneous Sills and Sill Junction Relationships: Geological Society, London, Memoirs, v. 29, no. 1, p. 199–208, doi:10.1144/GSL.MEM.2004.029.01.19.

Hansen, R. J., and P. J. J. Kamp, 2004, Late miocene to early pliocene stratigraphic record in northern taranaki basin: Condensed sedimentation ahead of northern graben extension and progradation of the modern continental margin: New Zealand Journal of Geology and Geophysics, v. 47, no. 4, p. 645–662, doi:10.1080/00288306.2004.9515081.

Herrera, C., M. Aldana, E. Science, and S. Bolívar, 2017, Depth to sources and Bouguer density determination of the Merida Andes , Venezuela , by means of a fractal analysis of gravity data: SEG expanded Abstracts, 2017, p. 1786–1792.

Holford, S. P., N. Schofield, and P. Reynolds, 2017, Subsurface fluid flow focused by buried volcanoes in sedimentary basins: Evidence from 3D seismic data, Bass Basin, offshore southeastern Australia: Interpretation, v. 5, no. 3, p. SK39-SK50, doi:10.1190/INT-2016-0205.1.

Holford, S. P., N. Schofield, C. A. L. Jackson, C. Magee, P. F. Green, and I. R. Duddy, 2013, Impacts of igneous in- trusions on source and reservoir potential in prospective sedimentary basins along the Western Australian continental margin: West Australian Basins Symposium, Proceedings of the Petroleum Exploration Society of Australia Symposium, 1–12.

Infante-Paez, L., and K. J. Marfurt, 2017, Seismic expression and geomorphology of igneous bodies: A Taranaki Basin, New Zealand, case study: Interpretation, v. 5, no. 3, p. SK121-SK140, doi:10.1190/INT-2016-0244.1.

Jackson, C. A. L., N. Schofield, and B. Golenkov, 2013, Geometry and controls on the development of igneous sill-related forced folds: A 2-D seismic reflection case study from offshore southern Australia: Bulletin of the Geological Society of America, v. 125, no. 11–12, p. 1874–1890, doi:10.1130/B30833.1.

Jackson, C. A. L., N. Schofield, and B. Golenkov, 2013, Geometry and controls on the development of igneous sill-related forced folds: A 2-D seismic reflection case study from offshore southern Australia: Bulletin of the Geological Society of America, 125, no. 11–12, 1874–1890, doi:10.1130/B30833.1.

Jackson, C. A.-L., 2012, Seismic reflection imaging and controls on the preservation of ancient sill-fed magmatic vents: Journal of the Geological Society, v. 169, no. 5, p. 503–506, doi:10.1144/0016-76492011-147.

Klarner S., O. Klarner, 2012, Identification of Paleo-Volcanic Rocks on Seismic Data: Updates in Volcanology – A Comprehensive Approach to Volcanological Problems, InTech.

Krueger, D. J., Funder, 2004, Towards a Balanced Social Psychology:Causes, Consequences and Cures for the Problem-seeking\rApproach to Social Behavior and Cognition: Behavioral and Brain Sciences, p. 313–376.

Kumar, P. C., and A. Mandal, 2017, Enhancement of fault interpretation using multi-attribute analysis and artificial neural network (ANN) approach: a case study from Taranaki Basin, New Zealand: Exploration Geophysics, no. November, doi:10.1071/EG16072.

Lam, N. S. N., and D. Quattrochi, 1992, On the issues of scale, resolution, and fractal analysis in the mapping sciences: Professional Geographer, v. 44, no. 1, p. 88–98, doi:10.1111/j.0033-0124.1992.00088.x.

Liborius-Parada, A., and D. Tazzo, 2012, Petrografía de la aureola de contacto de la granodiorita de El Carmen en las adyacencias del pico El Águila-vía Piñango, edo. Mérida, Venezuela: GEOS Venezuelan Journal of Earth Sciences, 42, 72–76.

Magee, C. et al., 2016, Lateral magma flow in mafic sill complexes: Geosphere, v. 12, no. 3, p. 809–841, doi:10.1130/GES01256.1.

Magee, C., C. A. L. Jackson, and N. Schofield, 2014, Diachronous sub-volcanic intrusion along deep-water margins: Insights from the Irish Rockall Basin: Basin Research, v. 26, no. 1, p. 85–105, doi:10.1111/bre.12044.

Magee, C., C. A.-L. Jackson, J. P. Hardman, and M. T. Reeve, 2017, Decoding sill emplacement and forced fold growth in the Exmouth Sub-basin, offshore northwest Australia: Implications for hydrocarbon exploration: Interpretation, v. 5, no. 3, p. SK11-SK22, doi:10.1190/INT-2016-0133.1.

Magee, C., E. Hunt-Stewart, and C. A. L. Jackson, 2013, Volcano growth mechanisms and the role of sub-volcanic intrusions: Insights from 2D seismic reflection data: Earth and Planetary Science Letters, v. 373, p. 41–53, doi:10.1016/j.epsl.2013.04.041.

Magee, C., J. D. Muirhead, A. Karvelas, S. P. Holford, C. AL. Jackson, I.D. Bastow, N. Schofield, C.T. Stevenson, C. McLean, W. McCarthy, and O. Shtukert., 2016, Lateral magma flow in mafic sill complexes: Geosphere, 12, no. 3, 809–841, doi:10.1130/GES01256.1.

Mark, N. J., N. Schofield, S. Pugliese, D. Watson, S. Holford, D. Muirhead, R. Brown, and D. Healy, 2017, Igneous intrusions in the Faroe Shetland basin and their implications for hydrocarbon exploration; new insights from well and seismic data: Marine and Petroleum Geology, no. November doi:10.1016/j.marpetgeo.2017.12.005.,

McLean, C. E., N. Schofield, D. J. Brown, D. W. Jolley, and A. Reid, 2017, 3D seismic imaging of the shallow plumbing system beneath the Ben Nevis Monogenetic Volcanic Field: Faroe–Shetland Basin: Journal of the Geological Society, v. 174, no. 3, p. 468–485, doi:10.1144/jgs2016-118.

Miles, A., and J. Cartwright, 2010, Hybrid flow sills: A new mode of igneous sheet intrusion: Geology, v. 38, no. 4, p. 343–346, doi:10.1130/G30414.1.

Morley, C., 2018, 3D seismic imaging of the plumbing system of the Kora volcano, Taranaki Basin, New Zealand: The influences of syn-rift structure on shallow igneous intrusion architecture: Geosphere, in press.

Naviset, S., C. K. Morley, D. H. Naghadeh, and J. Ghosh, 2017, Sill emplacement during rifting and inversion from threedimensional seismic and well data, Phitsanulok Basin, Thailand: Geosphere, v. 13, no. 6, p. 2017–2040, doi:10.1130/GES01466.1.

Olorunsola, O., J. Qi, L. Infante, B. Hutchinson, and K. Marfurt, 2016, Multiattribute seismic-facies expressions of a complex granite wash formation: A Buffalo Wallow field illustration: SEG Technical Program Expanded Abstracts 2016, p. 1884–1888, doi:10.1190/segam2016-13946878.1.

Planke, S., E. Alvestad, and O. Eldholm, 1999, Seismic characteristics of basaltic extrusive and intrusive rocks. The Leading Edge, 18, no. 3, 342-348. https://doi.org/10.1190/1.1438289

Planke, S., P. A. Symonds, E. Alvestad, and J. Skogseid, 2000, Seismic volcanostratigraphy of large-volume basaltic extrusive complexes on rifted margins: Journal of Geophysical Research: Solid Earth, v. 105, no. B8, p. 19335–19351, doi:10.1029/1999JB900005.

Qi, J., T. Lin, T. Zhao, F. Li, and K. Marfurt, 2016, Semisupervised multiattribute seismic facies analysis: Interpretation, v. 4, no. 1, p. SB91-SB106, doi:10.1190/INT-2015-0098.1.

Rabbel, O., O. Galland, K. Mair, I. Lecomte, K. Senger, J. B. Spacapan, and R. Manceda, 2018, From field analogues to realistic seismic modelling : a case study of an oil-producing andesitic sill complex in the Neuquén Basin , Argentina: Journal of the Geological Society, pp.jgs2017-116.

Reynolds, P., N. Schofield, R. J. Brown, and S. P. Holford, 2018, The architecture of submarine monogenetic volcanoes – insights from 3D seismic data: Basin Research, v. 30, p. 437–451, doi:10.1111/bre.12230.

Rojo, L., A. Escalona, and L. Schulte, 2016, The use of seismic attributes to enhance imaging of salt structures in the Barent Sea: First Break, 34, 49–57.

Sarkar, S., and K. J. Marfurt, 2017, Effect of volcanic bodies on hydrocarbon reservoirs in the northeastern part of the Chicontepec Foredeep, Mexico: Interpretation, v. 5, no. 3, p. SK1-SK10, doi:10.1190/INT-2016-0110.1.

Sarkar, S., S. Verma, and K. J. Marfurt, 2016, Seismic-petrophysical reservoir characterization in the northern part of the Chicontepec Basin, Mexico: Interpretation, 4, no. 3, T403–T417, doi: 10.1190/INT-2015-0168.1.

Schmiedel, T., S. Kjoberg, S. Planke, C. Magee, O. Galland, N. Schofield, C. A.-L. Jackson, and D. A. Jerram, 2017, Mechanisms of overburden deformation associated with the emplacement of the Tulipan sill, mid-Norwegian margin: Interpretation, 5, no. 3, SK23-SK38, doi:10.1190/INT-2016-0155.1.

Schofield, N., S. Holford, J. Millet, D. Brown, D. Jolly, S.R. Passey, D. Muirhead, C. Grove, C. Magee, J. Murray, and M. Hole, 2017, Regional magma plumbing and emplacement mechanisms of the Faroe-Shetland Sill Complex: implications for magma transport and petroleum systems within sedimentary basins: Basin Research, 29, no. 1, 41–63, doi:10.1111/bre.12164.

Senger, K., J. Millett, S. Planke, K. Ogata, C. H. Eide, M. Festøy, O. Galland, and D. A. Jerram, 2017, Effects of igneous intrusions on the petroleum system: a review: First Break, v. 35, no. 6, p. 47–56, doi:10.3997/1365-2397.2017011.

Spacapan, J. B., O. Galland, H. A. Leanza, and S. Planke, 2017, Igneous sill and finger emplacement mechanism in shale-dominated formations: a field study at Cuesta del Chihuido, Neuquén Basin, Argentina: Journal of the Geological Society, 174, no. 3, 422–433, doi:10.1144/jgs2016-056.

Thomson, K., 2007, Determining magma flow in sills, dykes and laccoliths and their implications for sill emplacement mechanisms: Bulletin of Volcanology, v. 70, no. 2, p. 183–201, doi:10.1007/s00445-007-0131-8.

Zhao, T., F. Li, and K. J. Marfurt, 2017, Seismic attribute selection for unsupervised seismic facies analysis using user guided data-adaptive weights: Geophysics, v. 83, no. 2, p. 1–62, doi:10.1190/geo2017-0192.1.

CHAPTER 3

USING MACHINE LEARNING AS AN AID TO SEISMIC GEOMORPHOLOGY, WHICH ATTRIBUTES ARE THE BEST INPUT?

ABSTRACT

Volcanic rocks with intermediate magma composition show distinctive patterns in seismic amplitude data. Depending on the processes by which they were extruded to the surface, these patterns may be chaotic, moderate amplitude reflectors, (indicative of pyroclastic flows) or continuous high amplitude reflectors (indicative of lava flows). I identify appropriate seismic attributes that highlight the characteristics of such patterns and use them as input to Self-Organizing Maps (SOM) to isolate these volcanic facies from their clastics counterpart. My analysis shows that such clustering is possible when the patterns are approximately self-similar, such that the appearance of objects do not change at different scales of observation. I propose a workflow that can help interpreters to decide what methods and what attributes to use as an input for machine learning algorithms, depending on the nature of the target pattern of interest, and apply it to the Kora 3D seismic survey acquired offshore in the Taranaki Basin, New Zealand. The resulting clusters are then interpreted using the limited well control and principles of seismic geomorphology.

INTRODUCTION

In today’s modern era, the most effective way to gain knowledge on how a certain geological feature like a lava flow appears in seismic data is to do a Google search and type a few key words such as “lava flow seismic” then go to the images section and even go through a couple of scientific publications, until we reach an “Aha moment” when we find patterns that appear similar to those in our data set. This type of pattern recognition is easy for a human interpreter but quite difficult for computers. The advantage of computers is that once such a task is well defined, they can apply the analysis to every voxel in a large 3D seismic data volume, perhaps identifying subtle features that may have been overlooked by an overworked interpreter. Machine learning pattern recognition of seismic data goes beyond automation of time-consuming analysis tasks. Specifically, each prediction can be weighted by a confidence value, which can be used in subsequent risk analysis.

Machine learning was first used by Alan Turing to decipher the Nazi “enigma” code. Since then, it has branched out to nearly all forms of language analysis, including voice recognition and translators, and expanded into visual communication, marketing, and social media. Early machine learning applications to seismic facies analysis include work by Meldahl et al. (2001) and West et al. (2002) who used multilinear feedforward neural networks with seismic attributes to produce a probability volume of gas chimneys, Linari et al. (2003) Coleou et al. (2003) and Poupon et al. (2004) used seismic amplitude waveform and SOM to define zones of interest. Similarly, Verma (2012), Roy et al. (2013) Roden et al. (2015), and Zhao et al. (2016) used volumetric seismic attributes fed into SOM algorithms to find different facies in shale resources plays. Qi et al. (2016) and Olorunsola et al. (2016) used generative topographic mapping (GTM) to try to separate salt from clastics, MTDs, from layered sediments in the Gulf of Mexico, and producing from tight facies in the Granite Wash in the Texas Pan Handle respectively. Recently, Lubo-Robles (2018) applied Independent Component Analysis of spectral components to try to predict sandy facies in the Miocene Moki A formation in Taranaki Basin, New Zealand.

Machine learning techniques are relatively simple mathematical algorithms that can learn from and generate clusters/classes based on patterns in (or interrelationships between) the data. Depending upon data availability, we can use either supervised or unsupervised algorithms. In supervised classification, the interpreter defines facies of interest, either by selecting specific voxels (Meldahl et al., 2011) or by drawing polygons around facies of interest (West et al., 2002; Qi et al., 2016) which serve as "training data" that are used to establish the relationship between input and output. Once trained, the algorithm is then applied to another subset of "validation data" (interpreted facies not used in the training step) to determine if the algorithm is sufficiently accurate. If the validation is successful, the algorithm is then applied to the entire seismic data volume.

In principle, unsupervised classification requires no interpreter input. In practice, the interpreter strongly biases the results of the algorithm by choosing a suite of attributes that best differentiate facies of interest. In a seismic interpretation context, this machine learning technique extracts patterns that exhibit a similar attribute expression for similar geologic facies, displaying these similar expressions, or clusters, using a 2D color-coded to allow subtle patterns to be identified by the interpreter (e.g., Zhao et al., 2016; Qi and Marfurt, 2016; Zhao et al., (2017).

Depending on the objective, both supervised and unsupervised techniques use seismic attributes as input. Where impedance and anisotropy attributes provide critical information for geomechanical clustering. In the absence of sufficient well control, instantaneous, geometric, spectral, and texture attributes provide critical information for interpreting seismic geomorphology from clustering (Zhao et al., 2016, Infante-Paez and Marfurt, 2017).

The focus of most recent studies in seismic interpretation has been focused on applying and comparing different machine learning methods including multilayer perceptron network, self-organizing maps, support vector machine, K-means, generative topographic maps (Meldahl et al., 2011; Roy and Marfurt, 2013; Snyder, 2016; Zhao et al., 2016; Qi et al., 2016) respectively.

I begin this chapter by defining the nature of the seismic patterns represented by volcanics in my seismic volume. I then propose a workflow that will allow interpreters to decide what machine learning algorithm to use, depending on the nature of the target pattern. Next, I compute mathematically independent candidate attributes that highlight the continuity (such as GLCM entropy), amplitude (peak spectral magnitude) and frequency (peak spectral frequency) of these target patterns, with the goal of determining which input attributes best differentiate the volcanics from the surrounding clastic sediments. Finally, I input the GLCM entropy, peak spectral magnitude and frequency attributes into SOM, to interpret the seismic geomorphology of the internal elements of the Kora volcano.

METHODOLOGY

Selection of the target patterns

The target patterns in my study include some of the internal and external elements of the Kora volcano, as well as adjacent volcanics from the Mohakatino Volcanic belt

(MVB). These volcanics form potential analogues to the volcanics in Songliao Basin, China (Figure 3.1) and andesites from Jatibarang field in Java (Figure 3.2) which have produced more than 1.2 billion of barrels of oil and > 2.7 TCF of gas between 1969 and 1990. (Kartanegara et al., 1996).

Figure 3.3 displays a vertical slice through the Kora 3D survey where multiple target patterns (TP) are highlighted by yellow boxes. Seismic-to-well-ties indicate that these patterns have been drilled by exploration wells (Figure 3.4) validating the presence of volcanics.

Nature of the target patterns

I define my human interpretation patterns as “monogenetic”, “composite” and “intricate” patterns where the goal is to examine relationships that can be evaluated by a machine.

Monogenetic seismic patterns

I define a monogenetic pattern as a facies that consists of a single seismic pattern. This pattern is statistically consistent, translational vertically and horizontally. The pattern is also consistent at different scales, such as conformal or chaotic reflectors within a 20x20x20 versus a 5x5x5 voxel window. Monogenetic seismic patterns are related to physical self-similarity, where the appearance of objects does not change at different scales of observation (Lam and Quattrochi, 1992; Dimri et al., 2011; Dasgupta, 2013; Herrera et al., 2017). Examples of monogenetic seismic patterns are shown in Figure 3.5.

Composite seismic patterns

Composite patterns are those facies that consist of two or more simpler patterns. Composite patterns do not entirely preserve their character laterally, vertically or at different scales but can still be distinguished from surrounding patterns. (Figures 3.6-3.7) for example.

Intricate seismic patterns

Intricate patterns are those facies that dramatically change their character with scale and location and are far from being self-similar, for example, Figure 3.8.

I hypothesize that using appropriate seismic attributes as input to a machine learning algorithm (SOM for example) monogenetic patterns will be represented by a single cluster. Composite patterns will be represented by two or more clusters, resulting in a machine learning classification that requires subsequent human “clumping”. Intricate patterns are represented by multiple clusters, providing an image that may offer little value over the original seismic amplitude volume. While composite and intricate patterns may be represented by more than one cluster, a given “cluster” may also represent more than one facies. For example, clustering based on reflector continuity and parallelism might result in marine shales and deepwater fans clumped together. To separate them the interpreter might add energy or peak frequency as additional input data to break them apart. For this reason, if the multiple clusters representing an intricate pattern are unique, they can be subsequently clumped after clustering to form a single facies. Such clumping is performed implicitly when computing the Bhattacharya distance when using generative topologic mapping (Qi et al., 2016) where a probability density function, rather than a single prototype vector is computed for each voxel in the training data set. The sum of these PDFs can then represent more intricate patterns.

Convolutional neural network (CNN) may provide and alternative means to addressing intricate patterns. In the simplest workflow, the interpreter provides the original seismic amplitude data. Internally, the machine convolves adjacent voxels, computing its own attributes for evaluation. Alternatively, Qi (2018) used CNN and a suite of input seismic attributes to predict fractures seen in image logs.

Computers have several advantages over humans: (1) they can perform repetitive analysis of billions of voxels without tiring, (2) they can be much more quantitative, and (3) they can easily compare similarities and differences between more than three attributes at the same voxel (4). In contrast, humans have advantages over machines in that they can (1) see patterns on a much larger scale, thereby identifying a pattern in context, (2) compare patterns to those seen in others seismic surveys or in outcrop, and (3) integrate patterns as discrete components or elements that result from a geologic process.

Seismic attribute selection

Figures 3.9-3.11 demonstrate the importance of the input attributes to unsupervised machine learning. The goal is to try to organize the people in Figure 3.9a who work at a university and determine which of them perform similar jobs. From the top to and moving clockwise we have the dean of the Mewbourne College of Earth and Energy Dr. J. Mike Stice, PhD candidate in geophysics Lennon Infante, geophysics professor Dr. Kurt. J. Marfurt, and geology professor Dr. Roger Slatt. From their headshots we can extract additional information, such as their hair length and smile (happiness). The fact that one of them is dean of the College of Earth and Energy, two of them are professors, and the last one is a student, suggest they have different incomes. These three attributes, the happiness, hair length and income, provide a means to place the two professors in the same cluster (Figure 3.9b). Although the SOM put these four people into three different clusters it cannot tell which cluster represents which job.

In reality, we cannot measure income from the input data (headshots). A more realistic scenario would be the one shown in Figure 3.10. Some of the attributes that can be extracted from the input data are gender, hair length, clothes type and happiness (smile on their faces). When the gender, clothes and hair length attributes are fed into SOM, we obtain three clusters which is the correct number of different jobs. However, one of the clusters is erroneous since it groups professor Marfurt with dean Stice who have different jobs. Selecting the happiness attribute instead of hair length produces different clusters (Figure 3.11). In this case the SOM outputs only one cluster. From this analogy, it is clear that the input attribute selection and not the SOM algorithm itself produces erroneous results.

Voxel based approach for classifying monogenetic seismic patterns

Given that the approximately self-similar target patterns of interest (Figure 3.4) preserve their character at different scales and distinct locations, I use the workflow described in Figure 3.12 to select attributes that differentiate the volcanics from each other and from the surrounding clastic sediments.

There are different approaches that a seismic interpreter can use to select input seismic attributes for clustering of seismic facies. A simple but time consuming and potentially dangerous approach is to apply all possible attributes and determine which combination best correlates with the desired facies. Kolkoney (1999) warms that this workflow may lead to false predictions. Principal component analysis reduces a suite of correlated attributes into a smaller number of composite attributes. Roden et al., (2015) use the first principal components to determine which attributes are most important in representing the seismic data volume. Unfortunately, such choices do not necessarily guarantee the differentiation of the pattern of interest, particularly if one or more of these patterns only represent 1-5% of the data. Moreover, this approach may be suitable as a first pass for exploring the data, but it could fail when trying to isolate a specific pattern such as a mass transport deposit (MTD) or pyroclastic flows. Thus, I recommend the calculation of seismic attributes based on the qualitative description of the patterns (Figure 3.13) (analogous to how a geologist describes facies in outcrops or in core). Because most commercial and research software that implement machine learning techniques do what they are supposed to do, e.g., organize the data into clusters, the challenge for interpreters in applying SOM and similar algorithms to seismic data is the attribute selection. For example, TP 3 in Figure (3.6) is characterized by semi-chaotic, low-to-moderate amplitude reflectors with occasional isolated continuous, moderate-amplitude reflectors that are parallel. During the description process, key words such as “chaotic reflectors” can help us think of seismic attributes that best highlight such features (such as the GLCM texture entropy attribute). TP 1 is characterized by continuous high-amplitude reflectors. TP2 is characterized by chaotic, moderate-amplitude reflectors, while TP3 and TP 4 are characterized by semi-continuous to semi-chaotic, moderate-to-high amplitude reflectors with few isolated parallel reflectors. Attributes that measure such observations include amplitude attributes (envelope, RMS amplitude, energy, colored inversion), continuity attributes (GLCM entropy, chaos, coherence), frequency attributes such as the peak frequency, average frequency and bandwidth, and conformity attributes (reflector convergence, parallelism). Spectral components are also helpful, but more difficult for a human interpreter to assign to a given seismic pattern. Seismic patterns exist at zones (geological age), so one can constrain the attribute analysis within a zone of interest bounded by seismic horizons to minimize variability not only to geology, but also to seismic resolution.

Seismic Attributes that assist interpreter's vs seismic attributes that assist machine learning

For *monogenetic* and *composite* seismic patterns to be successfully clustered using the voxel approach, all the input attributes should highlight the same sample (voxel) in the seismic trace. Therefore, we must differentiate between attributes that assist the interpreter in highlighting key geological features (Figure 3.14) and attributes that assist machine learning algorithm to isolate specific geological features (Figure 3.15). That is, if the target seismic features to map are faults, one should avoid using input attributes to machine learning such as coherency, most positive and most negative curvatures together. Though they do highlight the fault in a visual way that is clear to a human interpreter, they do not highlight the fault at the same seismic sample (voxel). The same principle applies to different facies such as sinkholes. If one is trying to isolate sinkholes using a clustering technique such as SOM, feeding complementary attributes such as most positive and most negative curvatures and coherency would not produce an accurate result since these attributes highlight various parts of the sinkhole, but not at the same voxel. The most obvious example are combinations of spectral components, that differentiate thicknesses and lithologies within a channel system, and coherence, that highlights the channel edges. Seismic noise also results in patterns that may be mentally "filtered out" by a human interpreter, but form (ideally, its own) noise clusters.

Seismic attribute expression of volcanic rocks that assist machine learning clusters.

Based on the descriptions (e.g., continuous versus chaotic, low amplitude versus high amplitude) of the target patterns, the input seismic attributes for clustering of these patterns would be three types of attributes that highlight amplitude, continuity and frequency content. Using the same composite section from Figure 3.3 as a reference, I compute a suite of candidate attributes to visually evaluate the attribute response of the target patterns (Figures 3.16-3.22). Figure 3.17 displays the peak spectral magnitude calculated from the continuous wavelet transform (CWT) (reference). This attribute gives a response similar to the RMS amplitude and highlights the strength of the reflectors. The peak spectral magnitude shows that there are differences in all TPs. TP 1 is characterized by high magnitude, whereas TP 2 is highlighted by low magnitudes. TP3 and TP4 on the other hand consist of low to moderate magnitude.

The gray level co-occurrence matrix (GLCM) provides a group of texture attributes homogeneity, entropy, dissimilarity, contrast, mean, energy, correlation and variance. Hall-Beyer (2007) defines texture as "an everyday term relating to touch that includes such concepts as rough, silky, and bumpy. When a texture is rough to the touch, the surface exhibits sharp differences in elevation within the space of your fingertip. In contrast, silky textures exhibit very small differences in elevation”. Seismic textures work in an analogous manner with elevation replaced by amplitude, and the probing a finger by rectangular or elliptical analysis window oriented along the structure. From these 8 attributes the most useful are the entropy and the homogeneity, (see, Gao et al., 2003; Qi et al.2016; Zhao et al., 2017; Gao 2017; Marfurt 2018) though they are somewhat coupled. Detailed examination of the entropy and homogeneity of TP 1 and TP2 (Figures 3.18-3.19) shows that TP 1 has high values of homogeneity and low values of entropy. The opposite is true for the TP2, suggesting we can separate these two patterns using these texture attributes. TP 3 and TP 4 display zones where the entropy is high to moderate. High values of entropy mean the reflectors are chaotic (not layer cake). Figure 3.19 shows the peak spectral frequency attribute which displays the dominant frequency for the entire section. In the volcanic sequence the peak spectral frequencies ranges between 40 to 50 Hz. Although TP 1, TP3 and TP 4 exhibit a similar range of frequencies, TP 2 is characterized by low to mid frequencies (15-25 Hz).

In the same way, Figures 3.21-3.23 show the magnitude of reflector convergence, the dip magnitude and coherence attribute, all co-rendered with the seismic amplitude, highlighting different aspects of the seismic patterns of interest, but not at the same voxel. Therefore, for the Kora 3D survey, I conclude that the attributes that would assist machine learning are: (1) the texture attributes which are a measure of continuity, (2) peak spectral magnitude that measure the strength of the reflectors and (3) peak spectral frequency which measures the dominant frequency. These attributes are mathematically independent, but coupled through the geology, making them candidates for SOM.

Self-organizing maps (SOM) and seismic geomorphology

In seismic interpretation, self-organizing maps (SOM) is a clustering technique that extracts similar patterns across multiple seismic attribute volumes and displays those similarities as a color-coded map, with similar colors representing clusters that a human interpreter can visualize as similar facies (Zhao et al., 2016). Because several of the attributes I use (GLCM entropy and homogeneity, peak magnitude and peak frequency) measure spatial patterns, SOM will be able to cluster spatial patterns as well. The SOM workflow used in this study is illustrated in Figure 3.24. The input attributes to feed the SOM are of three types: attributes that highlight the continuity- how layer cake the reflectors are- (homogeneity and entropy), the amplitude (peak magnitude) and the frequency (peak frequency) of the target patterns. These attributes are extracted from the raw amplitude data using software developed at the University of Oklahoma, (. e.g., Matos et al., 2011; Qi et al., 2016).

I input the previously computed seismic attributes into the SOM algorithm. Since I am using four attributes at each voxel, the analysis is in 4D attribute space. In this case, the objective of SOM is to fit a deformed 2D surface (called a manifold) to the distribution of the data points living in 4D space. Each data point is projected onto the nearest part of a manifold which is then mapped to a 2D color bar. In this manner, voxels that have a similar response (lie next to each other in 4D space) project onto nearby locations on the manifold and are displayed as similar colors. In contrast, voxels that exhibit a very distinct attribute behavior (lie far from each other in 4D space), project onto different parts of the manifold and appear as different colors. Details of SOM applied to seismic data can be found in Roy et al. (2013), Roden et al. (2015), and Zhao et al. (2016).

Internal elements of the Kora volcano

Integrating well reports from Kora -1,2 and 3 (where core data were acquired) and their seismic patterns, provide geological control to the chaotic moderate amplitude seismic pattern. Internally to the Kora volcano, the seismic data exhibit two main patterns: strong continuous (TP1) and moderate chaotic reflectors (TP 2). According to the core data and seismic-to-well ties from wells Kora-1 through 3, I interpret that the penetrated chaotic, moderate-amplitude reflectors are correspond to pyroclastic flows whereas the geological process corresponding to the strong, continuous reflectors remains unknown.

Figure 3.25 shows a vertical slice connecting the four Kora wells illustrating the distribution of TP1 and TP2. The same vertical slice is then shown with the SOM clusters (Figure 3.26). From these clusters, we can observe three distinctive colors (seismic facies). The Orange/yellowish color represent the continuous, high-amplitude reflectors (TP1), while the purple/dark blue colors represent the chaotic, moderate-amplitude reflectors (TP2). A third green color is more representative of the clastic sediments underlying and onlapping onto the volcano, while the geometry of the orange/yellow color appears to be more dominant adjacent to the Kora-4 well. Extracting the SOM clusters on top of the time structure map of the volcano shows its geomorphology. The orange/yellow facies occur mainly on the western flank of the volcano, while the purple/dark blue facies occurs more on the eastern flank and between the orange/yellow facies (Figure 3.27). The black solid line highlights these unknown facies. Based on and understanding of volcanic processes, geomorphology and structural relation of these facies to the volcanic cone, I interpret the orange/yellow facies to be lava flows such as those reported by Klarner and Klarner (2012), Holford et al. (2012) and McArdle et al. (2014).

External elements of the Kora Volcano and adjacent volcanoes

Subaqueous flows

Volcanic eruptions allow the volcano to grow. A coned geometry like the one observed in the Kora and nearby volcanoes suggests that the volcanoes grew by preferential addition of material to the summit area (Magee et al., 2013). Furthermore, a discontinuous to semi-chaotic with short (100 m) continuous reflectors, creating a distinctive seismic pattern (TP 3) can be seen as far as 20 km to the northwest form the Kora volcano. Fortunately, this and other similar seismic patterns have been penetrated by several wells offshore Taranaki Basin, including the Ariki-1, Arawa-1, Kanuka-1, Moana-1 and other wells (Well report series). Well-to-seismic ties coupled with completion reports indicate that this seismic pattern is representative of sediments with significant volcaniclastic content called the Mohakatino Formation named by Hansen and Kamp (2004). The Ariki-1 well drilled through semi-continuous, semi-chaotic seismic patterns (Figure 3.4) similar to the mass transport deposits (MTD) previously documented by Posamentier and Kolla (2003), Lee et al. (2004), Dallas et al. (2013), Qi et al., (2016) in steep slope clastic environments. In my survey, the MTD seem, at least partially originated from the west flank of the Kora volcano (Figures 3.28 a 3.28 b). The Ariki-1 well completion report defines cuttings from the interval 2256-2556 m as volcaniclastic deposits, where: “Tuffaceous material is most abundant in the lower part of the formation and decreases upwards, reflecting the waning of volcanic material”. The lithology varies from gray mudstones with a tuffaceous matrix including biotite, chlorite, pyrite and at the base, light to moderate gray sandy tuffs. These tuffs contain abundant angular to sub-angular, fine-to-medium-grained, poorly sorted clasts of biotite, garnet, olivine, hornblende, and aphanitic material together with quartz and feldspar of both sedimentary and volcanic origin. Comparable descriptions are also given for the cuttings of the other wells that drilled through similar seismic patterns in the Arawa-1, Kanuka-1, and Moana-1well series reports. Given the morphology of TP 3 (Figure 3.28a) it is possible to infer a depositional process. Figure 3.28c shows a scour-like base of about 3km width that spreads out in a fan-like geometry beyond 20 km the limits of the 3D survey reaching Ariki-1. This geometry is highlighted by SOM purple/dark blue facies where the chosen input seismic attributes (entropy/homogeneity, peak magnitude, peak frequency) highlight the characteristics of TP 3. Interestingly, although the nature of TP 3 is considered to be *composite*, it is still possible to isolate and map TP 3 because this pattern is very different from the background clastic sediments. The fact that reflectors in TP 3 are far from being parallel (indicative of tuff clouds settling in volcanic facies) and that they form a fan-like geometry, indicates that the process that deposited the volcaniclastic material was a subaqueous flow. I use the term volcanic mass transport deposit (VMTD) to describe these volcaniclastics.

Additionally, Figure 3.28b shows evidence of sill junctions that appear to have erupted lava onto the west flank of the Kora volcano which, could explain the spatial distribution of these flows in the western flank of Kora (Figure 3.27).

Pyroclastic flows from volcanoes adjacent to Kora

Given the proximity of TP 4 to the Kora volcano, it is reasonable to attribute TP 4 to a younger eruption in the history of this volcano. Nevertheless, the distribution of the submarine volcanoes of the MBV mapped by Giba (2010) (Figure 3.2b), depicts younger (8-4 Ma compared to Kora's 16-12 Ma) volcanoes to the East of Kora. According to the mapped geometry of these andesitic volcanoes, they appear to coalesce instead of forming a single volcanic cone like Kora. Furthermore, their aerial extent appears to be at least five times larger than Kora. Detailed examination of the Kora 3D seismic survey indicates that TP 4 exists only on the eastern section onlapping onto the Kora volcanic edifice (Infante-Paez and Marfurt 2017). Therefore, I interpret TP 4 to be related to the activity of the volcanoes located East of Kora which is also confirmed by the SOM clustering results (Figure 3.29) where the purple/dark blue facies appears to dominate the entire area, even though isolated blocks of orange/yellow facies can be observed within the purple/dark blue facies. The presence of these two facies is because the nature of TP 4 is "*composite*" consisting of two or more patterns. In this scenario the orange/yellow facies represents a greater content of clastic material being deposited within the volcanics in the basin. Due to the similarities of TP 2 and TP 4 and the fact that other andesitic volcanoes exist adjacent to Kora, I interpret TP 4 to be pyroclastic flows originated from the previously mentioned younger andesitic volcanoes from MVB.

Potentially enhanced volcanic reservoirs.

As stated in the previous sections, the submarine volcanoes in the Taranaki Basin represent potential reservoirs as indicated by the DST in Kora-1A and the good log and core porosity from the Kora and other wells. The uncertainty in this type of reservoir is how well connected those pores are. For that reason, an area of potentially enhanced flow capacity is that of the interpreted pyroclastic flows (TP 4) adjacent to the East flank of Kora. In this area, the volcanics are probably fractured due to the faults associated with the Kora and/or the adjacent andesitic volcanoes (Figure 3.29b) like in the case of the fractured andesites in the Jatibarang field in Indonesia where permeability is up to 10 D (Schutter, pers. Comm., 2018).

LIMITATIONS

Different authors (Meldahl et al., 2001; Roy et al., 2013; Qi et al., 2016; Sinha et al;2016; Sinha et al; 2017 Zhao et al. 2017; Kumar and Mandal, 2017; Qi, 2018) have used different methods, including MLFN, SOM and CNN to predict well production performance and to cluster different patterns (gas chimneys, faults, MTDs) in seismic data and. However, these patterns have different nature (e.g., monogenetic, composite and intricate) that present different levels of difficulty for machine learning. Thus, I propose that *monogenetic and composite patterns* can be mapped by feeding appropriate geometric, instantaneous, spectral, and seismic inversion-derived attributes to an unsupervised machine algorithm such as SOM. *Intricate* patterns (Figure 3.8) on the other hand, may need a different method, such as CNN, where the algorithm convolves adjacent amplitude values to generate its own “attributes”. At present there is not a single method

(SOM, GTM, MLFN, SVM, CNN) that is best to map seismic patterns. The clustering method chosen depends on the nature of the pattern that represents the facies of interest (Figure 3.12).

As seen in Figure 3.26, the voxel based approached is most useful in monogenetic patterns where we can easily differentiate the interpreted lava flow facies from the pyroclastic flows (TP 1 and TP 2 respectively). Similarly, Figures 3.28 and 3.29 show that the voxel-based approach is also useful in isolating composite seismic patterns, though they are represented by more than one cluster. The key to a successful clustering of a specific seismic facies is to determine the nature of that pattern. The limitation in this proposed workflow is twofold. First, a human interpreter needs to quantitatively define the nature of the target pattern. The illustrations shown here provide an example appropriate for volcanics in the Taranaki Basin. Second, once the pattern is recognized, the interpreter has to decide which attributes provide a quantitative measurement that serve as input to a machine learning algorithm. Our task as interpreters is to construct a dynamic library of the attribute expression of different geological facies in seismic data that can be updated as they are encountered with new facies and new attributes as they are developed.

CONCLUSIONS

From my experience in trying to isolate the extrusive volcanics related to the Miocene volcanism in Taranaki Basin, New Zealand, I realized that when trying to isolate a target pattern, interpreters usually describe it regarding their continuity, parallelism, amplitude and frequency. Therefore, a good rule of thumb as to what attributes to input for clustering of *monogenic* and *composite* patterns would be three types of attributes: attributes that highlight the amplitude (such as envelope, energy, RMS amplitude, relative acoustic impedance) attributes that highlight the continuity (such as GLCM entropy chaos), and attributes that highlight the frequency (peak spectral frequency, average spectral frequency, bandwidth, etc.) Furthermore, there is the need of a seismic attribute that measures the self-similarity of the different patterns in the seismic section (with a change in lateral and vertical location, and scale). Ideally, the interpreter draws a polygon around the target pattern to be mapped, and this new seismic attribute (self-similarity) would quantitatively evaluate whether the target pattern is monogenetic or more complex (intricate).

SOM and similar clustering algorithms do what they are supposed to do: cluster the attributes they are fed. Attributes that are good for 3D interactive interpretation may not be appropriate for machine learning. Thus, the need of a new set of seismic attributes that assist machine learning so that they can identify more complex facies such as *composite* and *intricate* seismic patterns.

Geologically, I propose that volcanics/volcaniclastics associated with eruptions or landslides from Kora and other nearby MVB volcanoes should be evaluated as potential migration pathways due to the good log porosity (and good core porosity and permeability from some cored wells) observed in wells penetrating the Kora volcano and the potentially fractured adjacent volcanics.

Chapter 3 Figures

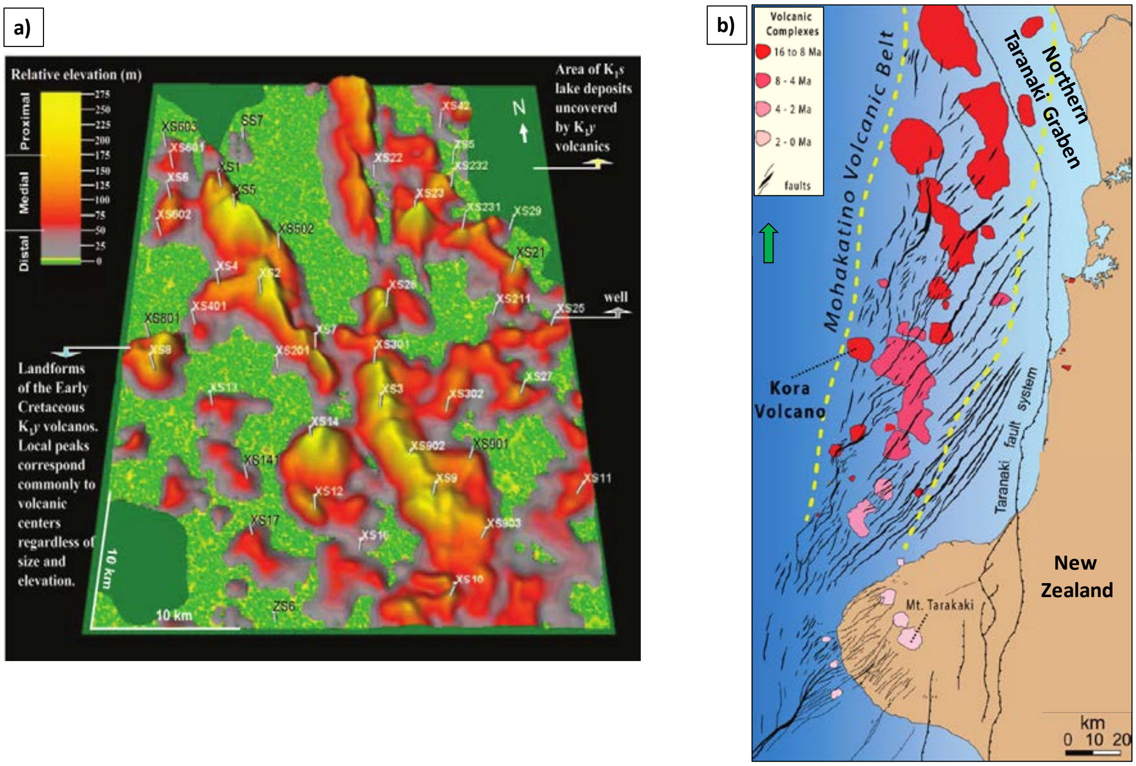

Figure 3.1. (a) Three-dimensional map of buried volcanos in the Xujiaweizi graben in the Songliao Basin, China showing several wells targeting the buried volcanoes (Chen and Wang, 2015). (b) buried volcanoes in the Taranaki Basin New Zealand. (After Giba et al., 2013 and Bischoff et al., 2017).

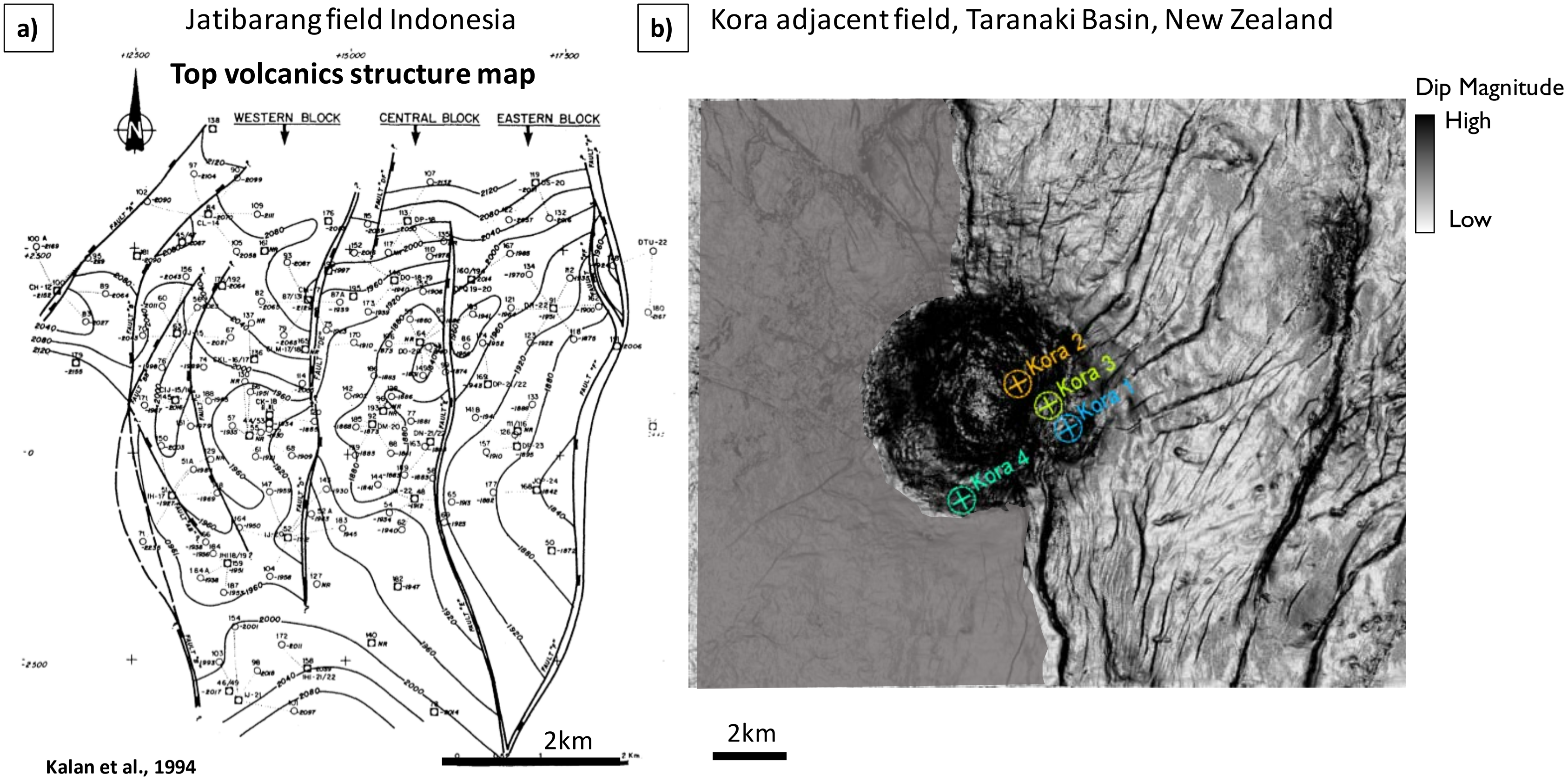

Figure 3.2. Comparison of the size and styles of a) the Jatibarang field in Java that produced more than 1.2 Bbl. from fractured andesites. After Kalan et al.,1994 and b) the Kora and adjacent volcanics. Even though the structural style in the Kora area is not exactly the same when compared to Jatibarang, the volcanics in Kora can potentially be fractured due to the radial and major rift faults.

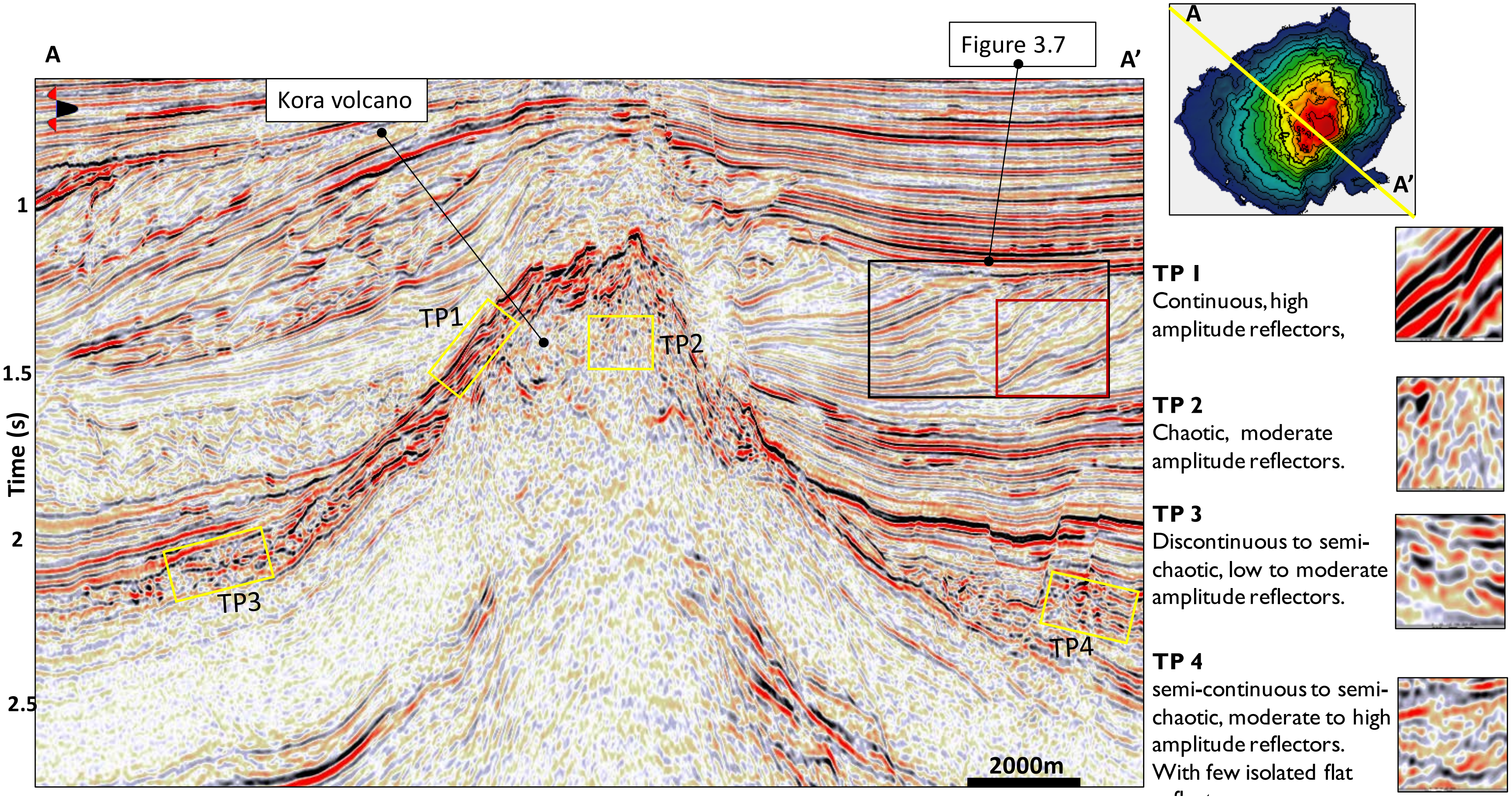

Figure 3.3. (a) Composite vertical slice through the Kora 3D survey where multiple patterns associated with the extrusive Kora volcano are highlighted by yellow boxes. (b) expanded image of these four patterns and their descriptions. TP= Target Pattern. Seismic data courtesy of NZP&M.

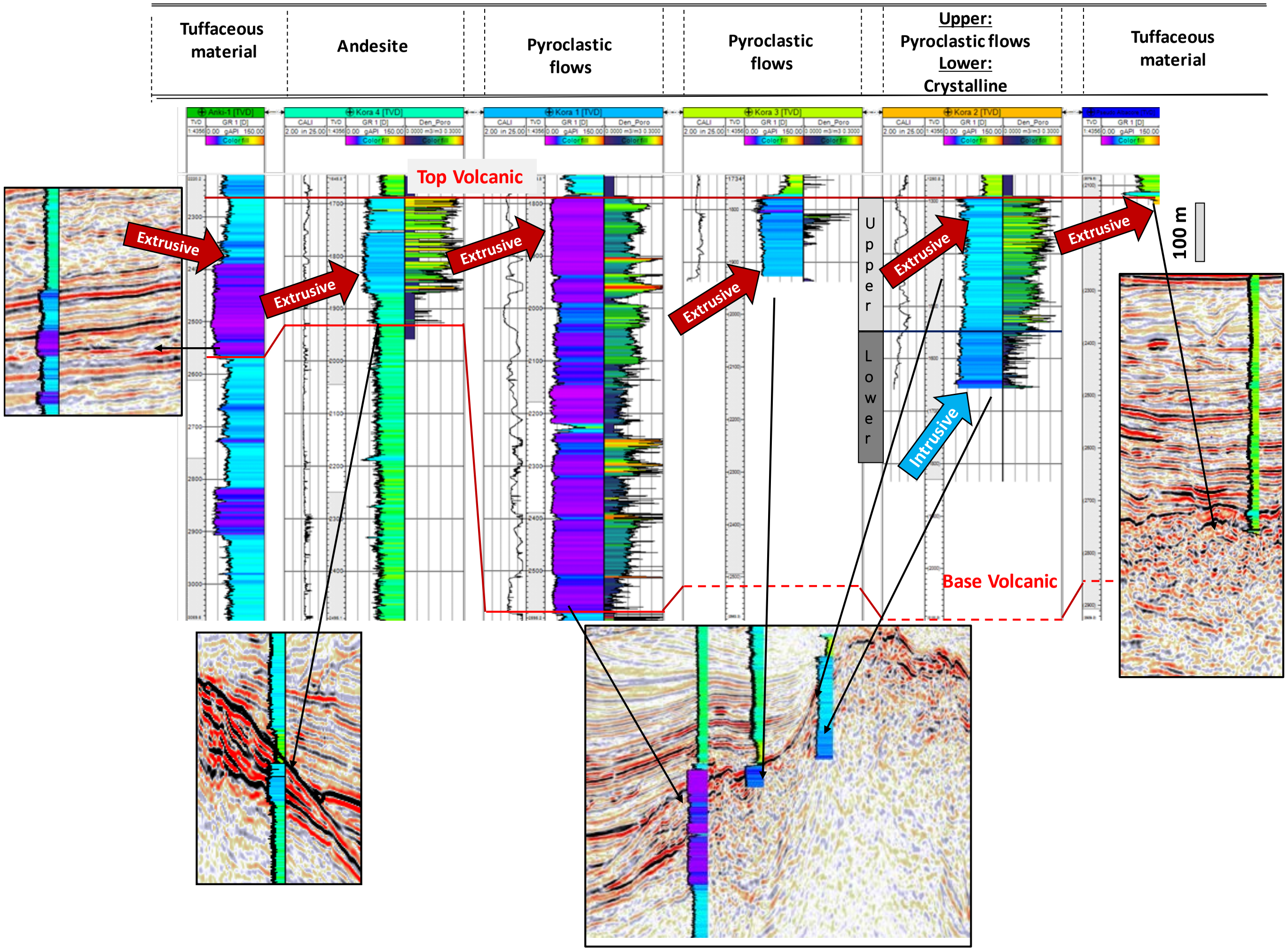

Figure 3.4. Wells that penetrate volcanoes and volcaniclastics and their corresponding seismic expression in the Kora 3D seismic survey. Track 1 displays the caliper log, track 2 the gamma ray, and track 3 the density porosity log. Note the low gamma-ray response in all the wells consistent with intermediate versus felsic-magma composition. (After Infante-Paez and Marfurt, 2017).

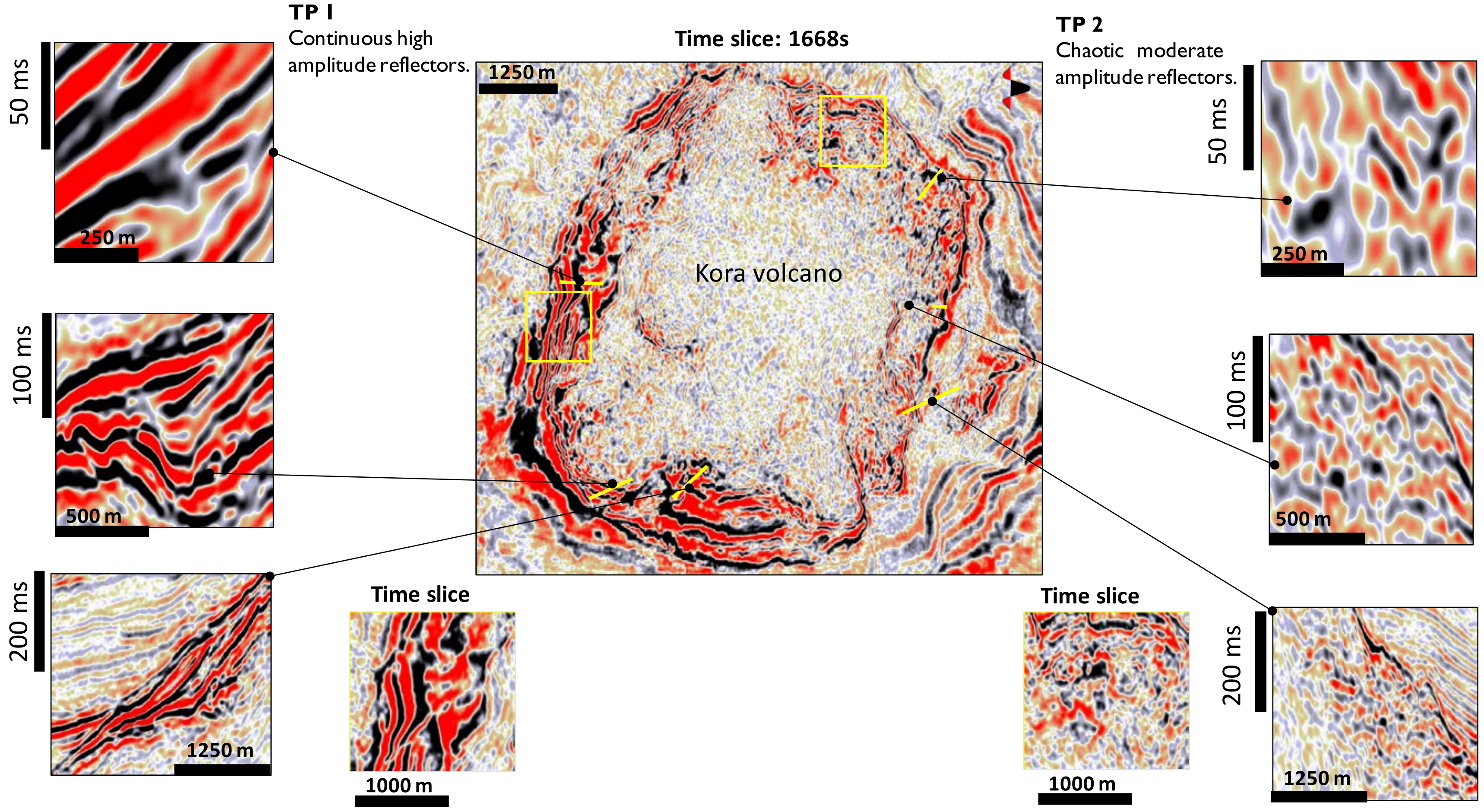

Figure 3.5. Examples of approximately self-similar “monogenetic” seismic patterns TP 1 and TP 2. Note the scale bar in the expanded boxes. These patterns are relatively easy for a machine to identify. Seismic data courtesy of NZP&M.

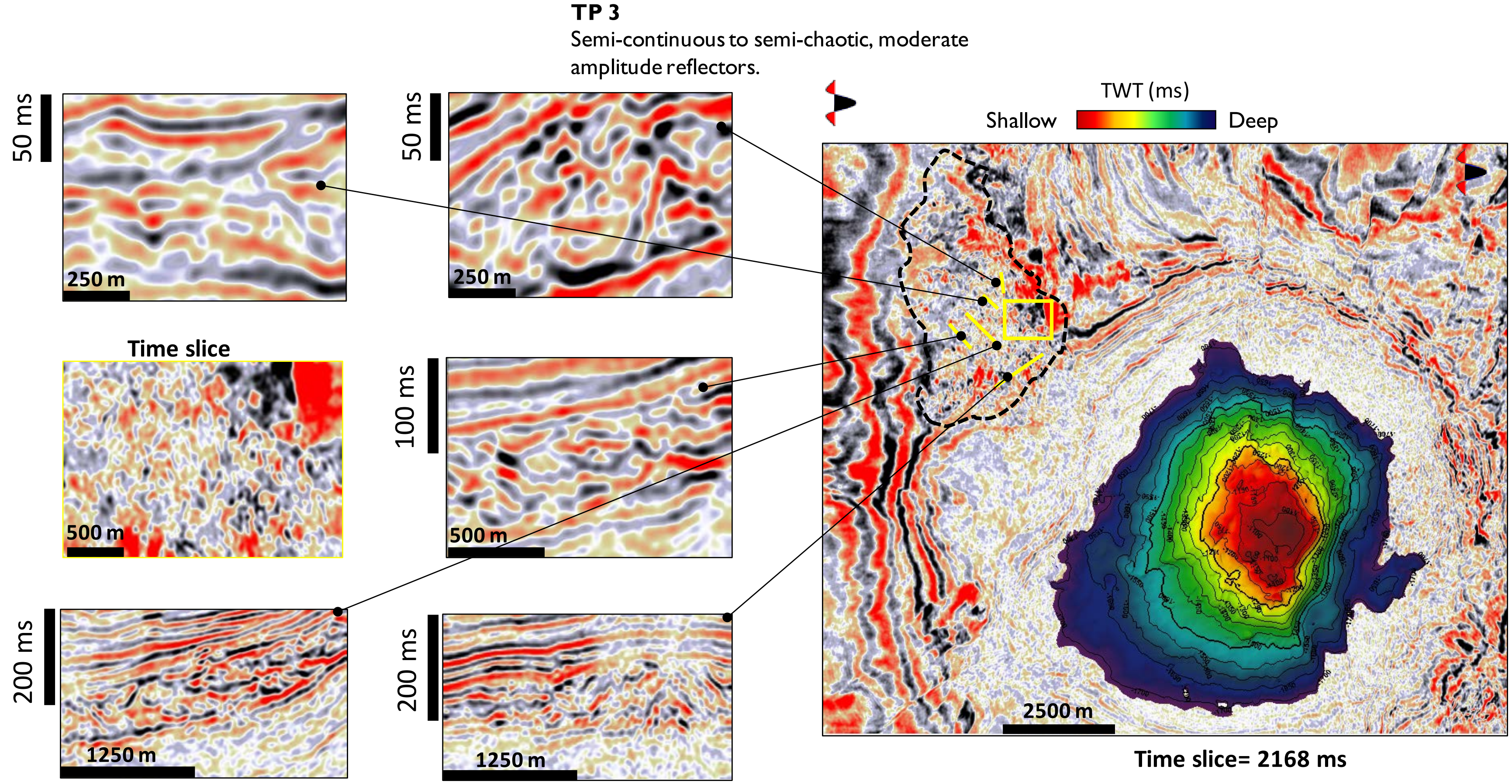

Figure 3.6. Example of a "composite" seismic pattern. Note the different scales in the expanded boxes show TP 3. Black dotted polygon in time slice shows the extension of TP 3. TP= Target Pattern. Seismic data courtesy of NZP&M.

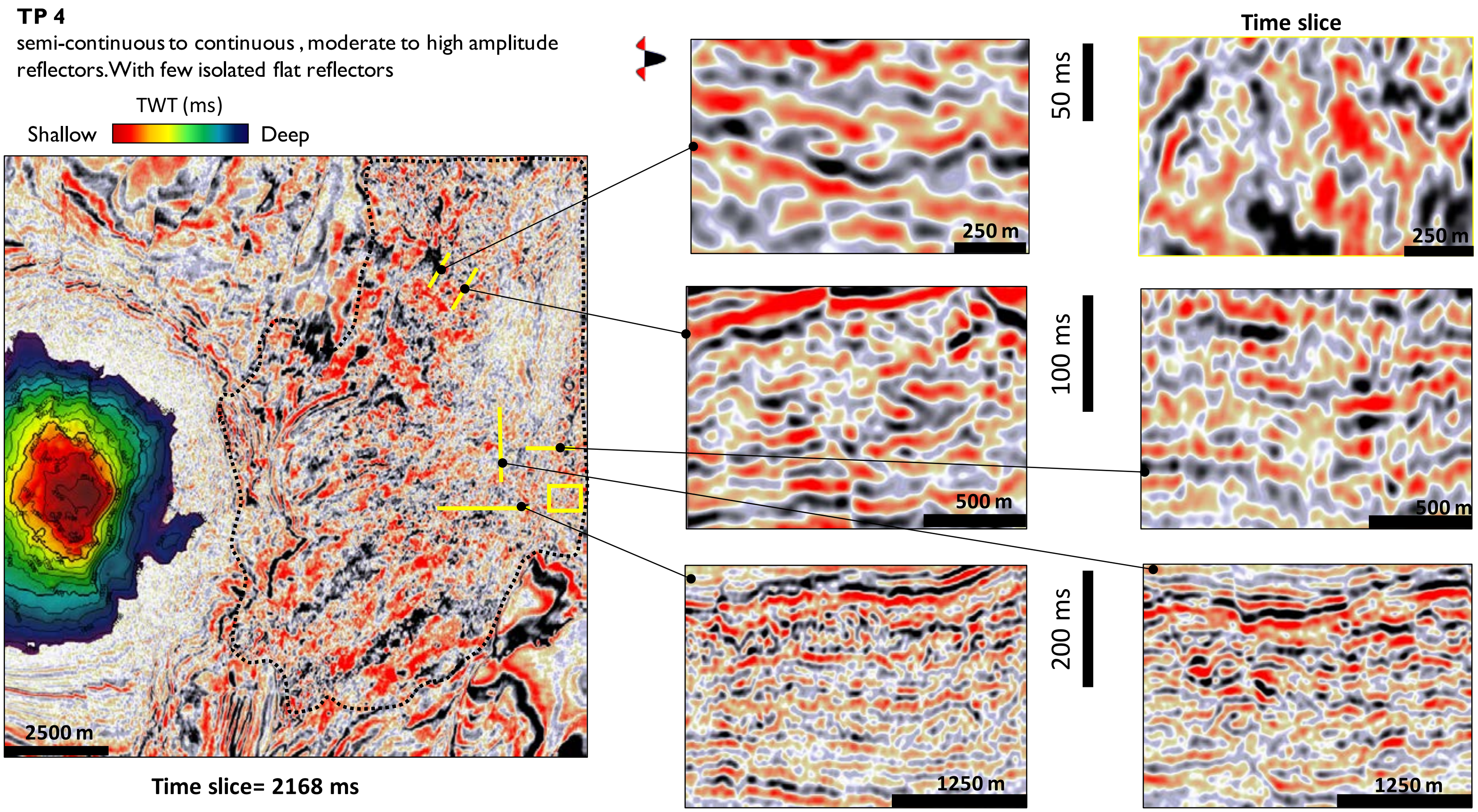

Figure 3.7. Examples of "*composite* seismic pattern. Note the different scales in the zoomed boxes. Black dotted polygon in time slice shows the extension of TP 4. TP= Target Pattern. Seismic data courtesy of NZP&M.

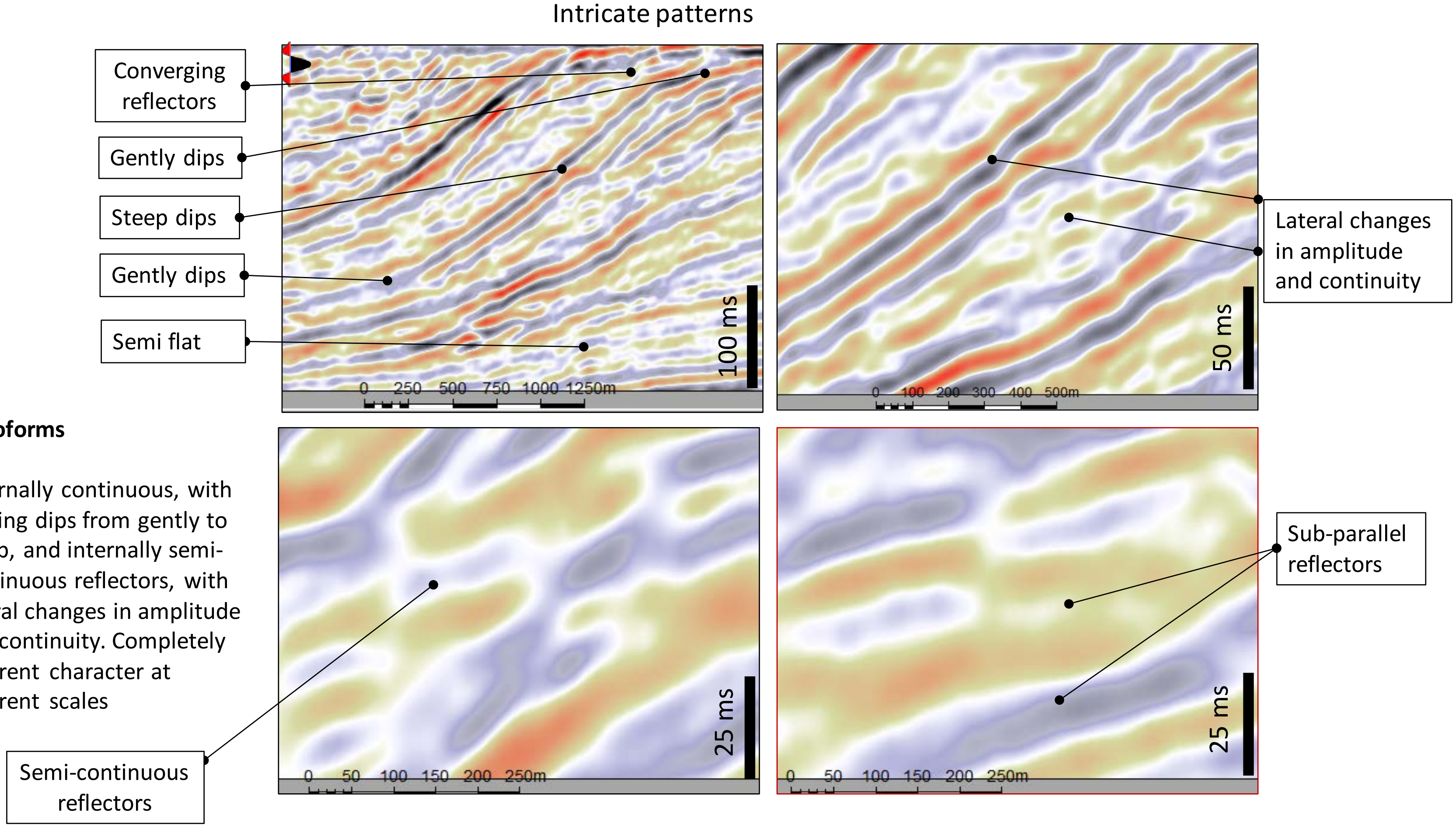

Clinoforms

Externally continuous, with varying dips from gently to steep, and internally semi-continuous reflectors, with lateral changes in amplitude and continuity. Completely different character at different scales

Figure 3.8. Example of an "*intricate*" seismic pattern. Notice the character of the pattern is not the same at different scales. The pattern also changes laterally form flatter, converging to more steeply dipping, subparallel reflectors. This pattern is more difficult for a machine to identify. Seismic data courtesy of NZP&M.

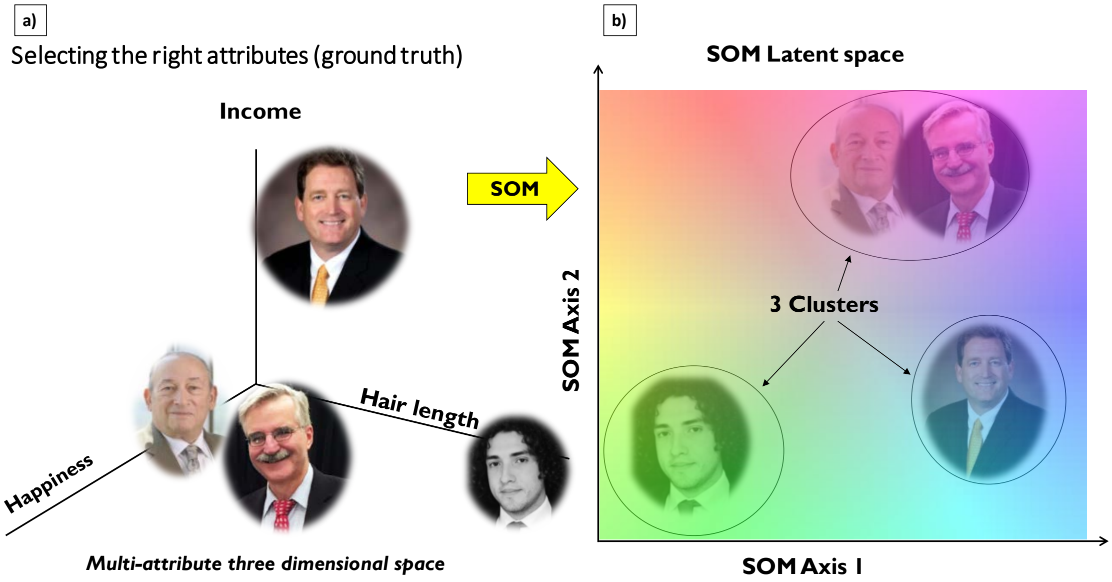

Figure 3.9. Headshots of four people who work at a University. a) The input data are three attributes that somehow distinguish them- hair length, happiness and income. (b) Using this combination of attributes, the machine learning algorithm correctly clusters the two professors into the same group and the student and the dean are into their own group. Notice 3 clusters where the two professors form 1 cluster and the student and the Dean two different clusters.

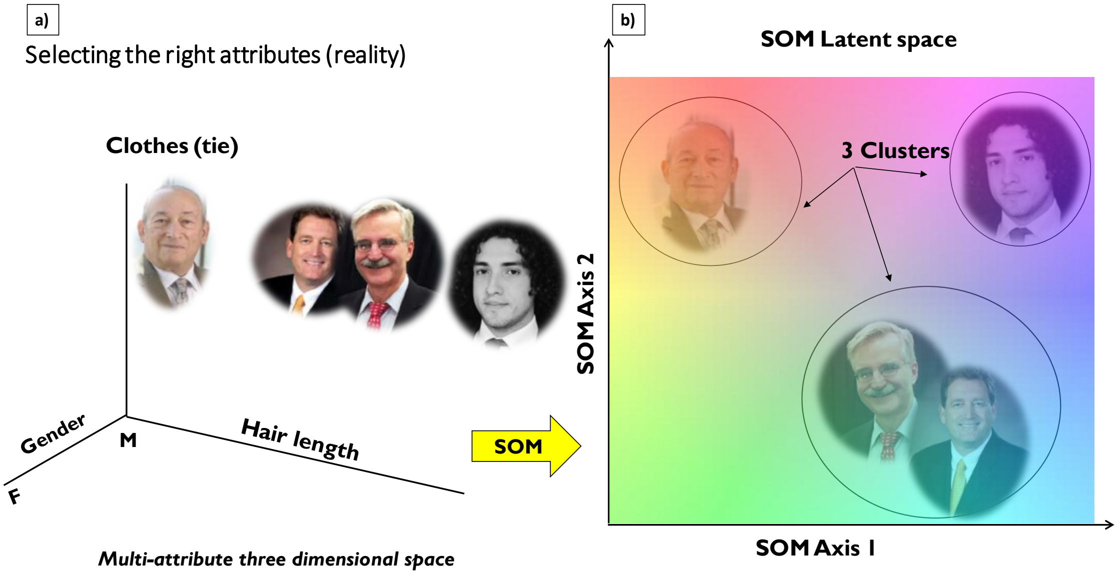

Figure 3.10. Headshots of the same four people shown in Figure 3.9 where the input attributes are hair length, gender, dress code. All four samples are male and have similar dress code (wearing a tie). For this reason, the clustering is driven by hair length alone, misclustering one of the professors with the dean

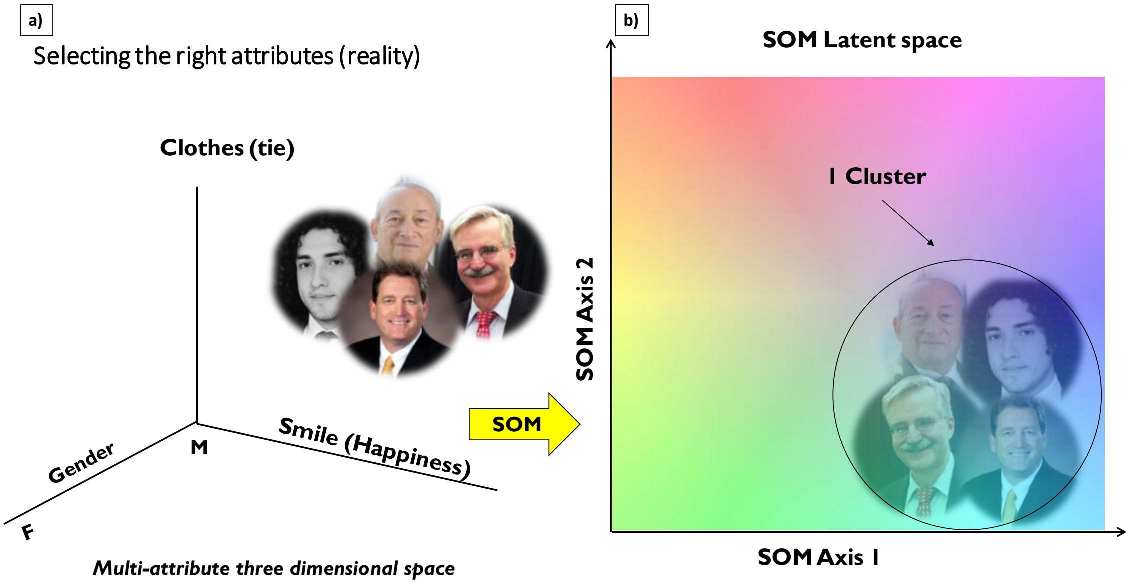

Figure 3.11. The same "samples" as in Figures 3.9 and 3.10 where attributes are clothing, gender and happiness. In this examples SOM results in only one clusters, suggesting happy conformity in this University, but no indication of the role occupied by each person.

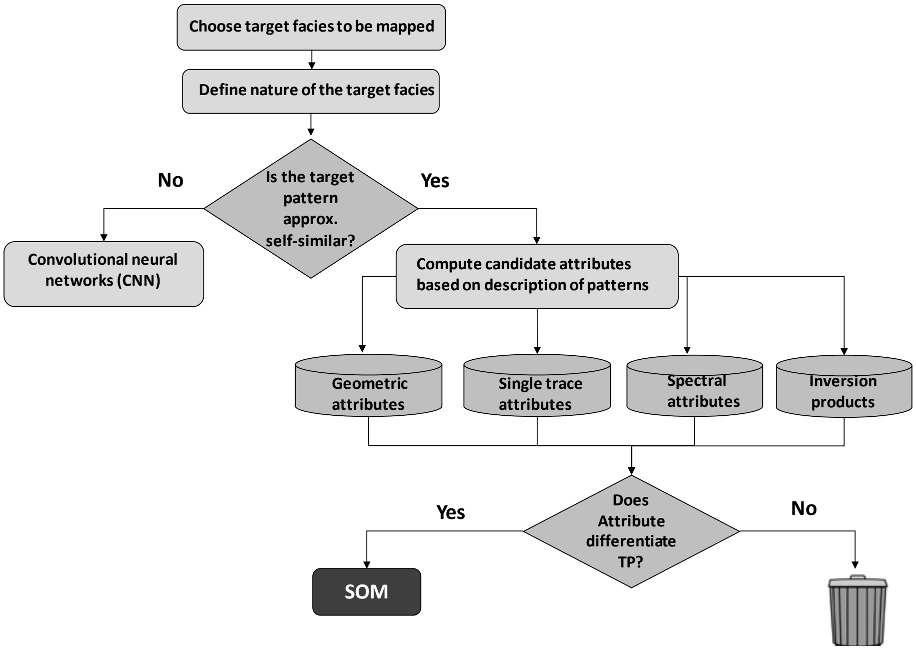

Figure 3.12. Proposed workflow to decide clustering of the patterns approach in seismic data.

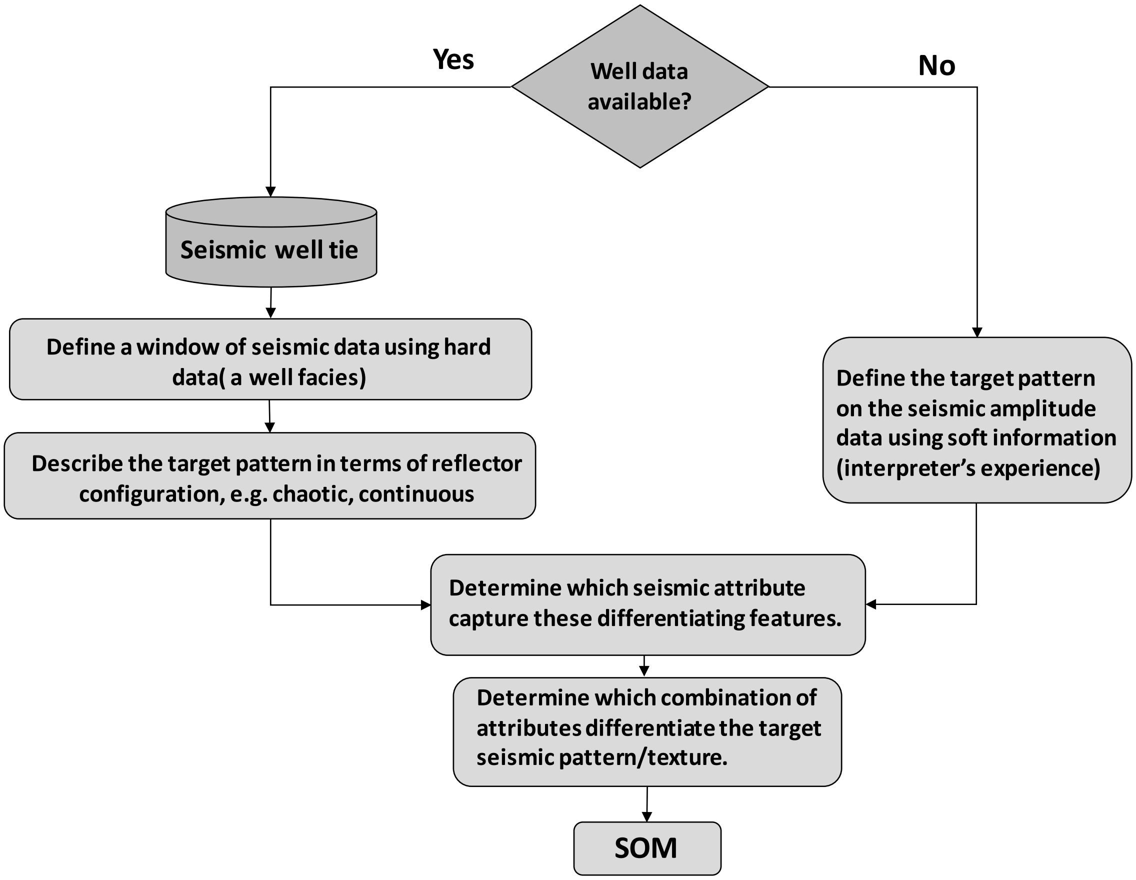

Figure 3.13. Proposed workflow to decide which seismic attributes to select for machine learning.

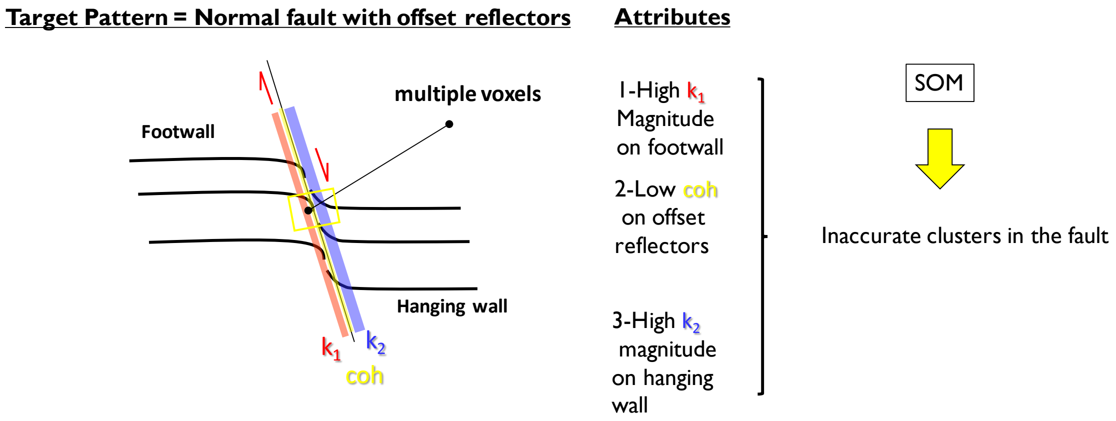

Figure 3.14. Cartoon showing a normal fault and its attribute response. Such red-yellow and blue pattern is easily recognized by a human interpreter. However, since they occur at laterally shifted voxels, they are more difficult to interpret for a machine. Most positive curvature, k1 (in red) illuminates the footwall, most negative curvature, k2 (in blue) illuminates the hanging wall, while coherence (in yellow) illuminates the fault discontinuity. After Qi, 2018.

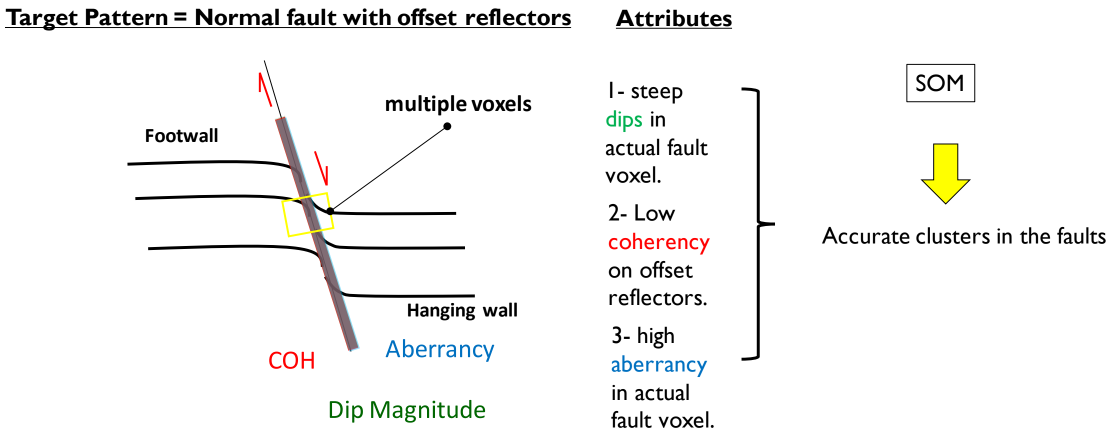

Figure 3.15. Cartoon showing the same normal fault as in the previous figure. The attributes are: Coherence, dip magnitude and aberrancy (Qi and Marfurt 2018). These three attributes image the fault at the exact same location (voxel) and are therefore amenable to machine learning for clustering). After Qi, 2018.

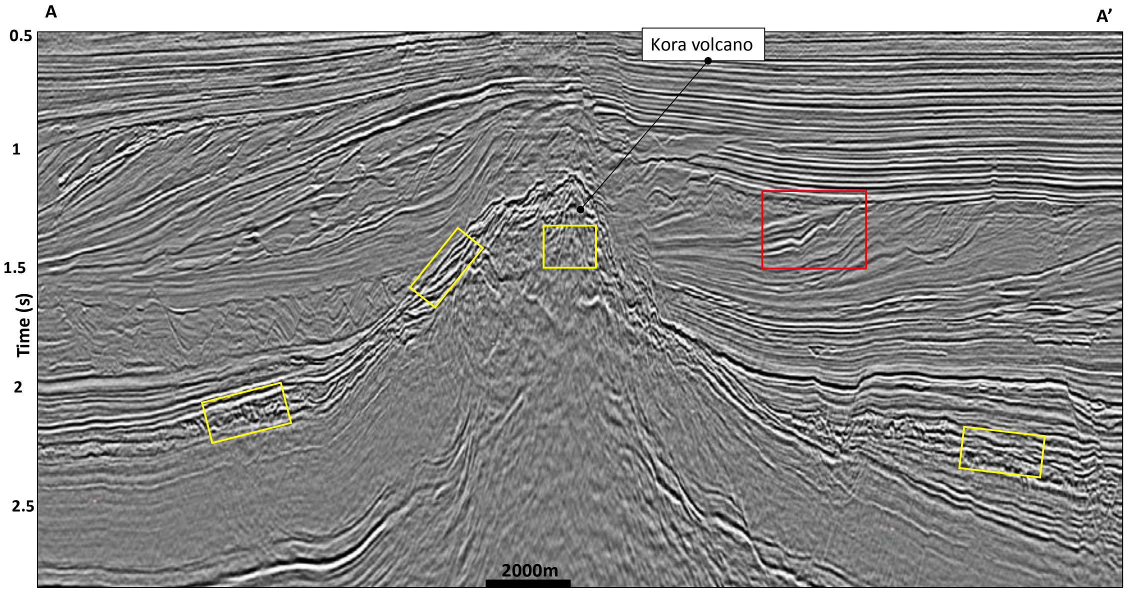

Figure 3.16. Same vertical amplitude slice as in Figure 3.3. The color scale has been changed to black and white, to facilitate co-rendering with seismic attributes. Yellow boxes represent extrusive volcanics and volcaniclastics. Seismic data courtesy of NZP&M.

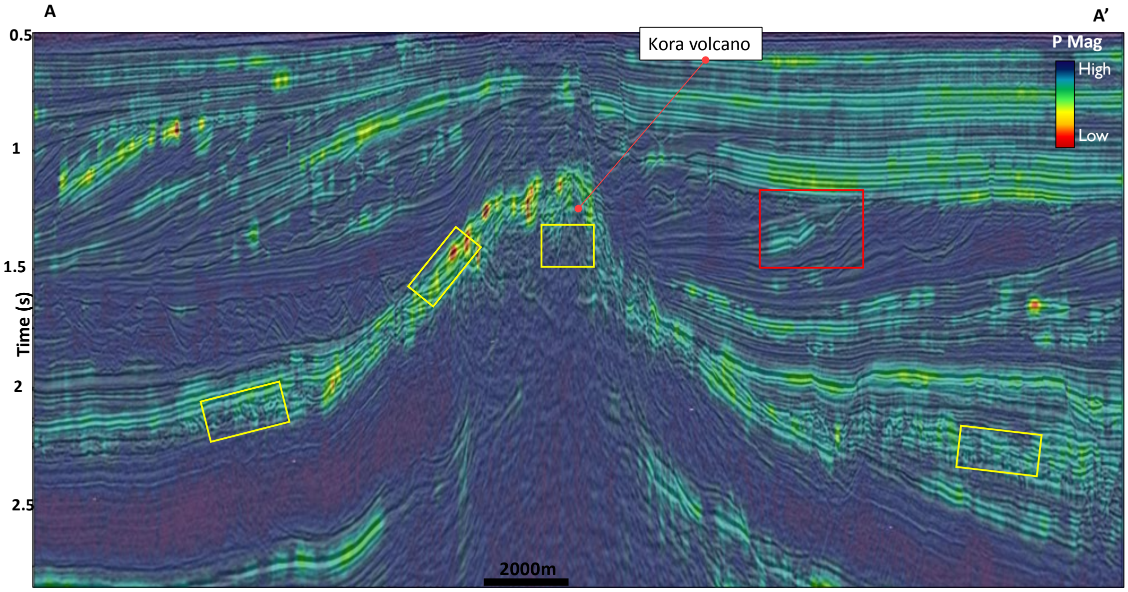

Figure 3.17. Vertical amplitude slice co-rendered with peak spectral magnitude. Same seismic section as in Figure 3.3. Yellow boxes represent extrusive volcanics and volcaniclastics. Seismic data courtesy of NZP&M.

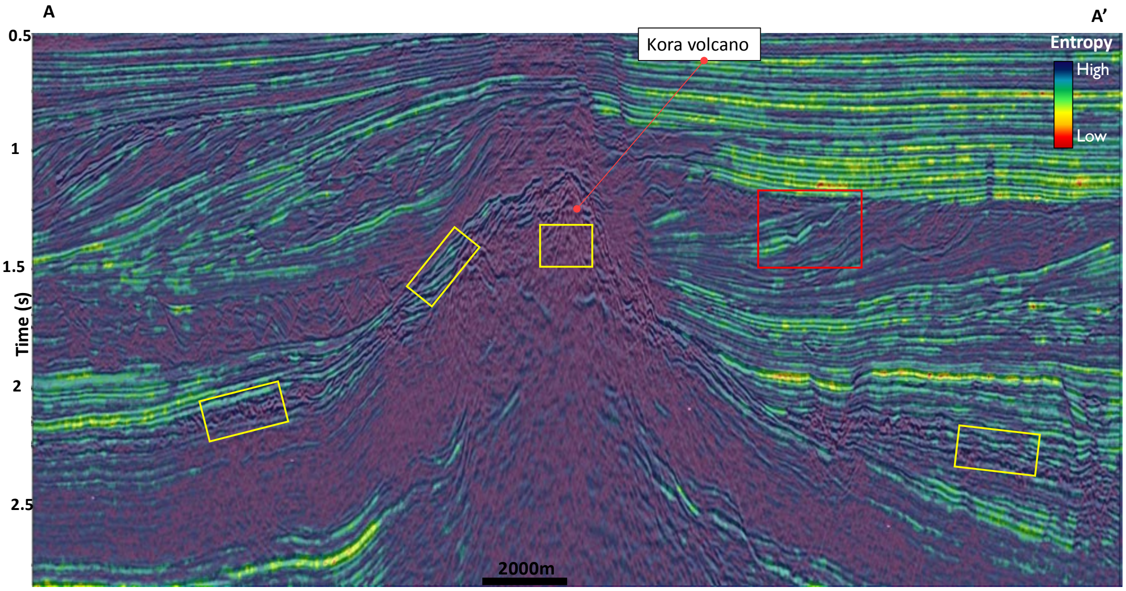

Figure 3.18. Vertical amplitude slice co-rendered with GLCM entropy. Same seismic section as in Figure 3.3. Yellow boxes represent extrusive volcanics and volcaniclastics. Seismic data courtesy of NZP&M.

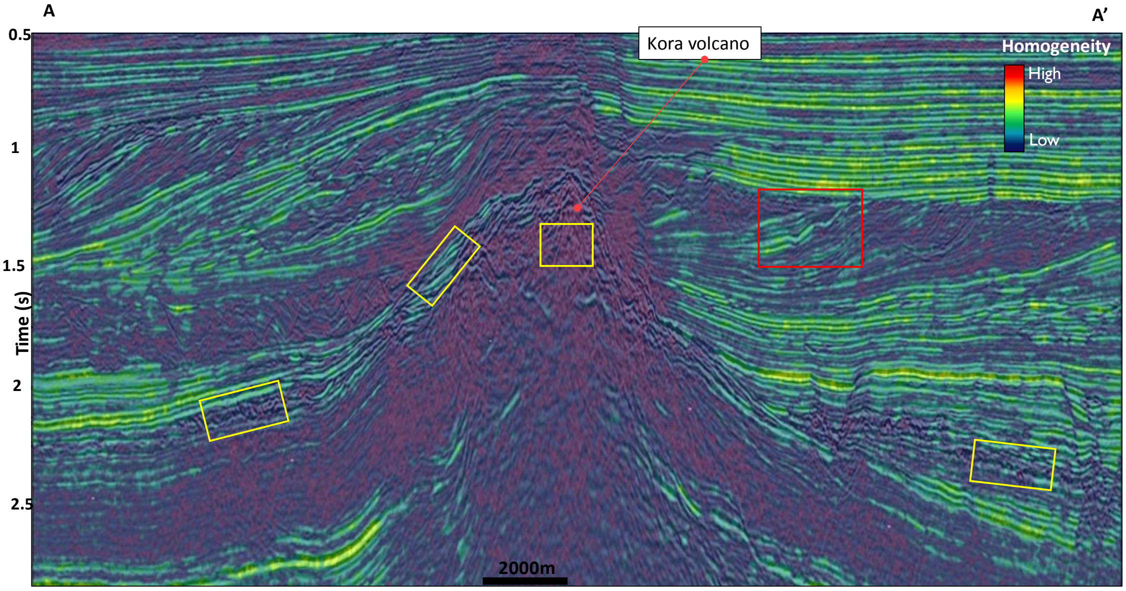

Figure 3.19. Vertical amplitude slice co-rendered with GLCM homogeneity. Same seismic section as in Figure 3.3. Yellow boxes represent extrusive volcanics and volcaniclastics. Seismic data courtesy of NZP&M.

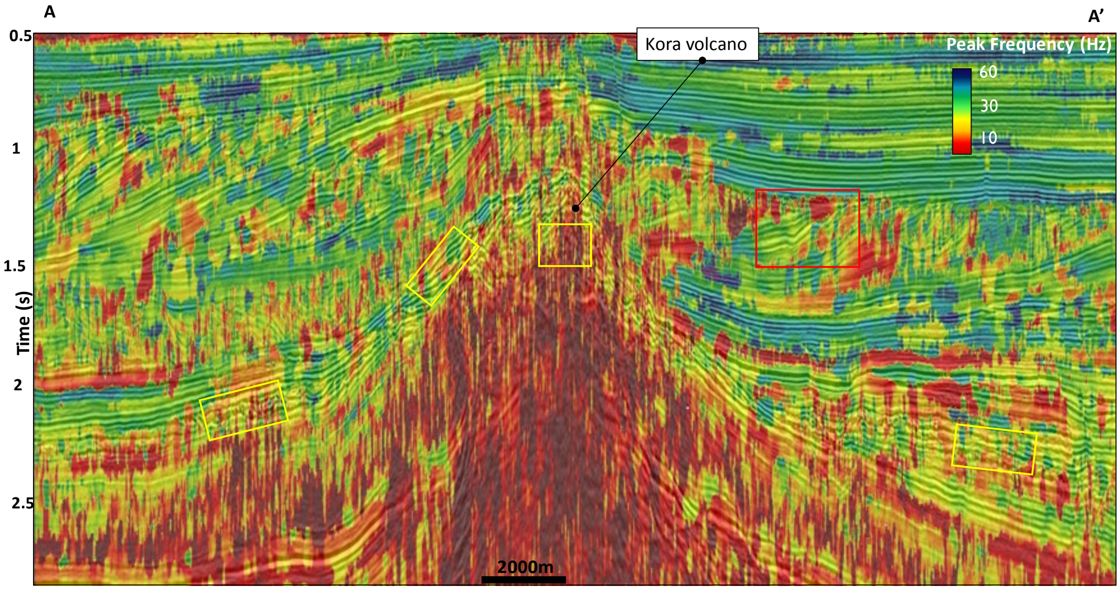

Figure 3.20. Vertical amplitude slice co-rendered with Peak spectral freq. Same seismic section as in Figure 3.3. Yellow boxes represent extrusive volcanics and volcaniclastics. Seismic data courtesy of NZP&M.

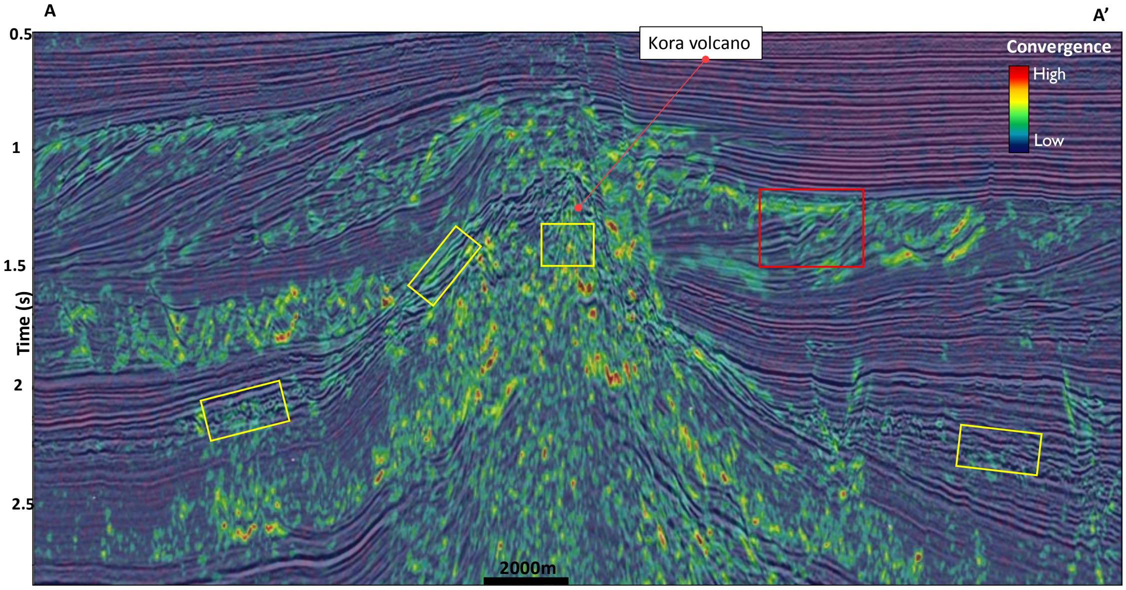

Figure 3.21. Vertical amplitude slice co-rendered with magnitude of reflector convergence. Same seismic section as in Figure 3.3. Yellow boxes represent extrusive volcanics and volcaniclastics. Seismic data courtesy of NZP&M.

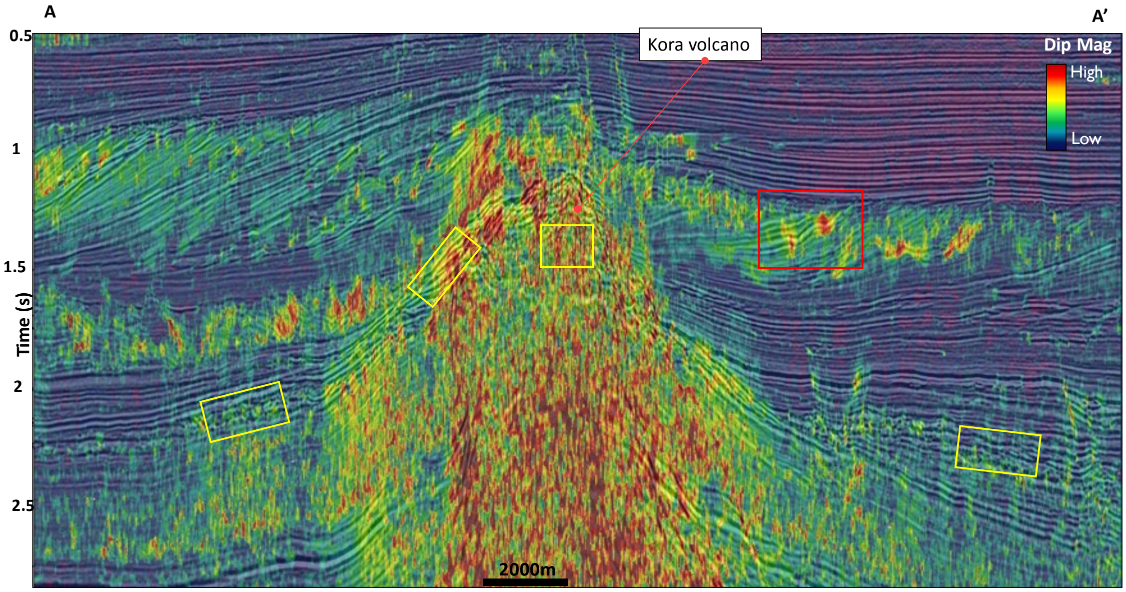

Figure 3.22. Vertical amplitude slice co-rendered with dip magnitude. Same seismic section as in Figure 3.3. Yellow boxes represent extrusive volcanics and volcaniclastics. Seismic data courtesy of NZP&M.

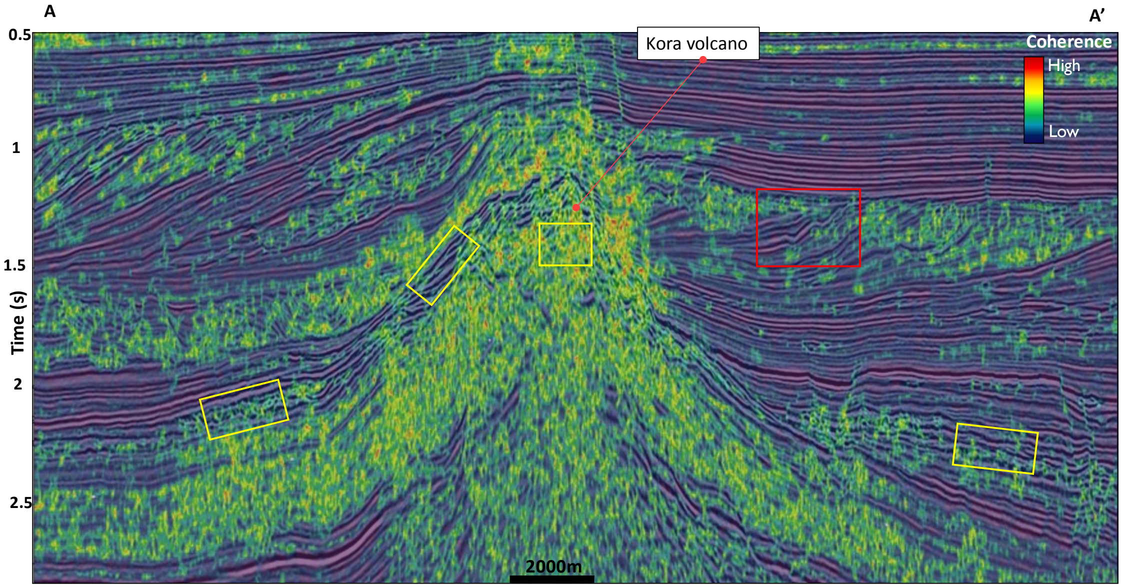

Figure 3.23. Vertical amplitude slice co-rendered with coherence. Same seismic section as in Figure 3.3. Yellow boxes represent extrusive volcanics and volcaniclastics. Seismic data courtesy of NZP&M.

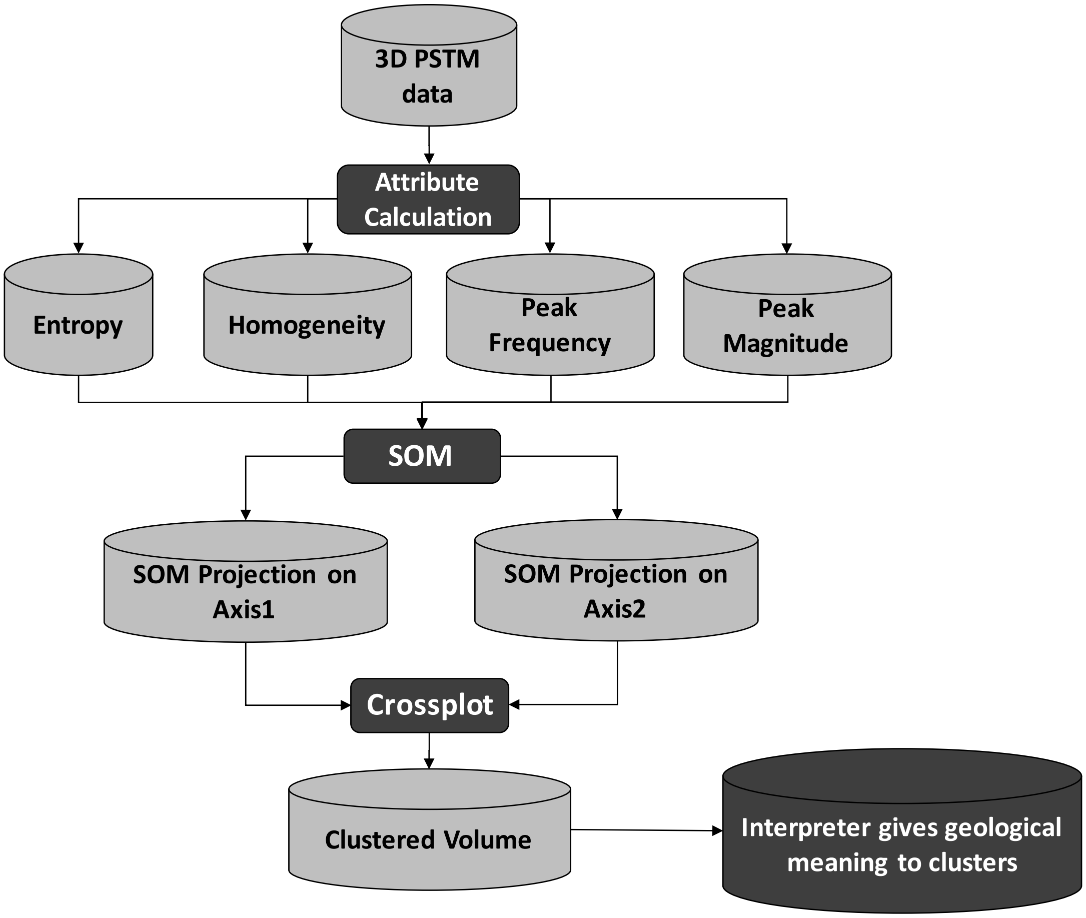

Figure 3.24. Workflow implemented for clustering analysis using Self-Organizing maps (SOM).

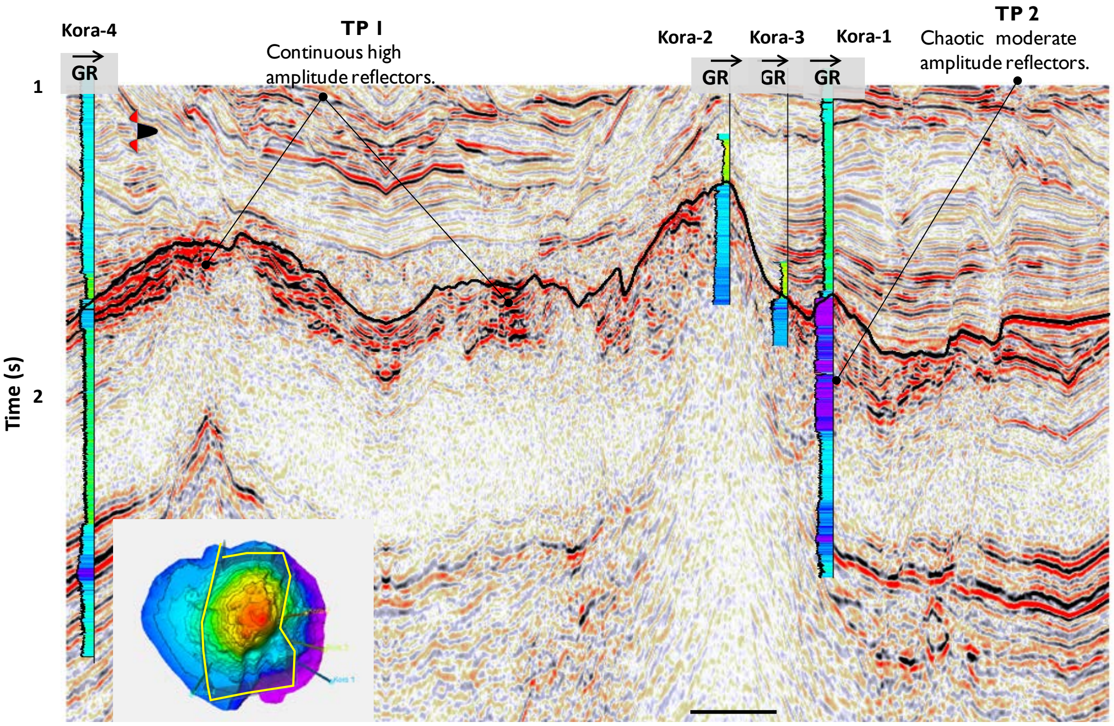

Figure 3.25. Vertical section connecting the four Kora wells through the seismic amplitude volume showing the distribution of TP 1 and TP 2. (After Infante-Paez and Marfurt 2017). Seismic data courtesy of NZP&M.

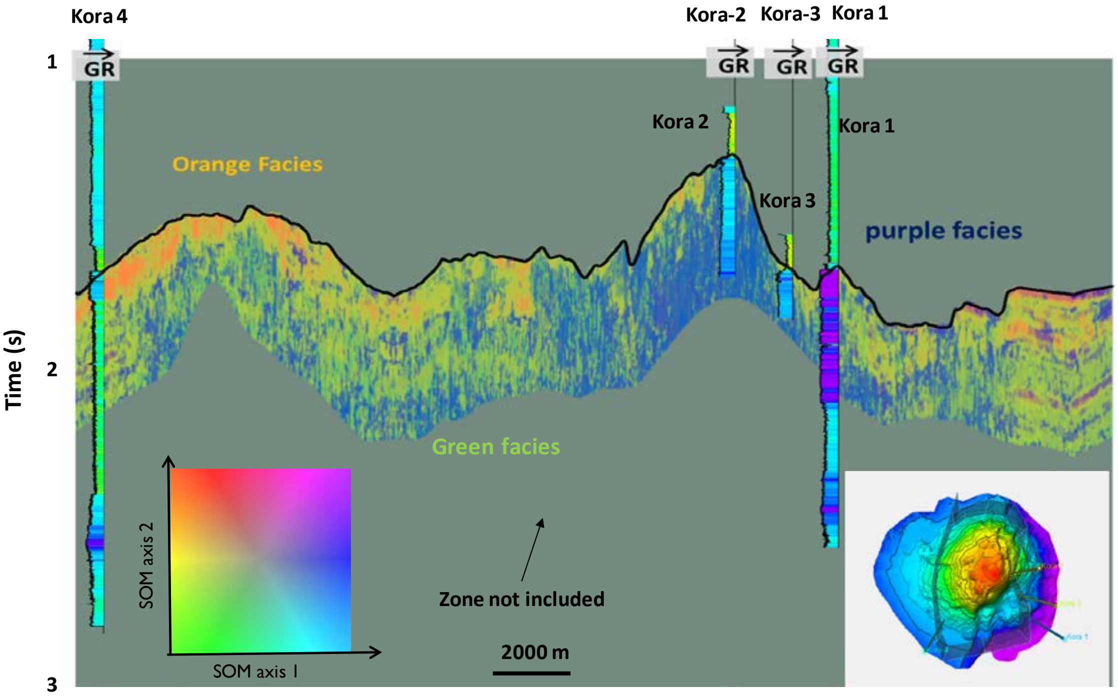

Figure 3.26. Vertical slice connecting the four Kora wells through the SOM clusters showing the two distinctive colors (purple-ish and yellow-ish) indicating two different facies. The green facies represent clastic sediments. Facies are colored based on the latent space projection. (After Infante-Paez and Marfurt 2017) Seismic data courtesy of NZP&M**.**

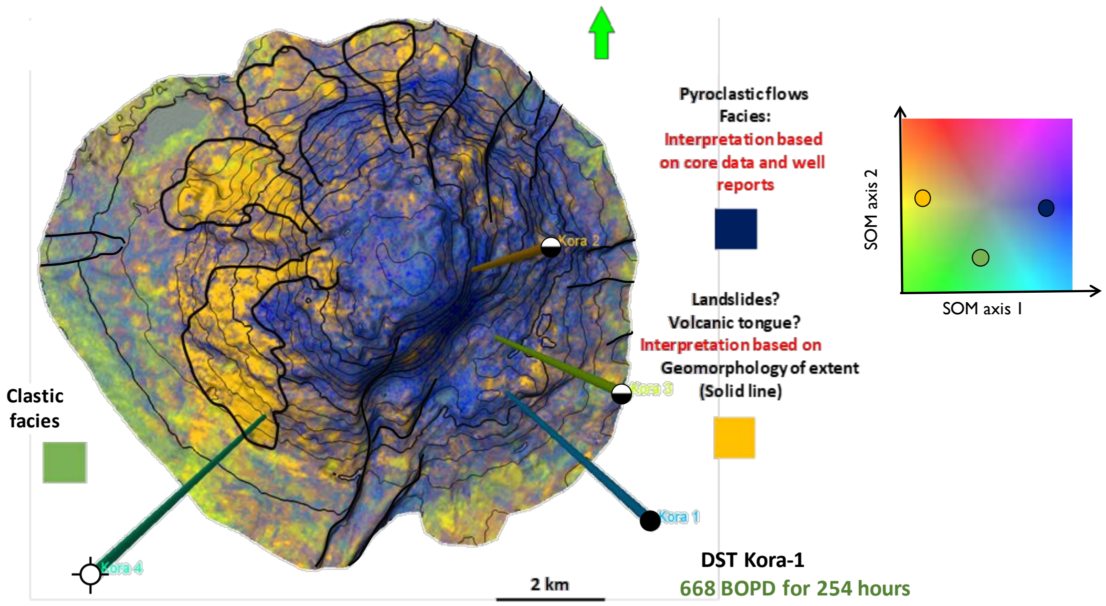

Figure 3.27. SOM clusters extracted along the top of Kora structure map. Core descriptions provided in the well completion reports for wells Kora-1,2 and 3 indicate the purple facies to be pyroclastic flows. In contrast, based on their geomorphology and structural relation to the volcanic cone the yellow/orange facies are interpreted to be lava flows such as those reported by Klarner and Klarner (2012) and Holford et al. (2012). Clusters are colored based on the latent space axes. (After Infante-Paez and Marfurt 2017)

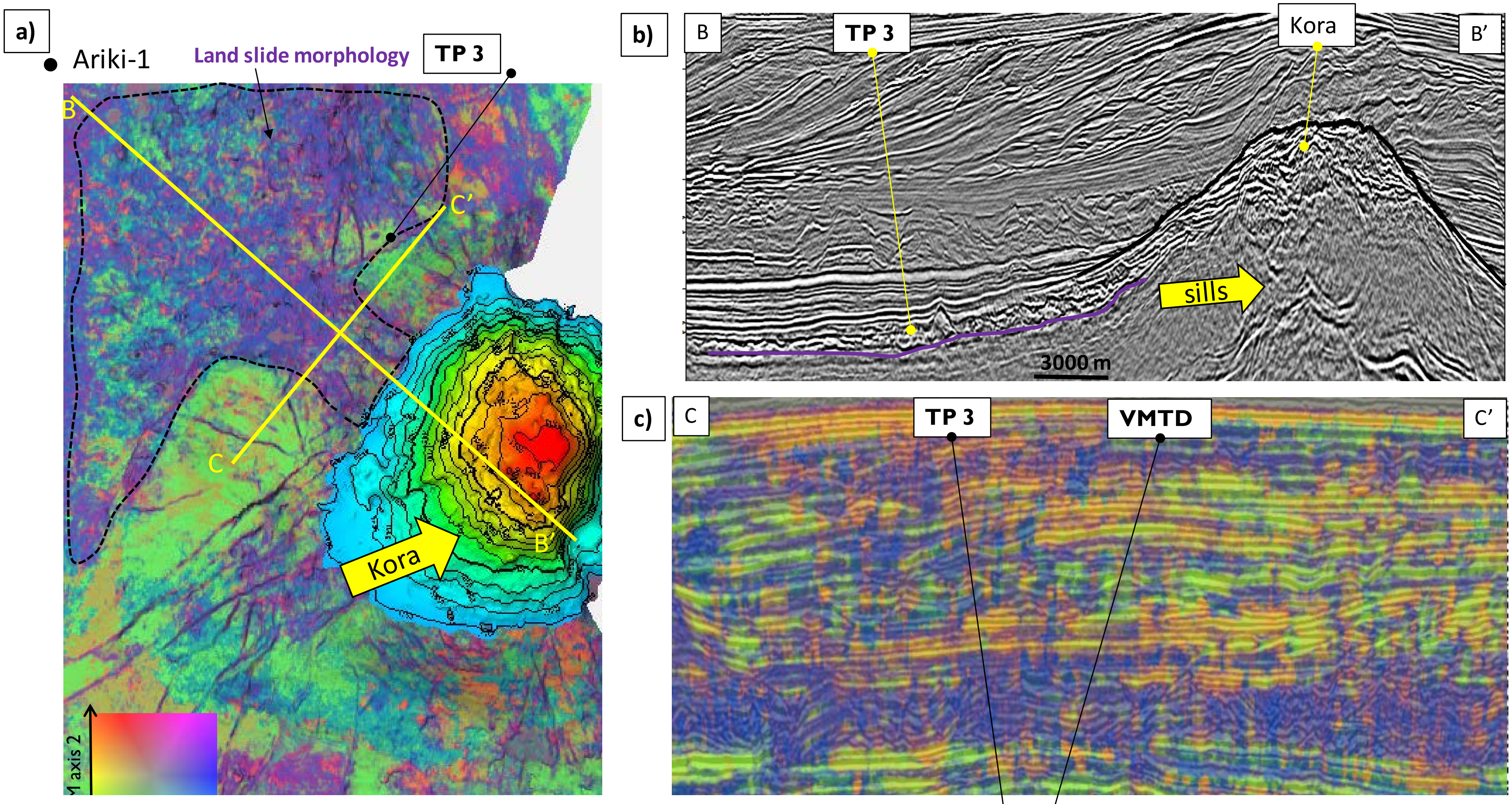

Figure 3.28. (a) SOM clusters extracted on a slice horizon close to the base of the Kora volcano indicated by the purple pick in (b). The colors in the horizon slice indicate similar facies (similar colors= similar facies) Notice the purple-ish colors in a fan-like geometry with a ~ 2 km scour, suggesting TP 3 are associated with a land slide from the west flank of the Kora volcano (b) A vertical slice through the seismic amplitude volume inside the subaqueous flow showing the extension of TP 3. (c) A vertical slice perpendicular to that in (b) through co-rendered amplitude and SOM clusters. Notice the distinct purple facies associated with the land slide or Volcanic Mass transport Deposit (VMTD).

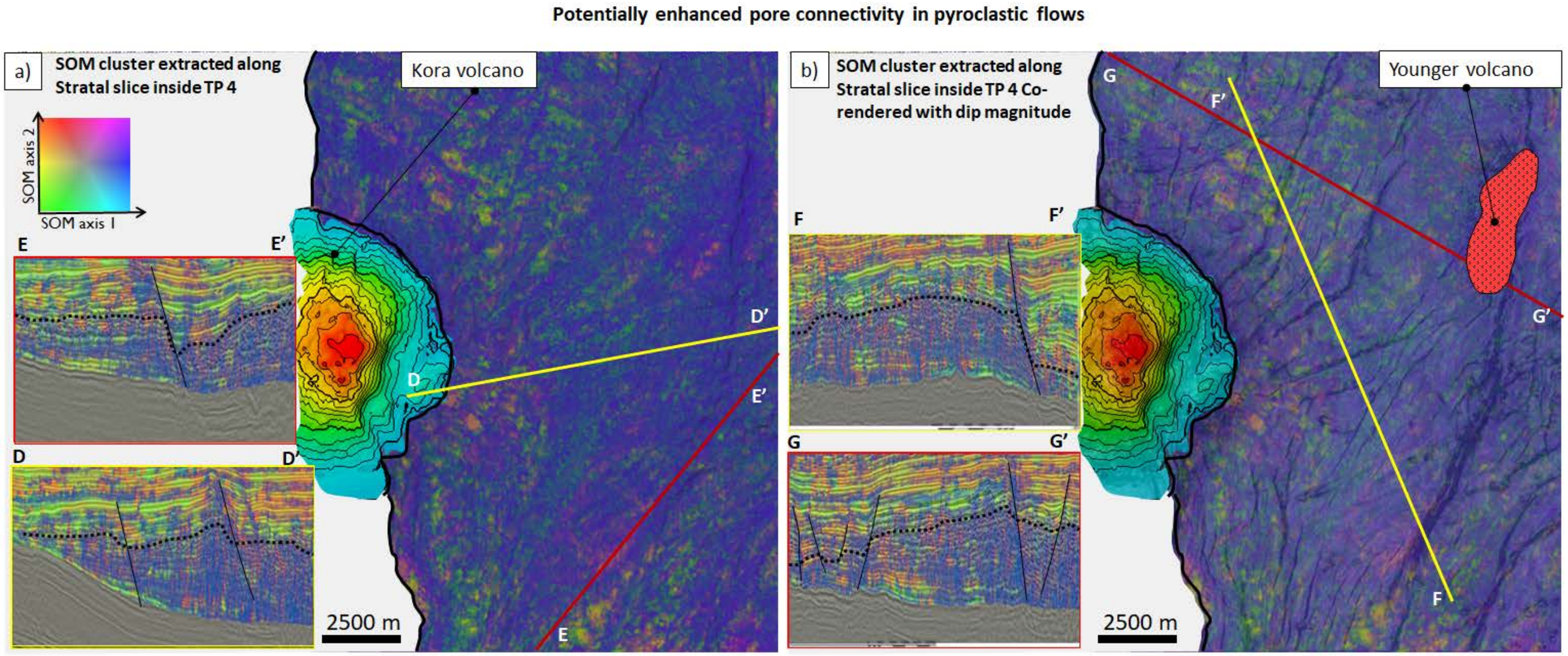

Figure 3.29. (a) SOM clusters extracted along a stratal slice inside the volcanics onlapping the eastern flanks of the Kora volcano (b) The same image co-rendered with dip magnitude attribute highlighting the normal faults. The area is completely dominated by the purple facies which according to Albacore-1 they are andesitic detritus probably derived from pyroclastic flows from adjacent younger volcanoes to the East of Kora.

REFERENCES

Coleou, T., M. Poupon, and K. Azbel, 2003, Unsupervised seismic facies classification: A review and comparison of techniques and implementation: The Leading Edge, 22, 942–953, doi: 10.1190/1.1623635

Crown Minerals, Albacore-1 well completion report. 2016. Web. 12 Dec. 2016. Petroleum Report Series PR 4183.

Crown Minerals, Ariki-1 Well. PPL38048. 2016. Web. 12 Dec. 2016. Petroleum Report Series PR 1038.

Crown Minerals, Ariki-1 Well. PPL38048. 2016. Web. 12 Dec. 2016. Petroleum Report Series PR 1038.

Crown Minerals, Capillary pressure and XRD mineralogy study of Kora Wells. 2016. Web. 12 Dec. 2016. Petroleum Report Series PR 4178.

Crown Minerals, Final Well Report, Kora-1 Kora-1A. PPL 38447. 2016. Web. 12 Dec. 2016. Petroleum Report Series PR 1374.

Crown Minerals, Final Well Report, Kora-2. PPL 38447. 2016. Web. 12 Dec. 2016. Petroleum Report Series PR 1441.

Crown Minerals, Final Well Report, Kora-3. PPL 38447. 2016. Web. 12 Dec. 2016. Petroleum Report Series PR 1441.

Crown Minerals, Final Well Report, Kora-4. PPL 38447. 2016. Web. 12 Dec. 2016. Petroleum Report Series PR 1443.

Crown Minerals, Hydrocarbon characterization study Tangaroa Play. 2016. Web. 12 Dec.

Dallas, B. D., L. J. Wood, and L. G. Moscardelli, 2013, Seismic geomorphology of early North Atlantic sediment waves, offshore northwest Africa: Interpretation, 1, no. 1, SA75–SA91, doi: 10.1190/INT-2013-0040.1.

Dasgupta, R., 2013, Determination of the fractal dimension of a shore platform profile: Journal of the Geological Society of India, 81, no. 1, 122–128, doi:10.1007/s12594-013-0011-0.

Dimri, F. V. P., R. P. Srivastava, and N. Vedanti, 2011, Encyclopedia of Solid Earth Geophysics: no. 1, doi:10.1007/978-90-481-8702-7.

Gao, D., 2003, Volume texture extraction for 3D seismic visualization and interpretation: Geophysics, 68, 1294– 1302, doi: 10.1190/1.1598122

Gao, Z., W. Tian, L. Wang, Y. Shi, and M. Pan, 2017, Emplacement of intrusions of the

Tarim Flood Basalt Province and their impacts on oil and gas reservoirs: A 3D seismic reflection study in Yingmaili fields, Tarim Basin, northwest China: Interpretation, 5, no. 3, SK51-SK63, doi:10.1190/INT-2016-0165.1.

Giba, M., A. Nicol, and J. Walsh, 2010, Evolution of faulting and volcanism in a back-arc basin and its implications for subduction processes: Tectonics, 29, TC4020, doi: 10.1029/2009TC002634.

Hall-Beyer, M., 2007, The GLCM tutorial, version 2.10, http://www.fp.ucalgary.ca/mhallbey/tutorial.htm, accessed 1 December 2016

Hansen, R. J., and P. J. J. Kamp, 2004, Late miocene to early pliocene stratigraphic record in northern taranaki basin: Condensed sedimentation ahead of northern graben extension and progradation of the modern continental margin: New Zealand Journal of Geology and Geophysics, 47, no. 4, 645–662, doi:10.1080/00288306.2004.9515081.

Holford, S., N. Schofield, J. MacDonald, I. Duddy, and P. Green, 2012, Seismic analysis of igneous systems in sedimentary basins and their impacts on hydrocarbon prospectivity: examples from the southern Australian margin: The APPEA Journal, 52, no. 1, 229-252, doi:10.1071/AJ11017.

Infante-Paez, L., and K. J. Marfurt, 2017, Seismic expression and geomorphology of igneous bodies: A Taranaki Basin, New Zealand, case study: Interpretation, 5, no. 3, SK121-SK140, doi:10.1190/INT-2016-0244.1.

Kartanegara, A.L., Baik, R.N. and Ibrahim, M.A., 1996, Volcanics oil bearing in Indonesia: American Association of Petroleum Geologists, A73.

Klarner, S., B. Ujetz, R. Fontana, and J. Altenkirch, 2006, Seismic signature of Upper Cretaceous volcanics; Santos Basin, Brazil: 68th Annual International Conference and Exhibition, EAGE, Extended Abstracts, 105.

Klarner, S. and O., Klarner, 2012, Identification of paleo-volcanic rocks on seismic data: In Updates in Volcanology-A Comprehensive Approach to Volcanological Problems, InTech.

Kumar, P. C., and A. Mandal, 2017, Enhancement of fault interpretation using multi-attribute analysis and artificial neural network (ANN) approach: a case study from Taranaki Basin, New Zealand: Exploration Geophysics, in press. doi:10.1071/EG16072.

Lam, N. S. N., and D. Quattrochi, 1992, On the issues of scale, resolution, and fractal analysis in the mapping sciences: Professional Geographer, 44, no. 1, 88–98, doi:10.1111/j.0033-0124.1992.00088.x.

Lee, C., J. A. Nott, F. B. Keller, and A. R. Parrish, 2004, Seis- mic expression of the Cenozoic mass transport complexes, deepwater Tarfaya-Agadir Basin, offshore

Morocco: Offshore Technology Conference, 16741.

Lubo-Robles, D., 2018, Development of Independent Component Analysis for reservoir geomorphology and unsupervised seismic facies classification in the Taranaki Basin, New Zealand: Master's thesis, University of Oklahoma.

Magee, C., E. Hunt-Stewart, and C. A. L. Jackson, 2013, Volcano growth mechanisms and the role of sub-volcanic intrusions: Insights from 2D seismic reflection data: Earth and Planetary Science Letters, 373, 41–53, doi:10.1016/j.epsl.2013.04.041.

Marfurt, K.J., 2018, Seismic attributes as the Framework for Data Integration Throughout the Oilfield Life Cycle: Distinguished instructor series, no. 21.

Mark, N. J., N. Schofield, S. Pugliese, D. Watson, S. Holford, D. Muirhead, R. Brown, and D. Healy, 2017, Igneous intrusions in the Faroe Shetland basin and their implications for hydrocarbon exploration; new insights from well and seismic data: Marine and Petroleum Geology, in press, doi:10.1016/j.marpetgeo.2017.12.005.

Matos, M., M. Yenugu, S. M. Angelo, and K. J. Marfurt, 2011, Integrated seismic texture segmentation and cluster analysis applied to channel delineation and chert reservoir characterization: Geophysics, 76, no. 5, P11–P21, doi: 10.1190/geo2010-0150.1.

McArdle, N., D. Iacopini, M. A. KunleDare, and G. S. Paton, 2014, The use of geologic expression workflows for basin scale reconnaissance: A case study from the Exmouth Subbasin, North Carnarvon Basin, northwestern Australia: Interpretation, 2, no. 1, SA163–SA177, doi: 10 .1190/INT-2013-0112.1.

Meldahl, P., Heggland, R., Bril, B., and de Groot, P., 2001, Identifying fault and gas chimneys using multi-attributes and neural networks: The Leading Edge, 20, 474–482. doi:10.1190/1.1438976

Olorunsola, O., J. Qi, L. Infante, B. Hutchinson, and K. Marfurt, 2016, Multiattribute seismic-facies expressions of a complex granite wash formation: A Buffalo Wallow field illustration: SEG Technical Program Expanded Abstracts 2016, 1884–1888, doi:10.1190/segam2016-13946878.1.

Posamentier, H.W., V. Kolla, 2003, Seismic geomorphology and stratigraphy of depositional elements in deep-water settings. Journal of Sedimentary Research, 73, 367-388.

Qi, J., T. Lin, T. Zhao, F. Li, and K. Marfurt, 2016, Semisupervised multiattribute seismic facies analysis: Interpretation, 4, no. 1, SB91-SB106, doi:10.1190/INT-2015-0098.1.

Qi, X., 2018, Seismic attribute assisted quantitative characterization for unconventional reservoirs: Ph.D. dissertation, The University of Oklahoma.

Roden, R., T. Smith, and D. Sacrey, 2015, Geologic pattern recognition from seismic attributes: Principal component analysis and self-organizing maps: Interpretation, 3, no. 4, SAE59–SAE83, doi: 10.1190/INT-2015- 0037.1.

Roy, A., B. Dowdell, and K. Marfurt, 2013, Characterizing a Mississippian tripolitic chert reservoir using 3D unsupervised and supervised multiattribute seismic facies analysis: An example from Osage County,: Interpretation for unconventional resources, 1, no. 2, 109–124, doi:10.1190/segam2012-1365.1.

Sinha, S., D. Devegowda, and B. Deka, 2016, Multivariate Statistical Analysis for Resource Estimation in Unconventional Plays Application to Eagle Ford Shales: Society of Petroleum Engineers. doi:10.2118/184050-MS.

Sinha, S., K. Marfurt, D. Devegowda, R. Lima, and S. Verma, 2017, Seismic Inversion Based SRV and Reserves Estimation for Shale Plays: Society of Petroleum Engineers. doi:10.2118/187137-MS.

Snyder, J., 2016, Correlating rate of penetration and bit trips to 3D surface seismic data, anadarko shelf, Oklahoma: M.S. Thesis, The University of Oklahoma.

Somasundaram, S., S. Bhat, A. Das, B. Mund, A. Beohar, and P. Shankar, 2017, Fracture detection and calibration in a tight volcanic gas reservoir, Barmer Basin, In- dia: First Break, 35, 101–106.

Verma S., A. Roy, R. Perez, and K.J. Marfurt, 2012, Mapping high frackability and high TOC zones in the Barnett Shale: Supervised Probabilistic Neural Networks vs. unsupervised multi-attribute Kohonen SOM: 82nd SEG Annual Meeting, 1-5, doi: 10.1190/segam2012-1494.1

West, P. B., R. S. May, E. J. Eastwood, and C. Rossen, 2002, Interactive seismic facies classification using textural attributes and neural networks: The Leading Edge, 21, 1042–1049, doi: 10.1190/1.1518444.

Zhao, T., F. Li, and K. J. Marfurt, 2017, Seismic attribute selection for unsupervised seismic facies analysis using user guided data-adaptive weights: Geophysics, 83, no. 2, 1–62, doi:10.1190/geo2017-0192.1.

Zhao, T., J. Zhang, F. Li, and K. J. Marfurt, 2016, Character- izing a turbidite system in Cantebury Basin, New Zealand, using seismic attribute and distance-preserving self-organizing maps: Interpretation, 4, no. 1, SB79–SB89, doi: 10.1190/INT-2015-0094.1.

CHAPTER 4

MEGA FORCED FOLDS ASSOCIATED WITH ANDESITIC VOLCANOES IN TARANAKI BASIN, NEW ZEALAND: IMPLICATIONS FOR HYDROCARBON EXPLORATION.

ABSTRACT

Subduction related volcanism like that seen in the Taranaki Basin, New Zealand can create structural deformations of varying orders of magnitude within the host rock. Such deformations include folding in both the strata that pre-dates and post-dates the volcanism. Similar types of folds have been commonly found to create structural closures of ~10 km^2 in extensional basins due to the emplacement of igneous sill. By performing seismic-to-well ties, three-dimensional (3D) mapping of the Eocene, Miocene and younger strata and examination of well completion reports, I show that there are spatial and causal relationships between andesitic volcanos and forced folds with structural closure of >20 km^2 that have the potential to host economic accumulation of hydrocarbons. Contractional deformation in the pre-magmatic sequence is interpreted to be due to elastic bending induced by the emplacement of a magma chamber within the upper crust at a unknown depth, where the deformed area extends across ~170 km^2 with a relief of up to 800 m. Whereas, deformation of the post-magmatic sequence is developed through differential compaction of the overlying softer sediments around the more rigid andesitic volcanoes. Here, I introduce the term “Mega Forced Folds”, to describe forced folds of >20 km^2 and could be as large as 170 km^2. These large structural closures are important because of their potential hydrocarbon storage capacity. In this study, a Mega forced fold in the post-magmatic sequence measures ~76 km^2, which if filled with

hydrocarbons could hold >1 billion of barrels of oil in place, assuming the presence of a mature source rock and charge (to spill point) of migrated hydrocarbons into the trap. Finding that demonstrates previously unidentified positive impacts to hydrocarbon exploration in sedimentary basins associated with subduction related volcanisms.

INTRODUCTION

Igneous bodies in sedimentary basins can have both a positive and/or negative impact on hydrocarbon exploration. For example, in some cases, the thermal effects of igneous intrusions can beneficially affect the maturity of source rocks, by increasing the geothermal gradient and placing immature source rocks within the oil window (Chen et al., 1999; Rodriguez Monreal et al., 2009; Holford et al., 2013). In other cases, this increase in temperature may adversely affect the maturity of hydrocarbons by overcooking the source rock (Barber, 1988; Kingston and Matzko, 2015). Buried volcanoes can potentially provide pathways for vertical fluid migration due to the higher bulk permeability of the volcanic complex compared to the surrounding sediments (Holdford et al., 2017). Igneous rocks can also act as seals and traps (Holford et al., 2013). If fractured, igneous rocks can serve as migration pathways (Rateau et al., 2013) or form the reservoir (Kartanegara et al., 1996; Schutter, 2003; Rodriguez and Montreal 2009; Zhang and Marfurt, 2011;). Deformation of the host rocks induced by igneous bodies, can result in forced folds. Forced fold were first defined by Stearns, (1978) as “folds in which the overall shape and trend are dominated by the shape of a forcing member below”. During the past two decades, several studies have shown evidence of the relationship between igneous sills and overlying forced folds (Hansen and Cartwright, 2006; Jackson et al., 2013; Magee et al., 2014; Alves et al., 2015; Schmiedel et al., 2017; Infante-Paez and Marfurt, 2017).

In this chapter, I analyze a series of folds that are spatially related to andesitic volcanoes. In order to understand that spatial relationship, I examine several 2D and 3D seismic surveys from different locations that connect exploration wells that targeted four-way dip closure of deepwater reservoirs.

Drilling History in Permit PEP 38485 Offshore Taranaki Basin, New Zealand

A total of sixteen wells have been drilled in the permit area PEP 38485, where nine of them targeted structural traps associated with volcanic cones.

According to well completion reports, the Kora-1 well was drilled in the 1980's by Arco Petroleum NZ Inc. to test the Eocene Tangaroa Sandstone member with a large dome structure associated with a Miocene age "volcano". The well was drilled to a TD of 3421m (11,224 ft.) and encountered significant indications of hydrocarbons in the top of the Miocene volcanic section and in the upper and lower Tangaroa Sandstone. Results of three drill stem tests (DST) evaluating the Tangaroa shows indicated that the Tangaroa Sandstone member was a tight formation. However, the Miocene volcanic sections were tested as a sidetrack Kora-1A. A long-term production test was conducted which resulted in 32 API oil flow of 668 BOPD for 254 hours. Following the success of hydrocarbons found in the Miocene volcanic wells Kora-2, Kora-3 and Kora-4 were drilled to keep testing this volcanic potential. Only shows were found in wells Kora-2 and Kora-3 whereas Kora-4 was barren of hydrocarbons. Therefore, the 3D Kora seismic survey was acquired in 2006 with the objective of imaging the Miocene Kora Volcano.

Mangaa-1

The Mangaa-1 well was the first exploration well drilled to total depth of 3553m by Hematite Petroleum N.Z Ltd. The primary objective of this well was the structural closure of the Upper Miocene-Pliocene Mangaa sands. Although not discussed in the well report series, I hypothesize that the targeted structural closure was due to differential compaction over the deepwater Miocene-Pliocene sediments related to an older volcano below the target turbidities. The well was plugged and abandoned. (Awatea-1 well completion report series)

Te Kumi-1

The Te Kumi-1well spudded on 21 March 1988, drilled to a TD of 3824 m on 21 April 1988. The well was drilled as an exploratory well in the PEP 38485 permit area, offshore New Zealand in the Tasman sea. The primary objective of this well was to evaluate structural closure and potential hydrocarbon production of the Pleistocene, Miocene and Eocene sediments. The well was plugged and abandoned as a dry hole. No testing was done (Te-Kumi-1 well completion report series).

Tua-Tua-1

The primary objective of the Tua-Tua-1 well was the Upper Eocene Tangaroa Sandstone. This well was drilled in Taranaki Basin, targeting an anticline which is dissected by a series of normal faults. This structure has three-way dip closure and is dependent upon a graben-margin normal fault to the East for complete closure (Tua-Tua-1 well completion report series).

Kora wells

The Kora-1 well was drilled in 1988 by Arco Petroleum NZ Inc. to test the Eocene Tangaroa Sandstone member with a large dome structure associated with a Miocene age “volcano”. The well was drilled to a TD of 3421 m (11,224 ft.) and encountered significant indications of hydrocarbons in the top of the Miocene volcanic section and in the Upper and Lower Tangaroa Sandstone. Results of three drill stem tests (DSTs) evaluating the Tangaroa shows indicated that the Tangaroa Sandstone member was a tight formation. The Miocene volcanic sections were tested as a sidetrack Kora-1A. A long-term production test was conducted which resulted in 32 API oil flow of 668 BOPD for 254 hours. Following the success of hydrocarbons found in the Miocene volcanic wells Kora-2, Kora-3 and Kora-4 were drilled to keep testing this volcanic potential. Only shows were found in wells Kora-2 and Kora-3 whereas Kora-4 was barren of hydrocarbons. For this reason, the 3D Kora seismic survey was acquired in 2006 with the objective of imaging the Miocene Kora Volcano (Kora-1 well completion report). No further Kora wells have been drilled to date.

Awatea-1

Awatea-1 was spudded on 24 September 1996 and reached Td of 3255 m on October 1996 as a vertical wildcat well drilled on a structural closure, offshore North Taranaki Basin (PEP 38485). The primary objective of the well was to penetrate and evaluate the Pliocene Mangaa Sands. The Mangaa sands encountered exhibited good reservoir quality but were water bearing. No testing or coring was performed. Awatea-1. The well was plugged and abandoned (Awatea-1 well completion report series). Although not discussed in the well report series, I hypothesize that the structural closure was in part due to the faults associated with the compaction of the paleo-sediments where an andesitic volcano formed.

Albacore-1

Albacore-1 was a vertical exploration well designed to evaluate two series of Lower Pliocene and Upper Miocene turbidities. The target was a combined stratigraphic and dip closed turbidite fans, draping a mid-Miocene volcanic edifice in the North Taranaki Basin in permit PEP 38485, offshore Taranaki New Zealand (Alabacore-1 well report series).

Kanuka-1

The Kanuka-1 well spudded on 23 October 2007 and reached a total depth of 2879m TD on 1 November 2007. The primary objective was to evaluate the hydrocarbon potential of the Lower to Upper Miocene sand sequences laid down in a basin floor fan setting. These units have variously been called the Mt. Messenger sands, Mohakatino sands and Moki sands. Secondary objectives were to understand the stratigraphy and reservoir quality of other formations within the Pliocene and Miocene section. Structural closure had been mapped from the Late Miocene down to proposed TD using recently (2006) reprocessed 2D seismic data. Closure is subtle and is more pronounced on the depth maps than on the TWT maps. Although not discussed in the well report series, I hypothesize that the structural closure was due to differential compaction over the deepwater Miocene-Pliocene sediments related to an older volcano below the target turbidities. This well was plugged and abandoned (Kanua-1 well completion report series).

The remaining of the exploration wells drilled in PEP 38485 (Figure 4.1) targeted four-way dip closures of the Eocene turbidities. However, these structures were not associated with magmatism, but rather with basement highs (Moana-1 well completion report series).

Potential hydrocarbon traps associated with andesitic volcanoes.

Subduction related volcanism can produce giant domes with four-way dip closure both in the pre-magmatic and post-magmatic sequences. In the pre-magmatic sequence, the host rock is “jacked-up” due to the emplacement or growth of a magma chamber in the lower crust because of the partial melting of the subducting slab. Once volcanism has ceased and a volcanic cone becomes buried by sediments of the post-magmatic sequence, the sediments around the volcano suffer differential compaction because they are softer than the more rigid volcanic edifices, resulting in a dome structure.

Exploration in the offshore Northern Taranaki Basin began in the 1980s. In PEP 38485 most of these wells targeted deepwater deposits either from the Late Eocene or Mid to Early Miocene. Of the 16 exploration wells drilled in PEP 38485, only six of them did not target structural trap associated with volcanoes. (Figures 4.2-4.6), suggesting that volcanoes can be beneficial to hydrocarbon exploration.

Summarizing the drilling history of permit PEP 38485, the main target plays in this area exhibit four-way dip closure of Eocene and Miocene-Pliocene turbidities (Figures 4.2-4.6). I hypothesize that the four-way dip closure of Eocene turbidites are associated with the emplacement of magma chambers that fed different Miocene volcanoes. Following Bischoff et al.’s (2017) terminology for strata that predate and postdate volcanism, the Eocene turbiditie plays in this study area are “pre-magmatic” turbidite plays and the four-way dip closure of the Miocene-Pliocene turbidites associated with differential compaction of softer sediments deposited around the more rigid volcanic cones are “post-magmatic” turbiditie plays.

Since the nature of these four-way dip closures is very different, I distinguish them based on their mechanisms. The Mega forced folds of the pre-magmatic sequence are formed by elastic bending of the host rock similar to the deformation induced by intrusive sills (Schmiedel et al., 2017). Whereas the Mega forced folds formed by differential compaction of the post-magmatic sequence are created by the greater loss of porosity of the sedimentary rocks compared to the more rigid andesitic volcanoes (Hansen and Cartwright, 2006). Here, I introduce the prefix “Mega” to indicate structures with large (>20 km^2) four-way dip closure areas that formed above emplaced large igneous bodies (e.g., a magma chambers or andesitic stratovolcanoes), in contrast to the forced folds of ~10 km^2 of closure area formed by igneous sills documented by Hansen and Cartwright, (2006).

Mega forced folds Mechanisms

Elastic Bending

The elastic bending model, as presented by Hansen and Cartwright (2006) and Schmiedel et al. (2017) is associated with intrusive sills where the volume of the magma intruded is responsible for the amount of uplift in the host rock. Figure 4.7 shows a composite vertical section where wells Ariki-1, Moana-1 and Kora-4 penetrate the top Oligocene and the top Eocene. The available well control reveals a difference in relief of at least 400- 500 m (~500 ms TWT) in the Eocene strata and 500-600 m (~600 ms TWT) in the Oligocene strata. The total uplift should be more than the difference in elevation found in wells Moana-1 and Kora-4 (~400 m) because Kora-4 drilled the flank rather than the crest of the Eocene strata (Figure 4.7). In this portion of the basin (west of Taranaki Graben) tectonic activity is absent (Giba et al., 2013). Therefore, the difference in relief is likely related to volcanism. There is no reason the 600 m uplift had been produced by a single vertical pipe that fed the Kora volcano. Such pipes have been reported to range from tens to hundreds of meters. Following Morley (2018, in press) I suggest that this uplift is due to the emplacement of a magma chamber located at unknown depth. A similar magnitude in uplift (about 500-700ms TWT) can be seen in seismic sections imaging Tua-Tua, and Te-Kumi volcanoes (Figures 4.5-4.6).

In terms of the reservoir trapped by these forced folds, they would be dependent upon the original depositional environment prior volcanism. The Mega forced folds formed by an elastic bending mechanism can trap reservoirs from any depositional environment (e.g., carbonates, deepwater-shallow water clastics etc.)

Differential Compaction

In contrast to the elastic bending mechanism, differential compaction folds are formed after the igneous activity had ceased and the volcanoes became extinct. These folds form because the sediments are less rigid than the volcanic cone, and thus, compact more under the load of subsequent sedimentation. The expression for such mechanism is associated with a divergent geometry of the stratal reflections within the overburden because of a more gradual evolution of fold amplitude during vertical loading under increased burial (Hansen and Cartwright, 2006). Thus, the structural relief of the sediments deposited on top of the volcanoes appears to “heal” as the strata become stratigraphically younger away from the volcano (Figure 4.8). Since the andesitic volcanoes from the Mohakatino Volcanic Belt grew in a deep-water environment the sediments that buried them are mostly deep water clastic sediments. In some cases, they are not completely buried by deep water clastics and are late buried by progradation of the continental shelf (Figure 4.11). Thus, the Mega forced folds associated with a differential compaction mechanism could be trapping either deep water or shallow water sediments.

Due to insufficient 3D seismic data to image multiple volcanoes in the Taranaki Basin, I am unable to construct a quantitative relationship between the size of the volcanoes and the area and relief of such compactional folds. Nevertheless, based on less optimum 2D seismic surveys, that, I found a positive relationship regarding the size of the andesitic volcanoes and the size of the compactional fold (Figures 4.2, 4.3 and 4.8).

The Kora submarine volcano as an example of mega forced folds associated with andesitic volcanoes.

The excellent data quality and three dimensionality of the Kora 3D survey allows me to better study the geometry and dimensions of these Mega forced folds. Relying on Morley (2018), the size of the forced folds developed due to elastic bending will depend mostly upon the size of the magma chamber. Figure 4.9 shows the Mega forced folds associated with the Kora Volcano. Based on the well data (Figure 4.7), the structural relief induced by the hypothesized magma chamber that fed the plumbing system of the Kora Volcano is up to 800 m of uplift in an area of ~ 170 km^2 (~13x14 km) within the pre-magmatic sequence. The amplitude (800 m) and lateral coverage of the uplift (170 km^2) is validated by the difference in elevation between wells Moana-1 and Kora-4 (Figure 4.7). On the other hand, the post-magmatic sequence deposited about and above the volcano suffers differential compaction resulting in the development of Mega forced folds that have a closure area of about 76 km^2 and a vertical relief up to 200 m. The pink polygon in Figure 4.10a defines the aerial extension of the Kora volcano in comparison to that of the forced folds. The spatial relationship of the Mega forced folds and the Kora volcano indicates a causative relationship between the two.

I use a deterministic approach to estimate the hypothetical capacity the differential compaction Mega forced folds of the post-magmatic sequence could store, if fully filled to the spill point. I assume a net to gross ratio (N/G) of 50%, an average porosity (Ø) of 20%, an oil saturation (So) of 80%, and a formation volume factor for oil at initial condition (Boi) of 1. These are reasonable ranges for a shallow water uncompacted sandstone reservoir. The bulk rock volume (Vb) is calculated using the surface of the Pleistocene along with a constant spill plane via commercial seismic interpretation software, which gives a bulk rock volume Vb of ~16 billion barrels.

$$OOIP = \frac{(Vb)(N/G)\,(\emptyset)(So)}{\mathrm{Boi}}. \qquad (1)$$

Inputting these values into PetroWiki 2018’s variant of the Original Oil in Place (OOIP) equation (1), gives OOIP of ~ 1.28 billion barrels. Estimation of hypothetical hydrocarbon volumes for the pre-magmatic sequence becomes more difficult since these strata have also been deformed by the plumbing system of the Kora volcano such as, sills, dikes, and possibly laccoliths. However, based on the bulk rock volume Vb of ~400 billion of barrels results in an accumulation that is at least one order of magnitude larger than the one stored by the post-magmatic sequence, assuming the trap is filled to the spill point.

A critical factor is the environment of deposition in which the volcanoes grew. The Kora volcano is thought to have formed in a deep marine environment of about 1300 m of water depth (Kora-1 well report series). Therefore, sediments that began burying Kora were deep water clastic sediments (mostly mudstones). However, Kora became completely buried by the progradation of the clastic shelf (Figure 4.11), indicating that the four-way dip closure of the sediments in the compactional folds are shallow water sediments from the shelf that are Pleistocene in age sediments, rather than forced folds which trap deep water sediments.

Although only some wells have been drilled into the structural traps created by the andesitic volcanoes (Mohakatino Volcanic Belt) in the offshore Taranaki Basin, there is still tremendous potential where other similar-size and larger volcanoes occur and create Mega forced folds. (Figures slides 4.12-4.18). From these vertical slices it is possible to note that compactional folds exist at different stratigraphic levels associated with the more rigid andesitic volcanoes.

Figure 4.19 summarizes the main finding of this chapter showing three different andesitic volcanoes that form at different ages and present compactional folds above them. The sediments draping on each one of these volcanoes are of different age and may represent different depositional environments. Furthermore, although most of these volcanoes were mapped by Giba (2010), there may be additional andesitic volcanoes that have not been mapped by the 2D seismic surveys, promising a myriad of untapped different potential plays in Taranaki Basin, New Zealand.

LIMITATIONS

Although the interpretation and findings in this chapter were exclusively from offshore New Zealand, I emphasize that similar “Mega forced folds” do occur in various sedimentary basins where volcanism is associated with subduction.

CONCLUSIONS

Contrary to the common belief, volcanism can be of significant help in creating Mega forced folds (giant structural traps).

The interpretation of the 3D Kora seismic survey reveals that there is a causal spatial relationship between the Kora volcano and Mega forced folds in the strata that pre-dates and post-dates the formation of the Kora volcano. I find that building of the Kora volcano can cause: (1) deformation of the pre-magmatic strata creating large scale folds (>170 km^2) with a topographic relief of up to 800 m. Such deformation is probably due to a magma chamber growth or inflation into the upper crust. (2) development of large (≈80 km^2) folds with topographic relief of up to 200 m in the post-magmatic sequence through differential compaction of sediments deposited around the more rigid Kora volcano.

These Mega forced folds have the potential to create giant fields depending on the size of the emplaced magma chamber and the size of the resulting eruptive volcano. In the Taranaki Basin, New Zealand, these volumes are greater than 1 billion of barrels in the post-magmatic sequence and even larger volumes in the pre-magmatic sequence. Of course, the trap is only one element of the petroleum system. Therefore, there must be a mature source rock that can charge the previously formed traps through adequate migration pathways, and top and lateral sealing rocks that prevent the hydrocarbons from escaping the trap.

It is my hope that this study can help remove the misconception that volcanic systems only pose a direct threat to hydrocarbon exploration in sedimentary basins affected by volcanism.

Chapter 4 Figures

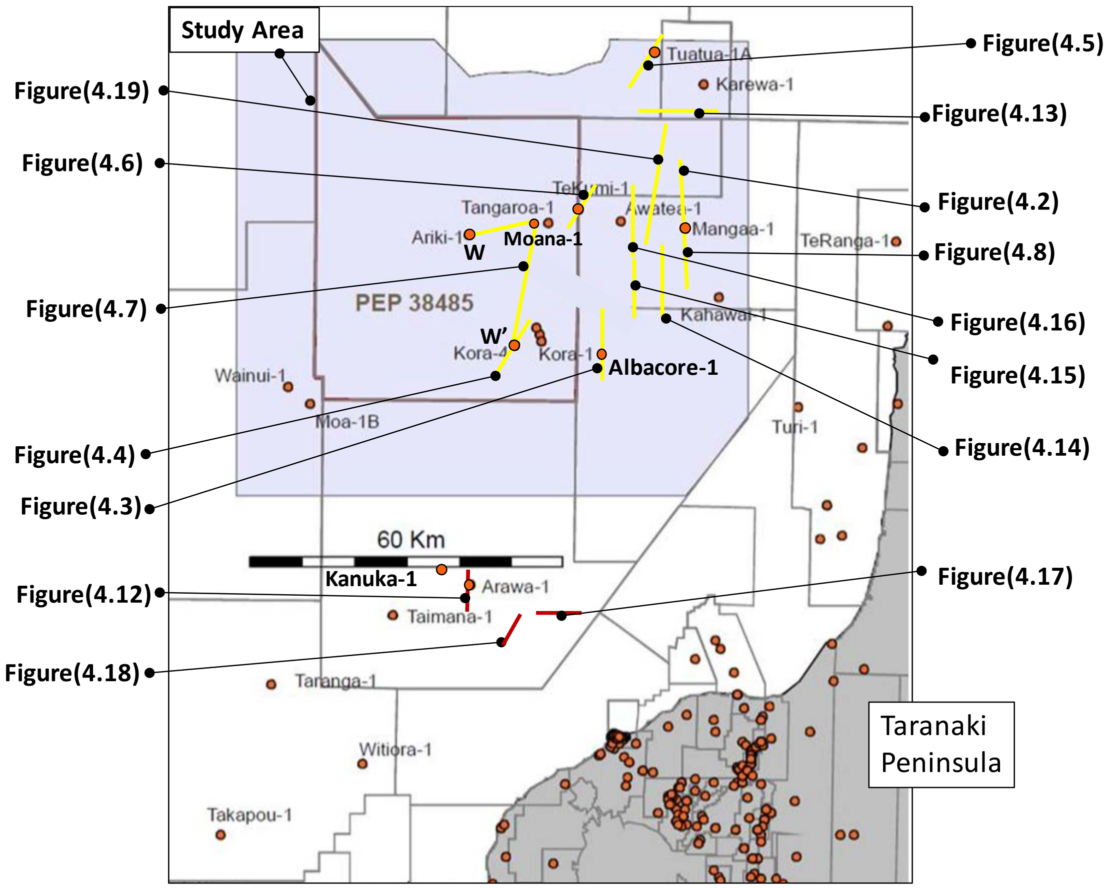

Figure 4.1. Study area showing exploration wells drilled in the offshore Taranaki Basin permit area PEP 38485 as well as the approximate location of the seismic vertical slices of subsequent figures.

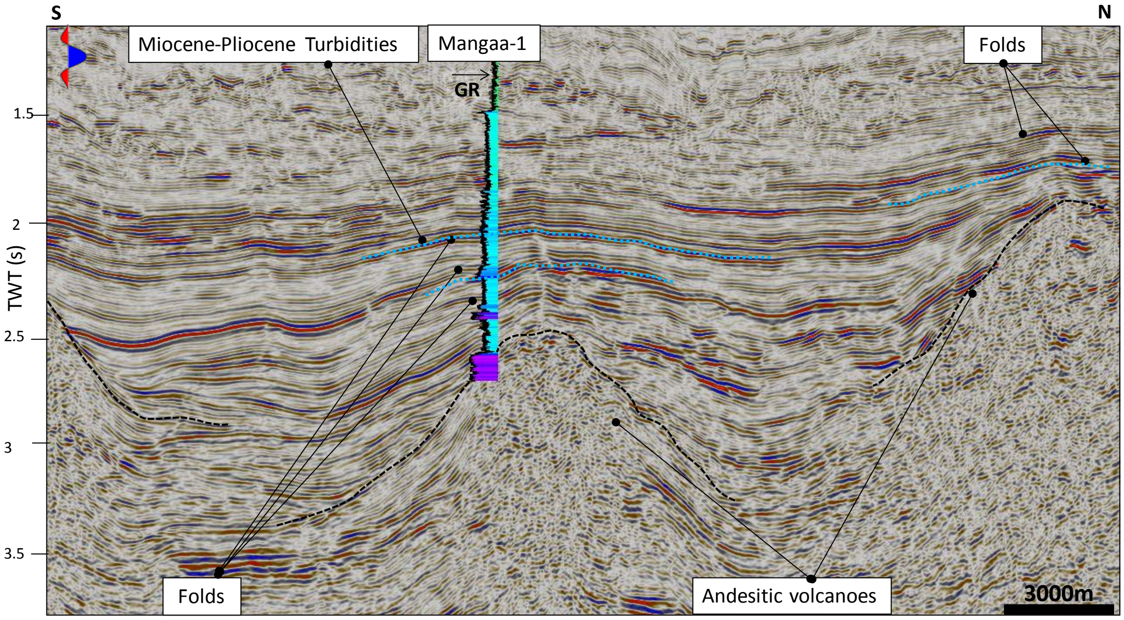

Figure 4.2. A N-S vertical slice through the seismic amplitude P95 2D survey showing the Mangaa-1 well which targeted the structural closure of Miocene –Pliocene turbidities associated with andesitic volcanoes. Blue dotted lines point to some folds. Seismic polarity indicated by the red-blue-red wavelet insert. Location of line shown in Figure 4.1. Seismic data courtesy of NZP&M).

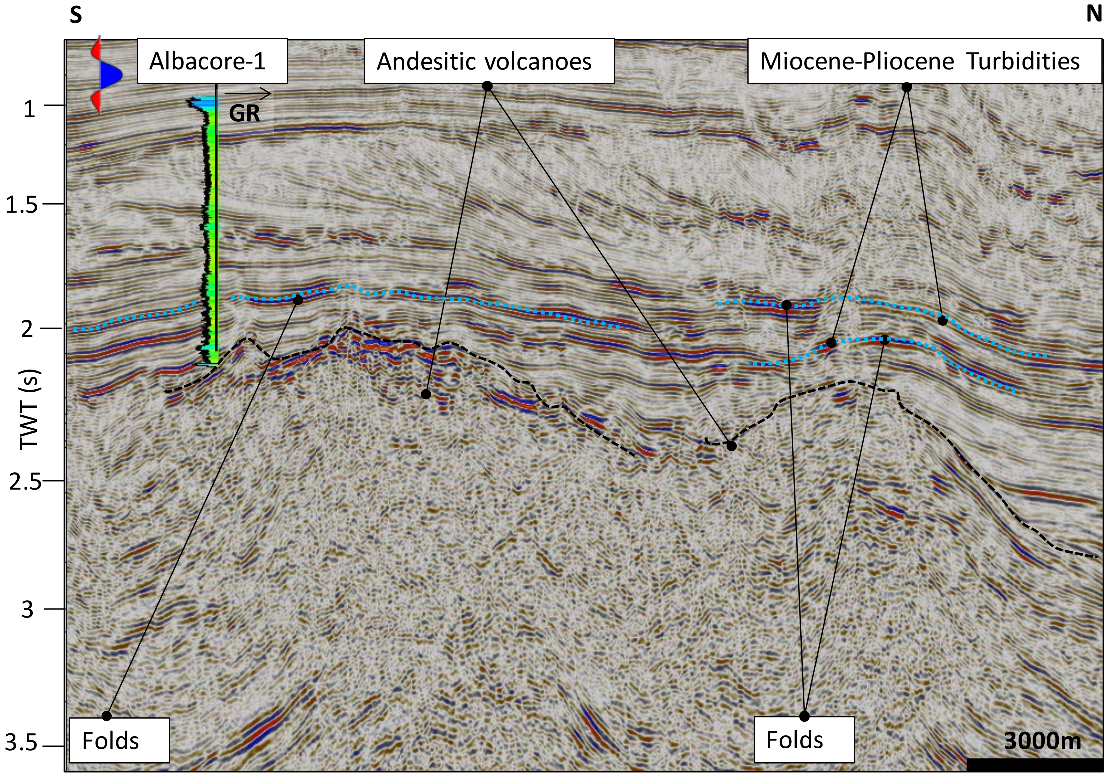

Figure 4.3. A N-S vertical slice through the seismic amplitude P95 2D survey showing the Albacore-1well targeting the structural closure of Miocene–Pliocene turbidities associated with andesitic volcanoes. Blue dotted lines point to some folds Location of line shown in Figure 4.1. Seismic data courtesy of NZP&M.

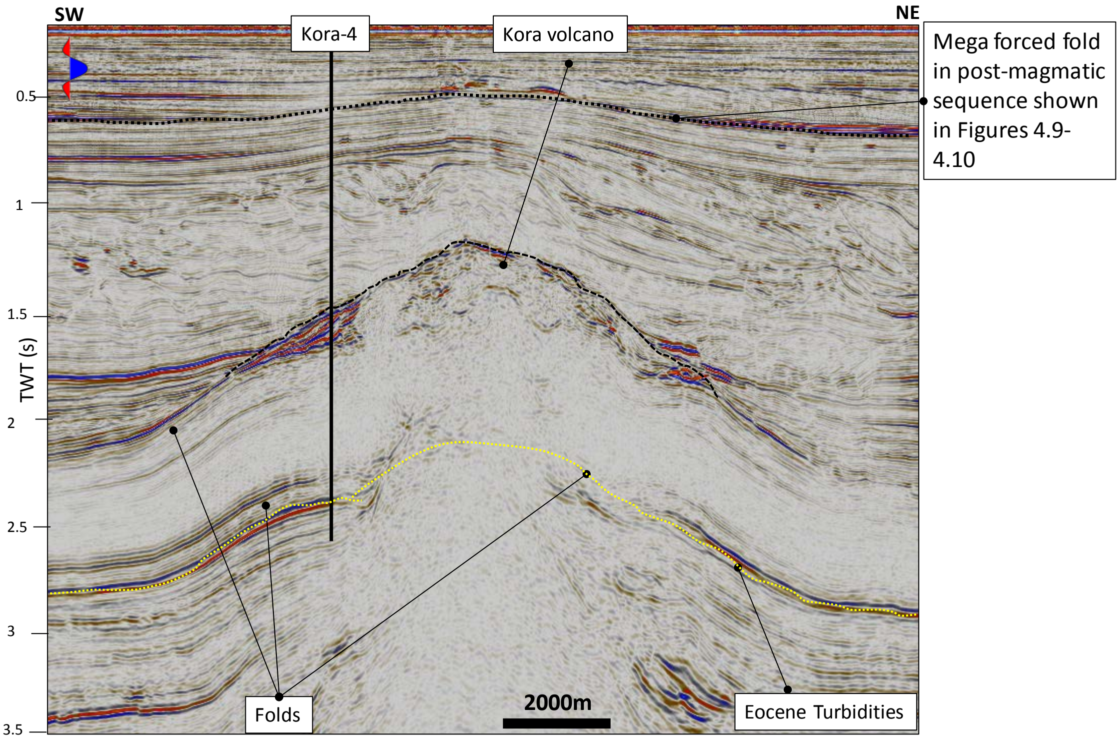

Figure 4.4. A N-S vertical slice through seismic amplitude volume showing the Kora-4 well targeting the structural closure of Eocene turbidities associated with the Kora volcano. Yellow dotted line indicates the Top Eocene. Location of line shown in Figure 4.1. Seismic data courtesy of NZP&M.

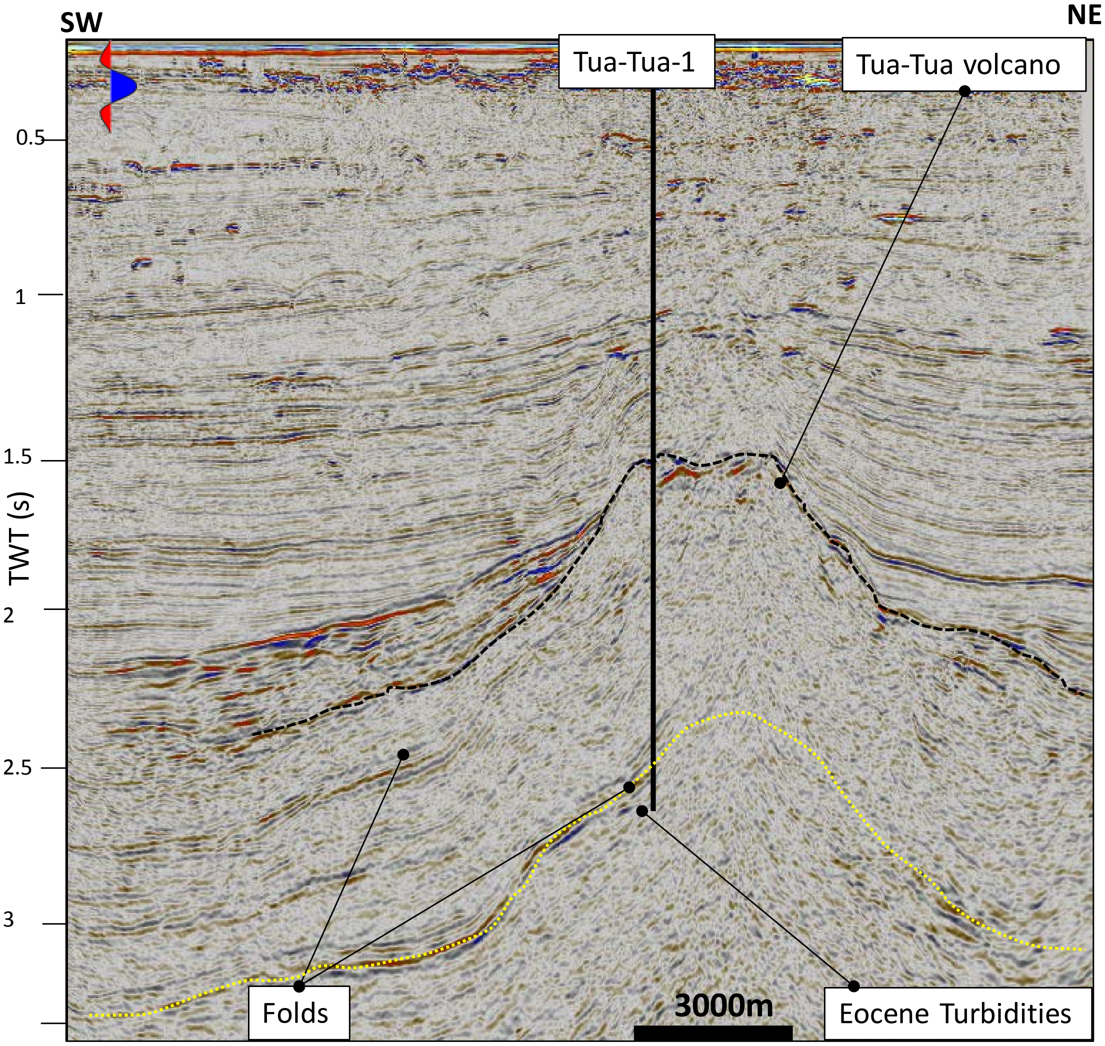

Figure 4.5. A NE-SW vertical slice through the seismic amplitude P95 2D survey showing the Te Kumi-1 well targeting the structural closure of Eocene turbidities associated with the Te-Kumi volcano. Yellow dotted line indicates the Top Eocene. Location of line shown in Figure 4.1. Seismic data courtesy of NZP&M.

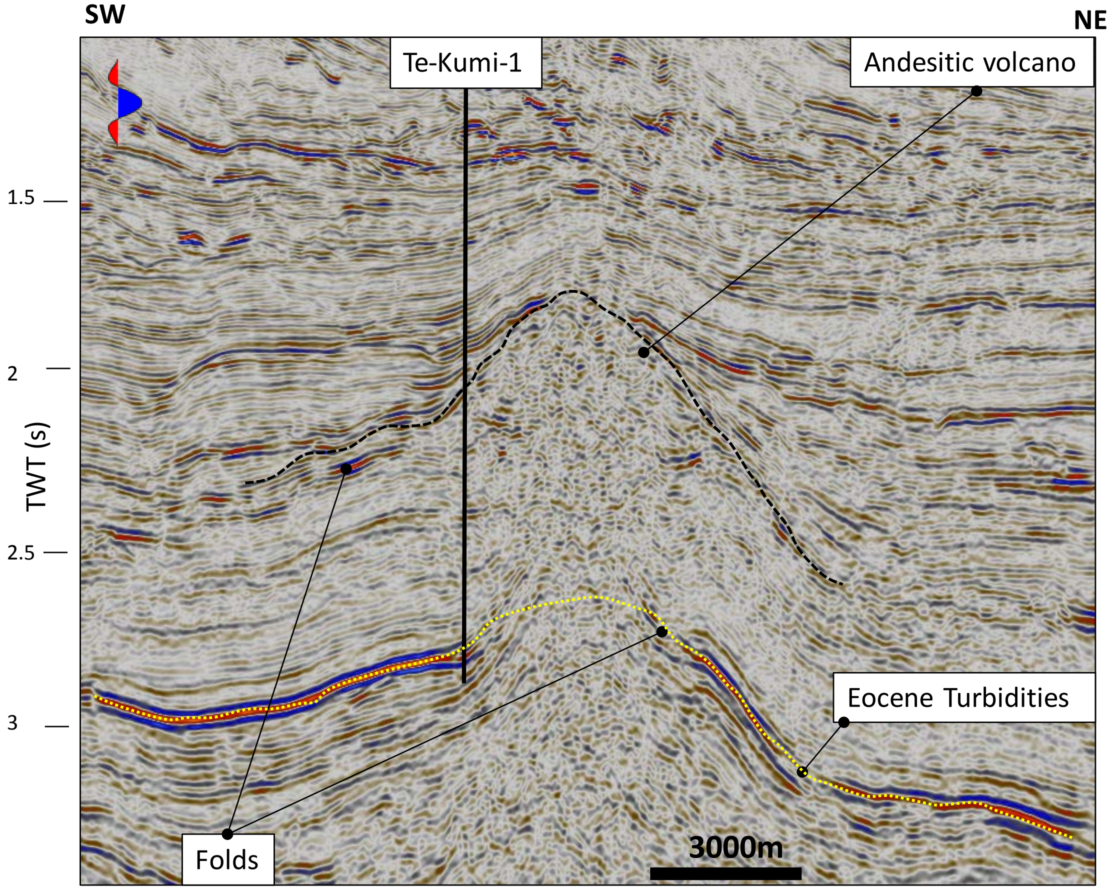

Figure 4.6. A NE-SW vertical slice through the seismic amplitude P95 2D survey showing well Te Kumi-1 targeting the structural closure of Eocene turbidities associated with the Te-Kumi volcano. Yellow dotted line indicates the Top Eocene. Location of line shown in Figure 4.1. Seismic data courtesy of NZP&M.

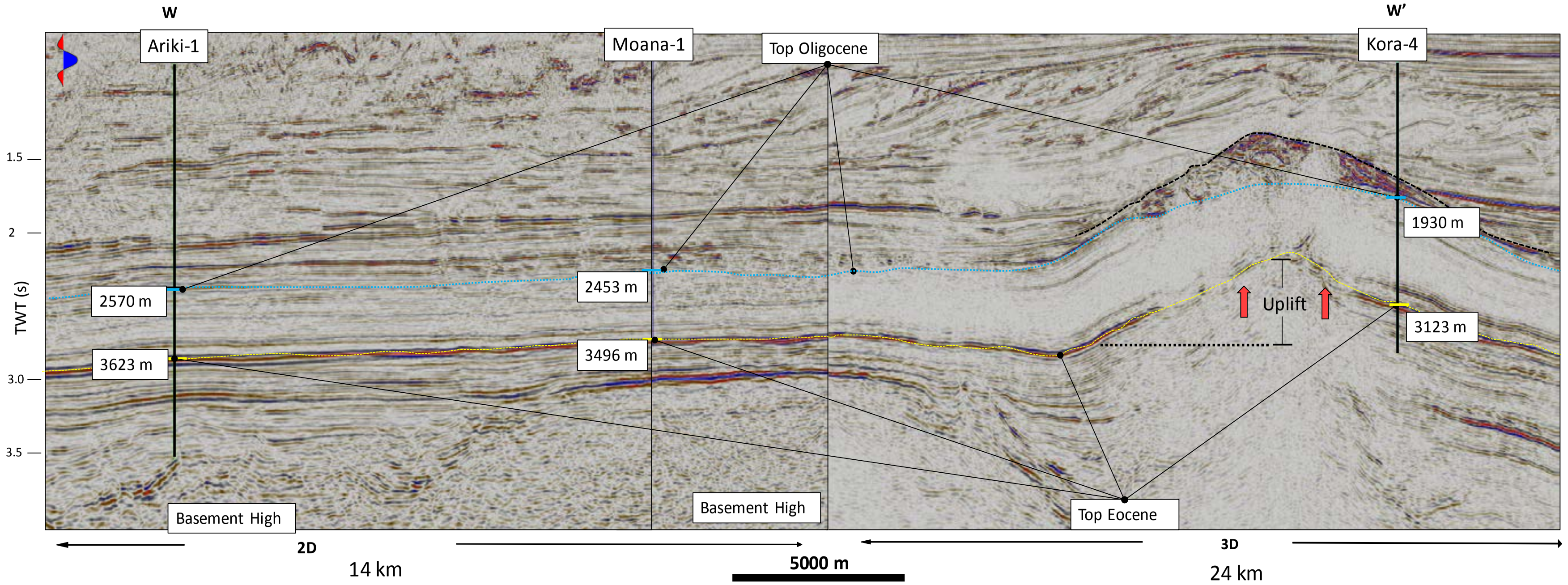

Figure 4.7. A composite vertical slice through seismic amplitude data connecting wells Ariki-1, Moana-1 and Kora-4. All three wells penetrate the Oligoene and Eocene. Notice the amount of uplift between Kora-4 and Moana-1 in the pre-magmatic sequence (Oligocene and older). Red arrows show the uplift in the area. Seismic data courtesy of NZP&M.

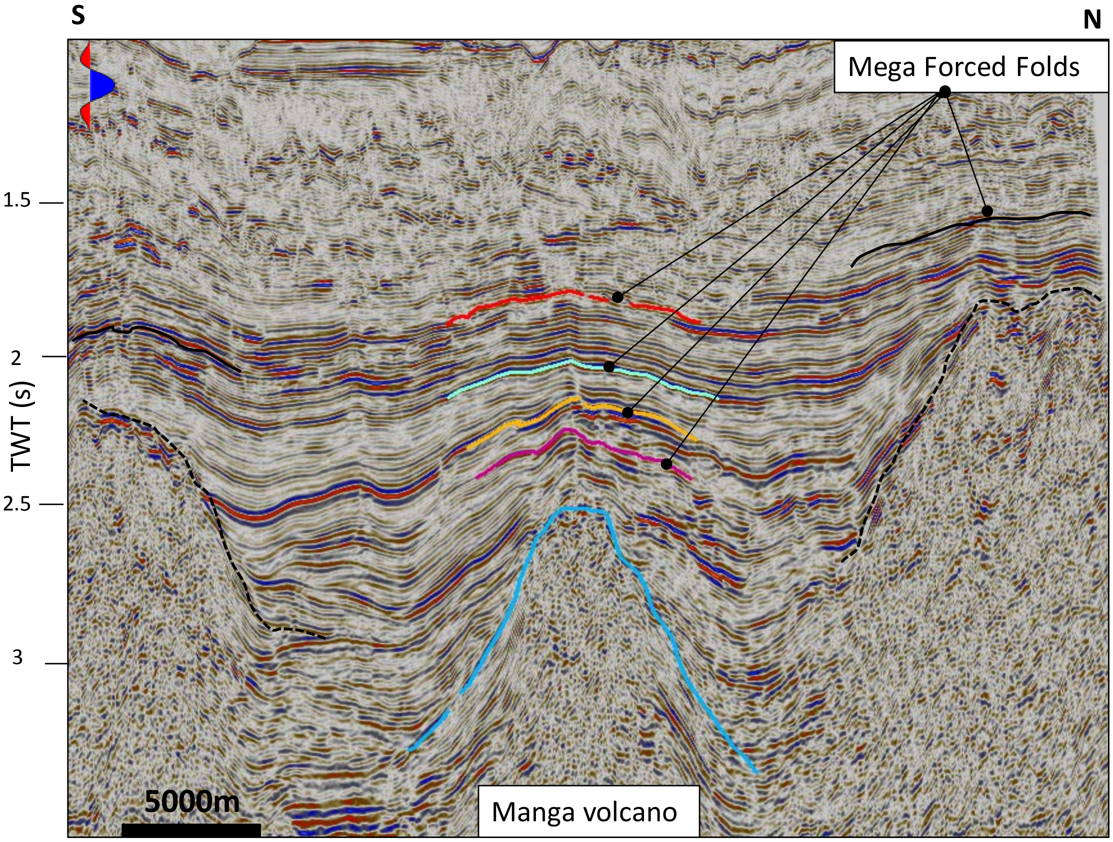

Figure 4.8. A N-S vertical slice through seismic amplitude P95 2D survey showing mega forced folds associated with the Manga volcano. Notice how the structural amplitude of the folds decrease as they decrease in age farther from the volcano. Location of line shown in Figure 4.1. Seismic data courtesy of NZP&M.

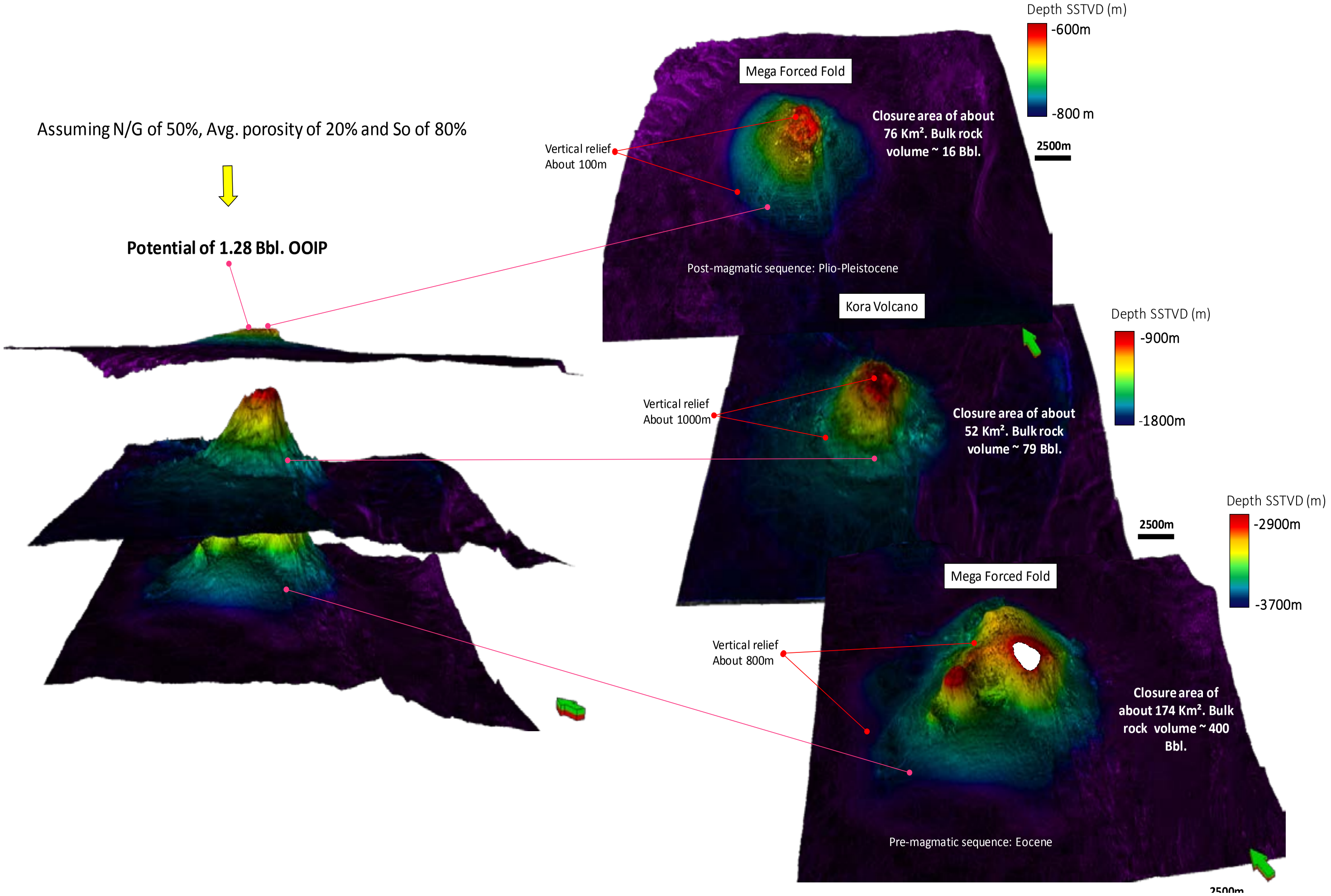

Figure 4.9. Mega forced folds associated with the Kora volcano. Strata in the pre-magmatic sequences are deformed by the emplacement of a magma chamber associated with the melting slab of the Pacific Plate because it subducts beneath the Australian Plate. Vertical relief in the pre-magmatic sequence is about 800 m and up to200 m in the post-magmatic sequence.

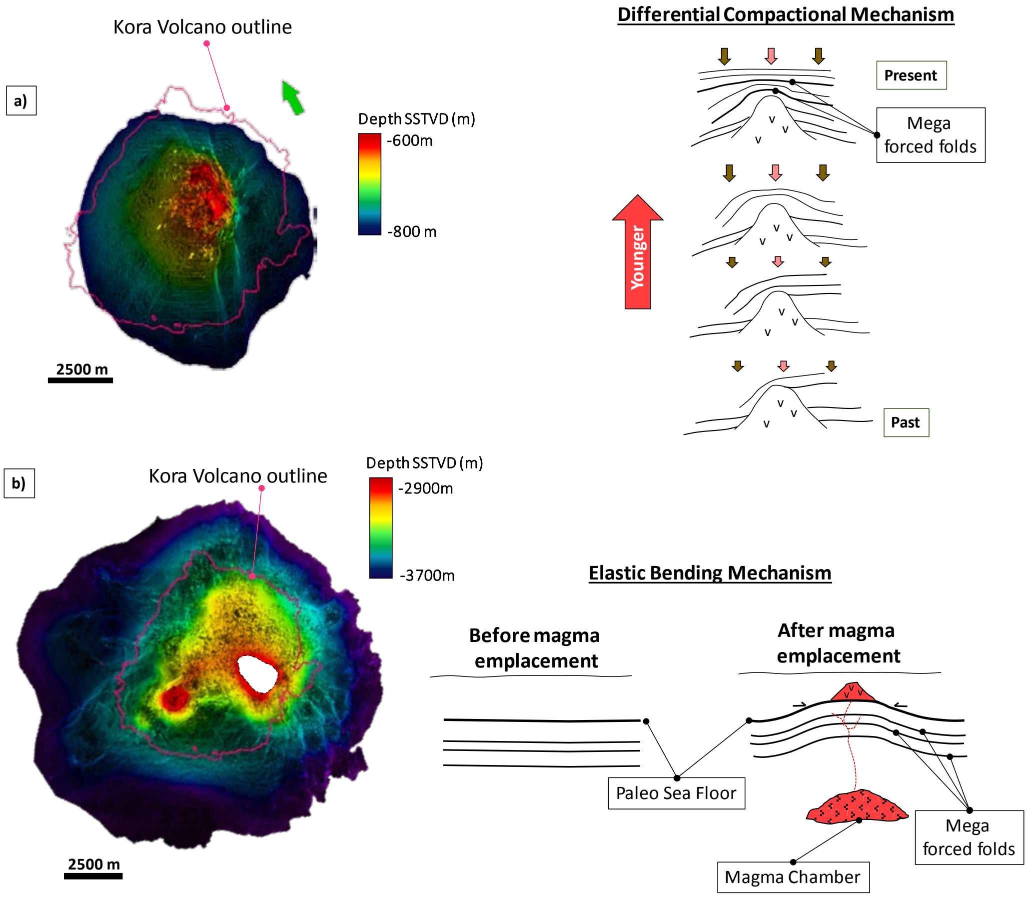

Figure 4.10. Mega forced folds associated with the Kora volcano showing (a) differential compaction mechanism on post-magmatic sequences according to Schmiedel et al. (2017) and (b) elastic bending mechanism on pre-magmatic sequence.

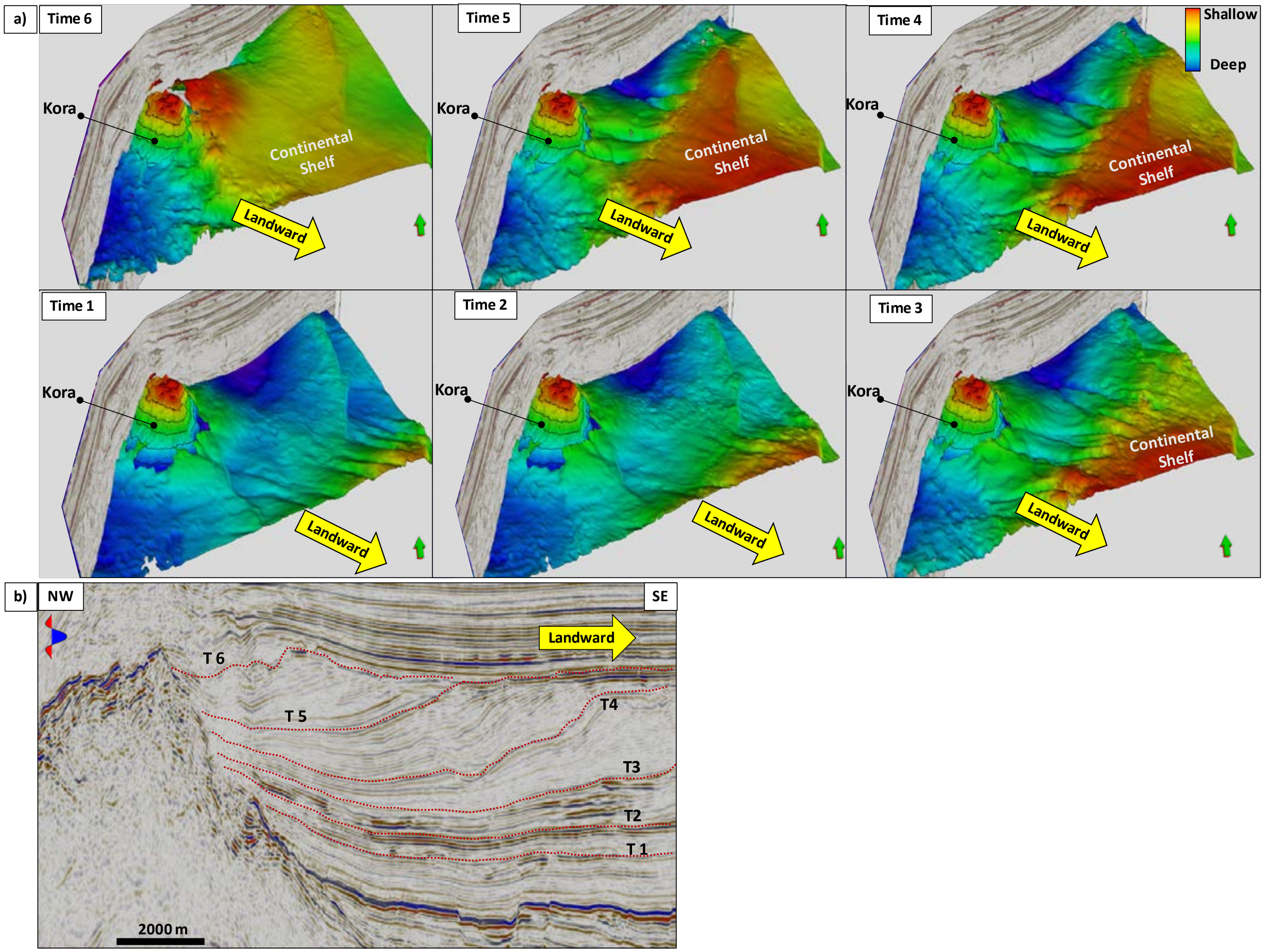

Figure 4.11. (a) Progradation of the continental shelf burying the Kora volcano beginning with a deeper horizon at time 1 (approximately Mid Miocene) and ending with a shallower horizon at time 6 (Pliocene). (b) Vertical section shows the position of the horizon slices for time 1 through 6.

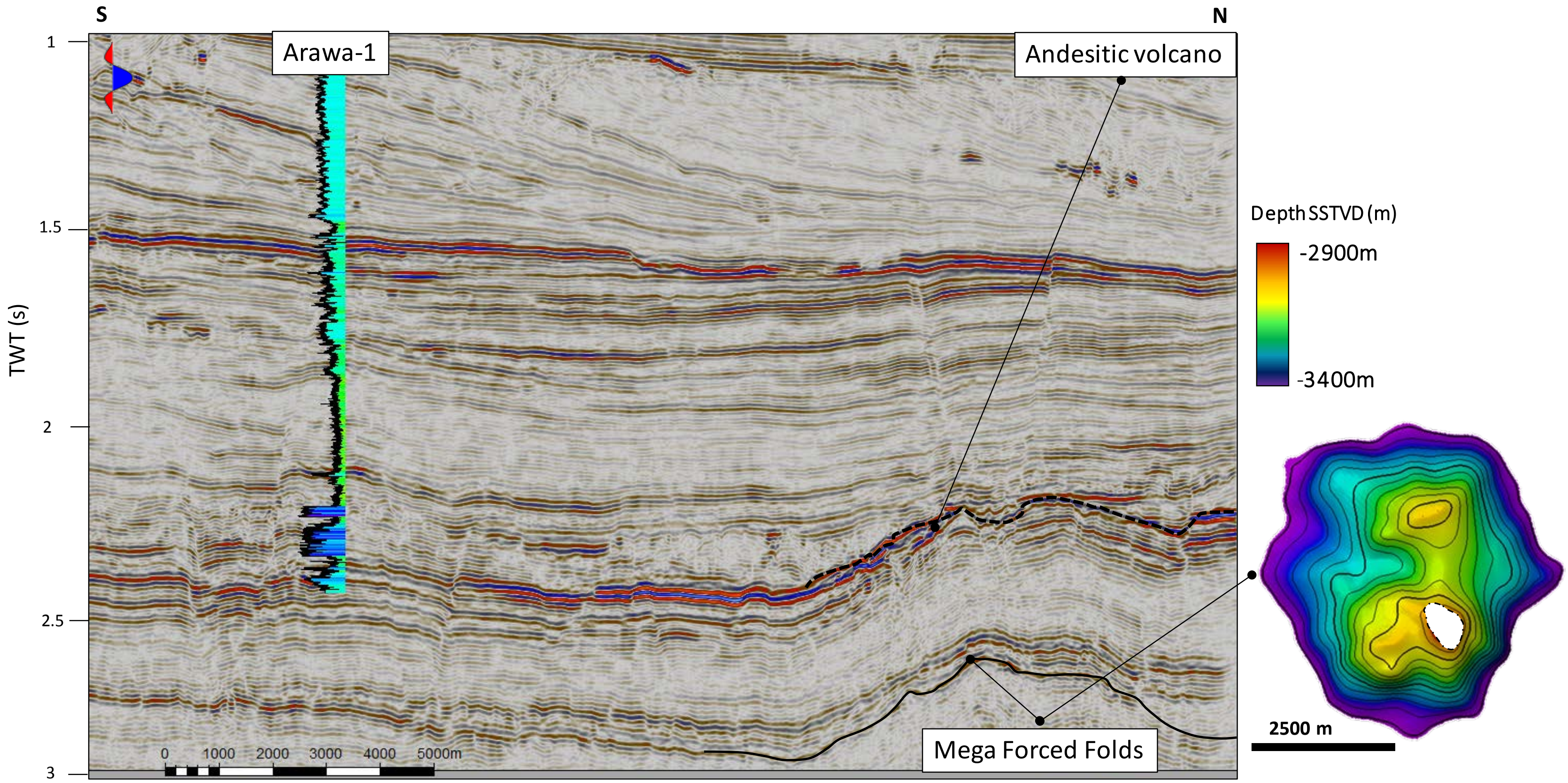

Figure 4.12. A N-S vertical slice through the seismic amplitude Parihaka volume showing folding of the pre-magmatic sequence, which I interpret to be due to the growth of the magma chamber. The low gamma ray response between t= 2.0- 2.5 s is due to the intermediate composition of the volcanics in Arawa-1. Location of line shown in Figure 4.1. Seismic data courtesy of NZP&M.

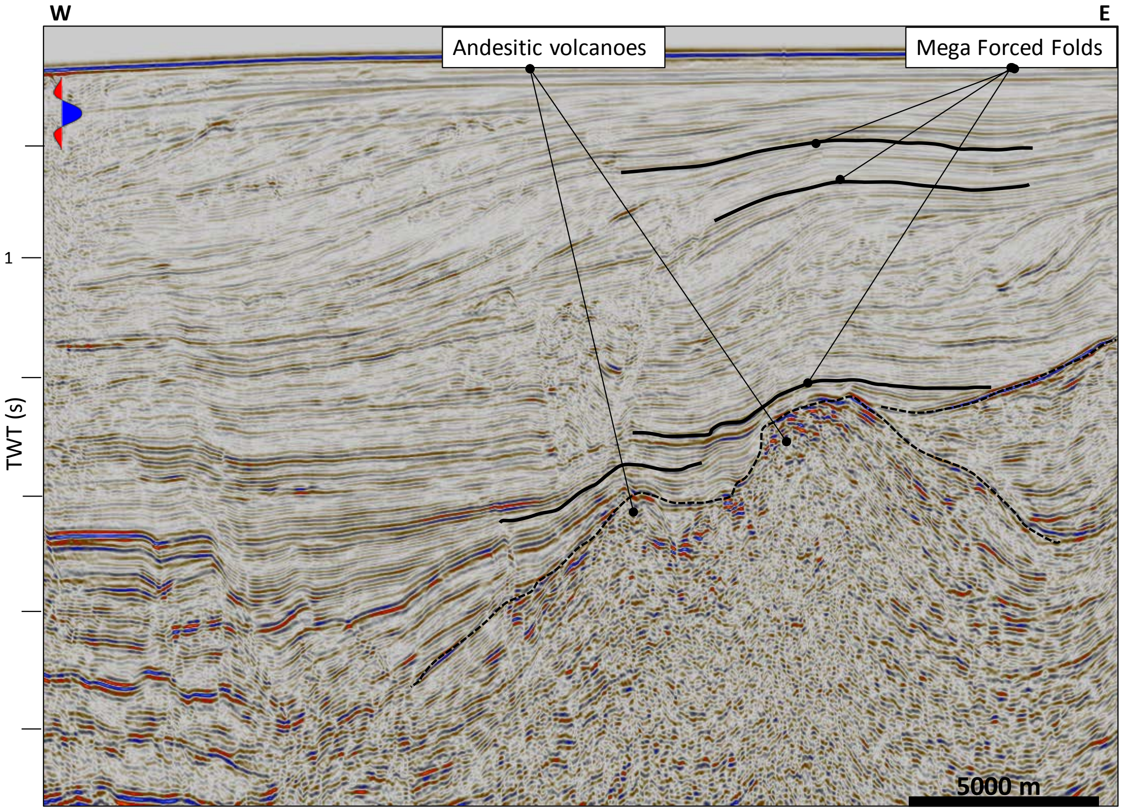

Figure 4.13. An E-W vertical slice through the seismic amplitude P95 2D survey showing folding of the post-magmatic sequence due to differential compaction of softer sediments about the more rigid andesitic volcanoes. Location of line shown in Figure 4.1. Seismic data courtesy of NZP&M.

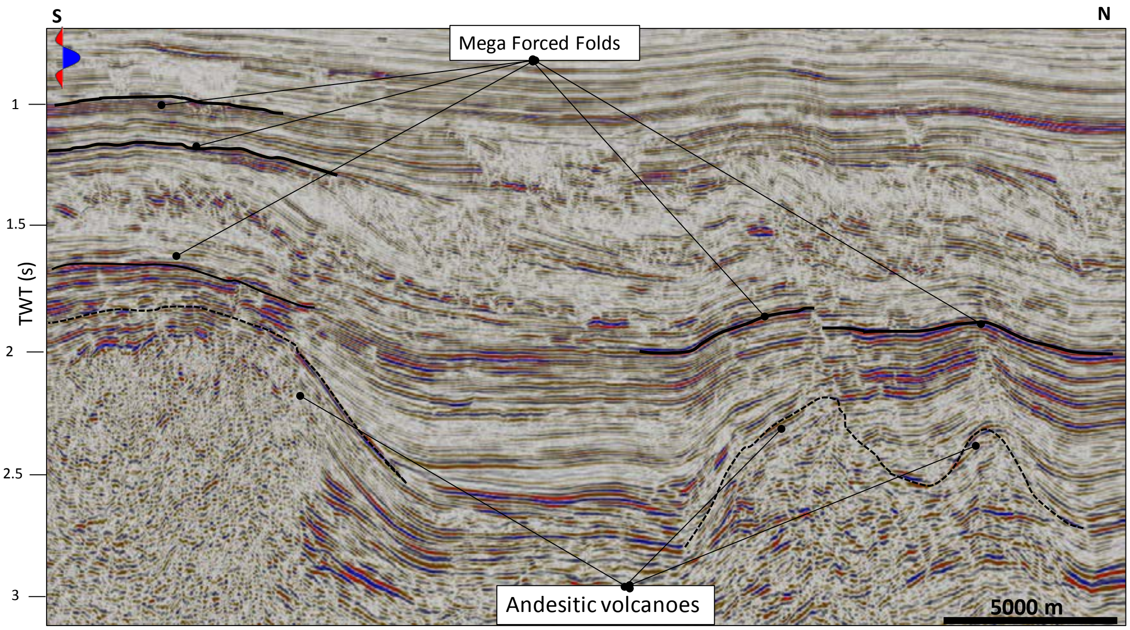

Figure 4.14 . A N-S vertical slice through the seismic amplitude P95 2D showing folding of different horizons of the post-magmatic sequence due to differential compaction of softer sediments about the more rigid andesitic volcanoes. Location of line shown in Figure 4.1. Seismic data courtesy of NZP&M.

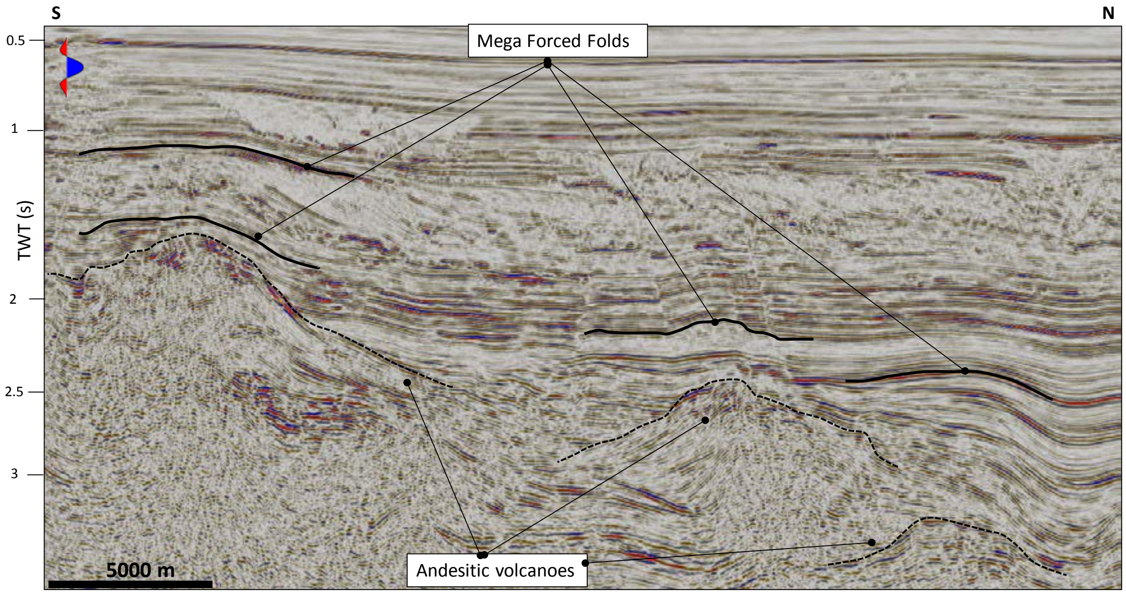

Figure 4.15 . A N-S vertical slice through the seismic amplitude P95 2D survey showing folding of different horizons of the post-magmatic sequence due to differential compaction of softer sediments about the more rigid andesitic volcanoes. Location of line shown in Figure 4.1. Seismic data courtesy of NZP&M.

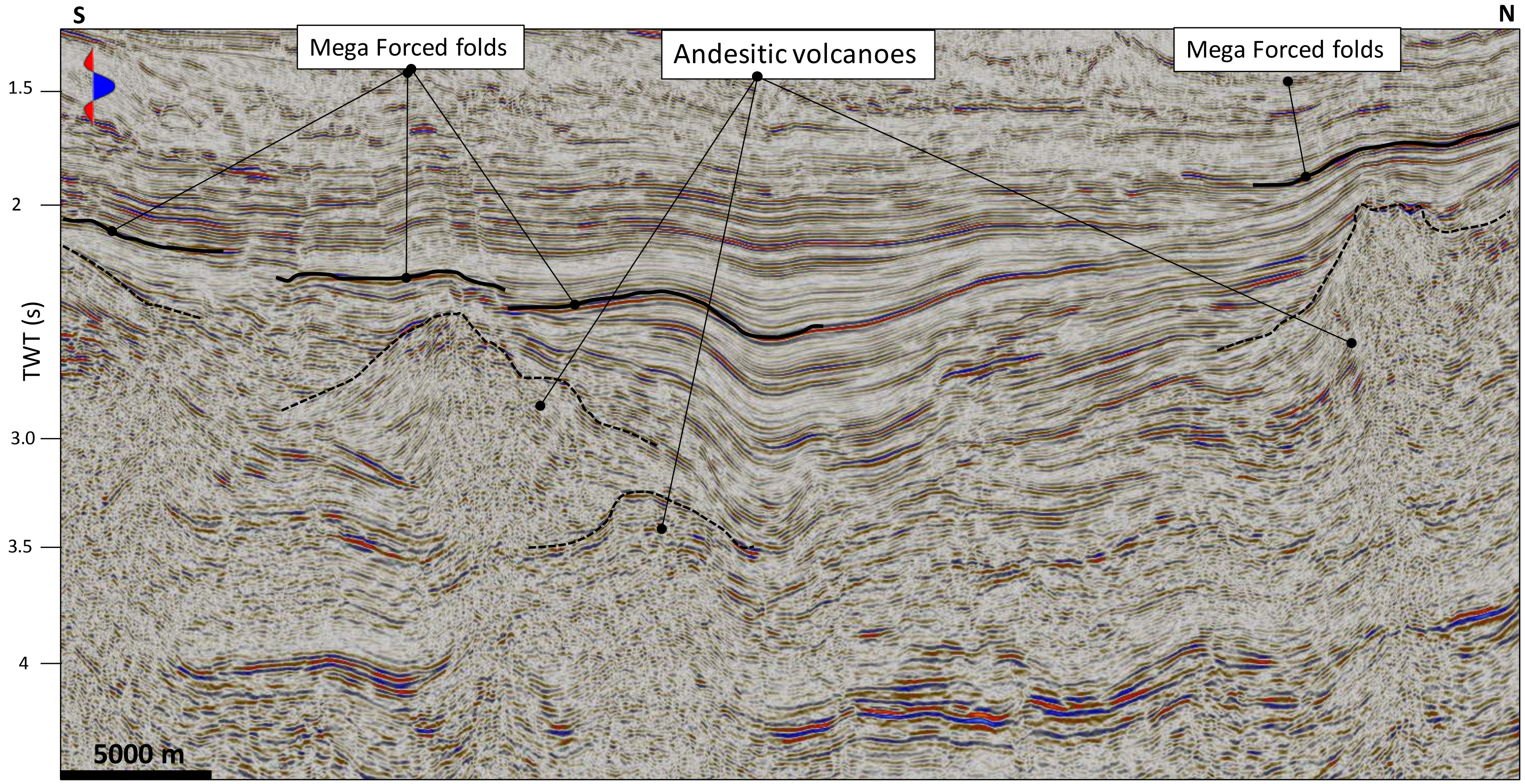

Figure 4.16. A N-S vertical slice through the seismic amplitude P95 2D survey showing folding of different horizons of the post-magmatic sequence due to differential compaction of softer sediments about the more rigid andesitic volcanoes. Location of line shown in Figure 4.1. Seismic data courtesy of NZP&M.

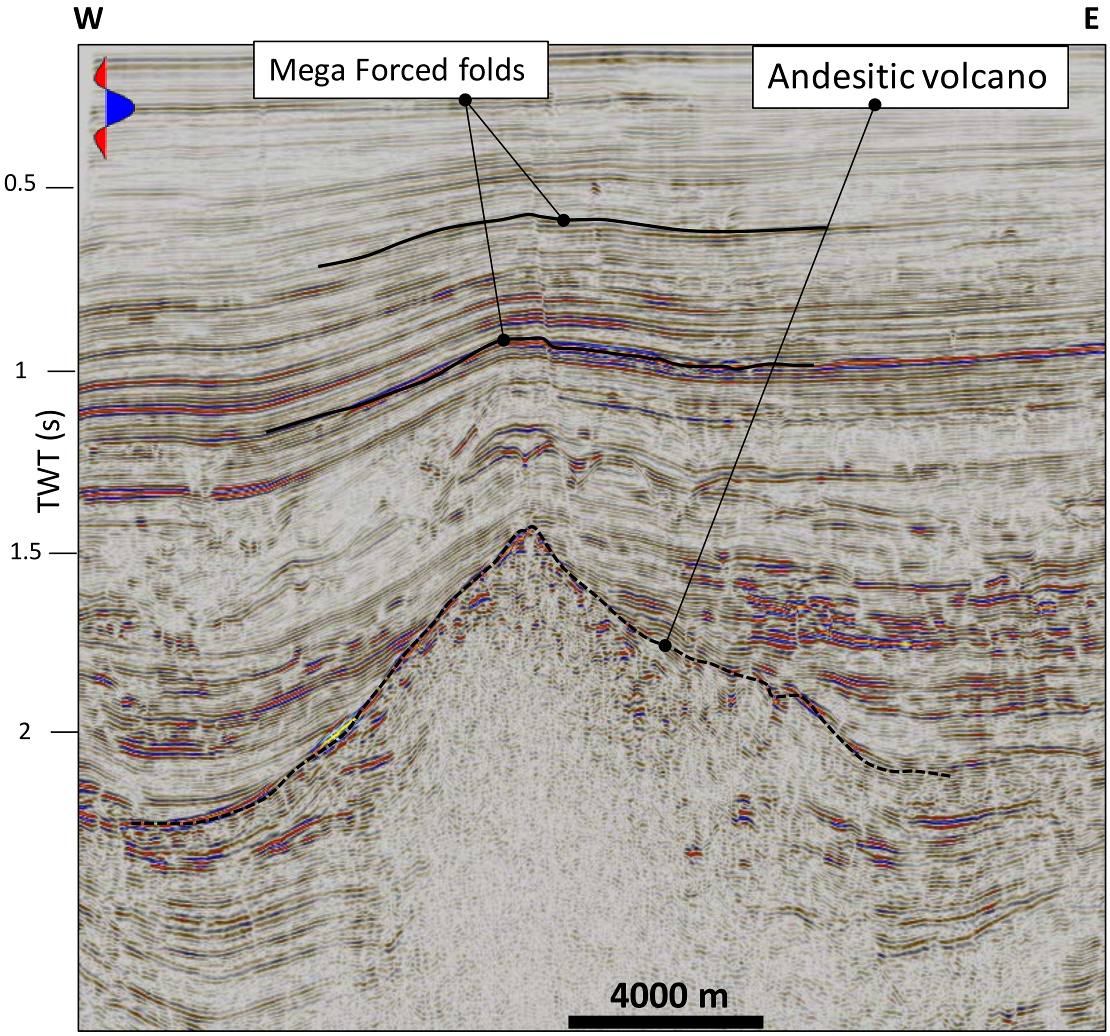

Figure 4.17. A N-S vertical slice through the seismic amplitude OMV 2005 2D survey showing folding of different horizons of the post-magmatic sequence due to differential compaction of softer sediments about the more rigid andesitic volcanoes. Location of line shown in Figure 4.1. Seismic data courtesy of NZP&M.

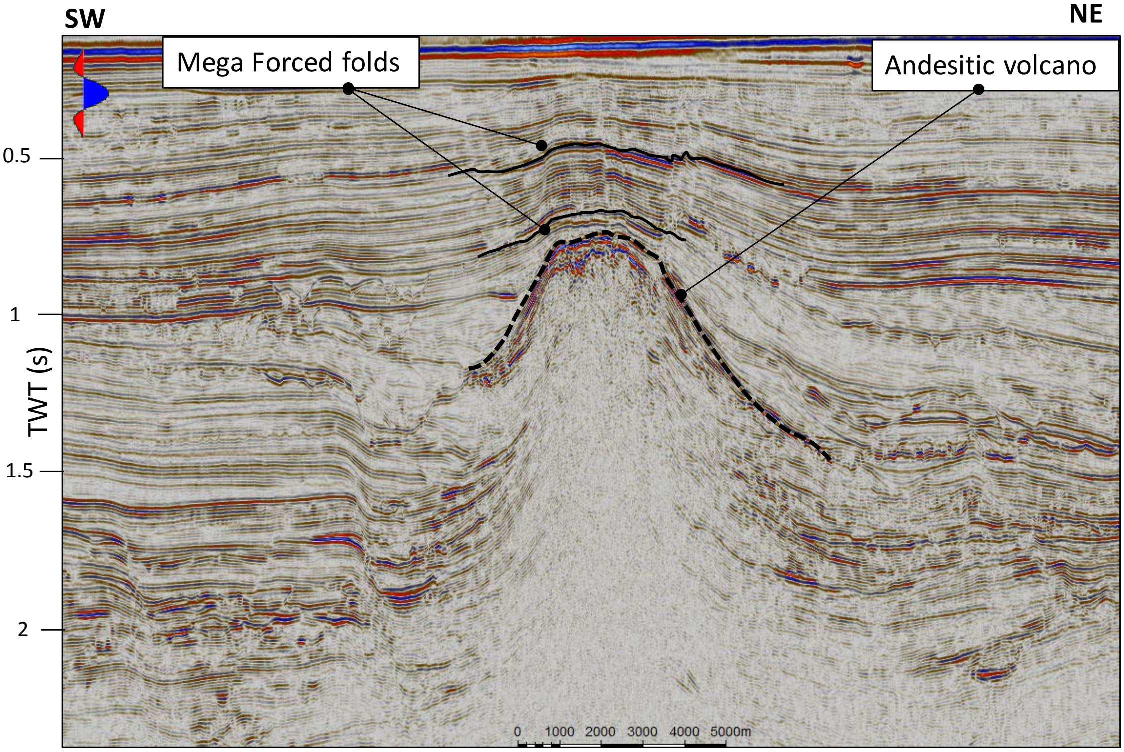

Figure 4.18. A N-S vertical slice through the seismic amplitude volume from the Parihaka 3D seismic survey showing folding of different horizons of the post-magmatic sequence due to differential compaction of softer sediments about the more rigid volcanic cone. Location of line shown in Figure 4.1. Seismic data courtesy of NZP&M.

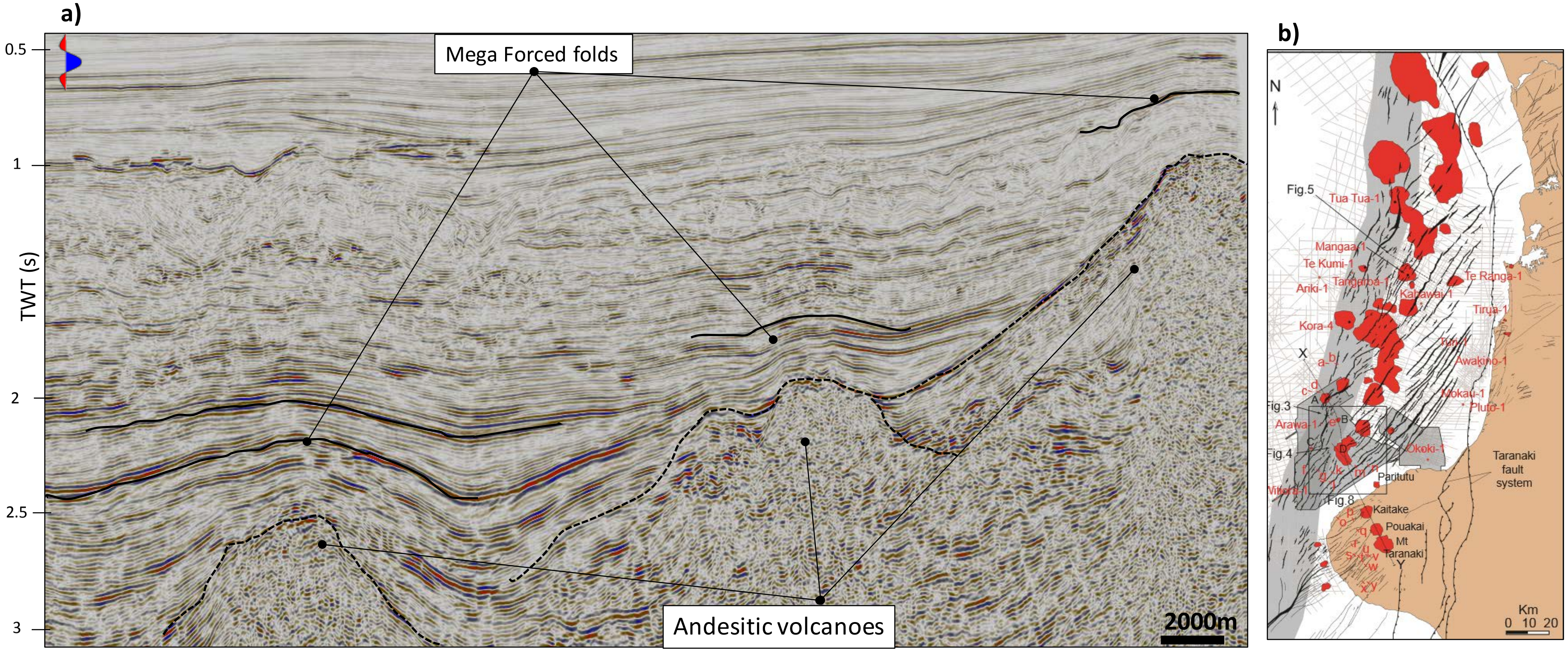

Figure 4.19. (a) A vertical slice through seismic amplitude showing mega forced folds of different ages of the post-magmatic sequence due to differential compaction of softer sediments about a more rigid volcanic cone. B) Map of the distribution of Miocene and younger submarine volcanoes in the Taranaki Basin New Zealand suggesting other potential traps (Giba et al., 2013). Seismic data courtesy of NZP&M.

REFERENCES

Alves, T., K. Omosanya, and P. Gowling, 2015, Volume rendering of enigmatic high-amplitude anomalies in southeast Brazil. A workflow to distinguish lithologic features from fluid accumulations: Interpretation, v. 3, no. 2, p. A1-A14.

Barber, P. M., T. Rasmussen, S. S. Rey, and R. Myklebust, 1988, The Exmouth Plateau deep water frontier: A case history, in P. G. Purcell and R. R. Purcell, eds., The North West Shelf, Australia: Proceedings of the Petroleum Exploration Society of Australia Symposium, 63–76.

Bergman, S. C., J. P. Talbot, and P. R. Thompson, 1992, The Kora Miocene submarine andesite stratovolcano hydrocarbon reservoir, northern Taranaki Basin, New Zealand: 1991 New Zealand Oil Exploration Conference Proceedings: Wellington, Ministry of Commerce, 178–206.

Bischoff, A. P., A. Nicol, and M. Beggs, 2017, Stratigraphy of architectural elements in a buried volcanic system and implications for hydrocarbon exploration: Interpretation, v. 5, no. 3, p. SK141-SK159, doi:10.1190/INT-2016-0201.1.

Crown Minerals, Albacore-1 well completion report. 2016. Web. 12 Dec. 2016. Petroleum Report Series PR 4183.

Crown Minerals, Final Well Report, Awatea-1. PPL 38447. 2016. Web. 12 Dec. 2016. Petroleum Report Series PR 2262.

Crown Minerals, Final Well Report, Kora-1 Kora-1A. PPL 38447. 2016. Web. 12 Dec. 2016. Petroleum Report Series PR 1374.

Crown Minerals, Final Well Report, Kora-2. PPL 38447. 2016. Web. 12 Dec. 2016. Petroleum Report Series PR 1441.

Crown Minerals, Final Well Report, Kora-3. PPL 38447. 2016. Web. 12 Dec. 2016. Petroleum Report Series PR 1441.

Crown Minerals, Final Well Report, Kora-4. PPL 38447. 2016. Web. 12 Dec. 2016. Petroleum Report Series PR 1443.

Crown Minerals, Final Well Report, Te-Kumi-1. PPL 38447. 2016. Web. 12 Dec. 2016. Petroleum Report Series PR 1386.

Crown Minerals, Final Well Report, Tua-Tua-1. PPL 38447. 2016. Web. 12 Dec. 2016. Petroleum Report Series PR 1389.

Crown Minerals, Kanuka-1 well completion report. 2016. Web. 12 Dec. 2016. Petroleum Report Series PR 3843.

Giba, M., A. Nicol, and J. Walsh, 2010, Evolution of faulting and volcanism in a back-arc basin and its implications for subduction processes: Tectonics, 29, p. TC4020, doi: 10.1029/2009TC002634.

Giba, M., J. J. Walsh, A. Nicol, V. Mouslopoulou, and H. Seebeck, 2013, Investigation of the spatio-temporal relationship between normal faulting and arc volcanism on million-year time scales: Journal of the Geological Society, v. 170, no. 6, p. 951–962, doi:10.1144/jgs2012-121.

Holford, S. P., N. Schofield, and P. Reynolds, 2017, Subsurface fluid flow focused by buried volcanoes in sedimentary basins: Evidence from 3D seismic data, Bass Basin, offshore southeastern Australia: Interpretation, v. 5, no. 3, p. SK39-SK50, doi:10.1190/INT-2016-0205.1.

Holford, S. P., N. Schofield, C. A. L. Jackson, C. Magee, P. F. Green, and I. R. Duddy, 2013, Impacts of igneous in- trusions on source and reservoir potential in prospective sedimentary basins along the Western Australian continental margin: West Australian Basins Symposium, Proceedings of the Petroleum Exploration Society of Australia Symposium, 1–12.

Infante-Paez, L., and K. J. Marfurt, 2017, Seismic expression and geomorphology of igneous bodies: A Taranaki Basin, New Zealand, case study: Interpretation, v. 5, no. 3, p. SK121-SK140, doi:10.1190/INT-2016-0244.1.

Jackson, C. A. L., N. Schofield, and B. Golenkov, 2013, Geometry and controls on the development of igneous sill-related forced folds: A 2-D seismic reflection case study from offshore southern Australia: Bulletin of the Geological Society of America, v.125, no. 11–12, p. 1874–1890, doi:10.1130/B30833.1.

Kartanegara, A.L., Baik, R.N. and Ibrahim, M.A., 1996, Volcanics oil bearing in Indonesia: American Association of Petroleum Geologists, A73.

Kingston, J., and J. R. Matzko, 1995, Undiscovered petro- leum of the Brazilian interior sag basins: Interna- tional Geology Review, 37,959–980, doi: 10.1080/00206819509465435.

Magee, C., C. A. L. Jackson, and N. Schofield, 2014, Diachronous sub-volcanic intrusion along deep-water margins: Insights from the Irish Rockall Basin: Basin Research, v. 26, no. 1, p. 85–105, doi:10.1111/bre.12044.

Morley, C., 2018, 3D seismic imaging of the plumbing system of the Kora volcano, Taranaki Basin, New Zealand: The influences of syn-rift structure on shallow igneous intrusion architecture: Geosphere, in press.

Planke, S., P. A. Symonds, E. Alvestad, and J. Skogseid, 2000, Seismic volcanostratigraphy of large-volume basaltic extrusive complexes on rifted margins: Journal of Geophysical Research: Solid Earth, v. 105, p. 19335–19351, doi:10.1029/1999JB900005.

Rateau, R., N. Schofield, and M. Smith, 2013, The potential role of igneous intrusions on hydrocarbon migration, West of Shetland: Petroleum Geoscience, v. 19, p. 259–272, doi: 10.1144/petgeo2012-035.

Rodriguez Monreal, F., H. J. Villar, R. Baudino, D. Delpino, and S. Zencich, 2009, Modeling an atypical petroleum system: A case study of hydrocarbon generation, migration and accumulation related to igneous intrusions in the Neuquen Basin, Argentina: Marine and Petroleum Geology, v. 26, no. 4, p. 590–605, doi:10.1016/j.marpetgeo.2009.01.005.

Schmiedel, T., S. Kjoberg, S. Planke, C. Magee, O. Galland, N. Schofield, C. A.-L. Jackson, and D. A. Jerram, 2017, Mechanisms of overburden deformation associated with the emplacement of the Tulipan sill, mid-Norwegian margin: Interpretation,v. 5, no. 3, p. SK23-SK38, doi:10.1190/INT-2016-0155.1.

Schutter, S. R., 2003, Hydrocarbon occurrence and exploration in and around igneous rocks: Geological Society of London, Special Publications, v. 214, p.7–33.

Spacapan, J. B., O. Galland, H. A. Leanza, and S. Planke, 2017, Igneous sill and finger emplacement mechanism in shale-dominated formations: a field study at Cuesta del Chihuido, Neuquén Basin, Argentina: Journal of the Geological Society, v. 174, no. 3, p. 422–433, doi:10.1144/jgs2016-056.

Stearns, D.W., 1978. Faulting and forced folding in the Rocky Mountains foreland. Geological Society of America Memoir 151, p.1-38.

Zhang, K., and K. J. Marfurt, 2011, Seismic attribute illumination of an igneous reservoir in China: The Leading Edge, 30, 266–270, doi: 10.1190/1.3567256.

Zou, C. N., 2013, Volcanic reservoirs in petroleum exploration: Beijing, China, Petroleum Industry Press.

CHAPTER 5

CONCLUSIONS AND RECOMMENDATIONS

In this dissertation I have shown that the seismic expression of igneous bodies often mimics that of other facies of exploration interest. Volcanic cones may appear similar to carbonate build ups and exhibit a similar high impedance contrast and internal reflectivity. Volcanic mass transport deposits look like siliciclastic mass transport complexes. If one does not properly account for polarity, igneous sills/volcanic piles can be easily misinterpreted to be hydrocarbon bright spots. In many situations, identification and linkage (in-context interpretation) of the diverse architectural elements that compose the volcanic system described in this study (igneous sills, forced folds) provide the means to avoid such interpretation pitfalls.

I also showed that volcanic rocks of andesitic composition show distinctive patterns in seismic data that can be exploited using machine learning algorithms to identify and map their geomorphology. I find that, clustering seismic attributes that highlight the continuity, amplitude and frequency of the volcanic facies using SOM, provides a means to identify architectural elements such as lava flows, pyroclastic flows and subaqueous landslides associated with the andesitic Kora Volcano. Although the patterns of interest in my research represent volcanics, I believe this approach can be applied to similar monogenetic seismic patterns.

In addition to acting as potential reservoirs, my study finds that andesitic volcanoes can create giant structural traps in both the pre- and post-magmatic sequences. Deformations of the pre-magmatic strata appear to be caused by inflation or growth of a magma chamber that results from subduction of oceanic crust underneath continental crust, whereas deformation of the post-magmatic sequence occurs due to differential compaction of softer sediments around the more rigid volcanic cone or sills. The volumetric capacity of potential hydrocarbons the Mega forced folds of the post-magmatic sequence above the Kora volcano can accommodate is more than 1.0 billion of barrels of oil if filled to spill point.

Although one should be careful in defining hydrocarbon prospects in andesitic volcanic terranes, the presence of igneous extrusive and intrusive rocks can pose a positive rather than a negative impact to hydrocarbon exploration in sedimentary basins. Therefore, I recommend interpreters to not condemn a new area because the presence of igneous rocks, but rather to properly evaluate their impact to petroleum systems.

APPENDIX 1

Special section: Subsurface expression of igneous systems and their impacts on petroleum systems.

Seismic expression and geomorphology of igneous bodies: A Taranaki Basin, New Zealand, case study.

Lennon Infante-Paez[1] and Kurt J. Marfurt[1]

1The University of Oklahoma (OU), School of Geology and Geophysics, Norman, Oklahoma, USA. E-mail: lennoninfante@ou.edu; kmarfurt@ ou.ed. Manuscript received by the Editor 24 December 2016; revised manuscript received 16 March 2017; published online 15 June 2017. This paper appears in Interpretation, Vol. 5, No. 3 (August 2017); p. SK121–SK140, 34 FIGS. http://dx.doi.org/10.1190/INT-2016-0244.1.

Seismic expression and geomorphology of igneous bodies: A Taranaki Basin, New Zealand, case study

Lennon Infante-Paez[1] and Kurt J. Marfurt[1]

Abstract

Very little research has been done on volcanic rocks by the oil industry due to the misconception that these rocks cannot be "good reservoirs." However, in the past two decades, significant quantities of hydrocarbons have been produced from volcanic rocks in China, New Zealand, and Argentina. In frontier basins, volcanic piles are sometimes misinterpreted to be hydrocarbon anomalies and/or carbonate buildups. Unlike clastic and carbonate systems, the 3D seismic geomorphology of igneous systems is only partially documented. We have integrated 3D seismic data, well logs, well reports, core data, and clustering techniques such as self-organizing maps to map two distinct facies (pyroclastic and lava flows), within a Miocene submarine volcano in the Taranaki Basin, New Zealand. Three wells; Kora-1–3 drilled the pyroclastic facies within the volcano encountering evidence of a petroleum system, whereas the Kora-4 well drilled the lava-flow facies, which was barren of hydrocarbons. By integrating results from geochemistry and basin modeling reports prepared for Crown Mineral, New Zealand, we concluded that the reason that Kora-4 was dry was due to a lack of source charge — not to the absence of reservoir quality. Moreover, the Kora-1 well drilled a thick sequence (>1000 m) of pyroclastic flows in this submarine volcano by chance and found high peaks of gas in the mudlogs near the top 25 m of this sequence. A long-term test in this upper volcanic section resulted in 32 API oil flow of 668 barrels of oil per day for 254 h — a result that challenges the misconception that volcanic rocks cannot be good reservoirs.

Introduction

Although igneous intrusive and extrusive rocks are common in the North Sea, New Zealand, northwest Australia, Argentina, offshore Brazil, China, and other oil provinces around the world, there is only limited documentation of the seismic expression of igneous rocks in 3D seismic data. In most cases, igneous rocks have limited impact on the exploration objective, unless someone is unfortunate to drill a bright spot having the wrong polarity (Alvez et al., 2015), or a nonmagnetic volcanic plug masquerading as a carbonate buildup (Klarner et al., 2006). In some cases, the thermal effects of igneous intrusions can beneficially affect the maturity of source rocks, by increasing the geothermal gradient and placing immature source rocks within the oil window (Holford et al. [2013] and this study). However, in others cases, this increase in temperature may adversely affect the maturity of hydrocarbons by overcooking the source rock (Barber et al., 1988; Kingston and Matzko, 1995). Volcanic facies can also act as seals/traps (Holford et al., 2013) and if fractured, they serve as migration pathways (Rateau et al., 2013). Similarly, a volcanic flow might form the reservoir (e.g., Zhang and Marfurt, 2011). Delpino and Bermudez (2009) draw on experiences in the Neoquen and San Jorge Basins of Argentina and Bolivia and find that igneous intrusions can increase and decrease reservoir permeability and may also give rise to fractures in overlying clastic reservoirs through differential compaction on batholiths. Farooqi et al. (2009) provide an excellent summary of the rich diversity of igneous reservoirs from around the world. One of the key means of identifying igneous extrusions and intrusions is through their morphology, either seen in a vertical section or through the attribute time and horizon slices. Planke et al. (2005), Klarner et al. (2006), Jackson et al. (2013), Alves et al. (2015), and Delpino and Bermudez (2009) as well as others find that igneous sills often appear to be of high amplitude and bowl shaped, climbing upward to form a stacked but offset pattern. Klarner et al. (2006), Pena et al. (2009), and Zhang and Marfurt (2011) all map the characteristic volcanic cones seen on the earth's surface, although the associated volcanic flows and tuff appear similar to mass-transport complexes and other sedimentary features, such as lava flows that mimic distributary channels mapped by McArdle et al. (2014). We have not seen any clear images of feeder stocks on data that we have analyzed from Mexico, China, or New Zealand, with the

---

[1] The University of Oklahoma (OU), School of Geology and Geophysics, Norman, Oklahoma, USA. E-mail: lennoninfante@ou.edu; kmarfurt@ou.ed.

Manuscript received by the Editor 24 December 2016; revised manuscript received 16 March 2017; published online 15 June 2017. This paper appears in *Interpretation*, Vol. 5, No. 3 (August 2017); p. SK121–SK140, 34 FIGS.

http://dx.doi.org/10.1190/INT-2016-0244.1.

chaotic column of amplitude beneath a volcanic cone being overprinted by velocity pull-up and degraded imaging on time-migrated data volumes. The second author has found near-vertical dikes to be very well-imaged by coherence volumes in the San Jorge, Santos, Neoquen, and Portiguar Basins of South America, although none of these images have been released for publication. Klarner et al. (2006) find that identifying easily imaged features is key to identifying subtler or potentially misleading architectural elements of a volcaniclastic system. Specifically, the presence of deeper sills near the shallower volcanic vents is a key warning that they may not be carbonate collapse features or buildups. Such feature identification and awareness is one of the main objectives of this special issue in *Interpretation*.

In addition to a specific geomorphology, igneous rocks often exhibit anomalous impedances. However, Klarner et al. (2006) find that high-impedance volcanic mounds and high-impedance carbonate buildups can be strikingly similar. Delpino and Bermudez (2009) use impedance inversion to confirm and help to map intrusive sills that finger upward. Alves et al. (2015) analyze a Brazilian survey and show that the polarity is opposite for igneous and gas-charged sand "bright spots." Zhang and Marfurt (2011) use well control to map the reservoir facies in a volcanic buildup in the Songliao Basin of northeast China. Sarkar et al. (2016) find that the interbed multiples associated with high-impedance volcanic sills can be stronger than underlying primaries, and if picked in the velocity analysis, they can give rise to erroneous images.

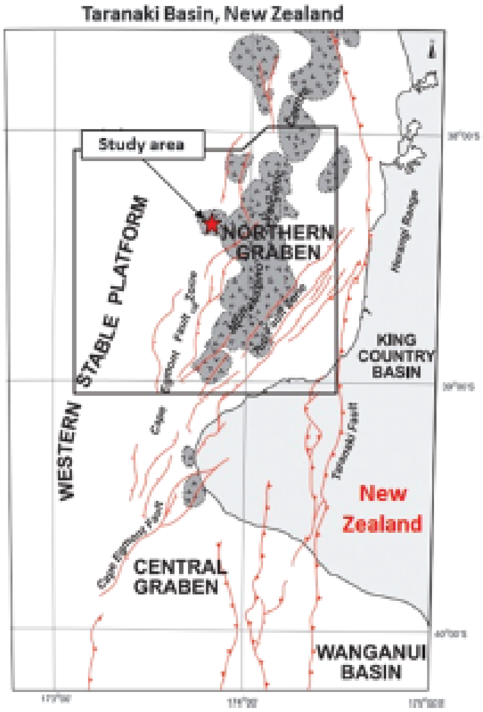

Figure 1. Location of the study area showing the structural style of the basin and the distribution of volcanic events. After King et al. (1993), King and Thrasher (1996), Thrasher et al. (2002), and Hansen and Kamp (2006).

Regardless of the nature of the igneous event, three fundamental questions need to be asked when exploring in basins affected by magmatic events. First, can we easily distinguish extrusive bodies such as volcanoes from carbonate buildups using seismic data? Second, do igneous bodies impact petroleum systems negatively or positively? Third, should we always categorize igneous bodies as being nonreservoirs? These are the questions that we will try to answer based on the data available for this research.

In this paper, we use seismic amplitude data to identify and map igneous intrusions such as hornfels, sills, and dikes (of which spatial and temporal associations are essential for distinguishing extrusive bodies such as volcanoes from carbonate buildups). We also compute geometric attributes from the 3D seismic amplitude data including dip magnitude, dip azimuth, and coherence to map the volcanic cone and associated faulting in the differentially compacted overburden. We use seismic stratigraphy principles and geomorphology combined with seismic texture and frequency attributes in a self-organizing clustering technique (self-organizing maps [SOMs]) to map productive and unproductive zones of the oil-bearing Miocene Kora volcano in the Taranaki Basin of New Zealand. Finally, we investigate the reasons of the absence of hydrocarbons in the unproductive zones through calibration of core and well data present in basin modeling, well completion, and geochemistry reports publicly available online in the New Zealand, Petroleum and Minerals (Ministry of Business, Innovation, and Employment, 2005).

Geologic background

The study area is in the Northern Graben of the Taranaki Basin, New Zealand (Figure 1). Although very extensive and complex, the evolution of the Taranaki Basin can be briefly summarized in three major phases of deformation: phase one, Cretaceous to Paleocene (approximately 84–55 ma) extension; phase two, Eocene to recent (approximately 40–0 ma) shortening; and phase three, Late Miocene to recent (approximately 12 ma) extension (Giba et al., 2010). Late Cretaceous extension was responsible for the breakup of Gondwana (King and Thrasher, 1992, 1996), whereas shortening in the Taranaki Basin is thought to have formed as a consequence of the subduction of the oceanic Pacific plate with the continental Australian Plate (Demets et al., 1994; Beavan et al., 2002). The last phase of deformation in the Taranaki Basin was the Miocene and younger extension. It was accompanied by volcanism that commenced at approximately 16 myr and continues at Mt. Taranaki today (Neall et al., 1986; Hayward et al., 1987; Bergman et al., 1992; King and Thrasher, 1992). These volcanic centers are mainly stratovolcanoes, of mostly low-medium K andesitic composition and, together with their north–northeast-trending alignment (Figure 1) parallel to the late Miocene subduction margin, suggest that magmas are derived from the subducting Pacific Plate beneath the basin (Bergman et al., 1992).

Data set

The data set available for this study is shown in Figure 2, and it includes approximately 200 km^2 of 3D prestack time migration (PSTM) seismic data acquired in 2006, six wells with four of them inside the 3D seismic survey (Kora-1–4) each with caliper, gamma ray, bulk density, neutron porosity, P-sonic resistivity logs, and some of them with photoelectric factor. The operator of these wells drilled in the 1980s was the former ARCO Petroleum New Zealand Inc. Basin modeling, geochemistry, and well-completion reports for all the wells as well as one 2D PSTM seismic line passing through one of the wells outside the 3D seismic survey are also available.

Drilling history

According to the well-completion reports, the Kora-1 well was drilled in the 1980s by ARCO Petroleum New Zealand Inc. to test the Eocene Tangaroa Sandstone member, with a large dome structure associated with a Miocene age volcano. The well was drilled to a TD of 3421 m (11,224 ft) and encountered significant indications of hydrocarbons in the top of the Miocene volcanic section and in the upper and lower Tangaroa Sandstone. Results of three drill stem tests (DSTs) evaluating the Tangaroa shows indicated that the Tangaroa Sandstone member was a tight formation. However, the Miocene volcanic sections were tested as a sidetrack Kora-1A. A long-term production test was conducted, which resulted in 32 API oil flow of 668 BOPD for 254 h. Following the success of hydrocarbons found in the Miocene, volcanic wells Kora-2–4 were drilled to keep testing this volcanic potential. Only shows were found in wells Kora-2 and Kora-3, whereas Kora-4 was barren of hydrocarbons. Therefore, the 3D Kora seismic survey was acquired in 2006 with the objective of imaging the Miocene Kora volcano.

Lateral extension of the Kora volcano and faults associated with cooling and collapse of volcanic edifice

Figure 3 shows a general view of the Kora volcano with an arbitrary inline and crossline in 3D view, in which different amplitude/facies can be easily identified. Within the volcano itself, we can identify two different facies: a high-amplitude continuous facies and a more chaotic moderate amplitude facies. A bright, shallow, low-frequency flat reflector appears above the volcano. This feature may indicate the presence of inorganic gases, such as water vapor, carbon dioxide, and sulfur dioxide, which are commonly found in volcanoes.

Extracting a time slice through the coherence attribute at 2050 ms shows a semicircular, low-coherence feature that delineates the extent of the volcano. The extension of the Kora volcano is approximately 6–7 km

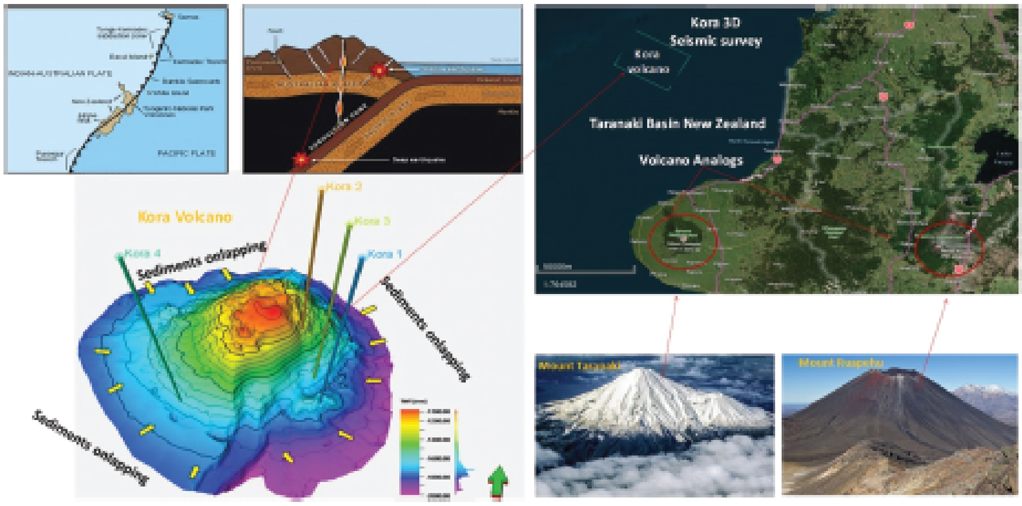

Figure 2. Above: model of the subduction of Pacific Plate with the Australian Plate. Below: 3D view of time-structure map of the Miocene Kora volcano and nearby modern onshore analogs.

in diameter, with a preserved peak height of approximately 1 km. These dimensions are comparable with the more modern Mount Taranaki (approximately 4 km in diameter and 2518 m of peak height) and Mount Ruapehu (approximately 6–7 km in diameter and 2797 m of peak height) analogs in the Taranaki Peninsula, New Zealand. Normal faults are observed as low-coherence radial patterns similar to those created by salt diapirs (Rojo et al., 2016) (Figure 4). Unlike salt diapirs that create these radial-fault patterns by upward migration breaking through the host rocks, the cooling and collapse episodes of the volcanic body are responsible for producing the radial-fault patterns. Such a hypothesis can be proposed because this deformation is observed in sediments above the volcano, which postdate the volcanic activity (the 2050 ms time slice cuts mainly postvolcanic sediments). Radial fault patterns like those created by the Kora volcano are likewise documented by Giba et al. (2013) also in the Northern Graben of the Taranaki Basin. Similarly, corendering volumetric dip azimuth and dip magnitude, we image the volcano and the radial normal faults, showing the direction in which both events are dipping. The different colors in the volcano indicate a dome structure (Figure 5).

Intrusive igneous bodies and seismic amplitude variability within the Kora volcano

Although not extensively documented in seismic data, the most common features related to igneous bodies are intrusive sills like those described by Planke et al. (1999), Holford et al. (2013), Jackson et al. (2013), and Alves et al. (2015) as well as more recently by Magee et al. (2016) and Cortez and Cetalte-Santos (2016). To catch the elements created by the episodic Miocene magmatic events, we create sequential vertical sections with different orientations through the amplitude volume (Figures 6, 7, 8, and 9). These vertical-amplitude sections show the dome shape of the top of the volcano exhibiting high amplitude. Its bright amplitude at the top is due to the high-impedance contrast between

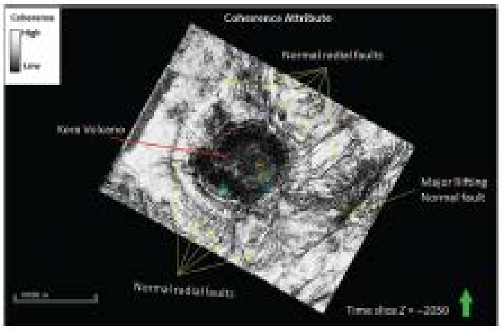

Figure 4. Time slice at 2050 ms through the coherence seismic attribute. The circular low-coherence feature (red arrow) delineates the extent of the volcano. Note the low-coherence radial fault pattern (yellow arrows). The four colored dots inside the volcano represent wells Kora-1–4.

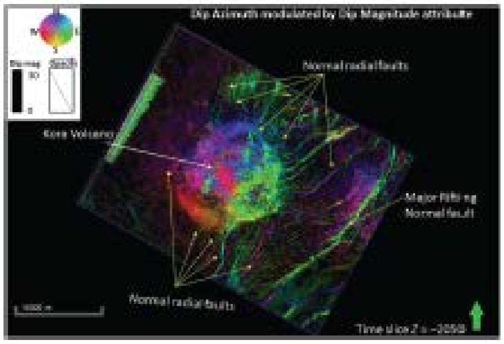

Figure 5. Time slice at 2050 ms through the dip azimuth modulated by dip magnitude seismic volumes. Like the previous figure, this attribute illuminates the volcano and the radial faults, showing the direction in which both events are dipping. The different colors in the volcano indicate a dome structure. The four black dots inside the volcano represent wells Kora-1–4.

Figure 3. A representative 3D composite section of the amplitude data showing the Kora volcano and the good signal-to-noise ratio, allowing the identification of different seismic facies related to the volcano.

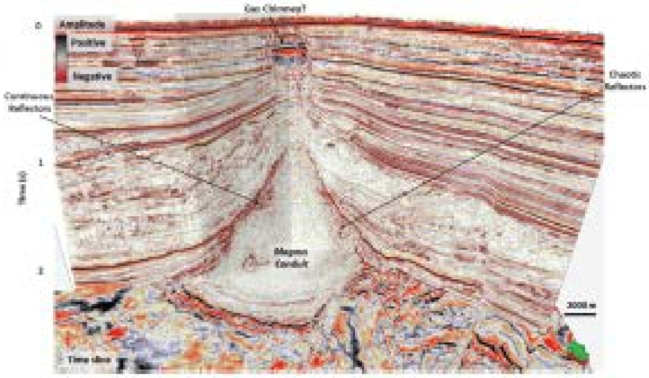

the siliciclastic sediments and volcanic rocks. Associated with this Miocene igneous intrusion are saucer-shaped sills, dikes, a gas chimney emanating from the center of the volcano, and the magma conduit distinguishable from other elements of the volcano by the anomalously low seismic amplitude. Sedimentary wedges also occurred at both sides of the volcano indicating that the igneous body is formed before the wedges (Figures 6-9).

Figure 10 displays a vertical amplitude section illustrating "saucer"-shaped intrusive bodies, in which the high-amplitude and discontinuous nature is evident. The upward migration of these intrusions deforms the surrounding sediments creating forced folds, faults (Jackson et al., 2013; Magee et al., 2014; Alves et al.,

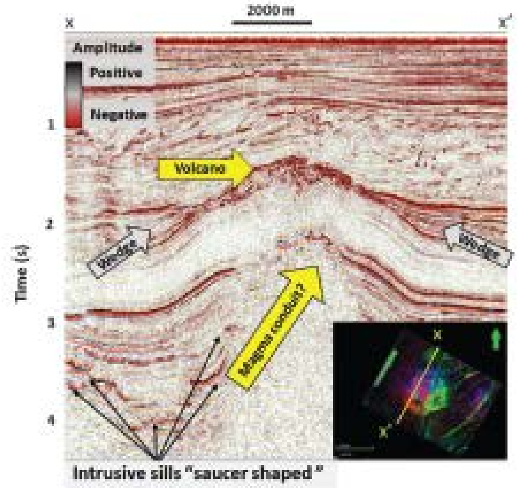

Figure 6. Vertical section XX' through the seismic amplitude volume. The high reflectivity of the top of the volcano is due to siliciclastic/igneous impedance contrast. The onlapping wedge at both sides of the volcano indicates that the volcano formed before than the wedges.

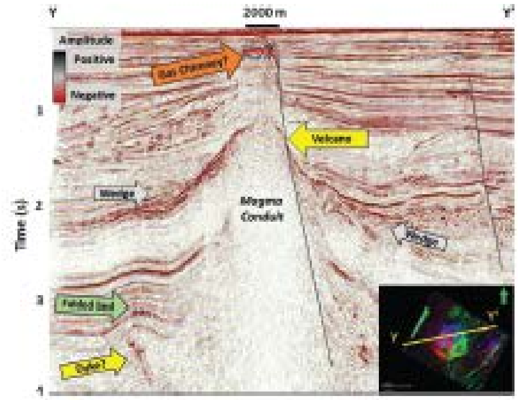

Figure 7. Vertical section YY' through the seismic amplitude volume. The orange arrow points to a localized high-amplitude, low-frequency event, which we interpret to be an inorganic gas chimney emanating from the volcano. Notice the same onlapping wedges at both sides of the volcano shown in the previous figure, indicating the volcano formed before the wedges.

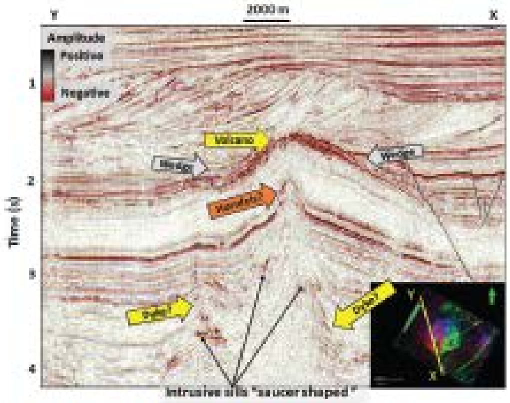

Figure 8. Vertical section XY' through the seismic-amplitude volume. The orange arrow indicates a pop-up structure, which is probably the result of magma rising and breaking into the host rock, creating a zone of hornfels. Note again the high reflectivity and the onlapping wedge at both sides of the volcano seen in the previous figures, indicating that the volcano formed before than the wedges.

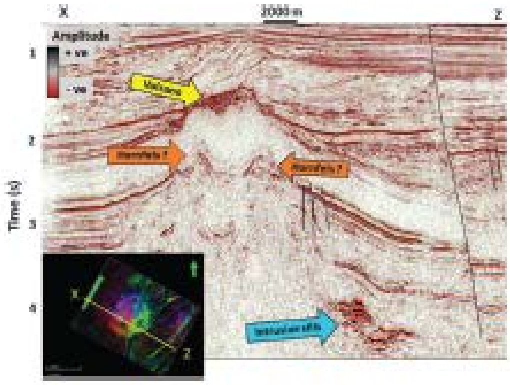

Figure 9. Vertical section XZ' through the seismic-amplitude volume. The orange arrows indicate two pop-up structure, which we interpret to be the result of magma rising and breaking into the host rock, creating a zone of hornfels. The cyan arrow indicates an intrusive sill characterized by localized high-amplitude reflectors.

2015), and possibly hornfels such as those described in outcrop by Liborius-Parada and Tazzo (2012) (Figures 8 and 9). The spatial distribution of these sills is illustrated using a set of corendered time slices through the instantaneous envelope attribute. Figure 11 shows the semicircular distribution of these intrusive sills about the volcano, allowing us to hypothesize that these intrusions are related to the same magma conduit that later created the Kora volcano in the Early Miocene. Such distributions of sills can be seen as evidence for multistage volcanic episodes within the Kora volcano edifice.

Lithologic composition of the volcanic/volcaniclastic sequences from well completion reports

A vertical random line through all the wells available in the study area shows different seismic facies regarding the volcanic/volcaniclastic sequence. Because the Ariki-1 well is outside the Kora 3D survey, we use an additional available 2D PSTM seismic section that augments the 3D seismic survey and ties the Ariki-1 well (Figure 12). The Ariki-1 well cuts through some chaotic seismic facies similar to mass-transport deposits (MTDs) documented by Posamentier and Kolla (2003), Lee et al. (2004), Dallas et al. (2013), and Qi et al. (2016) that originated from the western flank of the volcano. The well completion report reads cuttings from the interval 2256 to 2556 m as volcaniclastic deposits: Tuffaceous material is most abundant in the lower part of the formation and decreases upward, reflecting the waning of volcanic activity. The lithology varies from gray mudstones with a tuffaceous matrix, including biotite, chlorite, pyrite, and at the base, light to moderate gray sandy tuffs. These tuffs contain abundant angular to subangular, fine to medium poorly sorted clasts of biotite, garnet, olivine, hornblende, and aphanitic material together with quartz and feldspar of sedimentary and volcanic origin.

The Kora wells 1–3 drilled through the crest and eastern flank of the volcano, which are characterized by chaotic moderate amplitude. According to the Kora-1–3 well-completion reports, Kora wells-1–3 cut through a series of pyroclastic flows deposits of andesite composition dominated by plagioclase (andesine), hornblende, and pyroxene. Textural characteristics vary from sand-size andesite tuff breccia to clast-supported andesite agglomerates. Induration qualities also vary widely from unconsolidated to well-consolidated. Core data in Kora-1 indicate fair to good porosities (25% average), and good oil shows at the top 25 m, becoming fair through the base.

The Albacore-1 well cuts through salt/pepper seismic facies. The well completion report indicates the well drilled through 11 m of an aggregate of sandstone, siltstone, and mudstone in which andesitic detritus is a dominant constituent. This detritus is overall brownish gray, mainly fine to medium grained, moderately to poorly sorted, angular to subangular, and it is composed

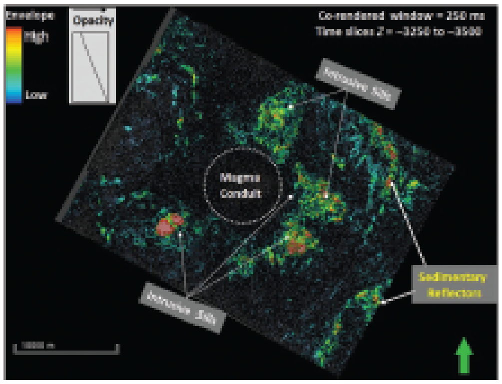

Figure 11. Corendered time slices through the envelope attribute volume illustrating the aerial distribution of the intrusive sills. Note the circular distribution of the sills about the magma conduit.

Figure 10. Vertical section YZ′ through the seismic-amplitude volume. The high-amplitude localized reflectors at the bottom of the figure represent intrusive sills. Their principal characteristics are high-amplitude "U" or "saucer"-shaped, described by Planke et al. (2005) and Cortez and Cetale-Santos (2016), which in turn give rise to the folding of the previously deposited sedimentary overburden as they rise (blue arrow).

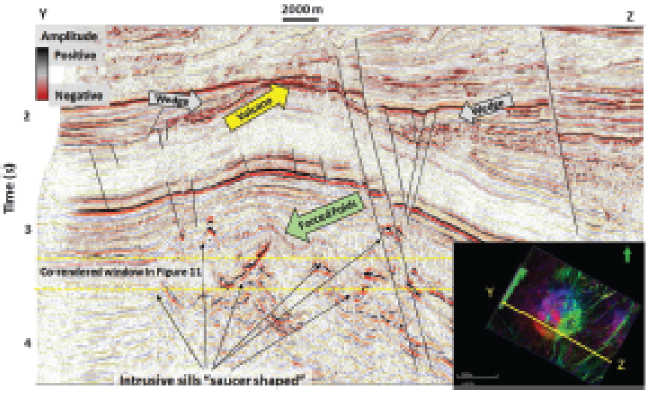

of 70% quarts and feldspars, common black pyroxene/hornblende with well-developed crystal faces, and yellowish green apatite or epidote.

Based on the analyzed seismic facies and core/cuttings integration, we can determine that the MTD-like facies on the western part are a result of volcanic subaqueous flow. The eastern crest and flanks of the volcano correspond to pyroclastic flows, and the salt-and-pepper-like facies in the eastern part refer to andesitic detritus mixed with clastic sands and mudstones (ADC) (Figure 12).

For utilitarian reasons, the well-log expression of this volcanic sequence is better illustrated by correlating the six wells using the top of the volcanic sequence as a flattened surface (Figure 13). Because the gamma-ray tool reads uranium, thorium, and potassium, the low gamma-ray response is due to the intermediate (in contrast to felsic) magma composition (Somasundaram et al., 2017) of the volcano (Kora-1 well report), which is mainly composed of calcium plagioclase, pyroxene, and some quartz (Bowen, 1922). Per the mineralogy report, the mineralogy composition is 42% plagioclase, 8% pyroxene, 6% quartz, and 31% of smectite clay giving an average grain density of 2.64 g/cm^3. This grain density of 2.64 g/cm^3 is used for calculating density porosity in the Kora wells, which ranges from 20% to 26%. In addition, a summarized well-log and a seismic expression of the volcanic architectural elements are shown in Figure 13.

The seismic well ties with the Kora wells indicate that wells Kora-1–3 penetrate the same chaotic moderate amplitude seismic facies, whereas the Kora-4 well penetrates the high-amplitude continuous seismic facies (Figure 14). Core pictures and descriptions available from the Kora completion well reports show that the volcanic rocks penetrated by Kora-1–3 wells represent a series of altered andesitic clasts with grain size all the way from tuff (volcanic ash) to pebbles representing several sequences of pyroclastic flows (Figure 15). This series of altered andesitic class exhibits a repeated pattern of fining-upward clasts every 5–8 m, which serves as evidence for multistage volcanic episodes within the Kora-volcano edifice. Furthermore, sidewall cores from the upper volcanic section were taken from Kora-1 well for porosity and permeability measurements. The Kora-1 well-completion report reads porosity ranges of 20%-26% and 170-240 mD of permeability, which agrees with the log-derived porosity.

Geomorphology of the Kora volcano

The conic geometry of the volcano makes it necessary to study it in different directions. Figure 16 shows the vertical section B-B′ in the northwest–southeast direction; such section crosses well Kora-4 illustrating the

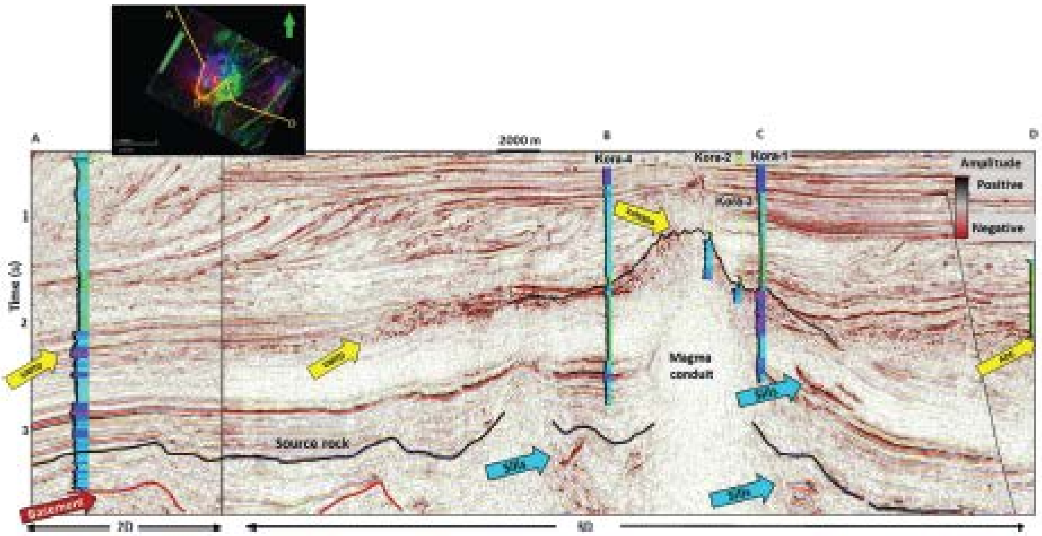

Figure 12. Vertical section ABCD showing an additional 2D PSTM seismic section that augments the 3D seismic survey and ties the Ariki-1 well. Kora wells 1–3 penetrate the volcano giving information about the chaotic moderate amplitude seismic facies. The yellow arrows indicate two different seismic facies: The Ariki-1 well on the western part identifies Tuffaceous sandstones to claystones, whereas the Albacore well to the east encounters andesitic detritus mixed with clastic deposits. Confirming that the unknown seismic facies are in fact related to the volcanic event. VMTD, volcanic mass-transport deposit; ADC, andesitic detritus mixed with clastic.

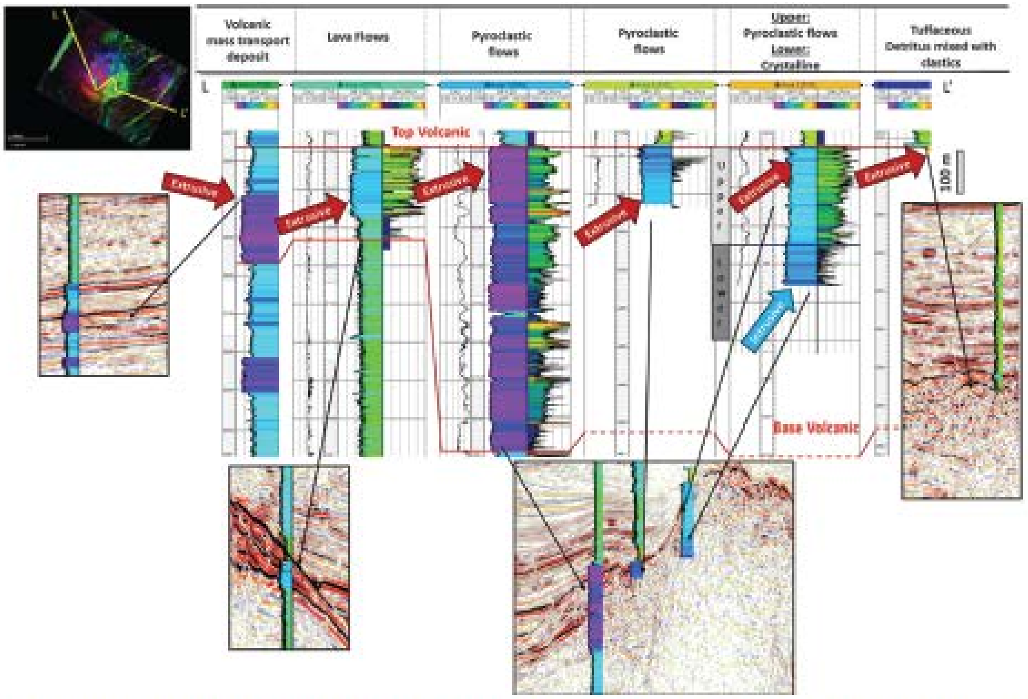

Figure 13. Correlation of all the wells available in this study. Track 1 displays the caliper log, track 2 displays the gamma ray, and track 3 displays the density porosity logs. Sections are flattened on top of the volcanic sequence for easier correlation. Note the low gamma-ray response in all the wells consistent with intermediate versus felsic-magma composition (Somasundaram et al., 2017). The Albacore well on the far right only shows the top few feet of the volcanic event. The average density porosity is approximately 25% in Kora-1. All wells are shown with their associated seismic expression.

Figure 14. Vertical section AA′ through the four Kora wells. The wells are tied to the seismic data using conventional seismic well-tie techniques. The seismic amplitude shows that the chaotic moderate-amplitude reflectors are penetrated by wells Kora-1–3, whereas the strong continuous reflectors are penetrated only by well Kora-4.

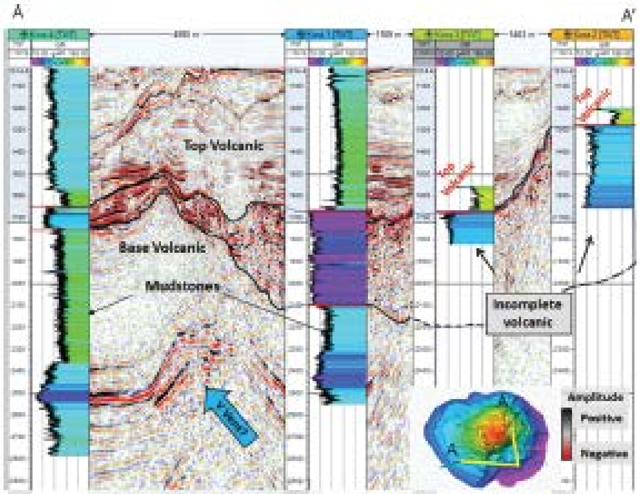

strong continuous and chaotic reflectors. We also notice two onlapping wedges at both sides of the volcano indicating that the volcanic activity originated before these events. There is also evidence of the magma conduit breaking the host rocks (blue arrow below). The north–south vertical section illustrates mainly the chaotic seismic facies penetrated by wells Kora-1–3. The magma conduit is also apparent in the seismic section evidenced by the anomalous low amplitudes in the center of the volcano; the onlapping wedges are also present (Figure 17). Similarly, the east–west vertical section shows two distinctive seismic facies within the volcano. Wells Kora-1 and 4 cut chaotic moderate amplitude and continuous high-amplitude reflectors, respectively, the onlapping wedges are also present (Figure 18). The presence of the onlapping wedges in the previous figures suggests that these sediments were shed from all directions.

Analyzing the core data from Kora-1–3, we can identify the chaotic moderate amplitude seismic facies as pyroclastic flows. Although the Kora completion well reports find no significant difference in mineralogic composition in volcanic rocks penetrated by Kora-1–3 to those penetrated by Kora-4, the slightly higher gamma ray in Kora-4 maybe due to higher clay content (possible higher alteration of plagioclase to clay rather than in situ clay sedimentation). Thus, the nature of the continuous high-amplitude seismic facies remains unknown. For this reason, we use clustering techniques and geomorphology to identify the architectural element represented by the continuous high-amplitude seismic facies.

SOMs and geomorphology

The SOM is a classification technique that extracts similar patterns inherent in multiple seismic attribute volumes and displays those similarities in a color-coded map, with different colors representing different facies (Zhao et al., 2016). The SOM with detailed steps in our workflow is shown in Figure 19. The input attributes to

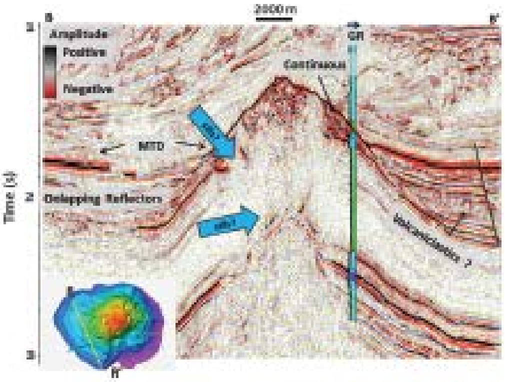

Figure 16. Magnified vertical magnified slice BB′ through the seismic amplitude volume showing the chaotic moderate amplitude reflectors adjacent to strong continuous reflectors penetrated by the Kora-4 well. An MTD is observed on the northwest flank of the volcano.

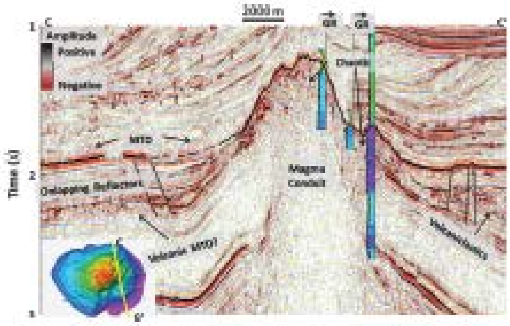

Figure 17. Magnified vertical section CC′ through the seismic amplitude volume showing the chaotic moderate amplitude reflectors penetrated by wells Kora-1–3 and the strong continuous reflectors in the northwest flank. Two different seismic facies are observed on the onlapping wedges.

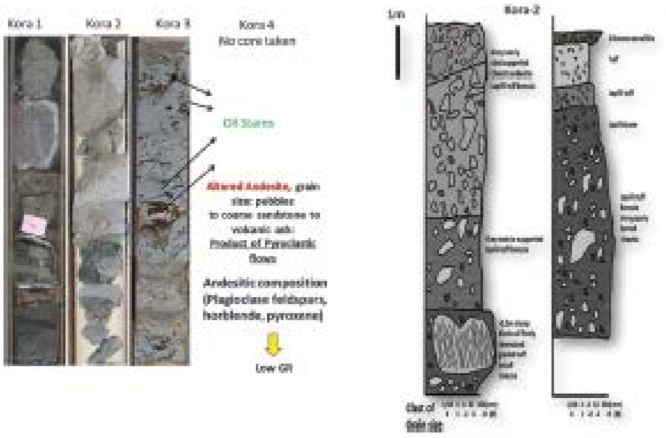

Figure 15. Core data available for wells Kora-1–3 and a cartoon of the volcanic facies present in Kora-2. The sticky note in Kora-1 is approximately 3 cm in length.

feed the SOM are texture (homogeneity and entropy), peak frequency, and peak magnitude attributes. These attributes are extracted from the raw amplitude data using software developed at the University of Oklahoma (e.g., Matos et al., 2011; Qi et al., 2016).

Hall-Beyer (2007) defines texture as "an everyday term relating to touch that includes such concepts as rough, silky, and bumpy. When a texture is rough to the touch, the surface exhibits sharp differences in elevation within the space of your fingertip. In contrast, silky textures exhibit very small differences in elevation." Seismic textures work in an analogous manner with elevation replaced by amplitude, and the probing of a finger by a rectangular or elliptical analysis window oriented along the structure.

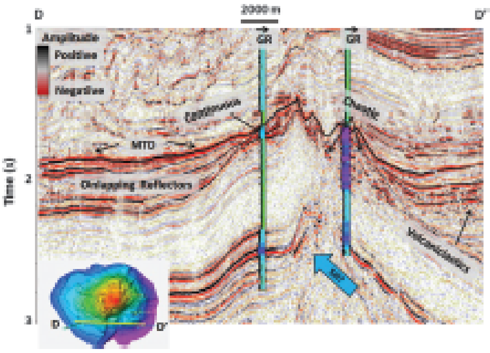

Figure 18. Magnified vertical section DD' through the seismic amplitude volume showing the chaotic moderate-amplitude reflectors penetrated by the Kora-1 well, whereas the strong western continuous reflectors are penetrated only by the Kora-4 well. An MTD is observed on the western flank of the volcano. Volcaniclastics are again present in the eastern onlapping wedge.

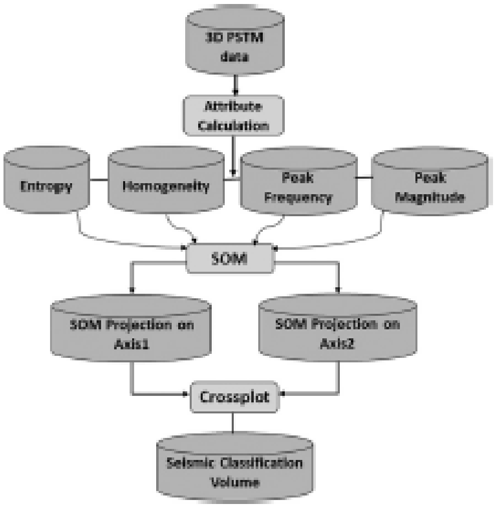

Figure 19. Workflow implemented for unsupervised seismic facies classification.

In general, texture attributes provide images that are somewhat fuzzy and not very useful for human interpretation. Rather, these attributes serve as input data to SOMs or other clustering algorithms.

The correlation of the Kora wells with the homogeneity and entropy texture attributes displays the continuous high-amplitude facies to have values of homogeneity and low values of entropy.

The opposite is true for the chaotic moderate-amplitude facies, suggesting that we can separate these two (Figures 20 and 21). The peak frequency modulated by peak magnitude attribute displays the dominant frequency for the entire volcanic sequence, ranging from approximately 40–55 Hz (Figure 22). Although exhibiting similar frequencies, low values of peak magnitude are observed in the center of the fence diagram (magma conduit) and in between different zones about the Kora-4 well.

Consequently, we input the previously computed seismic attributes into the SOM facies classification. Because we are using four attributes at each voxel, our analysis is in the 4D attribute space. In this case, the objective of SOM is to fit a deformed 2D surface (called a manifold) distribution of the data points living in 4D space. Each data point is projected onto the nearest part of manifold, which is then mapped to a 2D color bar. In this manner, voxels that have a similar response (they lie next to each other in 4D space) project onto nearby locations on the manifold and are displayed as similar colors. In contrast, voxels that exhibit a very distinct attribute behavior (they lie far from each other in 4D space), project onto different parts of the manifold and appear as different colors. Details can be found in Zhao et al. (2016) and Roden et al. (2015).

Figure 23 shows a vertical slice connecting the four Kora wells illustrating the distribution of the chaotic moderate and the continuous high-amplitude seismic facies. The same vertical slice is then shown with our SOM facies classification (Figure 24). From this classification, we can observe three distinctive colors (facies). The orange colors represent the continuous high-amplitude facies, whereas the purple colors represent the chaotic moderate amplitude facies. The third, green-ish, facies are more representative of the siliciclastic sediments underlying and onlapping onto the volcano. It is still not clear from this vertical slice what is the nature of this orange facies, which appear to be more dominant adjacent the Kora-4 well. Extracting the SOM classification on the top of the time-structure map of the volcano, we can observe its geomorphology. We observe the orange facies to be mainly distributed on the western flank of the volcano, whereas the purple facies appear to be more

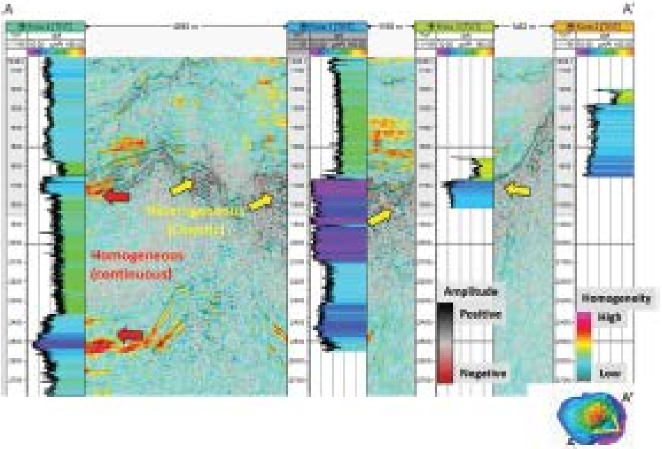

Figure 20. Vertical slice AA′ through the seismic amplitude volume corendered with the homogeneity seismic texture attribute. The chaotic moderate-amplitude reflectors correspond to low values of homogeneity, whereas the strong continuous reflectors correspond to high values of homogeneity.

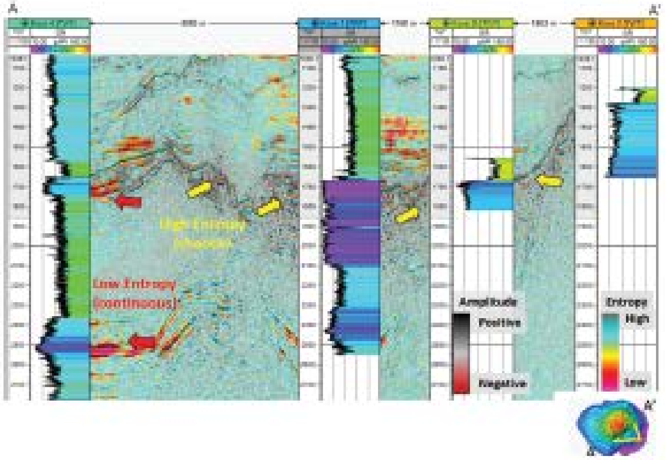

Figure 21. Vertical section AA′ through the seismic amplitude volume corendered with the entropy seismic texture attribute. Note that the chaotic moderate-amplitude reflectors correspond to high entropy, whereas the strong continuous reflectors correspond to low entropy.

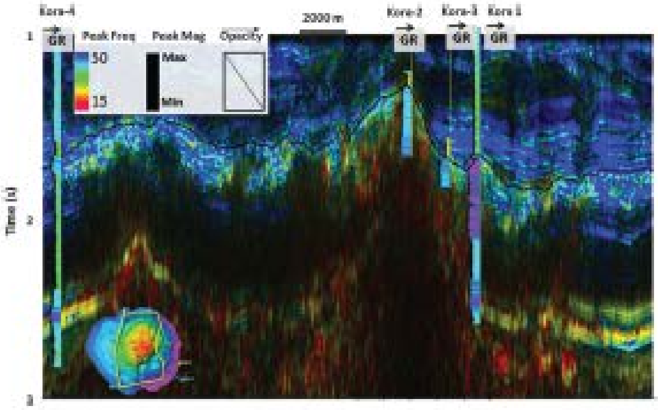

Figure 22. Vertical slice connecting the four Kora wells through the peak frequency modulated by peak magnitude attribute. Notice the frequency content of the volcanic sequence is cyan to blue indicating frequencies of approximately 45–55 Hz.

prominent in the eastern flank and between the orange facies (Figure 25). A solid black line is drawn to highlight these unknown facies. Based on the geomorphology and structural relation to the volcanic cone, we interpret the orange facies to be lava flows/volcanic tongues, such as those reported by Klarner et al. (2006) and McArdle et al. (2014). In terms of the spatial distribution in which pyroclastic and lava flows extend: One possible explanation to why the purple facies (pyroclastic flows) are more prominent in the eastern flank of the volcano and the orange (lava flows) facies dominate the western flank, may be related to the paleo-water currents flowing in the direction of the shoreline and evidenced by the ADC facies in the east (Figure 12; which appears to have been east-southeast, like today's Taranaki Peninsula shoreline), whereas the lava flows where dense enough to fight the water resistance and deposits mainly in the western flank.

Dry-hole analysis

To determine the failure of Kora-4 in the Miocene volcanics, we need information about the source rock in the Northern Graben of Taranaki Basin. According to the geochemistry report, a source rock (Waipawa Shale) interval is penetrated by well Ariki-1. Cuttings from this unit exhibit total organic matter ranges between 1.8% and 6%. These samples along with the crude oils from Kora-1 DTS's were analyzed by Geotechnical services Pty. Ltd. in 2005 for Crown Minerals, New Zealand. Their analysis based on biomarker profiles concluded that the Kora-1 oils from DTSs in the Miocene volcanics and the Eocene Tangaroa sandstone correlate well with the Paleocene Waipawa Black Shale

Figure 23. Vertical slice connecting the four Kora wells through the seismic amplitude volume showing the distribution of the chaotic moderate-amplitude and the strong continuous reflectors.

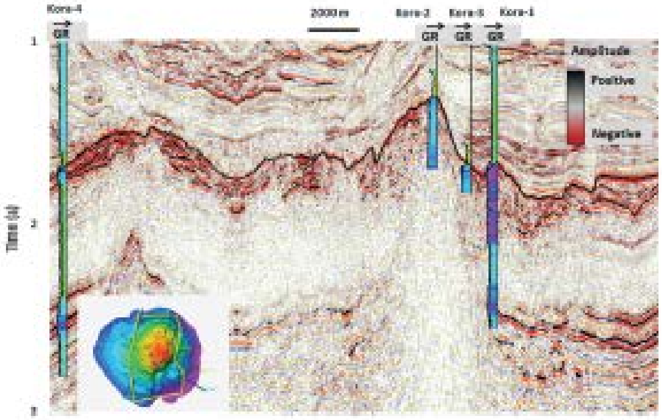

Figure 24. Vertical slice connecting the four Kora wells through the SOM classification showing the two distinctive colors (purple and yellow) indicating two different facies. The green facies represent sediments. Facies are colored based on our latent space axes.

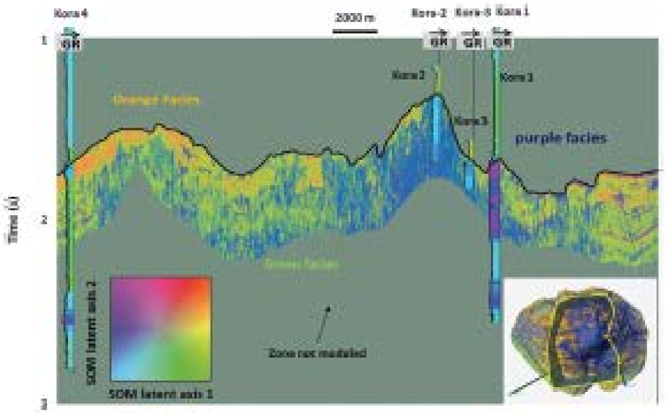

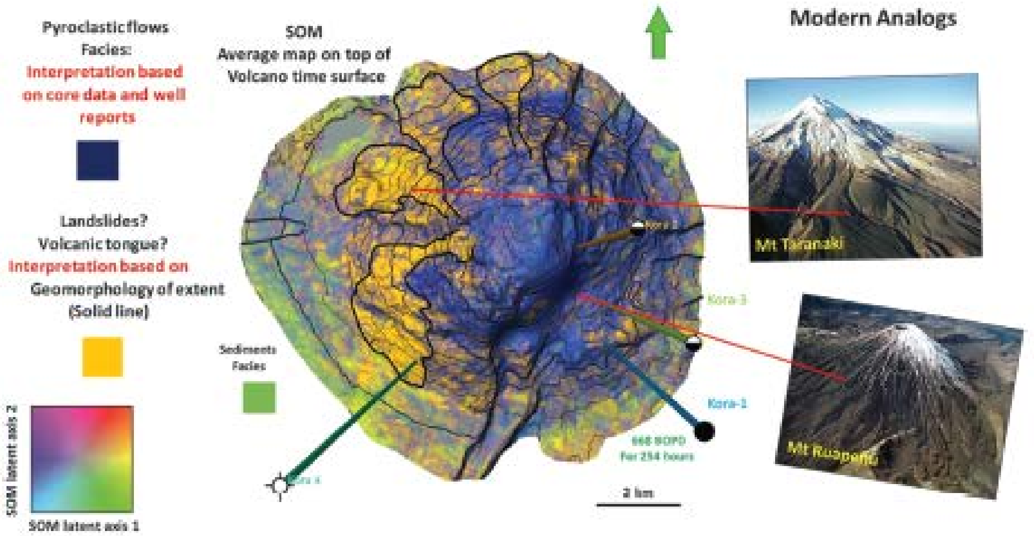

Figure 25. Seismic facies classification result using SOM. We interpret the purple facies to be pyroclastic flows based on the core descriptions provided in the wells completions reports for wells Kora-1–3. In contrast, the yellow facies we interpret to be lava flows/volcanic tongues, such as those reported by Klamer et al. (2006), are based on their geomorphology and structural relation to the volcanic cone. Facies are colored based on our latent space axes.

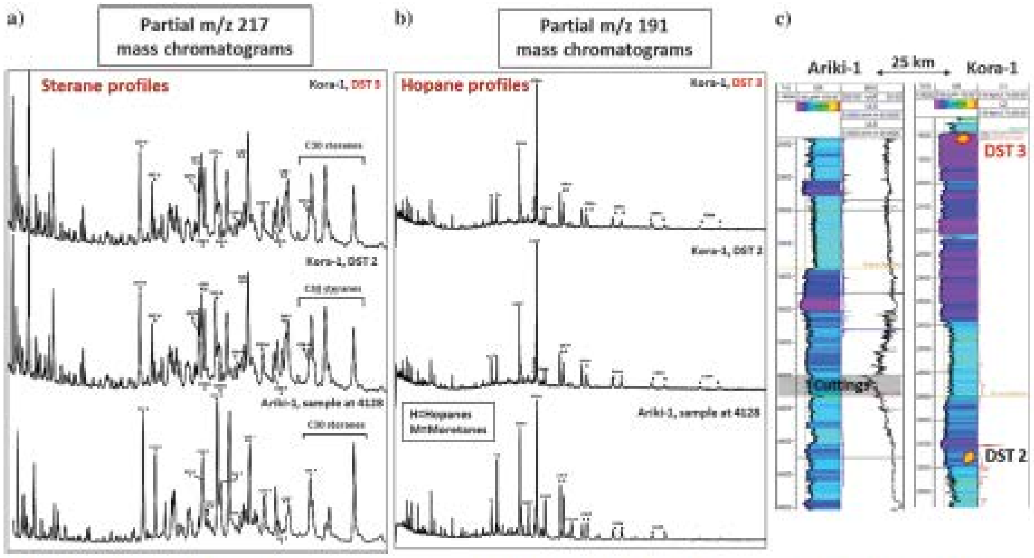

Figure 26. (a) Partial m/z 217 mass chromatograms showing the correlation between the sterene profiles of the Ariki-1 4128 m sample with the Kora-1 oils. (b) Partial m/z 191 mass chromatograms showing the correlation between the hopane profiles of the Ariki-1 4128 m sample with the Kora-1 oils. (c) Wells Ariki-1 and Kora-1 showing the gamma-ray log and the intervals analyzed for biomarkers. The second track in Kora-1 shows high kicks in the mudlogs. Figure reprinted with permission of Crown Minerals, New Zealand.

equivalent present in Ariki-1, (Figure 26). They also noticed that although the Ariki-1 analyzed cuttings samples were less mature (as one can observe in the low values of the resistivity log "LLD" in contrast to a mature source rock with high resistivity, like that described more recently by Infante-Paez et al., 2017) than the oils found in Kora-1, marine-derived sterane signatures, which include the presence of C30 components, characterize the Kora-1 oils and the Ariki-1 4128 m extract.

Altered thermal maturity

The difference in maturity from the samples in Ariki-1 and the Kora-1 crude oils is due to the ingenious activity present in nearby wells Kora-1–4 and absent in Ariki-1 (Figure 12). Evidence of the impact of this igneous activity in thermal maturity can be observed in the burial history and temperature profiles generated by the basin modeling report for Crown Minerals, New Zealand.

The Ariki-1 temperature profile obtained from bottom-hole data indicates a geothermal gradient of approximately 2.67°C/100 m (Figure 27), which is a normal gradient for passive margin basins (Nemčok 2016). In contrast, Figures 28 and 29 show the temperature and vitrinite reflectance R_o profile for wells Kora-1 and 4, respectively. Temperatures obtained for Kora-1 are more accurate because they were obtained from DST, whereas temperatures for Kora-4 were obtained from bottom-hole measurements. Although geothermal gradients for both Kora wells are similar (close to 3.25°C/100 m), the vitrinite reflectance measurements are substantially higher than the expected kinetics maturity trend (up to 5 R_o% in

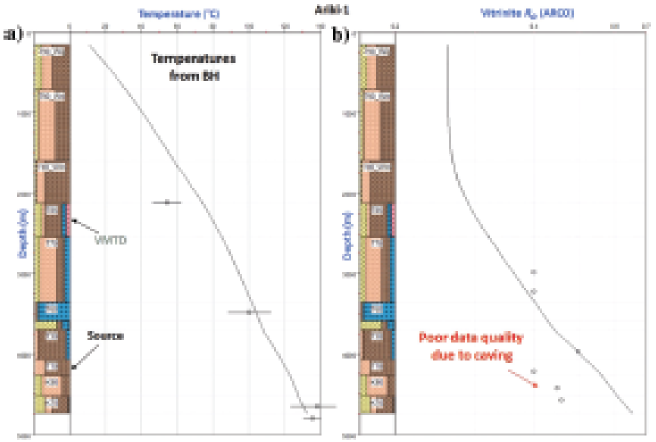

Figure 27. (a) Temperature profile of the Ariki-1 well. The circles with error bars are the BHT. (b) Vitrinite reflectance profile of the Ariki-1 well. The small circles are the measured vitrinite reflectance. Figure reprinted with permission of Crown Minerals, New Zealand.

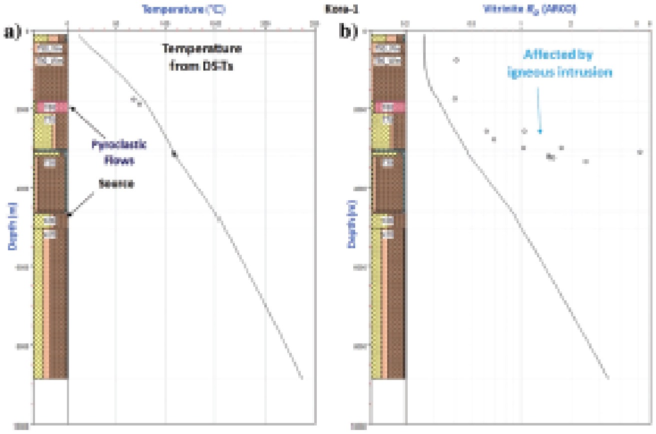

Figure 28. (a) Temperature profile of the Kora-1 well. The circles with error bars are the temperatures measured from DST. (b) Vitrinite reflectance profile of the Kora-1 well. The small circles are the measured vitrinite reflectance. Notice the offset of values of the measured R_o and the kinetics maturity model due to igneous activity. Figure reprinted with permission of Crown Minerals, New Zealand.

Kora-1). The higher R_o values are due to the excessive heat produced either by the igneous intrusions, streaming hot gases, or hydrothermal interactions with the surrounded rocks, as one can infer from the vertical amplitude sections (Figures 12 and 15–18).

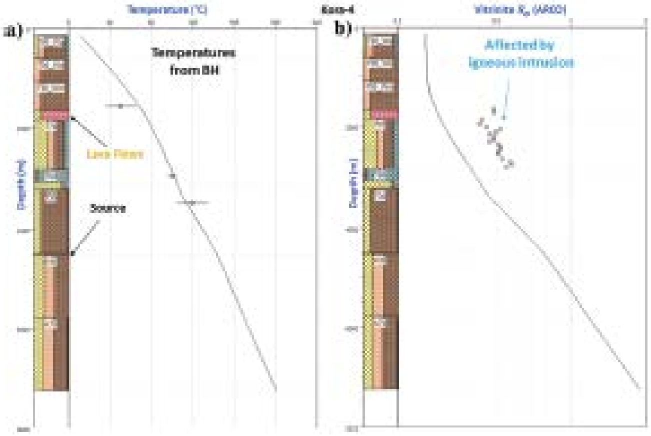

Figure 29. (a) Temperature profile of the Kora-4 well. The circles with error bars are the temperatures measured from BHT. (b) Vitrinite reflectance profile of the Kora-4 well. The small circles are measured vitrinite reflectance. Notice the offset of values of the measured R_o and the kinetics maturity model due to igneous activity. Figure reprinted with permission of Crown Minerals, New Zealand.

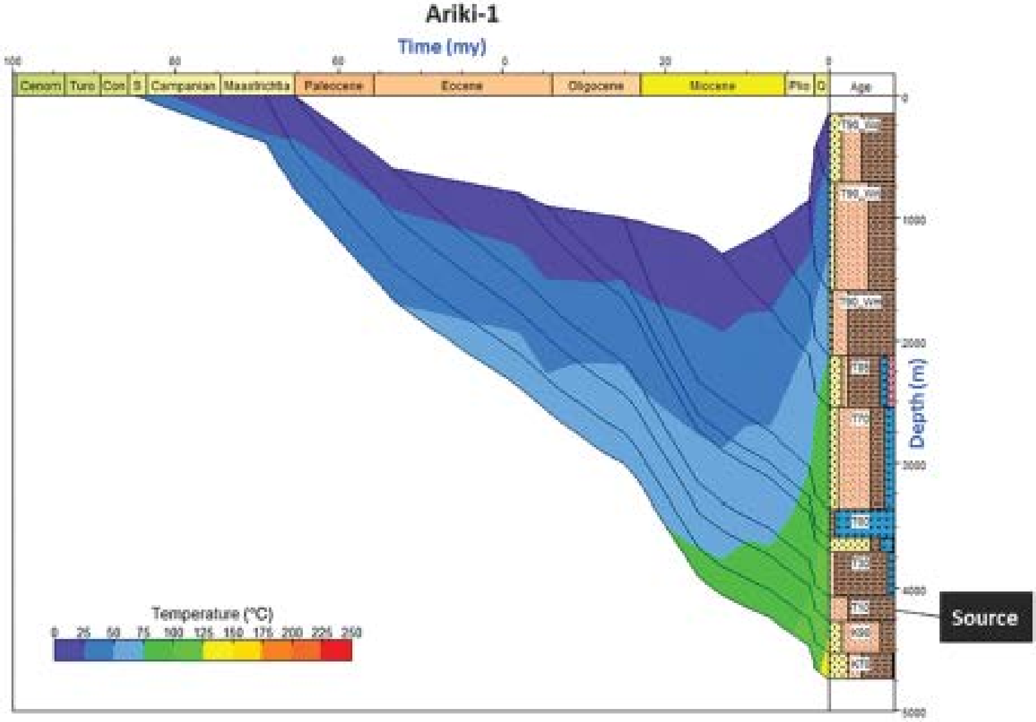

Figure 30. Burial history profile of the Ariki-1 well. Colors represent temperature based on the temperature profile from BHT. Colors represent temperature in °C. Figure reprinted with permission of Crown Minerals, New Zealand.

Migration pathways analysis

According to the basin modeling report, the Paleocene Waipawa source rock is believed to have spelled most of the hydrocarbons recently (5 ma) short after it entered the oil window (Figures 30 and 31). This hydrocarbon would have been stored in the Tangaroa sandstone, which is capped by the thick shale unit; furthermore, any movable hydrocarbon had to migrate through leaking faults. Figure 32 shows our interpreted horizons of the Paleocene Waipawa source rock, the top of the Eocene turbiditic Tangaroa Sandstone reservoir, and the top of the Miocene volcano with extracted dip magnitude and dip azimuth corendered with the dip magnitude, respectively (similar to Figure 5), in which the fault network can be observed. Figure 33 shows a 3D view of the mentioned horizons and the main faults

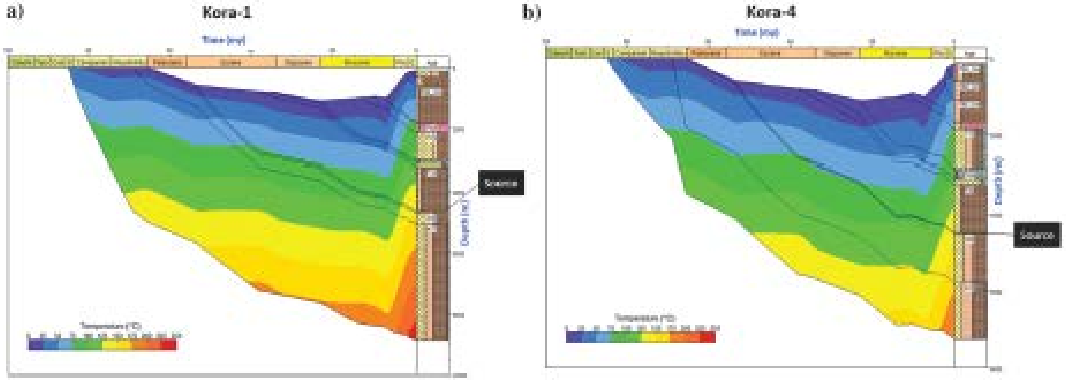

Figure 31. Burial history profile of the well Kora-1 and 4. Colors represent temperature based on the temperature profile from DST and BHT, respectively. Colors represent temperature in °C. Figure reprinted with permission of Crown Minerals, New Zealand.

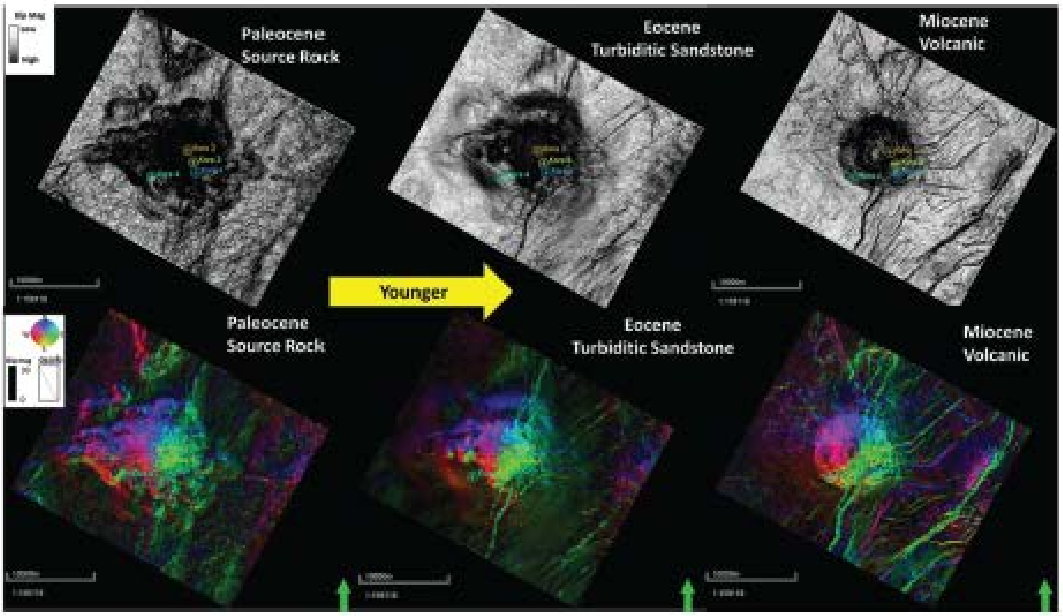

Figure 32. Dip magnitude (above) and dip magnitude modulated by dip azimuth (below) of the Paleocene Waipawa source rock, the Eocene turbidities, and the Miocene Volcanic, showing the evolution of the fault network. Notice the presence of the east-dipping faults (green) in the middle of the survey from the Paleocene through the Miocene.

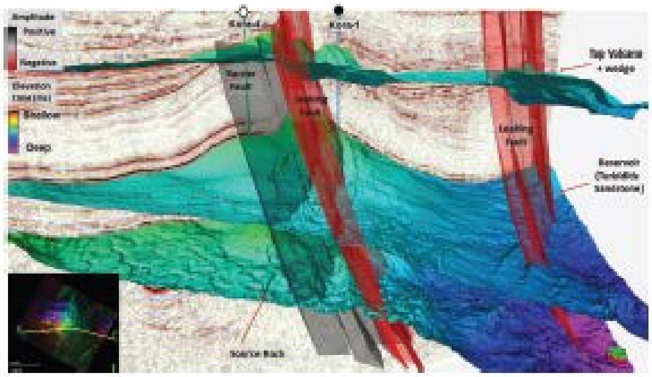

Figure 33. A 3D view of the base of the Paleocene, the Eocene, and the top of the Miocene volcanic. Three main faults (migration pathways) are mapped, which connect the source rock to the Miocene volcanics.

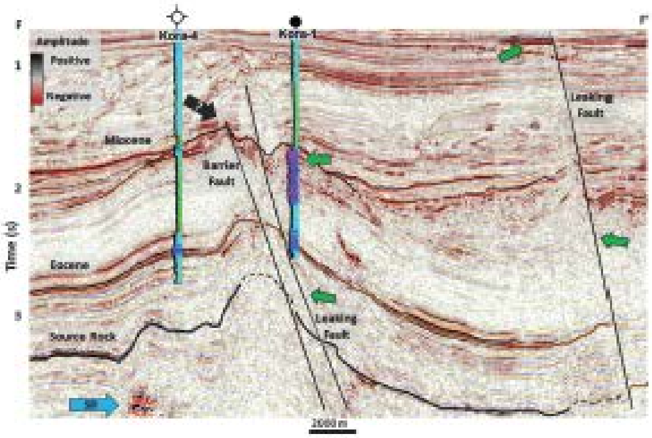

Figure 34. Vertical amplitude section connecting the Kora-1 and 4 wells. The previous three faults are displayed, showing the interpreted leaking and barrier faults. The green arrows point to the leaking faults and their evidence of hydrocarbons. The black arrow explains a second hypothesis. This points to possible evidence of hydrocarbon, assuming the barrier fault is leaking and the Kora-4 well is below the oil-water contact.

connecting the Paleocene source rock and the Miocene volcanics. It is noticeable that both faults connect the area drilled by Kora-1 and 4. Therefore, the fact that Kora-4 is a dry hole is most likely due to the poor migration pathways of the barrier fault because not even shows were found in this exploratory well. Alternatively, that barrier fault may have conducted hydrocarbons from the Paleocene Waipawa source rock to the lava-flow facies in the Miocene volcano, but then Kora-4 had to be positioned below the oil-water contact. This in addition with the good log porosity shown in Figure 13 makes us conclude that the reason Kora-4 did not encounter any hydrocarbons in the lava-flow facies was due to a source charge issue produced by a poor migration pathways, as shown in Figure 34.

Conclusion

Integrating well control and well reports, nearby modern volcano analogs and concepts of seismic geomorphology, we successfully map the distribution of the pyroclastic and lava flows, as well as deeper sills and dikes, which are probably responsible for the formation of the Miocene Kora volcano. In addition to geomorphology of shape and proximity to other components of the volcanic system, amplitude anomalies aided in the identification of intrusive sills, VMTDs, ADC sediments, magma conduits, and what we hypothesize to be hornfels.

Moreover, igneous bodies can indeed affect almost every element of the petroleum systems. As we showed in this case study, igneous intrusions can positively alter the maturity of the source rock moving it into the oil window. Igneous bodies can create structural traps (forced folds), migration pathways from cooling and collapse of the volcanic edifice (radial faults) or from upward migration breaking the host rock. Volcanic rocks can even form the reservoir, which, in this study, pyroclastic flows flowed 668 BOPD for 254 h with porosity ranges of 20%–25% and air permeability ranges of 170–240 mD.

Likewise, we would like to stress that the appearance of volcanic facies often mimics other facies of exploration interest. Small volcanic cones appear similar to carbonate buildups and exhibit a similar high impedance. The VMTDs look like siliciclastic mass-transport complexes. If one does not properly account for polarity, igneous sills can be easily misinterpreted to be hydrocarbon bright spots.

In many situations, igneous rocks exhibit high magnetic and gamma-ray anomalies. Common pitfalls are to ignore the impact of residual magnetism, or the removal of a magnetic anomaly by diagenetic alteration. Fortunately, identification and linkage of the diverse architectural elements that compose the volcanic system described in this and companion papers in this special section provide the means to avoid such interpretation pitfalls.

Acknowledgments

We would like to thank New Zealand Petroleum and Minerals for providing the Kora-3D seismic data to the public for use in research and education. Financial support for this effort is provided by the sponsors of the Attribute-Assisted Seismic Processing and Interpretation Consortium at the University of Oklahoma (OU). We thank our colleagues for their valuable input and suggestions. We would also like to thank the editors of this seismic expression of igneous bodies special section: C. Jackson, M. Giba, and T. Wrona for their valuable time and support. All the 3D seismic displays were made using licenses of Petrel provided to the OU for research and education courtesy of Schlumberger. We would also like to thank E. Da Silva for her time and dedication with the interpretation of the Kora horizon; A. Liborius for her help with the Kora-2 core description; and O. Olorunsola, A. Besov, and G. Machado for their moral support and posing relevant questions to this research. B. Weaver, R. Slatt, and Li at OU are appreciated for their invaluable insight.

References

Alves, T., K. Omosanya, and P. Gowling, 2015, Volume rendering of enigmatic high-amplitude anomalies in southeast Brazil: A workflow to distinguish lithologic features from fluid accumulations: Interpretation, **3**, no. 2, A1–A14, doi: 10.1190/INT-2014-0106.1.

Barber, P. M., T. Rasmussen, S. S. Rey, and R. Myklebust, 1988, The Exmouth Plateau deep water frontier: A case history, *in* P. G. Purcell and R. R. Purcell, eds., The North West Shelf, Australia, Proceedings of the Petroleum Exploration Society of Australia Symposium, 63–76.

Beavan, J., P. Tregoning, M. Bevis, T. Kato, and C. Meertens, 2002, Motion and rigidity of the Pacific Plate and implications for plate boundary deformation: Journal of Geophysical Research, **107**, ETG 19-1, doi: 10.1029/2001JB000282.

Bergman, S. C., J. P. Talbot, and P. R. Thompson, 1991, The Kora Miocene submarine andesite stratovolcano hydrocarbon reservoir, Northern Taranaki Basin, New Zealand: New Zealand Oil Exploration Conference Proceedings, Ministry of Commerce, 178–206.

Bergman, S. C., J. P. Talbot, and P. R. Thompson, 1992, The Kora Miocene submarine andesite stratovolcano hydrocarbon reservoir, Northern Taranaki Basin, New Zealand: New Zealand Oil Exploration Conference Proceedings, Ministry of Commerce, 178–206.

Bowen, N., 1922, The behavior of inclusions in igneous magmas: The Journal of Geology, **30**, 513–570, doi: 10.1086/622928.

Cortez, M., and M. Cetalle-Santos, 2016, Seismic interpretation, attribute analysis, and illumination study for targets below volcanic-sedimentary succession, Santos Basin, offshore Brazil: Interpretation, **4**, no. 1, SB37–SB50, doi: 10.1190/INT-2015-0097.1.

Crown Minerals, 2016a, Capillary pressure and XRD mineralogy study of Kora Wells, Web: Petroleum Report Series PR 4178.

Crown Minerals, 2016b, Final well report, Kora-1 Kora-1A, PPL 38447, Web: Petroleum Report Series PR 1374.

Crown Minerals, 2016c, Final well report, Kora-2, PPL 38447, Web: Petroleum Report Series PR 1441.

Crown Minerals, 2016d, Final well report, Kora-3, PPL 38447, Web: Petroleum Report Series PR 1441.

Crown Minerals, 2016e, Final well report, Kora-4, PPL 38447, Web: Petroleum Report Series PR 1443.

Crown Minerals, 2016f, Albacore-1 well completion report, Web: Petroleum Report Series PR 4183.

Crown Minerals, 2016g, Ariki-1 Well, PPL38048, Web: Petroleum Report Series PR 1038.

Crown Minerals, 2016h, Hydrocarbon characterization study Tangaroa Play, Web: Petroleum Report Series PR 3259.

Crown Minerals, 2016i, 3D basin modeling of PEP 38485, Offshore Taranaki Basin, Web: Petroleum Report Series PR 4313.

Dallas, B. D., L. J. Wood, and L. G. Moscardelli, 2013, Seismic geomorphology of early North Atlantic sediment waves, offshore northwest Africa: Interpretation, **1**, no. 1, SA75–SA91, doi: 10.1190/INT-2013-0040.1.

Delpino, D. H., and A. M. Bermudez, 2009, Petroleum systems including unconventional reservoirs in intrusive igneous rocks (sills and laccoliths): The Leading Edge, **28**, 804–811, doi: 10.1190/1.3167782.

DeMets, C., R. G. Gordon, D. F. Argus, and S. Stein, 1994, Effect of recent revisions to the geomagnetic reversal time scale on estimates of current plate motions: Geophysical Research Letters, **21**, 2191–2194, doi: 10.1029/94GL02118.

Farooqi, M. Y., H. Huijun, G. Li, N. Machin, T. Neville, A. Pal, C. Shrivastva, Y. Wang, F. Yang, C. Yin, J. Zhao, and X. Yang, 2009, Evaluating volcanic reservoirs: Oilfield Review, **21**, 36–47.

Giba, M., A. Nicol, and J. Walsh, 2010, Evolution of faulting and volcanism in a back-arc basin and its implications for subduction processes: Tectonics, **29**, TC4020, doi: 10.1029/2009TC002634.

Giba, M., J. J. Walsh, A. Nicol, V. Mouslopoulou, and H. Seebeck, 2013, Investigation of the spatio-temporal relationship between normal faulting and arc volcanism on million-year time scales: Journal of the Geological Society, **170**, 951–962, doi: 10.1144/jgs2012-121.

Hall-Beyer, M., 2007, The GLCM tutorial, version 2.10, http://www.fp.ucalgary.ca/mhallbey/tutorial.htm, accessed 1 December 2016.

Hansen, R. J., and P. J. Kamp, 2006, An integrated biostratigraphy and seismic stratigraphy for the late Neogene continental margin succession in northern Taranaki Basin, New Zealand: New Zealand Journal of Geology and Geophysics, **49**, no. 1, 39–56, doi: 10.1080/00288306.2006.9515146.

Hayward, W. B., R. P. King, and R. E. Fordyce 1987, Paleogeography and tectonic history of Taranaki Basin: Geological Society of New Zealand.

Holford, S. P., N. Schofield, C. A. L. Jackson, C. Magee, P. F. Green, and I. R. Duddy, 2013, Impacts of igneous intrusions on source and reservoir potential in prospective sedimentary basins along the Western Australian continental margin: West Australian Basins Symposium, Proceedings of the Petroleum Exploration Society of Australia Symposium, 1–12.

Infante-Paez, L., L. F. Cardona, B. McCullough, and R. Slatt, 2017, Seismic analysis of paleotopography and stratigraphic controls on total organic carbon: Rich sweet spot distribution in the Woodford Shale, Oklahoma, USA: Interpretation, **5**, no. 1, T33–T47, doi: 10.1190/INT-2015-0151.1.

Jackson, C. A., N. Schofield, and B. Golenkov, 2013, Geometry and controls on the development of igneous sill-related forced folds: A 2-D seismic reflection case study from offshore southern Australia: Geological Society of America Bulletin, **125**, 1874–1890, doi: 10.1130/B30833.1.

King, P. R., G. H. Scott, and P. H. Robinson, 1993, Description, correlation and depositional history of Miocene sediments outcropping along North Taranaki coast: Institute of Geological & Nuclear Sciences Ltd., p. 199.

King, P. R., and G. P. Thrasher, 1992, Post-Eocene development of the Taranaki Basin, New Zealand: Convergent overprint of a passive margin: Geology and Geophysics of Continental Margins, **53**, 93–118.

King, P. R., and G. P. Thrasher, 1996, Cretaceous Cenozoic geology and petroleum systems of the Taranaki Basin, New Zealand: Institute of Geological & Nuclear Sciences 2.

Kingston, J., and J. R. Matzko, 1995, Undiscovered petroleum of the Brazilian interior sag basins: International Geology Review, **37**, 959–980, doi: 10.1080/00206819509465435.

Klarner, S., B. Ujetz, R. Fontana, and J. Altenkirch, 2006, Seismic signature of Upper Cretaceous volcanics; Santos Basin, Brazil: 68th Annual International Conference and Exhibition, EAGE, Extended Abstracts, 105.

Lee, C., J. A. Nott, F. B. Keller, and A. R. Parrish, 2004, Seismic expression of the Cenozoic mass transport complexes, deepwater Tarfaya-Agadir Basin, offshore Morocco: Offshore Technology Conference, 16741.

Liborius-Parada, A., and D. Tazzo, 2012, Petrografía de la aureola de contacto de la granodiorita de El Carmen en las adyacencias del pico El Águila-vía Piñango, edo. Mérida, Venezuela: GEOS Venezuelan Journal of Earth Sciences, **42**, 72–76.

Magee, C., C. A. Jackson, and N. Schofield, 2014, Diachronous sub-volcanic intrusion along deep-water margins: Insights from the Irish Rockall Basin: Basin Research, **26**, 85–105, doi: 10.1111/bre.12044.

Magee, C., J. D. Muirhead, A. Karvelas, S. P. Holford, C. A. Jackson, I. D. Bastow, N. Schofield, C. T. Stevenson, C. McLean, W. McCarthy, and O. Shtukert, 2016, Lateral magma flow in mafic sill complexes: Geosphere, **12**, 809–841, doi: 10.1130/GES01256.1.

Matos, M., M. Yenugu, S. M. Angelo, and K. J. Marfurt, 2011, Integrated seismic texture segmentation and cluster analysis applied to channel delineation and chert reservoir characterization: Geophysics, **76**, no. 5, P11–P21, doi: 10.1190/geo2010-0150.1.

McArdle, N., D. Iacopini, M. A. KunleDare, and G. S. Paton, 2014, The use of geologic expression workflows for basin scale reconnaissance: A case study from the Exmouth Subbasin, North Carnarvon Basin, northwestern Australia: Interpretation, **2**, no. 1, SA163–SA177, doi: 10.1190/INT-2013-0112.1.

Ministry of Business, Innovation, and Employment, 2005, Online Exploration Database, https://data.nzpam.govt.nz/GOLD/system/mainframe.asp, accessed September 2015.

Moscardelli, L., and L. Wood, 2008, New classification system for mass transport complexes in offshore Trinidad: Basin Research, **20**, 73–98, doi: 10.1111/j.1365-2117.2007.00340.x.

Neall, V. E., R. B. Stewart, and I. E. M. Smith, 1986, History and petrology of the Taranaki volcanoes: Royal Society of New Zealand Bulletin, **23**, 251–263.

Nemčok, M., 2016, Rifts and passive margins: Structural architecture, thermal regimes, and petroleum systems: Cambridge University Press.

Pena, V., S. Chávez-Pérez, M. Vázquez-García, and K. J. Marfurt, 2009, Impact of shallow volcanics on seismic data quality in Chicontepec Basin, Mexico: The Leading Edge, **28**, 674–679.

Planke, S., E. Alvestad, and O. Eldholm, 1999, Seismic characteristics of basaltic extrusive and intrusive rocks: The Leading Edge, **18**, 342–348, doi: 10.1190/1.1438289.

Planke, S., T. Rasmussen, S. S. Rey, and R. Myklebust, 2005, Seismic characteristics and distribution of volcanic intrusions and hydrothermal vent complexes in the Vøring and Møre basins, *in* A. G. Dore and B. A. Vining, eds., Petroleum geology: North-West Europe and global perspectives, Proceedings of the 6th Petroleum Geology Conference: Geological Society, 833–844.

Posamentier, H. W., and V. Kolla, 2003, Seismic geomorphology and stratigraphy of depositional elements in deep-water settings: Journal of Sedimentary Research, **73**, 367–388, doi: 10.1306/111302730367.

Qi, J., T. Lin, T. Zhao, F. Li, and K. J. Marfurt, 2016, Semisupervised multiattribute seismic facies analysis: Interpretation, **4**, no. 1, SB91–SB106, doi: 10.1190/INT-2015-0098.1.

Rateau, R., N. Schofield, and M. Smith, 2013, The potential role of igneous intrusions on hydrocarbon migration, West of Shetland: Petroleum Geoscience, **19**, 259–272, doi: 10.1144/petgeo2012-035.

Roden, R., T. Smith, and D. Sacrey, 2015, Geologic pattern recognition from seismic attributes: Principal component analysis and self-organizing maps: Interpretation, **3**, no. 4, SAE59–SAE83, doi: 10.1190/INT-2015-0037.1.

Rojo, L., A. Escalona, and L. Schulte, 2016, The use of seismic attributes to enhance imaging of salt structures in the Barent Sea: First Break, **34**, 49–57.

Roy, A., M. Matos, and K. J. Marfurt, 2011, Application of 3D clustering analysis for deep marine seismic facies classification — An example from deep water northern Gulf of Mexico: GCSSEPM 31st Annual Bob. F. Perkins Research Conference, 410–439.

Sarkar, S., S. Verma, and K. J. Marfurt, 2016, Seismic-petrophysical reservoir characterization in the northern part of the Chicontepec Basin, Mexico: Interpretation, **4**, no. 3, T403–T417, doi: 10.1190/INT-2015-0168.1.

Schutter, S. R., 2003, Hydrocarbon occurrence and exploration in and around igneous rocks: Geological Society of London, Special Publications, 7–33.

Somasundaram, S., S. Bhat, A. Das, B. Mund, A. Beohar, and P. Shankar, 2017, Fracture detection and calibration in a tight volcanic gas reservoir, Barmer Basin, India: First Break, **35**, 101–106.

Thrasher, G. P., B. Leitner, and A. W. Hart, 2002, Petroleum system of the Northern Taranaki Graben: New Zealand Petroleum Conference Proceedings: Ministry of Economic Development, 1–6.

Zhang, K., and K. J. Marfurt, 2011, Seismic attribute illumination of an igneous reservoir in China: The Leading Edge, **30**, 266–270, doi: 10.1190/1.3567256.

Zhao, T., J. Zhang, F. Li, and K. J. Marfurt, 2016, Characterizing a turbidite system in Cantebury Basin, New Zealand, using seismic attribute and distance-preserving self-organizing maps: Interpretation, **4**, no. 1, SB79–SB89, doi: 10.1190/INT-2015-0094.1.

Lennon Infante-Paez received a bachelor's degree in geophysical engineering from Simon Bolivar University, Venezuela, and a master's degree in geology from the University of Oklahoma (OU) under R. Slatt. He is a student member of AAPG and SEG completing his doctorate in geophysics at OU studying under AAPG member K. Marfurt. His technical research interests include analysis of petroleum systems, quantitative and qualitative seismic interpretation, unconventional reservoir characterization, petrophysics, and seismic expression of igneous rocks.

Kurt J. Marfurt received a Ph.D. (1978) in applied geophysics from Columbia University's Henry Krumb School of Mines in New York, where he also taught as an assistant professor for four years. He joined the University of Oklahoma (OU) in 2007, where he serves as the Frank and Henrietta Schultz professor of geophysics within the ConocoPhillips School of Geology and Geophysics. He worked for 18 years in a wide range of research projects at Amoco's Tulsa Research Center, after which he joined the University of Houston for eight years as a professor of geophysics and the director of the Allied Geophysics Lab. He has received the following recognitions: SEG best paper (for coherence), SEG best presentation (for seismic modeling), as a coauthor with Satinder Chopra best SEG poster (for curvature) and best AAPG technical presentation, and as a coauthor with Roderick Perez-Altamar for best paper in *Interpretation* (on a resource play case study). He also served as the SEG/EAGE Distinguished Short Course Instructor for 2006 (on seismic attributes). In addition to teaching and research duties at OU, he leads short courses on attributes for SEG and AAPG. He currently serves as editor-in-chief of the SEG/AAPG publication *Interpretation*. His primary research interest is in the development and calibration of new seismic attributes to aid in seismic processing, seismic interpretation, and reservoir characterization. Recent work has focused on applying coherence, spectral decomposition, structure-oriented filtering, and volumetric curvature to mapping fractures and karst with a particular focus on resource plays.